

eIF4A2 is a regulator of hypoxic translation and colorectal tumour cell survival

Hannah Bolland, BSc (Hons), M.Med.Sci.

School of Medicine

Division of Cancer and Stem Cells

Thesis submitted to The University of Nottingham for the degree of Doctor of Philosophy

December 2019

Abstract

Colorectal cancer is the third most common cancer, leading to 700,000 deaths a year worldwide. Regions of hypoxia (<1% O_2) are present in around 50% of colorectal tumours. Hypoxia is associated with resistance to chemotherapy, radiotherapy and worse patient outcome. The process of protein synthesis, in particular, translation initiation, is a tightly regulated process orchestrated by the interaction between the mRNA strand, ribosome, RNA binding proteins and eukaryotic initiation factors. Hypoxia reprograms protein output by altering mRNA translation efficiency and components of the protein synthesis machinery to aid cell survival. eIF4A2 is an ATP dependent RNA helicase required to unwind complex secondary structures present in the 5'UTR of transcripts to allow for translation to occur. eIF4A2 is differentially expressed in a variety of cancers and has previously been shown to directly interact with components of miRNA repression machinery. It was therefore hypothesised that eIF4A2 plays a role in normoxic and hypoxic colorectal cancer cell survival through its regulation of translation of proteins required for hypoxic survival. This thesis aimed to investigate the hypoxic regulation and expression of eIF4A2 in colorectal cancer cells in addition to the effect of eIF4A2 knockdown on the hypoxic survival of colorectal cancer cells. A final aim of this thesis is to identify the differentially expressed transcripts bound to eIF4A2 under normoxic and hypoxic conditions in colorectal cancer cells. A variety of cell-based assays were used to identify that eIF4A2 mRNA expression is increased under hypoxic conditions across a panel of colorectal cancer cell lines. Furthermore, eIF4A2 was found to be under the transcriptional control of HIF2α at both the RNA and protein level in two colorectal cancer cell lines. eIF4A2 was found to be required for hypoxic colorectal cancer cell survival in both 2D and 3D assays, this effect was found to be tumour specific as no negative effect on cell survival was observed in a normal colon epithelial cell line following eIF4A2 knockdown. A global RIP-SEQ approach was used to uncover novel transcripts bound to eIF4A2 and differentially expressed between normoxia and hypoxia. Such transcripts up regulated in hypoxia in comparison to normoxia when bound to eIF4A2 were found to be enriched for pathways including metabolism, endocytosis, carbon metabolism, focal adhesion and lysosome along with many other pathways in line with the major changes in hypoxia. 5'UTR analysis revealed that hypoxic eIF4A2 bound transcripts possessed longer and more thermodynamically stable 5'UTRs. This suggests a higher dependence on eIF4A2 to be efficiently unwound. The work presented in this thesis for the first time demonstrates that colorectal cancer cells require eIF4A2 for their survival in both normoxia and hypoxia. Furthermore, the work presented in

this thesis uncovers novel hypoxic eIF4A2 bound transcripts and novel pathways potentially regulated by eIF4A2 in hypoxic conditions. These results lead us to the hypothesis that eIF4A2 is a master regulator of the molecular adaption to hypoxia, enabling cell proliferation and survival in hypoxia by regulating the translation of proteins in amino acids synthesis and endocytic pathways.

Acknowledgments

Firstly I would like to thank my supervisors Alan McIntyre and Abdol Shams Nateri for giving me the opportunity to research such an intellectually challenging and enjoyable project for the past 3 years. Thank you to Bowel and Cancer Research for funding this project!

Thank you to Chris Carroll for never ending trips to the shop and our shared love for quality memes. I will miss you very much. I would like to thank Phil Clark, Pam Collier, Anna Grabowska and Alison Ritchie for their work on the xenograft experiments, Latch, Wakkas and Declan for the tissue microarrays and Bev Bramley for organising all of our science lives. Thank for you Abhik for your time and patience in teaching me how to score an enormous TMA. Thank you to Graeme Denton and Vicki Norris for keeping the lab running safely and smoothly.

Can't forget to thank Mum and Dad who have been a constant source of encouragement and support all my life, I promise I will get a real job and stop being a student now! Thank you to Sam Bestall for your advice and friendship. Thank you to all members of the TVBL past and present who have helped along the way, you have all been great friends and I will miss working with you all. Special thank you to Kiren, Andy and Claire, I will miss you so much!! Thank you to Dave for your support, patience and love; I promise not work weekends and learn to say no to people.

Lastly a special thanks goes to Alan, who I feel has gone above and beyond what is expected of a supervisor. I cannot begin to thank you enough for your support and enthusiasm for "awesome" science. I could not have asked for a better person to guide me through my PhD. I will miss Nottingham so much.

Contents

List of Abbreviations

4EBP	Eukaryotic translation initiation factor 4E binding protein
5FU	Fluorouracil
5hmC	5-Hydroxymethylcytosine
5-mC	5-methylcytosine
FdUMP	Fluorodeoxyuridylate
^{18}F-FAZA	^{18}F-fluroazomycin arabinoside
^{18}F-FMISO	^{18}F-fluoromisonidazole
43SPIC	43S pre-initiation complex
ABC	ATP-binding cassette transporter
ADP	Adenosine di-phosphate
AGO	Argonaute
ANGPTL4	Angiopoietin-like 4
AKT	Protein kinase B
ALODA	Aldolase,Fructose-Bisphosphate A
ALDOC	Aldolase C, fructose bisphosphate
AP1	Activator protein 1
APC	Adenomatous polyposis coli
ARRB1	Arrestin beta 1
ARID5B	AT-Rich interaction domain 5B
ARNT	Aryl hydrocarbon receptor nuclear translocator
AML	Acute myeloid leukemia
ANOVA	Analysis of variance
ATCC	American Type Culture Collection
ATF	Activating transcription factor
ATP	Adenosine triphosphate
AXIN	Axin
AXUD1	AXIN1 up-regulated 1
BCL2	B-cell lymphoma 2
BCL-xL	B-cell lymphoma extra large

bHLH	Basic helix-loop-helix
Bip	Binding immunoglobulin protein
BLI	Bioluminescent intensity
BMP	Bone morphogenetic protein
BNIP3	BCL2 interacting protein 3
BOLD MRI	Blood oxygenation level dependent magnetic resonance imaging
BRCA	Breast cancer type 1 susceptibility protein
BSA	Bovine serum albumin
c-JUN	Transcription factor AP-1
CAIX	Carbonic anhydrase 9
CBC	crypt base columnar stem cells
CBP	CREB binding protein
ccRCC	Clear cell renal cell carcinoma
CD1	Cluster of differentiation 1
CDH22	Cadherin-like protein 22
CDK1	Cyclin-dependent kinase
cDNA	Complementary DNA
CEBP	CCAAT-enhancer-binding proteins
ChIP	Chromatin immunoprecipitation
ChIP-SEQ	Chromatin immunoprecipitation sequencing
CHMP6	Charged multivesicular body protein 6
CHOP	CEBP homologous protein
CIMP	CpG island methylator phenotype
CIN	Chromosomal instability
CK1	Casein kinase 1
CML	Chronic myelogenous leukemia
CNOT7	CCR4-NOT transcription factor complex subunit 7
$CoCL_2$	Cobalt (II) chloride
Co-IP	Co-immunoprecipitation
CpG	5’-C-phosphate-G-3’
CRC	Colorectal cancer

C-TAD	C-terminal transactivation domain
Ct	Cycle threshold
CTH	Cystathionine gamma-lyase
DAB	3,3’-Diaminobenzidine
DEPTOR	DEP domain-containing mTOR-interacting protein
DDX	DEAD-box protein
DMEM	Dulbecco’s Modified Eagle Medium
DMDA-PatA	Des-methyl,des-amino pateamine A
DMSO	Dimethylsulfoxide
DNA	Deoxyribonucleic acid
dNTP	Deoxynucleoside triphosphate
DVL	Dishevelled
E2F	E2 factor
ECM	Extracellular matrix
EDTA	Ethylenediaminetetraacetic acid
EE	Early endosome
eEFs	Eukaryotic elongation factors
EGFR	Epidermal growth factor receptor
EHD	EH domain containing protein
eIF	Eukaryotic initiation factor
EJC	Exon junction complex
ELK1	ETS transcription factor ELK1
EPO	Erythropoietin
ER	Endoplasmic reticulum
Erb	Estrogen receptor beta
ERK	Extracellular signal-regulated kinase
ETS1	Protein C-ets-1
ETV4	ETS translocation variant 4
EMT	Epithelial-mesenchymal transition
ENO	Enolase
FAP	Familial adenomatous polyposis

FBS	Fetal bovine serum
FBX02	F-box only protein 2
FDA	Food and Drug Administration
FDG-PET	Fluorodeoxyglucose positron emission tomography
FGF-2	Basic fibroblast growth factor
fLUC	Firefly luciferase
FOS	FOS proto-oncogene, AP-1 transcription factor subunit
FOSL2	Fos-related antigen 2
FOXP1	Forkhead box P1
FPKM	Fragments per kilobase of transcripts per million mapped reads
FZD	Frizzled
G_4	G-quadruplex
GADD34	Growth arrest and DNA damage includible protein
GAPDH	Glyceraldehyde 3-phosphate dehydrogenase
GATA	GATA binding factor
GCN2	General control nonderepressible 2
GDP	Guanosine diphosphate
GFP	Green fluorescent protein
GLUT	Glucose transporter protein
GO	Gene ontology
GRK5	G protein-coupled receptor kinase 5
GSK3	Glycogen synthase kinase 3
GTP	Guanosine triphosphate
GW182	Trinucleotide repeat containing gene 6A protein
H&E	Hematoxylin and eosin
HAP	Hypoxia activated prodrug
HER2	Human epidermal growth factor receptor 2
HIF	Hypoxia inducible factor
HK1	Hexokinase 1
HMGB1	High mobility group box 1
HNPCC	Hereditary non-polyposis colorectal cancer

HRE	Hypoxia response element
HRI	Heme-regulated eIF2a kinase
HSPA	Heat shock protein family A
iCLIP	Individual-nucleotide resolution UV crosslinking immunoprecipitation
IDH2	Isocitrate dehydrogenase
IgG	Immunoglobulin G
IGF1R	Insulin like growth factor 1 receptor
INSIG2	Insulin induced gene 2
IPTG	Isopropyl β-d-1-thiogalactopyranoside
IRES	Internal ribosome entry site
ISR	Integrated stress response
ITAF	IRES trans-acting factors
JMJD1A	Jumonji domain containing 1A
KEGG	Kyoto Encyclopedia of Genes and Genomes
KIF5B	Kinesin family member 5B
LacO	Lac operon
LDHA	Lactate dehydrogenase
LEF	Lymphoid enhancing factor
LGR5	Leucine-rich repeat-containing G-protein coupled receptor 5
LOH	Loss of heterozygosity
LOX	Lysyl oxidase
LRP	Lipoprotein receptor-related protein
m^6A	N^6-Methyladenosine
m^7G	7-Methylguanosine
MAPK	Mitogen-activate protein kinase
MATRIX	Mass spectrometry analysis of activate translation facto using ribosome density fractionation and isotopic labeling experiments
Mcl-1	Myeloid cell leukemia 1
MDM2	Mouse double minute 2 homolog
MDR1	Multi drug resistance gene 1
Meis1	Meis homeobox 1

MEK	Mitogen-activate protein kinase kinase
MFE	Minimum free energy
MGMT	O^6-methylguanine DNA methyltransferase
MIF	Macrophage migration inhibitory factor
miRNA	microRNA
MLH1	Human mutL homolog 1
MLST8	Target of rapamycin complex sub unit LST8
MMR	Mismatch repair
MNK	MAP kinase-interacting serine/threonine-protein kinase 1
MOI	Multiplicity of infection
mRNA	Messenger RNA
mRNP	Messenger ribonucleoprotein complex
MSH	MutS homolog 2
MTI-MMP	Membrane type 1 matrix metalloproteinase
mTOR	Mammalian target of rapamycin
Myc	Myc proto-oncogene protein
NBF	Neutral buffered formalin
NEURL3	Neuralized E3 ubiquitin protein ligase 3
NF- κβ	Nuclear factor kappa-light-chain-enhancer of activated B cells
NHL	Non-Hodgkin lymphoma
NOD	Nucleotide-binding oligomerization domain protein
NOTCH1	Notch receptor 1
NOXA	Phorbol-12-myristate-13-acetate-induced protein
NSCLC	Non-small-cell lung carcinoma
N-TAD	N-terminal transactivation domain
OCT4	Octamer-binding transcription factor 4
ODDD	Oxygen dependent degradation domain
ORF	Open reading frame
P4HA1	Prolyl 4-Hydroxylase sub unit alpha 1
PA	Phosphatidic acid
PAN	Poly(A)-nuclease

PAR-CLIP	Photoactivatable ribonucleoside-enhanced crosslinking a immunoprecipitation
PAS	Per-Arnt-Sim
PatA	Pateamine A
PABP	Poly(A)-binding protein
PARD6A	Partitioning defective 6 homolog alpha
PBS	Phosphate buffered saline
PDAC	Pancreatic ductal adenocarcinoma
Pdcd4	Programmed cell death protein 4
PERK	Protein kinase RNA-like endoplasmic reticulum kinase
PET	Positron emission tomography
PFA	Paraformaldehyde
P-gp	P-glycoprotein
PHD	Prolyl-hydroxylase
PHGDH	Phosphoglycerate dehydrogenase
PI3K	Phosphoinositide 3-kinase
PIC	Pre-initiation complex
PIP_2	Phosphatidylinositol 4,5-bisphosphate
PIP_3	Phosphatidylinositol (3,4,5)-triphosphate
PIP5K1C	Phosphatidylinositol-4-phosphate 5-kinase type 1 gamma
PIP-SEQ	Protein interaction profile sequencing
PKM	Pyruvate kinase
PKR	Protein kinase R
PLD2	Phospholipase D2
PMS2	Mismatch repair endonuclease PMS2
POL	RNA polymerase
PRAS40	Proline-rich Aky substrate of 40kDa
PRE	Pumilio response element
PROTOR	Protein-rich protein 5
pSILAC	Stable isotope labelling with amino acids in cell culture
PSD4	PH and SEC7 domain-containing protein 4

PTEN	Phosphtase and tensin homolog
PTM	Post translational modification
qRT-PCR	Quantitative reverse transcription polymerase chain reaction
RAS	Ras GTPase
RAB11FIP4	Rab11 family-interacting protein 4
RAF	RAF proto-oncogene serine/threonine-protein kinase
RB	Retinoblastoma
RBM4	RNA binding motif 4
RBP	RNA binding protein
RCC	Renal cell carcinoma
REDD1	Regulated in development and DNA damage response
RHEB	Ras homolog enriched in brain
RIBO-SEQ	Ribosome profiling
RICTOR	Rapamycin-insensitive companion of mammalian target of rapamycin
RIP	RNA immunoprecipitation
RIPA	Radioimmunoprecipitation assay buffer
RIP-SEQ	RNA immunoprecipitation sequencing
RNA	Ribonucleic acid
RNA-SEQ	Ribonucleic acid sequencing
rRNA	Ribosomal RNA
RTK	Receptor tyrosine kinase
RUNX1	Runt-related transcription factor 1
S6kinase	Ribosomal S6 kinase
SCID	Severe combined immune deficient
SF2	Superfamily 2 helicases
sFRP	Secreted Frizzled-related proteins
SHAPE	Selective 2’-hydroxyl acylation analysed by primer extension sequencing
SHMT2	Serine hydroxymethyltransferase
shRNA	Short hairpin RNA
siRNA	Small interfering RNA
SLC01B3	Solute carrier organic anion transporter family member 1B3

SLC6A18	Solute carrier family 6, member 18
SMAD	SMAD family member
SNAIL2	Zinc finger protein SNAI2
snoRNPs	Small nucleolar RNA
SRC	Steroid receptor co-activator
SSU	Small sub unit
STAT	Signal transduced and activator of transcription
SUMO	Small ubiquitin-like modifier
TAB182	Tankyrase 1-binding protein of 182kDa
T-ALL	T-cell acute lymphoblastic leukemia
TBS	Tris buffered saline
TBS-T	Tris buffered saline with Tween
TCF	Helix-loop-helix transcription factor family of proteins
TET1	Ten-eleven translocation methylcytosine dioxygenase 1
TF11B	Transcription initiation factor IIB
TGF	Transforming growth factor
Tie2	Angiopoietin-1 receptor
TMA	Tissue microarray
TOP	5'Terminal oligopyrimidine tract
TOR	Target of rapamycin
TP53	Tumour protein p53
TRAP-SEQ	Targeted purification of polysomal mRNA
tRNA	Transfer RNA
$tRNAi_{met}$	Initiation methionyl transfer RNA
TSC	Tuberous sclerosis protein
TSS	Transcription start site
uORF	Upstream open reading frame
UPR	Unfolded protein response
UPW	Ultra pure water
UTR	Untranslated region
UV	Ultraviolet

VEGF	Vascular endothelial growth factor
VEGFR	Vascular endothelial growth factor receptor
VHL	Von Hippel-Lindau
WT	Wild type
XIAP	X-linked inhibitor of apoptosis
XRN1	5’-3’ exoribonuclease 1
YTHDC2	YTH domain containing 2
ZBTB33	Zinc finger and BTB domain containing 33
ZFYVE9	Zinc finer FYVE-Type containing 9
ZNF143	Zinc finger protein 143

List of Figures and Tables

Chapter 1: Introduction

Figure 1.1. Schematic of the small intestinal epithelium displaying the key epithelial cell types.

Figure 1.2. Functional domains of the HIF isoforms.

Figure 1.3. HIF1α regulation under normoxic and hypoxic conditions

Figure 1.4. Schematic overview of translation initiation.

Figure 1.5. Biphasic response to hypoxic conditions is mediated via 2 distinct pathways.

Figure 1.6. Motifs present within the DEAD box family of proteins

Figure 1.7. Schematic overview of eIF4A catalytic cycle.

Chapter 2: Methods and Materials

Table 2. Master mix components per sample for cDNA synthesis

Table 2.1. Master mix components per sample for qRT-PCR.

Figure 2. Structure of the pLKO-puro-IPTG-3xLacO inducible vector.

Table 2.3. Reagents, time in minutes and number of washed performed to perform rehydration of immunohistochemical samples.

Table 2.4. Reagents, time in minutes and number of washed performed to perform dehydration of immunohistochemical samples.

Table 2.5. Components per sample for RIP lysis buffer.

Table 2.6. Components per sample for RIP Immunoprecipitation Buffer.

Table 2.7. Components per sample for Proteinase K Buffer.

Chapter 3: eIF4A2 Hypoxic Expression and Regulation in Colorectal Cancer

Figure 3.1. eIF4A2 mRNA expression under hypoxic conditions across a panel of colorectal cancer cell lines

Figure 3.2. eIF4A1 mRNA expression under hypoxic conditions across a panel of colorectal cancer cell lines.

Figure 3.3. CA9 mRNA expression under hypoxic conditions across a panel of colorectal cancer cell lines

Figure 3.4. Representative immunoblot images of eIF4A1 and eIF4A2 protein expression following hypoxic time course

Figure 3.5. Representative images of hypoxic localisation of eIF4A1 protein in colorectal cancer cells.

Figure 3.6. Representative images of hypoxic localisation of eIF4A2 protein in colorectal cancer cells.

Figure 3.7. eIF4A2 and CA9 staining and localisation of colorectal cancer spheroids.

Figure 3.8. Validation of HIF1α, HIF2α knockout of HCT116 and LS174T cell lines at the mRNA level.

Figure 3.9. eIF4A1 and eIF4A2 mRNA expression following HIF1α or HIF2α knockout in HCT116 and LS174T cell lines

Figure 3.10. eIF4A2 protein expression following HIF1 and HIF2 KO in HCT116 and LS174T cell lines.

Figure 3.11. Representative image of CNOT7 interaction with eIF4A2 in colorectal cancer cells.

Figure 3.12. Representative images of eIF4A2 nuclear staining intensities of normal matched tissue cores.

Figure 3.13. Representative images of eIF4A2 nuclear staining intensities of colorectal cancer tissue cores.

Figure 3.14. Representative images of eIF4A2 cytoplasmic staining intensities of colorectal cancer tissue cores

Figure 3.15. Representative images of eIF4A2 cytoplasmic staining intensities of normal matched tissue cores.

Figure 3.16. Representative images of eIF4A2 infiltrating cells staining intensities.

Figure 3.17. Representative images of CA9 and eIF4A2 co-localisation of colorectal tumour and matched normal tissue controls of core 68

Figure 3.18. Representative images of CA9 and eIF4A2 co-localisation of colorectal tumour and matched normal tissue controls of core 128

Figure 3.20. eIF4A2 3'UTR mRNA sequence.

Table 3. *In silico* analysis of the eIF4A2 promoter for transcription factor binding sites.

Table 3.1. *In silico* analysis of the eIF4A1 promoter for transcription factor binding sites.

Chapter 4: Functional Consequences of eIF4A2 Inhibition

Figure 4. Structural formula of the natural product Silvestrol ($C_{34}H_{38}O_{13}$).

Figure 4.1. Structural formula of the natural product Hippuristanol ($C_{24}H_{46}O_5$).

Figure 4.2. Structural formula of the natural product Pateamine A ($C_{31}H_{45}N_3O_4S$).

Figure 4.3. siRNA knockdown of eIF4A2 on cell survival

Figure 4.4. Validation of eIF4A2 IPTG inducible system at the RNA level in HCT116 cells

Figure 4.5. Validation of eIF4A2 IPTG inducible system at the RNA level in LS174T cells.

Figure 4.6. Validation of eIF4A2 IPTG inducible system at the protein level in HCT116 cells.

Figure 4.7. Effect of sheIF4A2 on cell growth in HCT116 and LS174T cells under normoxic and hypoxic conditions.

Figure 4.8. Representative images of LS174T sheIF4A2 spheroids failing to form.

Figure 4.9. HCT116 sheIF4A2 spheroid growth rates.

Figure 4.10. Representative images of HCT116 sheIF4A2 knockdown spheroids

Figure 4.11. Representative images of eIF4A2 knockdown in HCT116 spheroids.

Figure 4.12. Representative images of sheIF4A2 HCT116 necrotic cores.

Figure 4.13. Representative images of differing patterns of necrosis between HCT116 sh69 and HCT116 sh94 cells.

Table 4. HCT116 sheIF4A2 experimental groups for xenograft (CSU1774).

Figure 4.14. sheIF4A2 xenograft growth rates and average body weights.

Figure 4.15. Growth curves of the HCT116 sheIF4A2 xenograft in comparison to historical data from HCT116 wild type cells of the same administration route.

Figure 4.16. Pilot study of HCT116 and LS174T wild type cells.

Table 4.1. HCT116 sheIF4A2 experimental groups for xenograft (CSU 1784).

Figure 4.17. Tumour growth rates of HCT116 sheIF4A2 xenografts (CSU1784).

Figure 4.18. Log transformation of HCT116 sheIF4A2 xenograft tumour volumes.

Figure 4.19. Log transformation of HCT116 sheIF4A2 xenograft tumour diameters.

Figure 4.20. H&E staining of HCT116 shCTL + IPTG xenograft samples (CSU1784).

Figure 4.21. H&E staining of HCT116 shCTL + IPTG xenograft samples (CSU1784).

Figure 4.22. H&E staining of HCT116 sh84 + IPTG xenograft samples (CSU1784).

Figure 4.23. H&E staining of HCT116 sh84 + IPTG xenograft samples (CSU1784).

Figure 4.24. Quantification of necrosis in shCTL and sheIF4A2 xenograft tumours (CSU1784).

Chapter 5: Identification of Hypoxic eIF4A2 bound mRNAs in Colorectal Cancer Cells using a RIP-SEQ Approach

Figure 5. c-MYC 5'UTR secondary structure.

Figure 5.1. Overall results of FPKM cluster analysis from eIF4A2 RIP-SEQ experimental conditions.

Figure 5.2. Volcano plots showing overall distribution of differentially expressed genes from the eIF4A2 RIP-SEQ.

Figure 5.3. Co-expression of differentially expressed genes from eIF4A2 RIP-SEQ.

Table 5. Differentially bound upregulated genes in the eIF4A2 1% 0_2 RIP vs eIF4A2 normoxic RIP enriched for the endocytic pathway.

Table 5.1. Differentially bound upregulated genes in the eIF4A2 1% 0_2 RIP vs eIF4A2 normoxic RIP enriched for the carbon metabolism pathway.

Table 5.2. Differentially bound upregulated genes in the eIF4A2 1% 0_2 RIP vs eIF4A2 normoxic RIP enriched for the biosynthesis of amino acids pathway

Table 5.3. Differentially bound upregulated genes in the eIF4A2 1% 0_2 RIP vs eIF4A2 normoxic RIP enriched for the lysosome pathway.

Table 5.4. Differentially bound upregulated genes in the eIF4A2 1% 0_2 RIP vs eIF4A2 normoxic RIP enriched for the lysosome pathway

Figure 5.4. KEGG pathway analysis of differentially bound eIF4A2 1% 0_2 bound upregulated genes in comparison to eIF4A2 normoxic bound genes.

Figure 5.6. KEGG pathway analysis of differentially bound eIF4A2 1% 0_2 bound downregulated genes in comparison to eIF4A2 normoxic bound genes.

Figure 5.7. qRT-PCR validation of eIF4A2 normoxic and hypoxic RIP for biosynthesis of amino acid selected top transcripts.

Figure 5.8. qRT-PCR validation of eIF4A2 normoxic and hypoxic RIP for carbon metabolism selected top transcripts.

Figure 5.9. qRT-PCR validation of eIF4A2 normoxic and hypoxic RIP for endocytosis selected top transcripts.

Figure 5.10. qRT-PCR validation of eIF4A2 normoxic and hypoxic RIP for HIF isoforms..

Figure 5.11. Representative images of immunoblot validation of eIF4A2 dependent transcripts identified from RIP-SEQ.

Figure 5.12. Representative images of immunoblot validation of eIF4A2 knockdown on CTH protein expression.

Figure 5.13. Representative images of immunoblot validation of eIF4A2 RIP-SEQ targets following eIF4A1 knockdown.

Figure 5.14. Representative images of immunoblot validation of eIF4A2 RIP-SEQ targets following eIF4A1 knockdown.

Figure 5.15. Cell survival of colorectal cancer cells following siRNA knockdown of endocytic genes identified from the eIF4A2 RIP-SEQ.

Figure 5.16. Average 5'UTR length and predicted free energy of eIF4A2 bound transcripts that were found to be upregulated or downregulated under hypoxic conditions identified from the eIF4A2 RIP-SEQ.

Figure 5.17. Representative MFE plots of the most upregulated and downregulated transcripts when bound to eIF4A2 under hypoxic conditions.

Figure 5.18. KEGG pathway of endocytosis, transcripts in red highlight eIF4A2 bound transcripts upregulated under hypoxic conditions.

Contents

Abstract 2
Acknowledgments 4
Contents 5
List of Abbreviations 5
List of Figures and Tables 15
1.0 Introduction 24
1.1 Cancer 24
1.2 Colorectal Cancer 24
1.2.1 Biology of the Intestine 24
1.2.2 Development of Colorectal Tumours 25
1.2.3 APC and Colorectal Tumour Development 27
1.3 Colorectal Cancer Incidence and Survival Rates 27
1.4 Tumour Hypoxia 28
1.5 HIF Transcription Factors 29
1.5.1 Hypoxia and Treatment Resistance 33
1.5.2 Targeting HIF Transcription Factors 34
1.5.3 Hypoxia Activated Pro Drugs (HAPs) 34
1.5.4 Methods of Detecting Hypoxia 35
1.6 Overview of Eukaryotic Cap Dependent Translation 36
1.6.1 Protein Synthesis 36
1.6.2 Translation Initiation 37
1.6.3 Elongation 41
1.6.4 Termination 42
1.7 Non-canonical Cap Dependent Translation 42
1.8 Cap Independent Translation 43
1.9 Translation Initiation in Malignant Cells 43
1.10 Protein Synthesis and the Response to Stress 44
1.10.1 eIF2 Phosphorylation 44
1.10.2 mTOR/eIF4F Signalling Axis 45
1.11 Protein Synthesis and the Response to Hypoxia 46
1.11.1 REDD/TSC1 signalling axis 47
1.11.2 Alternative Modes of Translation in Response to Hypoxia 47
1.11.3 IRES 48
1.11.4 Formation of Novel Protein Complexes to Facilitate Cap Binding 48
1.11.5 Hypoxic Switch in eIF4F Isoforms 49

1.12 The RNA Helicase eIF4A 50
1.13 eIF4A Isoforms 52
1.13.1 eIF4A1 52
1.13.2 eIF4A2 53
1.14 Project Aims 54
2.0 Methods and Materials 55
2.1 Cell Culture 55
2.1.1 Culture of Adherent Cells 55
2.1.2 Cryopreservation of Cells 55
2.1.3 Cell Counting 55
2.2 Hypoxic Culture Conditions 55
2.3 Western Blot 56
2.3.1 Protein Extraction 56
2.3.2 Protein Quantification – Bradford Assay 56
2.3.3 Gel Electrophoresis 56
2.3.4 Gel Transfer 57
2.4 Co-immunoprecipitation of Endogenous Proteins 57
2.5 RNA Extraction 58
2.6 cDNA Synthesis 58
2.7 Quantitative PCR 59
2.8 Nucleic Acid Transfection of Adherent Cells 59
2.8.1 Oligofectamine siRNA Reverse Transfection 59
2.9 Assessment of Cell Viability 60
2.9.1 Clonogenic Assay 60
2.10 Generation of eIF4A2 Inducible Knockdown Cell Line 60
2.10.1 Transduction of Lentiviral Particles 61
2.10.2 Single Cell Clonal Selection 62
2.11 Immunocytochemical Staining 62
2.12 3D Cell Culture 63
2.12.1 Formation of Spheroids 63
2.12.2 Preparation of Spheroids for Immunohistochemistry 63
2.13 Immunohistochemistry 64
2.14 eIF4A2 Human Colorectal Cancer Tissue Micro Array 65
2.15 RNA Immunoprecipitation 65
2.16 RIP-qPCR Data Analysis 67
2.17 RNA Immunoprecipitation Sequencing (RIP-SEQ) 68

2.17.1 Sample Collection and Preparation 68
2.17.2 RNA Quality Control 68
2.17.3 Library Preparation 68
2.17.4 Clustering and Sequencing 69
2.17.5 Data Analysis 69
2.17.8 GO and KEGG Analysis of Differentially Expressed Genes 70
3.0 eIF4A2 Hypoxic Expression and Regulation in Colorectal Cancer 71
3.1 Introduction 71
3.2Regulation of Gene Expression under Hypoxic Conditions 71
3.3 Transcriptional Co-operation with HIF 72
3.4 RNA Helicase Gene Expression under Hypoxic Conditions 72
3.5 Expression of eIF4A1 and eIF4A2 under Hypoxic Conditions in Colorectal Cancer Cells 75
3.5.1 eIF4A1 and eIF4A2 Hypoxic mRNA Expression 75
3.5.2 eIF4A1 and eIF4A2 Hypoxic Protein Expression 79
3.5.3 eIF4A1 and eIF4A2 Hypoxic Localisation 80
3.5.4 eIF4A2 Expression in Colorectal Cancer Spheroids 82
3.5.6 Regulation of eIF4A1 and eIF4A2 by HIF1α and HIF2α 84
3.5.7 in silico Analysis of eIF4A1 and eIF4A2 Promoter Regions 89
3.5.8 Investigation of eIF4A2 Hypoxic Binding Partners 92
3.5.9 eIF4A2 Expression in Human Colorectal Patient Samples 93
3.6 Discussion 101
3.6.1 Regulation of eIF4A2 at the Transcriptional Level 101
3.6.2 Regulation of eIF4A2 at the Protein Level 103
3.6.3 Investigation of eIF4A2 Hypoxic Binding Partners 106
3.6.4 Concluding Statements 107
4.0 Functional Consequences of eIF4A2 Inhibition 108
4.1 Introduction 108
4.1.1 Inhibition of Components of Protein Synthesis Machinery 108
4.2 Pre-Clinical Inhibitors of eIF4A 108
4.2.3 Silvestrol 109
4.2.4 Hippuristanol 110
4.2.5 Pateamine A 110
..... 111
4.3 Results 113
4.3.1 siRNA inhibition of eIF4A2 and its effects on cell survival 113

4.3.2 Generation of an IPTG inducible sheIF4A2 colorectal cancer cell line 115
4.3.4 qPCR validation of sheIF4A2 cell lines 115
4.3.5 Immunoblot validation of sheIF4A2 cell lines 118
4.3.6 Effect of eIF4A2 Inhibition on Cell Growth 119
4.3.7 sheIF4A2 and its effects on 3D spheroid culture 121
4.3.8 Immunohistochemical analysis of sheIF4A2 knockdown spheroids 124
4.3.9 sheIF4A2 Spheroid Necrosis 125
4.3.10 HCT116 sheIF4A2 xenograft 128
4.3.11 Immunohistochemical Analysis of HCT116 sheIF4A2 Xenografts 136
4.4 Discussion 141
4.4.1 The effect of eIF4A2 inhibition of colorectal cancer cell survival 141
4.4.2 The generation of an inducible sheIF4A2 line and its effects on colorectal spheroid growth 142
4.4.3 eIF4A2 knockdown and its effects on xenograft growth rate 143
4.5 Concluding Remarks 143
5.0 Identification of hypoxic eIF4A2 bound mRNAs in Colorectal Cancer Cells using a RIP-SEQ Approach 144
5.1 Introduction 144
5.1.1 The eIF4A Dependent Translatome 144
5.2 Results 148
5.2.1 eIF4A2 binds to a Distinct Subset of mRNAs Under Hypoxic Conditions 148
5.2.2 Cluster Analysis of Differentially Expressed Genes 149
5.2.3 Screening of Differentially Expressed Genes 151
5.2.4 Co-expression Analysis of Differentially Expressed Genes 152
5.2.5 KEGG Pathway Analysis 152
5.2.6 qPCR validation of RIP-seq 162
5.2.7 Immunoblot Validation of RIP-SEQ Top Targets 168
5.2.8 Functional Validation of RIP-SEQ Targets 172
5.2.9 5'UTR Analysis of eIF4A2 bound hypoxic transcripts 174
5.3 Discussion 178
5.3.1 eIF4A2 Dependent Pathways under Hypoxia: Possible Mechanisms 178
5.3.2 RIP-Seq Methodology Limitations and Future Investigations 184
5.3.3 5'UTR Analysis Limitations and Future Investigations 184
5.3.4 Concluding Statements 186
6.0 Discussion and Future Directions 187
6.1 eIF4A2 Hypoxic Regulation and Expression 187

6.2 Hypoxic eIF4A2 Bound Transcripts 189
6.3 Targeting Endocytosis in Hypoxia 189
6.4 Limitations of Methodology 190
6.5 Final Conclusions 190
7.0 Appendix 192
8.0 Bibliography 196

1.0 Introduction

1.1 Cancer

Cancer is a multistep process involving the accumulation of genetic mutations, gene amplifications, chromosome rearrangements and epigenetic modifications of tumour suppressor genes and tumour oncogenes in somatic cells, and in some cases germ line cells The malignant phenotype is a combination of more than one of the aforementioned mechanisms leading to proto-oncogene activation and tumour suppressor gene loss (Vicente-Duenas et al, 2013). Notable tumour suppressor genes that are commonly silenced in colorectal cancer (CRC) include loss of the adenomatous polyposis coli (*APC*) gene which will be discussed in more detail in the following sections. Conversely, mutations in proto-oncogenes may lead to their activation and concur a growth advantage to the cell as they commonly encode for proteins that regulate proliferation and differentiation. Significant examples of activating point mutations include those within the *ras* family of proto-oncogenes (N-*ras*, K-*ras*, H-*ras*). Mutations in the K-*ras* gene have been shown to be present in 50% of colon carcinomas (Porru et al, 2018).

In addition to *de novo* mutations, inherited predispositions to the disease add to the genetic complexity of malignancies. Well known high penetrance predispositions include mutations in the *APC* gene in CRC (Houlston and Tomlinson, 2000). Mutations in this gene are rare and display Mendelian inheritance. The complexity of mutations that define malignancies has been organised into the recently revisited “Hallmarks of Cancer”, which include the induction of angiogenesis, sustained proliferation and activation of invasion and metastasis among other traits that are required to form a malignancy are extensively reviewed in Hanahan and Weinberg 2011 (Hanahan and Weirnberg, 2011).

1.2 Colorectal Cancer

1.2.1 Biology of the Intestine

The physiological organisation of gastric epithelial cells is along a crypt-villus axis; with a pool of 4-16 colon stem cells located at the bottom of the crypt. Intestinal epithelial cells display a very short half-life as a result of constant exposure to pathogens and have therefore evolved the ability to regenerate rapidly (Peterson and Artis, 2014). These stem cells then migrate along the crypt villus axis and as they do, differentiate into different cell types (Barker et al, 2008). Paneth cells, involved in maintenance of the gut flora, goblet cells, secrete mucus, enterocytes, which make up 80% of the small intestine and possess absorptive functions for nutrients crossing the epithelium and lastly enteroendocrine cells,

which secrete hormones such as serotonin (Umar, 2011). The progenitor cells then undergo apoptosis once they reach the top of the villus and are shed into the intestinal lumen (Barker et al, 2008). The rate of turnover of each crypt occurs every 3-5 days. This process of differentiation is regulated by gradients of proteins including WNT, bone morphogenetic protein (BMP) and (transforming growth factor β (*TGFβ*) (Umar, 2011). The crypt base columnar stem cells (CBCs) express high levels of Lgr5, a Wnt target gene, and through lineage tracing experiments have been shown to give rise to all the cell types residing within the intestinal crypts (Shiokawa and Okamoto, 2017).

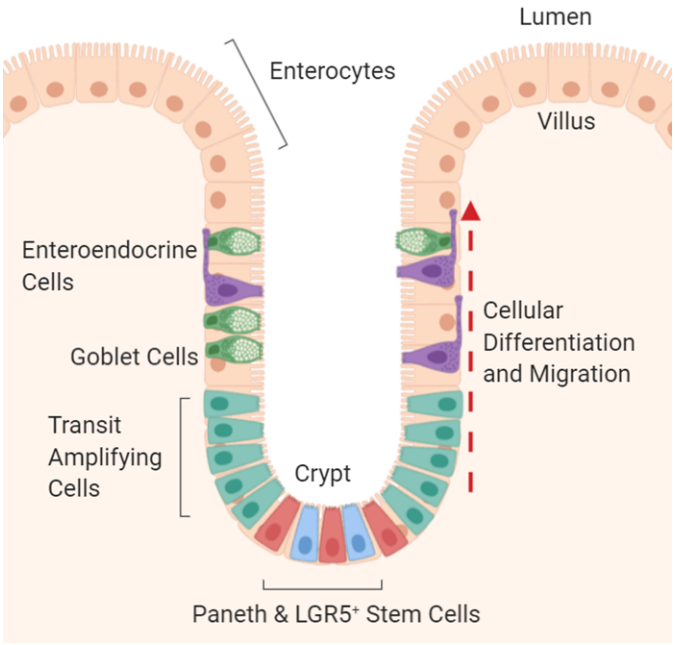


Figure 1.1 Schematic of the small intestinal epithelium displaying the key epithelial cell types. LGR5+ stem cells and paneth cells are located at the base of the intestinal crypts. These cells then migrate up the walls of the crypt and as the do differentiate into all cell types present within the crypt. These include goblet, paneth, transit amplifying cells, enterocytes and enteroendocrine cells. Once these cells reach the top of the crypt, they undergo apoptosis and are shed into the intestinal lumen. This process of differentiation is regulated by gradients of proteins including WNT, BMP and TGF-B (Umar, 2011). Figure adapted from Kuratnik and Giardina, 2013. Illustration created using BioRender.

1.2.2 Development of Colorectal Tumours

Colorectal cancer (CRC) encompasses malignancies of the colon and rectum and begins with the development of an adenocarcinoma, whereby epithelial gastrointestinal cells, typically in the form of a polyp, acquire sequential mutations that concur a selective advantage for self-renewal and proliferation (Leslie et al, 2002). These normal epithelial cells transform into hyper proliferative mucosa resulting in a benign adenoma, which will

eventually give rise to the development of a malignant carcinoma termed the “adenoma-carcinoma sequence” (Day, 1984). Each stage in the process is accompanied by morphological, histological and genetic changes (Fleming et al, 2012).

Sporadic somatic mutations account for around 70% of all CRCs; intrinsic genomic instability allows for the acquisition of new mutations occurs through one or a combination of the following 3 mechanisms; chromosomal instability, microsatellite instability and aberrant CpG island methylation (Armaghany et al, 2012). Chromosomal instability (CIN) is observed in 65-70% of sporadic CRC and refers to the gain or loss of large portions of chromosomes leading to an imbalance in chromosome number and loss of heterozygosity (LOH) (Nguyen and Duong, 2018). Key genes mutated in CRC include *APC*, *BRAF* and *KRAS* which subsequently effects downstream processes such as motility and cell differentiation (Nguyen and Duong, 2018). CpG island methylator phenotype (CIMP) is identified by the hypermethylation of the promoter and therefore silencing of tumour suppressor genes such as *MLH1* and *MGMT (*Mojarad et al, 2013*)*. Microsatellites are mono or dinucleotide repeats found within the human genome, however their repetitive nature predisposes them to increased transcriptional errors during replication (Nojadeh et al, 2018). Microsatellite instability arises from the inactivation of DNA mismatch repair genes resulting in an inability of the cell to repair errors within microsatellite repeats during replication, leading to a change in the size of microsatellites. This poses a problem if the microsatellite is located within a coding region of a gene as it may lead to the formation of an alternative transcript with a subsequent alternative protein isoform (Nojadeh et al, 2018).

Hereditary conditions, which concur an increased risk of CRC development, include familial adenomatous polyposis (FAP) and hereditary non-polyposis colon cancer (HNPCC) accounting for ~10% of CRC cases (Fearnhead et al, 2002). FAP displays an autosomal dominant pattern of inheritance and is characterised by the presence of several hundred or thousand colorectal polyps alongside a germline mutation in the APC gene. In the majority of FAP patients, 95% of APC mutations are frameshift resulting in a truncated protein with abnormal function (Heinimann et al,1998). HNPCC is an autosomal dominant condition associated with an increased risk of colorectal cancer without an abnormal increase in the number colon polyps and is associated with 5-8% of all CRC cases (Vasen et al, 2013). HNPCC is associated with mutations of DNA mismatch repair (MMR) genes, commonly MSH2 and MLH1 (Vasen et al, 2013).

1.2.3 APC and Colorectal Tumour Development

An important genetic mechanism contributing to both sporadic and familial CRC cases include mutations or loss of the APC gene and dysregulation of components of the Wnt/b-catenin signalling pathway (Powell et al, 1992). Around 95% of APC mutations are classified as frameshift or point mutations resulting in a truncated form of the APC protein; with the majority of mutation occurring between codons 1250 and 1514, termed the "mutation cluster region" (Miyoshi et al, 1992). These mutations affect the number of β-catenin binding repeats present in the mature protein hindering its ability to bind to and degrade β-catenin. The APC tumour suppressor protein plays an integral role in the Wnt signalling pathway by regulating the degradation of the transcription factor β-catenin. Loss of APC prevents the formation of the degradation complex allowing for increased nuclear translocation of β-catenin leading to increased expression of Wnt target genes (Aoki and Taketo, 2007). β-catenin is present as cytosolic, nuclear and bound to e-cadherin at adherens junctions. In the absence of Wnt signalling cytosolic β-catenin is rapidly phosphorylated and targeted for proteosomal degradation by the "destruction complex" which consists of AXIN, APC, GSK3 and CK1, maintaining low levels of cytosolic and nuclear β-catenin (Aoki and Taketo, 2007). Wnt ligand binding to frizzled (FZD) receptors and low-density lipoprotein receptor related protein (LRP) co-receptors, activates and recruits Disheveled (DVL) and Axin to the membrane thereby disrupting the formation of the destruction complex (Cadigan and Waterman, 2012). This allows accumulation of β-catenin where is translocates to the nucleus and interacts with the T-cell factor/lymphoid enhancer factor (TCF/LEF) family of transcription factors to trans-activate target genes (Cadigan and Waterman, 2012). Wnt/β-catenin target genes regulate diverse process such as proliferation, differentiation and cell-to-cell adhesion (Mah et al, 2016).

1.3 Colorectal Cancer Incidence and Survival Rates

With an estimated 1.4 million diagnoses and 500,000 deaths in 2012 (Ferlay et al, 2015), CRC is the third most commonly diagnosed and fourth leading causes of cancer death worldwide. CRC burden varies amongst countries; results from the GLOBOCAN database from 2018 demonstrate that incidence and mortality rates of the disease correlate with present human development levels, with rapid increases observed in low and middle income countries (Eastern Europe, Asia, South America) and likely reflect the adoption of a more western lifestyle (Bray et al, 2018). Non modifiable risk factors such as age are strongly associated with an increase in CRC incidence and mortality (Bray et al, 2018).

Current survival statistics for the UK indicate that 59% of people diagnosed with the disease will survive for 5 years or more (Cancer Research UK, 2019). The current mainstay treatment for CRC is surgery combined with neoadjuvant radiotherapy for stage II/III rectal cancer and adjuvant chemotherapy for high-risk stage II/III colon cancer (NICE, 2019). Current NICE guidelines recommend Capecitabine as monotherapy for CRC or Oxaliplatin in combination with 5-flurouracil (5-FU) and Folinic acid (NICE, 2020). Both Capecitabine and 5-FU are classed as antimetabolites, specifically pyrimidine analogues. 5-FU is converted into the active metabolite 5-fluoroxyuridine monophosphate (F-UMP), replacing uracil and so is incorporated into RNA, inhibiting RNA processing and therefore cell growth (Longley et al, 2003). More recently introduced adjuvant agents for CRC treatment include the anti-vascular endothelial growth factor (VEGF) humanized monoclonal antibody Bevacizumab and the anti-EGFR monoclonal antibody Cetuximab (Kazazi-Hyseni et al, 2010) (Lenz et al, 2007).

1.4 Tumour Hypoxia

Oxygen homeostasis in eukaryotes is essential in order to maintain aerobic metabolism and to maintain intracellular bioenergetics. Physiological oxygen concentrations (physoxia) vary between organs/cells and is an important factor to consider when studying oxygen concentrations across tumour types. In organs such as the liver and kidneys, oxygen levels range from 5-10% O_2, the brain 2-6% O_2, the kidney 7-12% O_2 and the intestine 3.5-6% O_2 (Brooks et al, 2007)(Carreau et al, 2011). Organs such as the lungs display a gradient distribution in oxygen concentrations (Jagnnathan et al, 2016). Cellular 0_2 concentration is generally defined as normoxia (~20% 0_2), physoxia (~1-13% O_2), hypoxia (~0.1-1% 0_2) and anoxia being the lack of oxygen (Soni and Padwad 2017)(McKeown, 2014).

Hypoxia (<1% 0_2/pO_2<9mmHg) is a common feature of the microenvironment within solid tumours. Physiological oxygen concentrations of the colon epithelium stand at 6.8% O_2 whilst colorectal tumour oxygen concentration stands at 1.3% O_2 (McKeown, 2014). Interestingly, previous studies have demonstrated accumulation of Pimonidazole staining localised to the lumen suggesting the colonic epithelium experiences physiological levels of hypoxia (Zheng et al, 2015). Due to the high proliferative and metabolic rates observed in malignant cells, tumours rapidly outgrow their oxygen supply. In order for tumours to grow beyond 1mm in diameter, the tumours must establish their own vasculature (Vaupel, 2004). These newly formed blood vessels exhibit a chaotic architecture with poor blood flow and fail to meet the oxygen demands of the growing tumour, further increasing the levels of hypoxia within the tumour (Harris et al, 2015). Furthermore newly formed blood

vessels often display an increase in permeability due to defects in basement membrane architecture and endothelial cell lining (Vaupel, 2004). Tumour cells experience dynamic changes in oxygen concentrations with both acute transient bouts of hypoxia and reoxygenation from poorly formed and leaky blood vessels and changes in perfusion and blood flow over time (Michiels, 2004).

The transcriptional response to hypoxia is orchestrated by the hypoxia inducible factors (HIFs) and includes the upregulation of more than 100 hypoxia response genes such as VEGFA, glucose transporter protein 1 (*GLUT1*), and carbonic anhydrase 9 (*CA9*), which contribute to a more malignant phenotype (Dengler et al, 2015). Genes that are transcriptionally activated by hypoxia are reviewed elsewhere by Semenza (Semenza, 2003). This response includes adaptive changes in metabolism, pH regulation, angiogenesis, invasion, metastasis, evasion of apoptosis and many hallmarks of cancer. Clinically, hypoxia is associated with resistance to chemotherapy and radiotherapy and increased metastasis and is therefore associated with poor patient prognosis as reviewed in (Horsman and Overgaard, 2016) (Young-Kim and Yong Lee, 2017).

1.5 HIF Transcription Factors

HIF is a heterodimeric transcription factor composed of two basic helix-loop-helix proteins (bHLH) belonging to the PAS family (Wang et al, 1995). HIF consists of two sub units: an oxygen sensitive HIF1α (analogues HIF2α and HIF3α) and a constitutively expressed HIFβ sub unit (also known as ARNT, aryl nuclear translocator) (Ziello et al, 2007). The two transactivation domains of HIF1α, the NH2 terminal (N-TAD) and the COOH terminal (C-TAD), are responsible for its transcriptional activity (Ziello et al, 2007). The C-TAD of HIF1α allows it to interact with the co activating transcription factor, CREB binding protein (CBP/p300) to modulate the transcription of target genes (Masoud and Li, 2015). All isoforms also possess a Per-ARNT-Sim (PAS) domain responsible for the heterodimerization (Masoud and Li, 2015). Additional transcription factors co-operate with HIF1α in order to fine-tune the transcriptional response, these include AP1, E2F and MIF *(*Villar et al, 2012*).* The oxygen dependent degradation domain (ODDD) overlapping the NTAD is crucial in mediating oxygen regulation stability that is absent in the HIFβ sub unit (Ziello et al, 2007). HIF1α and its analogue HIF2α shared 50% homology at the amino acid level (Ratcliffe, 2007). The most recently discovered HIF3 analogue, which lacks the C-TAD shared by HIF1α and HIF2α, and negatively effects gene expression by competing with HIF1α and HIF2α to down regulate the expression of angiogenic genes (Hara et al, 2001)(Kobayashi et al, 2015).

Six splice variant isoforms of HIF3α exist, with the most studied, HIF3A4 acting as a negative regulator of HIF1α (Dengler et al, 2014).

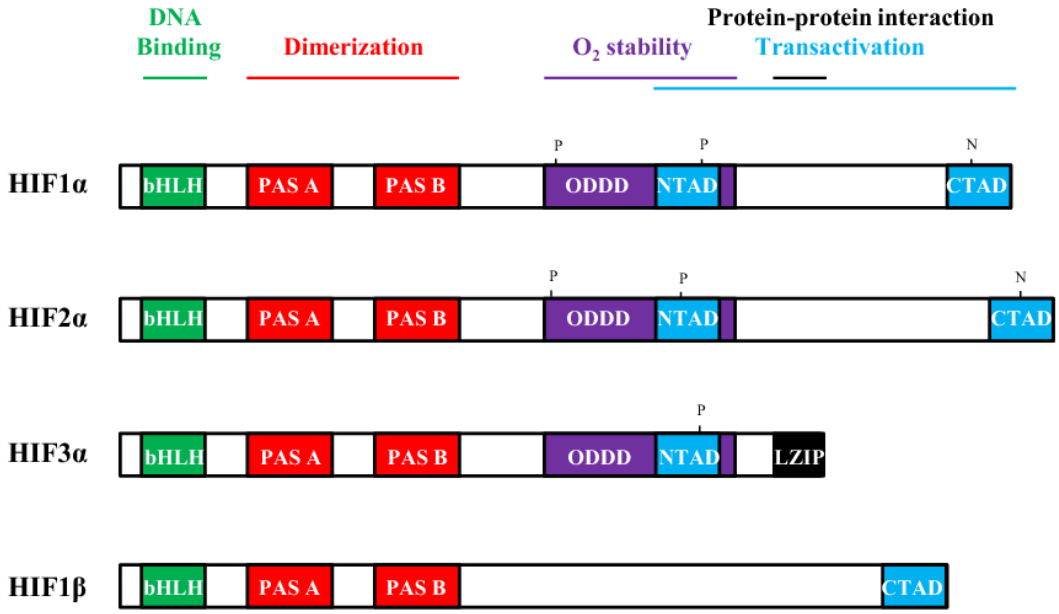


Figure 1.2 Functional domains of the HIF isoforms. All isoforms possess a bHLH domain responsible for DNA binding as highlighted in green, a PAS domain highlighted in red responsible for dimerization, the ODD domain (purple) which overlaps with the NTAD domain (blue) are responsible for mediating oxygen regulation stability and is absent in the HIF1β isoform. The NTAD domain (blue also) is responsible for their transcriptional activities. Figure taken from Ravenna et al 2015.

Despite these similarities, HIF1α and HIF2α also regulate distinct target genes unique to each analogue; genes specific to HIF1α include *CA9*, BCL2 interacting protein 3 (*BNIP3*) and lactate dehydrogenase (*LDHA*) glycolytic genes. Genes specifically under the control of HIF2α include cyclin D1, octamer binding transcription factor 4 (Oct-4) and TGFα (Dengler et al, 2014). Shared target genes include VEGF and GLUT1, however these are cell/tissue type dependent relationships *(*Sena et al, 2015*)* Furthermore HIF1α and HIF2α display differential expression across tissue and cell types with HIF1α appearing to be expressed in almost cell types, whereas HIF2α expression is limited to renal, endothelial, hepatic and lung cell types (Keith, Johnson and Simon, 2011). Indeed previous research has demonstrated divergent roles of HIF1α and HIF2α in colorectal cancer; HIF1α deficient colorectal cancer cells displayed decreased rates of proliferation, in contrast HIF2α deficient cells exhibited enhanced anchorage independent growth in soft agar assays, stimulated tumour growth and high HIF2α expression was correlated with advanced tumour stage (Imamura et al, 2009). HIF1α and HIF2α are over expressed in the vast

majority of human cancers, with these cancers displaying a more aggressive phenotype and poor patient prognosis (Imamura et al, 2009).

Under normoxic conditions 2 proline residues, P402 and P546, located in the ODDD of HIF1a are hydroxylated by prolyl4hydroxylases 1-4 (PHDs) (Choudry and Harris, 2017). PHD enzymes are dioxygenases that are 2-oxoglutarate dependent and oxygen dependent. Iron (Fe_{2+}) and ascorbate are required as cofactors in this reaction (Choudry and Harris, 2017). This leads to the rapid degradation of the HIF1α/HIF2α subunit by the proteasome by tethering to the beta domain of the von Hippel-Lindau protein (pVHL) (as part of an E3 ubiquitin ligase complex) (Choudry and Harris, 2017).

Under hypoxic conditions the enzymatic activity of PHDs are inhibited, HIF1α ODD is not hydroxylated, and thus stabilized. HIF1α translocates to the nucleus where it dimerises with HIF1β and associates with its cofactors CBP/p300 (Majmundar et al, 2010). This HIF heterodimer then binds to the hypoxic response element (HRE) in the promoter of hypoxia response genes. Hypoxic response elements contain the core recognition sequence 5'RCGTF3' where R denotes a purine residue (A/G) (Majmundar et al, 2010). Negative regulation of HIF1α protein levels are achieved via interaction with p53 directly or indirectly via MDM2 (Bardos and Ashcroft, 2005).

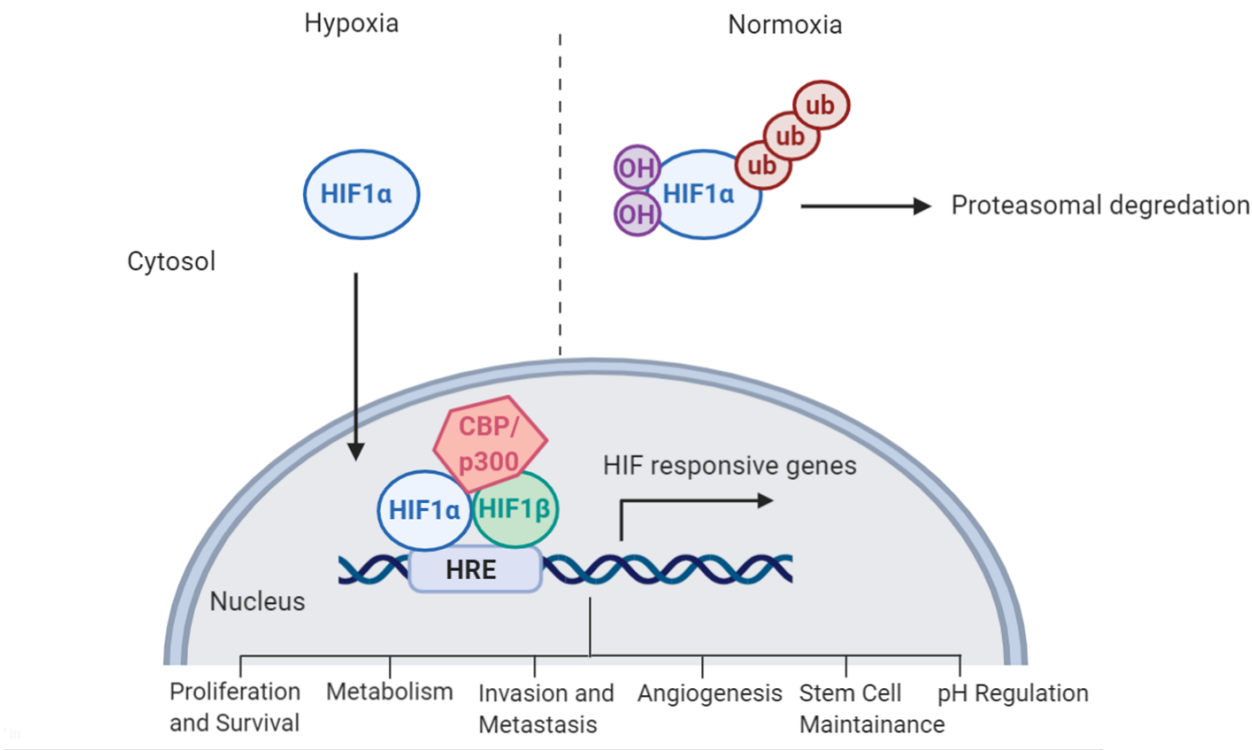


Figure 1.3. HIF1α regulation under normoxic and hypoxic conditions. Under normoxic conditions HIF1α is hydroxylated by oxygen dependent PHDs leading to rapid degradation via ubiquitin-proteasome degradation. Under hypoxic conditions the enzymatic activity of PHDs are inhibited, HIF1α is not stabilised and can translocated to nucleus where it where it dimerises with HIF1β and associates with its cofactors CBP/p300 and binds to the HRE within the promoter regions of target genes. This activates the transcription of genes involved in cellular processes including proliferation and survival, metabolism, invasion and metastasis, angiogenesis, stem cell maintenance and pH regulation. Figure adapted from Favaro, 2013. Illustration created with BioRender.

Oxygen independent stabilisation of HIF1α under normoxic conditions occurs notably via growth factor binding to cognate receptors and activating the downstream Phosphoinositide 3-kinase (PI3K) and mitogen-activate protein kinase (MAPK) signalling pathways and the subsequent activation of mammalian target of rapamycin (mTOR) and protein kinase B (AKT) (Iommarini et al, 2017). Once activated mTOR phosphorylates the 4E-BP family of proteins (4E-BP1) which act as negative regulator of the cap binding protein, eukaryotic initiation factor 4E (eIF4E) (Showkat et al, 2014). The phosphorylated form of 4E-BP1 prevents it from sequestering eIF4E, allowing it to form part of the eIF4F complex required for cap dependent translation (Showkat et al, 2014). This then results in enhanced translation of the HIF1α protein. mTOR additionally phosphorylates ribosomal S6 kinase, in turn stimulating translation (Magnuson et al, 2012). Furthermore activation of the RAS/RAF/MEK/ERK signalling cascade via activation of RAS by certain growth factors

leads to the phosphorylation of MAP kinase interacting kinase (MNK) (Shveygert et al, 2010). MNK has the ability to directly phosphorylate eIF4E resulting in an increase in global mRNA translation in turn leading to increased translation of the HIF1α protein (Shveygert et al, 2010).

1.5.1 Hypoxia and Treatment Resistance

Clinically, hypoxia is associated with resistance to chemotherapy and radiotherapy and is therefore associated with poor patient prognosis as reviewed in (Horsman and Overgaard, 2016) (Young-Kim and Yong Lee, 2017). Gray and colleagues were the first to demonstrate that the effects of ionizing radiation were significantly inhibited in the absence of oxygen (Gray et al, 1953). Oxygen has a high affinity for the free radicals generated during ionizing radiation. Oxygen binds covalently to the radical forming a peroxy radical, this "fixes" the damage subsequently leading to DNA strand breaks (Brown, 2007). Under hypoxic conditions, cellular thiols can donate a hydrogen atom to the radical and restore it to its undamaged form (Brown, 2007). Hypoxia acts to increase the radiation survival curve, that is hypoxic cells require a higher amount of ionizing radiation to achieve the same cell survival as normoxic cells (Brown, 2007).

Resistance mechanisms to chemotherapeutic are complex and diverse and can be broadly classed into 3 groups: 1) intrinsic tumour cell factors such as expression of drug efflux pumps 2) pharmacokinetic properties of the drug 3) extrinsic cell conditions within the tumour microenvironment such as hypoxia, acidosis, vasculature and interstitial pressure (Liao et al, 2014). One key mechanism hypoxia promotes drug resistance is through the upregulation of transcripts encoding drug efflux pumps one example being the multidrug resistance 1 (*MDR1*) gene (Comerford et al, 2002). Hypoxic upregulation of MDR1 has been observed in a variety of malignancies including colon and gastric (Chen et al, 2014) (Comerford et al, 2002). *MDR1* encodes a membrane bound P-glycoprotein (P-gp) that belongs to the class of ABC transporters and is capable of transporting a wide range of chemotherapeutic agents; previous research has revealed the presence of a HRE within the promoter MDR1 transcript conferring HIF1α dependence (Comerford et al, 2002). The same study demonstrated a 7.1 fold increase in MDR1 mRNA expression alongside enhanced efflux in both transformed and non-transformed cells following exposure to 18 hours hypoxia demonstrating functional significance of increased MDR1 transcript and protein levels (Comerford et al, 2002). A second mechanism contributing to hypoxic drug resistance involves alterations in cell cycle and proliferation. Many pro-apoptotic (BNIP3, NOXA) and anti-apoptotic proteins (Bcl-2, Bcl-xL, Bid, p53, survivin) are under control of

HIF1a and in the majority of cells HIF1α acts as a suppressor of apoptosis (Flament et al, 2010). Additional notable hypoxic adaptations associated with drug resistance include metabolic reprogramming, reduction in DNA damage repair and induction of autophagy which are reviewed in extensive detail elsewhere (Rohwer and Cramer, 2011). Furthermore hypoxia acts as a driving force to promote clonal selection of tumour cells that are deficient p53 to apoptosis resistance and genomic instability (Luoto et al 2013).

1.5.2 Targeting HIF Transcription Factors

Targeting HIF transcription factors directly has proved challenging, partly due to the requirements of targeting protein-protein interactions without affecting other pathways. Inhibition is usually achieved by modulating mRNA expression, protein level (translation or degradation), HIF1α/HIF1β dimerization, HIF1α DNA binding to the HRE or altering HIF1α transcriptional activity (Choudry et al, 2018). FDA approved therapies that inhibit HIF activity include Topotecan and Trastuzumab (Beppu et al, 2005) (Soni and Padwad, 2016). Recently developed HIF1α inhibitors currently in clinical trials include the HIF1α mRNA antagonist (RO7070179), currently in Phase Ib proof of mechanism trial in patients with hepatocellular carcinoma (NCT02564614) (Clinical Trails, 2019). EZN-2968, a HIF1α antisense oligonucleotide has been shown to inhibit HIF1α mRNA and protein levels and the expression of HIF1α target genes *in vivo* in both prostate and glioblastoma cell lines under normoxic and hypoxic conditions alongside inhibition of tumour cell growth (Greenberger et al, 2008). Furthermore EZN-2968 lead to a reduction in tumour growth in DU145 xenograft models (Greenberger et al, 2008). EZN-2968 has shown good tolerability profiles in Phase I clinical trials in patient with advanced solid tumours (NCT01120288) (Clinical Trails, 2019).

In contrast, promising results have been obtained targeting HIF2α in clear cell renal cell carcinoma (ccRCC) cell lines, pVHL defective xenografts and most recently clinical trials (Yu et al, 2017). PT2385 a selective small molecule HIF2α inhibitor, directly binds to the PAS B domain and allosterically blocks the heterodimerization of HIF2α with ARNT/HIF1β while having no effect on HIF1α (Xie et al, 2018). An additional compound PT2977, is an orally administered HIF2α inhibitor with improved potency compared to PT2385. Patients with advanced solid tumours were treated once daily in a dose-escalation trial (20-160mg) and showed no treatment related dose limiting toxicities (Papadopolous et al, 2018).

1.5.3 Hypoxia Activated Pro Drugs (HAPs)

Despite the challenges faced in directly targeting HIF transcription factors, advances have been made specifically targeting hypoxic tumour cells, with the development of

bioreductive pro drugs such as hypoxia activated pro-drugs (HAPS) (Liang et al, 2015). As a general mechanism, HAPs are inactive in normoxic cells and undergo selective reduction via endogenous oxidoreductases under hypoxic conditions releasing the active antineoplastic drug (Liang et al, 2015). HAPs can be divided into 2 classes based on the hypoxic threshold required for activation; Class I HAP such as benzotriazinine and N-oxides require mild hypoxia for activation, Class II HAPs such Evofosfamide require severe hypoxia for their activation (Spiegelberg et al, 2019). Despite demonstrating early success in phase 2 clinical trials for the treatment of pancreatic cancer in combination with gemcitabine, Evofosafamide (TH-302) has recently been shown to be ineffective in increasing overall survival of advanced pancreatic cancer in a large phase 3 clinical trial study (NCT01746979) (Spiegelberg et al, 2019). One limitation preventing HAPs from fulfilling their potential is the failure to identify and stratify patients based on their tumour hypoxia who may benefit from HAP treatment. Tarloxotinib (TH-4000), a molecular targeted HAP inhibiting pan-HER has shown promise in EGFR mutant NSCLC xenografts (Patterson et al, 2015). Unfortunately in two recent phase 2 clinical trials in HNSCC (NCT0245842) and NSCLC (NCT02449681), despite the use of HX4 PET imaging to assess baseline hypoxia for a more targeted approach, the trial was terminated as patients failed to reach the primary endpoint (Mistry et al, 2017). The development, synthesis and evaluation of HAPs is extensively reviewed in (Hunter, Wouters, Wilson, 2016).

1.5.4 Methods of Detecting Hypoxia

Accurate measurements of tumour hypoxia are crucial in order to correctly stratify patients in order to receive the appropriate treatment. A large number of clinical trials utilizing hypoxia activated pro-drugs have failed, or failed to provide the promised response as seen in *in vitro* studies (Spiegelberg et al, 2019). These disappointing results have been attributed to poor or lack of patient stratification and so patients who not possess hypoxic tumours ultimately receive hypoxia targeted treatment which fail to elicit a positive response (McKenna et al, 2018). Furthermore, development of individualised treatment for each patient will require regular and reliable assessment of the changing tumour landscape using a variety of biomarkers.

Historically measurements of tumour hypoxia involved the use of invasive pO_2 electrodes (Aguilera and Brekken, 2014*)*. More modern and non-invasive techniques now include immunohistochemical analysis of exogenously administered drugs such as Pimonidazole, a 2-nitroimidazole that forms adducts with thiol groups in proteins within hypoxic cells both *in vitro* and *in vivo* (Aguilera and Brekken, 2014). Additional proteins upregulated by

hypoxia may also be stained for by immunohistochemical analysis such as CAIX, GLUT-1 and LDHA (Hammond et al, 2014). Non-invasive oxygen enhanced imaging techniques have also been developed such as Blood oxygenation level dependent (BOLD) MRI which is able to detect differences in tumour blood oxygenation based on the paramagnetic properties of oxygenated and deoxygenated haemoglobin (O'Connor et al, 2019). However this technique is largely dependent on blood flow, is influenced by vascular volume, pH, vessel density and local haematocrit; furthermore it cannot be directly interpreted as oxygen concentration (Hallac, Zhou and Mason, 2014*)*. Alternative imaging modalities include positron emission tomography (PET) which displays a higher specificity for hypoxic tissues and offers a range of radiotracers to allow for 3D tumour representation (Price, Robinson, Koh, 2013). Commonly used radiotracers include ^{18}F-fluromisonidazole (^{18}F-FMISO), a nitroimidazole derivative and the second generation 2-nitroimidazole compound ^{18}F-Fluroazomycin arabinoside (^{18}F-FAZA) (Xu et al, 2017).

1.6 Overview of Eukaryotic Cap Dependent Translation

1.6.1 Protein Synthesis

Protein synthesis is a tightly regulated, energetically demanding and highly conserved process across all living cells both prokaryotes and eukaryotes. Regulation of translation is of particular importance in response to physiological stress to the cell as adaptation in mRNA translation efficiencies from the existing pool of mRNAs provide a much more rapid response than changes in transcriptional regulation (Hershey et al, 2012). The majority of cellular capped mRNAs are translated via the canonical cap dependent pathway which consists of three distinct phases; initiation, termination and elongation; with the majority of regulation exerted at the initiation phase hence why it is often referred to as the rate limiting step of translation (Hershey et al, 2012). The process of translation in eukaryotes is the most energy consuming process in the cell and has evolved to include a large number of initiation factors (eIFs), regulatory translation factors, and long and complex 5' and 3'untranslated regions (UTRs) which play a role in regulating the translation efficiency and fate of mRNAs (Hinnebusch et al, 2016). Over twenty eIFs are involved in the regulation of translation initiation and include the following: 1,1a,2,2a,2B,2-y,2A,2D,3 (and associated sub units a-m), 4A1, 4A2, 4E,4G, 4B, 4H,5,5A,5B,6. Each eIF and their specific functions are extensively reviewed in (Sharma, Bressler, Patel et al, 2016).

Furthermore, mRNAs do not exists as naked strands, they are associated with and interact with RNA binding protein (RBPs) and non-coding RNAs (miRNA, PIWI interacting RNAs and large non coding RNA) which together form complex structures known as messenger

ribonucleoprotein particles (mRNPs) (Hentze et al, 2018). RBPs are collectively referred to a *trans*-acting factors. mRNPs are responsible for the regulation of mRNA life cycle including nuclear export, localisation within the cell, translation and eventual decay and may undergo remodelling at each stage of the mRNA life cycle (Hentze et al, 2018). A single RBP can contain multiple RNA binding domains and exist on a scale of selectivity (Dominguez et al, 2018). For example, Pumilio domain containing proteins display high specificity, binding only to the RNA consensus sequence, the Pumilio Response Element (PRE) (5'UGUANAUA-3') within the 3'UTR of mRNA targets (Bohn et al, 2018). Factors that influence the dynamic composition of mRNPs include the local context of the binding site, which is the primary sequence and structure of the mRNA which will determine the affinity for any RBP or miRNA (Mitchell and Parker, 2014). The local context also includes the PABP and the 5' 7-methylguanosine (m^7G) cap of the mRNA strand. The cellular concentration of the binding factor and the presence of competing binding sites is an additional factor that can influence mRNP formation (Mitchell and Parker, 2014). This principle has been proven in the context of miRNA binding whereby ncRNA "decoys" can compete with miRNAs for binding, thereby reducing the number of miRNAS bound to the 3'UTR of a target leading to increase in the expression of such transcripts (Mitchell and Parker, 2014). mRNPs can assemble into larger and more complex structures such as P bodies and stress granules which contain mRNAs that are stalled and not engaged in active translation and are often induced during periods of physiological stress to the cell in order to conserve energy (Decker and Parker, 2012).

1.6.2 Translation Initiation

The process of initiation begins with the recruitment of pre-assembled 43SPIC which consists of; the 40S ribosomal sub unit, the ternary complex (eIF2-GTP-$tRNA_i^{Met}$), eIFs (1, 1a, 2, 3, 5) to the 5' 7-methylguanosine (m^7G) cap of the mRNA strand (Pestova et al, 2001). All eukaryotic mRNAs possess a 5'm^7G cap, an evolutionary conserved modification that orchestrates cap related functions such as nuclear export, cap dependent translation, recruitment of initiation factor and pre-mRNA processing. It also serves to protect the mRNA from 5' to 3' exonuclease cleavage (Ramanathan et al, 2016). The ribosomal sub unit itself has no real affinity for the 5'cap and so must be aided through the eIFs (Ramanathan et al, 2016). Binding of the 43SPIC is aided by the heterotrimeric eIF4F complex which consists of 3 sub units: 1) eIF4E, a cap binding protein 2) eIF4G, a large scaffold protein with interactions with eIF3 and eIF4A 3) eIF4A, an ATP dependent RNA helicase required to unwind secondary structures present in the 5'UTR to enable scanning that would otherwise impede translation (Pestova et al, 2001). The eIF4F complex is able to recruit the small

ribosomal subunit via eIF4G affinity to eIF1 and eIF5 (Yamamoto et al, 2005). Circularization of the mRNA strand is achieved via the binding eIF4G to the poly (A) binding protein (PABP) (Kahvejian et al, 2005). This circularization of the mRNA strand is thought to promote the recruitment of free ribosomal small subunits (SSUs) from the cytosol and may additionally be involved in recycling of SSUs from termination to initiation within a polysome (Kahvejian et al, 2005). Following recruitment of the 43SPIC and the eIF4F complex to the cap, the PIC scans in a 5' to 3' direction in an ATP dependent reaction referred to as "ribosomal scanning" facilitated by eIF4A, who's activity is facilitated by eIF4B and eIF4H (Hinnebusch, 2011). The PIC scans each base pair for the anti-codon of the Met-tRNAi, once the start codon has been reached (typically AUG), this triggers eIF1 dissociation from the 40S subunit and irreversible hydrolysis of eIF2-GTP and subsequent release of eIF2 and GDP (Hinnebusch, 2011). Additionally eIF5B-GDP and eIF1a are released from the PIC followed by 60S large sub unit joining and formation of the final 80S initiation complex (Hinnebusch, 2011).

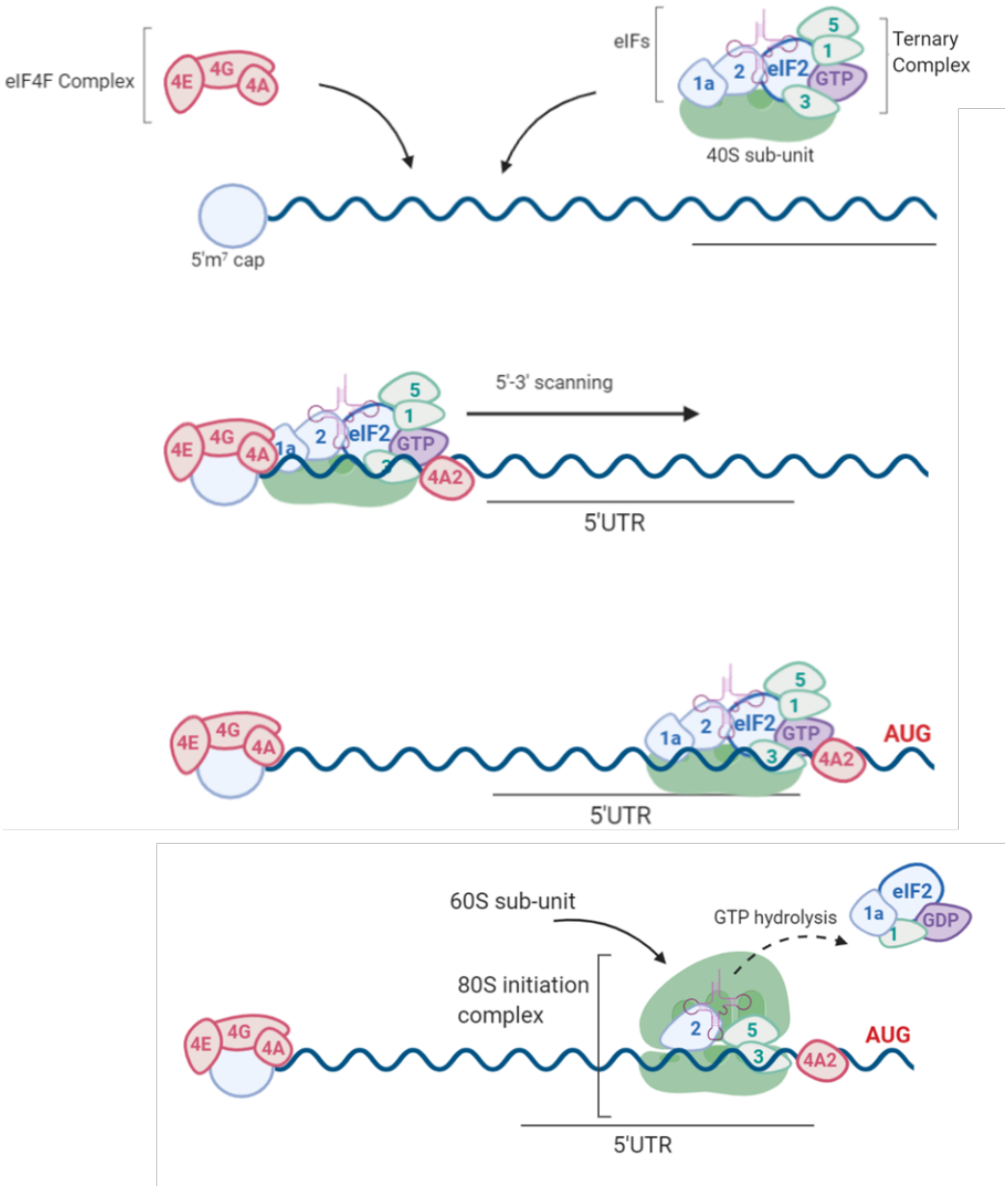


Figure 1.4. Schematic overview of translation initiation. Initiation begins with the recruitment of pre-assembled 43SPIC which consists of; the 40S ribosomal sub unit, the ternary complex (eIF2-GTP-$tRNA_i^{Met}$), eIFs (1, 1a, 2, 3, 5) to the 5'm^7G cap. This is aided by the heterotrimeric eIF4F complex (eIF4A, eIF4E, eIF4G). eIF4A is required to unwind secondary structures present in the 5'UTR to enable scanning that would otherwise impede translation. The PIC scans in a 5' to 3' direction until it reaches the start codon (AUG). This causes GTP hydrolysis and dissociation of eIF1a, 1, eIF2 and GDP followed by recruitment of the 60S sub unit and formation of the final 80S initiation complex. Illustration created using BioRender.

Fully assembled ribosomes can be divided into two distinct categories with regards to their translational status and therefore their location within the cytoplasm; polysomes and monosomes (Heyer and Moore, 2016). Polysomes consist of an mRNA strand occupied by two or more ribosomes, with radioactive amino acid incorporation studies indicating demonstrating that the majority of peptide binds are formed on polysomes, indicating active translation (Noll, 2008). Monosomes consist of a mixture of mRNAs bound by an individual ribosome along with large and small ribosomal subunits that associated in the absence of mRNA (Noll, 2008). Monosomes are thought to be newly assembled subunits around the start codon and are therefore considered to be translationally inactive (Pringle et al, 2019). The location of individual transcripts can be identified within a polysome or a monosomes to determine if they are being actively translated via polysome profiling or ribosome footprinting, these methods will be described in more detail later on in this thesis (Pringle et al, 2019).

The untranslated regions of transcripts contain a variety of regulatory elements and play a crucial role in the regulation of gene expression and exert the majority of their effects at the translation initiation level (Barrett et al, 2012). In order for a transcript to be efficiently translated, the ribosome must be able to access the AUG start codon; in order to do so, the 5'UTR and associated secondary structures must be unwound by eIF4A to allow the ribosome to start scanning (Barrett et al, 2012). RNA secondary structured is the collection of base pairs that form in 3D; the hydrogen bonds formed between the base pairs are responsible for the thermodynamic stability of an RNA (Zhang et al, 2019). The canonical base pairing are Watson-Crick pairing (C.G, G.C, A.U and U.A), however there are additional non canonical ways in which bases can pair, allowing RNA duplexes to form a variety of secondary structures such as stem loops, hairpin loops and pseudoknots (Zhang et al, 2019). Recent studies using eIF3 PAR-CLIP and SHAPE have identified a stem loop present in the 5'UTR of transcripts recognised by eIF3 and targeting mRNAs for translational activation or repression (Lee et al, 2015). This subset of mRNAs recruited by eIF3 are enriched for transcripts involved in apoptosis, cell cycle and cell differentiation (Lee et al, 2015). The amount of free energy (ΔG) required to unwind a secondary structure can be predicted using algorithms that take into account the most likely combination of base pairing such the Vienna RNA package (Mathews and Turner, 2006). eIF4A is sensitive to sequence motifs and secondary structures; highly structured 5'UTRs are inhibitory to translation and are therefore more dependent on eIF4A to be unwound (Wolfe et al, 2014). UTRs with a high GC content alone have been shown to lead to a reduction on translation

efficiency. Indeed the requirement of eIF4A is directly proportional to the degree of 5'UTR secondary structure (Svitkin et al, 2001).

Furthermore, many oncogenes have been shown to possess long and GC rich 5'UTRs that contain secondary structures known as G-quadruplexes (Kumari et al, 2007). RNA G-quadruplexes are formed when non-Watson-Crick interactions form between 4 guanine nucleotides that lead to a square planar arrangement known as G-quartet (Kumari et al, 2007). These square planer structures of G-rich regions can then stack upon one another on different parallel planes linked by one nucleotide (A or C) (Kumari et al, 2007). Originally identified in DNA, they have been found to be enriched in gene promoters, telomeres and 5'UTRs (Fay et al, 2017). The NRAS and VEGF 5'UTR has been found to contain an RNA-quadruplex *in vitro*, however this still needs to be confirmed *in vivo* (Kumari et al, 2007). RNA quadruplexes are thermodynamically stable and so depend more so on eIF4A for their translation. Indeed, Wolfe et al demonstrated that RNA quadruplexes cases eIF4A dependent oncogene translation in cancer for transcript including MYC, MYC, NOTCH1 and CDK6 (Wolfe et al, 2014). An additional cis-acting regulatory element found within 5'UTRs are 5'TOP sequences; these are poorly translated under normal conditions, however their translation is activated downstream of mTOR signalling following growth factor stimulation and control the translation of transcripts regulating proliferation, metabolism and metastasis (Meyuhas and Kahan, 2015).

1.6.3 Elongation

Elongation refers to the migration of the ribosome along the mRNA stand and formation of the polypeptide chain following recognition of each codon (Merrick, 2004). Ribosomes possess 4 binding sites, one for the mRNA strand and the remaining 3 for transfer RNA (tRNA) and are termed P (peptidyl site), A (acceptor/aminoacyl site) and E (exit site) (Merrick, 2004). The P site binds to the tRNA holding the polypeptide chain of amino acids, the A site binds to the aminoacyl tRNA which holds the new amino acids to be added to the growing polypeptide chain, and finally the E site serves as an exit point for the completed polypeptide chain (Merrick, 2004). Elongation is regulated by a group of RNA binding proteins known as eukaryotic elongation factors (eEFs) (Sasikumar et al, 2013). Following recognition of the start codon, the 80S ribosome is positioned with the anti-codon of Met-tRNAi in the P site, base paired with the start codon (Dever and Green, 2012). In the A site sits the second codon of the ORF which is followed by subsequent binding of the cognate aminoacyl-tRNA. eEF1A binds aminoacyl-tRNA in a GTP dependent manner delivering it to the A site of the ribosome triggering GTP hydrolysis by eEF1A, releasing the factor and

allowing the aminoacyl tRNA to be accepted into the A site. eEF1A:GDP is recycled to eEF1A by eEF1B, an exchange factor (Dever and Green, 2012).

1.6.4 Termination

Termination occurs following entry of the stop codon (UAA/UAG/UGA) into the A site of the ribosome (Korostelev, 2011). Termination is catalysed by another distinct group of eukaryotic translation factors known as eukaryotic translation termination or release factors (eRF1, eRF3) eRF1 is responsible for stop codon recognition and peptidyl-tRNA hydrolysis, eRF3 acts as a GTPase, accelerating peptide release and increasing efficiency of termination at the stop codon (Hellen, 2018). Following recognition of the stop codon, the eRF1:eRF3:GTP complex binds to the A site of the ribosome, hydrolysis of GTP occurs and eRF3 is released (Korostelev, 2011). The ribosomal subunits are still closely bound to eRF1, the mRNA strand and the P-site deacylated tRNA which is now termed the post termination complex, and must now be dissociated to allow subsequent rounds of translation to occur. However, it is important to note that full dissociation of the ribosomal sub units is sometimes not achieved, allowing for "re-initiation" to take place (Hirokawa et al, 2002). Translation re-initiation is a process by which ribosomes translate multiple ORFs present within a single transcript, without fully undergoing complete recycling between the ORFs (Rogers et al, 2017).

1.7 Non-canonical Cap Dependent Translation

Alternative non canonical yet still cap-dependent modes of translation also exist, these include; leaky scanning, translation re-initiation, ribosome shunting and eIF4E independent cap recognition (Kwan and Thompson, 2018). Leaky scanning occurs when there are several AUG start codons present on a transcript whereby the first AUG codon is a weaker initiation codon triplet causing the ribosome to skip past it and continue scanning for the next initiator codon (Hinnebusch, 2011). If both the AUG codons are in frame with each other, this results in the translation of two isoforms of the same protein, one with the addition of an N-terminal extension. Alternatively, if the 2 AUG codons are part of two overlapping ORFs but with different reading frames, this will lead to the expression of two different proteins from the same mRNA strand (Hinnebusch, 2011).. An upstream open reading frame (uORF) is an initiator codon that is out of frame with the main ORF and found upstream within the 5'UTR (Barbosa et al, 2013). This causes the ribosome to initiate translation upstream, terminate translation following identification of a stop codon at the end of the uORF and then re-initiate translation further downstream once it reaches the main ORF (Barbosa et al, 2013). First discovered in plant pararetrovirsuses, and still

poorly understood, ribosome shunting involves recruitment of the ribosome to the 5'cap where it begins to scan, however it is able to physically bypass or "shunt over" secondary structures such as 5'hairpin loops in order to reach the initiator codon (Pooggin et al, 2012).

1.8 Cap Independent Translation

Internal ribosome entry sites (IRES), are *cis*-regulatory mRNA elements that allow mRNAs to bypass the canonical cap dependent translation machinery and directly recruit the 40S sub unit to an internal section of the mRNA (Komar and Hatzoglou, 2011). Typically this occurs during times when cap dependent translation is compromised, such as ER stress, hypoxia, and amino acid depletion (Spriggs et al, 2008). It is currently estimated that around 10% of cellular mRNAs contain IRES elements. IRES *trans*-acting factors (ITAFs) have been identified as a class of proteins which bind cellular IRESs and help to recruit the ribosome (Spriggs et al, 2008). It is interesting to note that a large portion of mRNAs containing IRES elements are involved in the regulation of cell growth, apoptosis and the stress response (Komar and Hatzoglou, 2011). However there is no a clear cut divide between mRNAs which are cap dependent and those which are IRES driven. A key example being neurogranin, a calmodulin binding protein present in neuronal cells; which is translated by both cap dependent and IRES translation (Pinkstaff et al, 2001). A number of studies have now demonstrated a requirement for eIF4A in the remodelling of a number of IRES structures to allow the ribosome to bind; these include the c-myc and N-myc IRES (Spriggs et al, 2009).

1.9 Translation Initiation in Malignant Cells

Translation initiation is the rate limiting step in protein synthesis and is tightly controlled by the availability of eIFs in response to extracellular and intracellular stimuli. Due to their rapid and uncontrolled growth, malignant cells are more metabolically active and so display increased rates of protein synthesis (Martineau et al, 2014). In fact the metabolic demands of cancer cells are often coupled to the size and protein synthesis rates (Dolfi, Chan, Qiu et al, 2013). Malignant cells require increased translation of key oncogenic proteins to promote tumorigenesis and cancer cell survival. Furthermore almost all oncogenic signalling pathways that are frequently mutated and hyper activated in cancers (PI3K/AKT/mTOR, Myc, Ras), ultimately converge onto the translation machinery leading to changes in the translational efficiency of a subset of mRNAs (Cintas and Guillermet-Guibert, 2017). This subset of mRNAs encode for proteins that regulate many of the hallmarks of cancer such as increased angiogenesis, proliferation and EMT (Cintas and Guillermet-

Guibert, 2017). In addition cancer cells use alternative modes of translation under stress conditions in order to maintain the synthesis of oncogenic proteins essential for survival. Deregulated protein synthesis and translational control is now a well-recognized characteristic of tumour cells (Bhat et al, 2015).

1.10 Protein Synthesis and the Response to Stress

Malignant cells often experience environmental stresses such oxidative stress, metabolic, mechanical, genotoxic to which the cell must adapt in order to survive (Fulda et al, 2010). Many types of cellular stress inhibit cap dependent translation; for example in response to the unfolded protein response (UPR), cap dependent translation is inhibited to reduce global protein biosynthesis in order to reduce the burden on the endoplasmic reticular (ER), thereby allowing the proper folding of proteins to prevent the accumulation of unfolded proteins in the ER (Pakos-Zebruka et al, 2016). In response to nutrient deprivation or hypoxia, as the most energy consuming process in the cell, cap dependent translation is inhibited in order to conserve energy (Chee et al, 2019). The inhibition of cap dependent translation is orchestrated via two signalling axis: mTOR/eIF4F axis and eIF2 phosphorylation (Chee et al, 2019). However it is important to note that under stress conditions, global translation is not simply “turned down” or “turned off”. Instead the translational efficiency of a sub set of mRNAs required to promote cell survival and to adapt to stress are maintained and in some instances increased (Chee et al, 2019).

1.10.1 eIF2 Phosphorylation

One key mechanism through which cells regulate the rate of protein synthesis is through a family of kinases that phosphorylate the alpha sub unit of eIF2 (Pakos-Zebruka et al, 2016). 4 separate kinases orchestrate the integrated stress response (ISR) in response to different stresses: 1) amino acid depletion/ general control non-derepressible 2 (GCN2) 2) Viral infection/double stranded RNA dependent protein kinase (PKR) 3) Heme deprivation/ heme regulated eIF2α kinase (HRI) 4) ER stress/ PKR like ER kinase (PERK) (Pakos-Zebrucka et al, 2016). All kinases share a common phosphorylation site on the alpha sub unit of eIF2α on serine 51 (Jiang and Wek, 2005). eIF2α phosphorylation leads a reduction in the exchange of eIF2-GDP to eIF2-GTP required to deliver Met-tRNAiMet to the 43SPIC resulting in a global down regulation of protein synthesis as it is unable to form part of the ternary complex required for cap dependent translation (Pakos-Zebrucka et al, 2016). However eIF2α phosphorylation levels begin to recover within 4-8 hours, and so the response to prolonged stress experienced by the cell is orchestrated by the eIF4F/mTOR axis (Rajesh et al, 2015).

1.10.2 mTOR/eIF4F Signalling Axis

The second key mechanisms used by eukaryotic cells to control the rate of translation is through the mTOR/eIF4F axis. mTOR, a Ser-Thr kinase downstream of PI3K/AKT is responsible for sensing and co-ordinating stimuli such as oxygen and amino acid availability in order to regulate proliferation, growth, lipid metabolism and autophagy (Laplante and Sabatini, 2009). mTOR exists as 2 structurally and functionally distinct protein complexes known as TOR complex and 2 (TORC1 and TORC2). mTORC1 consists of 1) the scaffold protein regulatory-associated protein of TOR (Raptor) 2) the catalytic component mTOR 3) the GTPase β-sub unit like protein g βL (mLST8) 4) proline-rich AKT substrate of 40kDa (PRAS40) 5) dishevelled Egl-10 pleckstrin [DEP] domain contain mTOR interacting protein (Deptor) (Peterson et al, 2009). mTORC2 also contains mTOR, MLST8 and Deptor, however in addition to these components it exclusively contains 1) rapamycin-insensitive companion of TOR (Rictor) 2) mammalian stress-activated protein kinase (SAPK) interacting protein (mSIN1) 3) proline-rich protein 5 (Protor) (Siddiqui and Sonenberg, 2015) (Guertin and Sabatini, 2007).

Under normal conditions mTORC1 is activated by the PI3K/Akt pathway; in response to growth factor and hormone stimulation, PI3K is activated and phosphorylates phosphatidyl inositol 3,4 (PIP_2) which generates phosphatidyl inositol 3,4,5 (PIP_3) leading to the recruitment of Akt to the plasma membrane where is it subsequently phosphorylated (Harrington et al, 2005). Activated Akt phosphorylates the tuberous sclerosis complex (TSC2) component of the TSC1/TSC2 complex (Brugarolas et al, 2004). The TSC1/TSC2 complex serves as a GTPase-activator protein (GAP) for the Ras-homolog enriched in brain (Rheb) protein (Long et al, 2005). Phosphorylation of TSC2 by AKT is thought to inhibit its GAP activity, allowing Rheb levels to accumulate in its GTP-bound form. GTP bound Rheb is then able to stimulate the kinase activity of mTOR. Phosphatase and tensin homologue (PTEN) acts a negative regulator of the PI3K/Akt pathway (Long et al, 2005). PDCD4 acts as a negative regulator of cap dependent translation via inhibition of eIF4A and is negatively regulated my mTOR signalling (Vikhreva et al, 2014).

mTORC1 phosphorylates and inactivates 4E-BP1, a negative regulator of eIF4E; under stress conditions the kinase activity of mTORC1 is reduced, limiting its availability to phosphorylate 4E-BP1 (Showkat et al, 2014). 4E-BP1 is then able to bid to eIF4E, sequestering it, and preventing it from forming part of the eIF4F complex (Showkat et al, 2014). In addition mTORC1 phosphorylates the S6 kinase (S6K), leading to increased activity of EF2 and ribosomal protein S6, and enhancing translational efficiency (Magnuson et al,

2012). However under stress conditions mTORC1 kinase activity is reduced, preventing the phosphorylation of S6K, reducing global translation rates (Magnuson et al, 2012). mTOR is a positive regulator of protein synthesis and mutations in upstream regulators of translation lead to hyperactive eIF4E signalling through constitutively active mTOR leading to a global increase in protein synthesis rates (Hardt et al, 2011).

1.11 Protein Synthesis and the Response to Hypoxia

Under hypoxic conditions, ATP production switches from oxidative phosphorylation to a less efficient anaerobic glycolysis and so energy expensive processes such as protein synthesis undergoes a global downregulation in order to conserve energy (Koumenis et al, 2002). mRNA translation under hypoxic conditions is regulated mainly at the translation initiation stage in biphasic response mediated through two distinct and independent pathways: the first occurring rapidly within 1-2 hours and mediated primarily by PERK activation as part of the UPR and eIF2a phosphorylation as described previously (Koumenis et al, 2002). Exposure of NIH3T3 cells to 24 hours 1% O_2 leads to a 50% reduction in the rate of ^{35}S-methionine incorporation which is completely reversible within 1 hour of returning to normoxia (Lang et al, 2002). Under anoxic conditions (0-0.2% O_2) a maximum inhibition of protein synthesis was observed after 1-2 hours and subsequently is partially restored after 8 hours (Koritzinsky, 2006*).* This initial restoration in translation is necessary to allow for the translation of stress response proteins crucial to the molecular adaption to hypoxia.

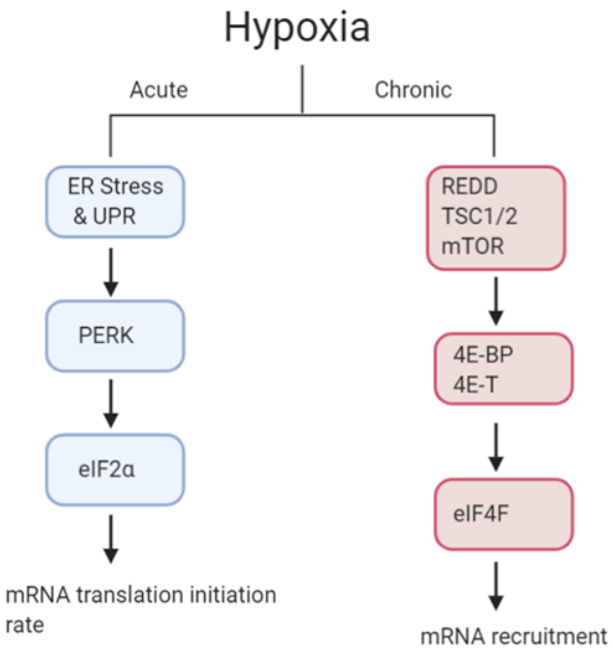


Figure 1.5. Biphasic response to hypoxic conditions is mediated via 2 distinct pathways. The response to acute hypoxia occurs within 1-2 hours and is under the control of eIF2α phosphorylation via PERK activation. Chronic hypoxia leads to the sequestering of eIF4E by 4E-BP1 preventing it from forming part of the eIF4F complex. Figure adapted from Koritzinksy et al, 2006. Illustration created using BioRender.

1.11.1 REDD/TSC1 signalling axis

Under hypoxic conditions 4E-BP phosphorylation is regulated by a novel pathway distinct from those activated by amino acid deprivation or depletion in ATP levels (PI3K/AKT). Instead mTOR inhibition is achieved via the regulated in development and DNA damage protein (REDD1)/ TSC1/TSC2 signalling axis (Schonenberger and Kovacs, 2015). Hypoxia induces the rapid de novo transcription and mRNA synthesis of REDD1, which acts as a negative regulator of mTOR phosphorylation. REDD1 promotes the release of TSC2 from its inhibitory 14-3-3 proteins and subsequent inhibition of mTORC1 (DeYoung et al, 2008). REDD1 overexpression alone is sufficient to inhibit mTORC1 activity (DeYoung et al, 2008). mTOR is no longer able to phosphorylate 4E-BP, allowing it to bind to eIF4E, sequestering it from the eIF4F complex (DeYoung et al, 2008).

1.11.2 Alternative Modes of Translation in Response to Hypoxia

In face of the global downregulation of protein synthesis, the translation of a subset of mRNAs crucial for the molecular adaptation to hypoxia are maintained. These transcripts

are essential for the adaptive response to hypoxia and include the well-known hypoxia response genes as mentioned earlier in this thesis (Chee et al, 2019). In order for theses transcripts to be translated under hypoxic conditions malignant cells employ two alternative methods of translation; 1) hypoxic induction of IRES translation 2) formation of novel protein complexes to facilitate cap binding 3) a switch in eIF4F isoforms (Chee et al, 2019).

1.11.3 IRES

Under hypoxic conditions, malignant cells are able sustain translation of key survival proteins via IRES dependent translation initiation in order to bypass the eIF4F complex and escape the global downregulation of protein synthesis (Young et al, 2008). Such transcripts that have been experimentally proven to contain an IRES have been shown to possess long, GC rich, highly structured 5'UTRs and include VEGF, and c-MYC and transcripts that play important roles in proliferation, regulation and apoptosis and differentiation (Lang et al, 2002)(Stonley et al, 1998). IRES translation does not depend on eIF4E, instead recruiting ITAFs which function as RNA chaperones (Komar and Hatzoglou, 2011). However a number of papers have now reported the requirement for eIF4A in the remodelling of IRES in order for them to support cap independent translation. EGFR has been experimentally proven to contain an IRES that supports its hypoxic translation, but requires the helicase activity of eIF4A to "remodel" the IRES before they are able to function (Webb et al, 2015). Furthermore eIF4A is required to remodel the IRES of c-myc, N-myc and BiP (Spriggs et al, 2009)(Thoma et al, 2004). It may seem an attractive explanation that under the hypoxic global downregulation of protein synthesis, translation of onco-proteins is sustained solely via IRES translation. However this is not the case, as IRES translation is only implicated in translation ~3-5% of cellular mRNAs and cannot account for the full and relatively high translational capacity of hypoxic cancer cells. Therefore hypoxic tumour cells must rely on alternative methods of translation (Holkik and Sonenberg, 2005).

1.11.4 Formation of Novel Protein Complexes to Facilitate Cap Binding

Initial experiments investigating the mechanism of the hypoxic translation of EGFR utilised RNA immunoprecipitation experiments to identify a novel interaction between HIF2α and the 3'UTR of EGFR (Uniacke et al, 2012). HIF2α was shown to directly bind to the EGFR 3'UTR between nucleotides 4295 and 4861 and was shown to activate its translation (Uniacke et al, 2012). siRNA inhibition of HIF2α and not HIF1α lead to a significant reduction in the rate of global protein synthesis, highlighting a role specifically for HIF2α in hypoxic protein synthesis (Uniacke et al, 2012). The same study, employing

immunoprecipitation experiments, went onto discover that HIF2α interacts with RNA binding motif-4 (RBM4) via a CGG trinucleotide RBM4-binding motif present within its 3'UTR. The same observation was not found for HIF1α (Uniacke et al, 2012). m^7-GTP bead pull down to immunoprecipitate the RBM4:HIF2α complex revealed eIF4E2, an eIF4E homologue, as an additional component of the RBM4:HIF2α complex. The study hypothesised that RBM4 binds to specific regions in the 3'UTR of target genes (similar to that of the RBM4 binding motif) to recruit HIF2α and termed these regions "RNA hypoxic response elements"(rHRE). Knockdown of eIF4E2 prevented the translation of transcripts identified by PAR-CLIP including EGFR, the same effect was not found for eIF4E (Uniacke et al, 2012). Additional inhibition of eIF4E using Rapamycin prevented the accumulation of eIF4E in the normoxic polysome but showed no effect on the recruitment of eIF4E2 to the hypoxic polysome. Silencing of the RBM4:HIF2α:eIF4E2 complex prevented the translation of transcripts containing rHRE in hypoxic but not in normoxia (Uniacke et al, 2012). This evidence supports the notion of an oxygen dependent switch in eIF4E isoforms.

1.11.5 Hypoxic Switch in eIF4F Isoforms

Further studies have expanded on Uniacke and colleagues work and have demonstrated a switch in eIF4G isoform in response to hypoxia; hypoxia promotes a switch from eIF4G1 to eIFG3. Together this work has proposed 2 distinct eIF4F complexes; the "normoxic" eIF4F complex consisting of eIF4E, eIF4A and eIF4G1 and the "hypoxic" eIF4F complex consisting of eIF4E2, eIF4A and eIF4G3 (Ho et al, 2016). The same study utilising pSILCAC/mass spectrometry in conjunction with RNA-seq was able to define oxygen responsive transcripts based on their hypoxic and normoxic translational efficiencies to group them into Class I, II, III mRNAs (Ho et al, 2016). Class I mRNAs are efficiently translated by the normoxic eIF4F complex, Class II mRNAs can be translated by both the normoxic and hypoxic eIF4F complex, independent of O_2 and Class III mRNAs can only be translated by the hypoxic eIF4F complex. Such transcripts represent ~25%, ~60% and ~15% of the combined normoxic and hypoxic translatome (Ho et al, 2016). However this study does not investigate the switch in eIF4A isoform, nor do they provide any clarification as to which eIF4A isoform they probed for. This information was also lacking from the materials and methods so one is unable to draw any conclusions about the roles of eIF4A1 or eIF4A2 from this study. This study supports the global reorganisation of translational efficiencies during hypoxic conditions, governed via the hypoxic eIF4F complex. This provides evidence that targeting eIF4A in cancer cells may prevent the hypoxic adaption that allows them to survive under such conditions.

1.12 The RNA Helicase eIF4A

The eIF4A RNA helicases belong to the superfamily 2 (SF2) and within the sub family of DEAD-box proteins and play a central role in many stages of the RNA life cycle including RNA metabolism, RNA export, translation initiation, translation termination, ribosome biogenesis, mRNA degradation and the formation of the spliceosome (Linder et al, 2006). RNA helicases catalyse the separation of RNA duplexes and the structural rearrangement of RNA and RNA/protein interactions in an ATP dependent manner stimulated by RNA (Gilman et al, 2017). DEAD box proteins are characterised by 9 conserved motifs: Q-motif, motif I, motif Ia, motif Ib, motif II, motif III, motif IV, motif V and motif VI. Motif II is also referred to as the Walker B motif and contains the amino acid sequence (asp,glu,ala,asp) D-E-A-D, giving the family its name. These motifs contribute to the proteins ATP binding and hydrolysis, RNA binding and duplex unwinding properties (Gilman et al, 2018)



Figure 1.6. Motifs present within the DEAD box family of proteins. Motifs outlined in red represent the ATP binding domains of these proteins. Motifs outlined in purple are represent the RNA interaction domains. Figure adapted from Tuteja et al, 2008. Illustration created with BioRender.

The 9 conserved motifs are located in the cleft of the helicase core formed by 2 domains that resemble the bacterial recombination protein recombinase A (RecA) (Andreou and Klostermeier, 2013). In the absence of RNA the helicase core resides in an open conformation, binding of RNA and ATP leads to a closed conformation state and stabilises the closed helicase core; the nucleotides bind in the inter-domain clef and interact with residues from motifs I, II, V and VI (Andreou and Klostermeier, 2013). With the RNA now clamped inside the helicase core, the duplex is destabilised and the first strand can dissociate. The helicase core remains in a closed conformation following ATP hydrolysis and only returns to the open state following phosphate release. The opening of the helicase core allows for the release of the second RNA strand (Andreou and Klostermeier, 2013). Following ADP dissociation the helicase core can undergo catalytic cycles of open and closed states.

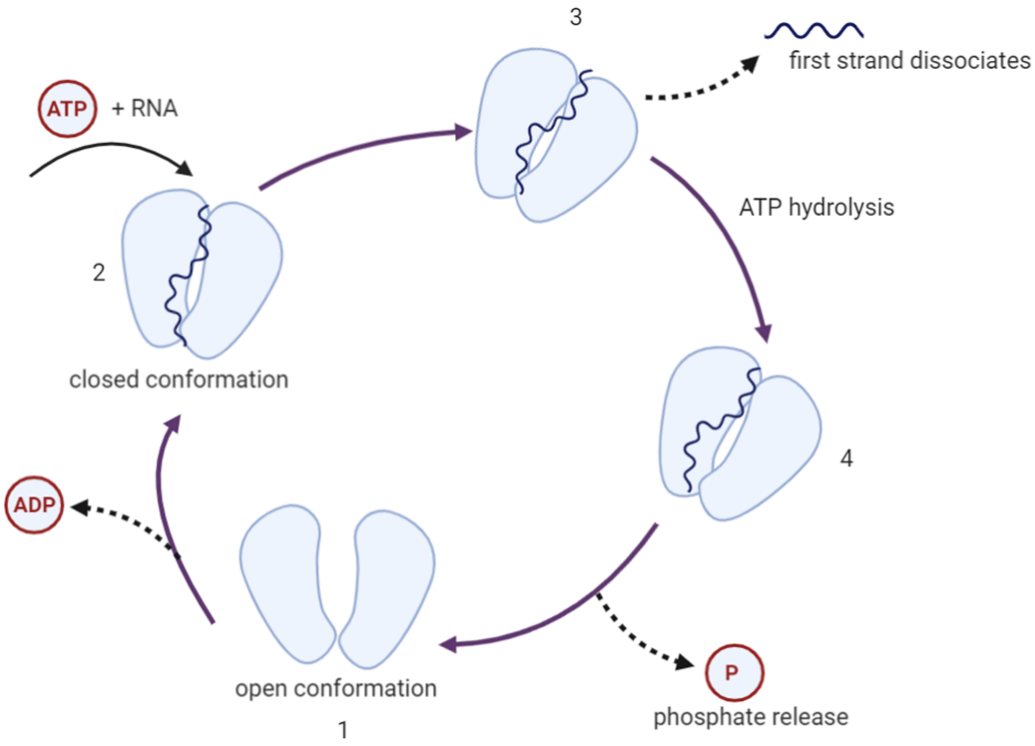


Figure 1.7. Schematic overview of eIF4A catalytic cycle. 1) In the absence of RNA and ATP the helicase core remains in an open conformation 2) cooperative binding of ATP and RNA stabilises the closed conformation of the helicase core 3) the interaction between the helicase motifs bound to the RNA and ATP leads to the destabilisation of the RNA duplex and leads to the dissociation of the first RNA strand 4) the helicase core remains in the closed conformation following ATP hydrolysis and only remain to the open conformation following release of phosphate. The helicase core is now ready to go through subsequent cycles of open and closed states. Figure adapted from Andreou and Klostermeier, 2013. Illustration created with BioRender.

Single molecule FRET experiments have revealed that this transition between open and closed confirmations takes on average 1.7 seconds to complete a cycle (Sun et al, 2014). It is important to note that the unwinding rate of eIF4A depends in the thermodynamic stability of the duplex and not of its length or sequence (Rogers et al, 1999).

1.13 eIF4A Isoforms

There are 3 eukaryotic isoforms of eIF4A: eIF4A1, eIF4A2 and eIF4A3. Only eIF4A1 and eIF4A2 play a role in in translation initiation are cytoplasmic, eIF4A3 only displays ~60% similarity to eIF4A1 and eIF4A2 and instead plays a role in the formation of the exon junction complex (EJC) and which regulates pre-mRNA splicing (Raza et al, 2015). For this reason eIF4A3 will not be discussed in detail in this thesis. Around 90% of eIF4A exists as free form with only a small proportion being recruited into the eIF4F complex (Pelletier et al, 2016). eIF4A must also form a complex with eIF4G in order to be incorporated into the eIF4F complex, it achieves this via a Huntington, Elongation Factor 3, PR65/A, TOR (HEAT) domain present in eIF4G which binds to both the RecA like domains of the helicase core of eIF4A and subsequently closing the domains (Oberer et al, 2005). However, when bound to eIF4G the RecA like domains are not fully closed, instead they remain in a "half open" conformation and in this state RNA binding is promoted and an increased rate of phosphate rate is also observed (Hilbert et al, 2011). Therefore eIF4A binding to eIF4G stimulates its helicase activity (Oberer et al, 2005). eIF4A1 also binds to PDCD4, its negative regulator; whereby PDCD4 binds to 2 molecules of eIF4A rendering it in a closed state and unable to bind to eIF4G, unable to be part of the eIF4F complex (Suzuki et al, 2008).

Both eIF4A1 and eIF4A2 share 91% similarity at the amino acid level and were originally thought to be functionally interchangeable (Raza et al, 2015). Both can assemble into the eIF4F complex where their helicase activity is stimulated by eIF4B and eIF4H. eIF4A1 suppression does leads to an increase in eIF4A2 transcription, however eIF4A2 cannot rescue the effects of eIF4A1 inhibition (Galicia-Vezquez et al, 2012). It has now been demonstrated that they display distinct functions and patterns of expression. It is important to note that in the literature there is a lack of research distinguishing the distinct roles of eIF4A1 and eIF4A2 with the majority of research focusing on eIF4A1 (Raza et al, 2015).

1.13.1 eIF4A1

eIF4A1 is expressed in actively proliferating cells and is generally the more abundant isoform in comparison to eIF4A2. Deregulated eIF4A1 expression has been observed in a variety of malignancies including lung, breast and colon (Liang et al, 2017). Furthermore

only eIF4A1 has been shown to act in a positive feedforward loop with MYC via the presence of an E-box within the eIF4A1 promoter (Lin et al, 2008).

It is important to note that previous studies have demonstrated that eIF4A1 remains unaffected by hypoxia in HCT116 cells exposed to either 16 or 40 hours 1% 0_2 (Lai et al, 2016). An additional study also confirmed that eIF4A1 was not found to accumulate to the hypoxic polysome of HEK293 cells following exposure to 1% 0_2 for 9 hours (Chen et al, 2019).

1.13.2 eIF4A2

eIF4A2 is expressed more so in quiescent cells; over expression has been associated with better patient prognosis in both breast cancer NSCLC (Yan et al, 2011)(Shaoyan et al, 2013). In comparison to eIF4A1, eIF4A2 seems to have been neglected in the literature. Particularly in hypoxia, a literature search reveals only 1 paper published on eIF4A2 in hypoxia. The paper demonstrated that eIF4A2 mRNA was upregulated under both hypoxic and acidosis conditions and additionally, simultaneous acidosis and hypoxia, a feature commonly found in solid tumours. However the paper provides no further investigation into the role of eIF4A2 in hypoxia (Sorensen et al, 2015).

In additional to its role in translation initiation, eIF4A2 has been demonstrated to be the only component of the eIF4F complex required for miRNA mediated translation repression (Meijer et al, 2013). It has been demonstrated that only eIF4A2 co-immunoprecipitates with CNOT7, a component of the CCR4-NOT complex (Meijer et al, 2013). Furthermore the same study uncovered a correlation between the degree of 5'UTR secondary structure and the presence of miRNA target sites within their 3'UTR. An additional conclusion from the same study was that transcripts with short unstructured 5'UTRs are unaffected by miRNA mediated regulation (Meijer et al, 2013). This paper supports the notion that eIF4A2 may possess dual roles in translation, acting as both an activator of translation, via unwinding of complex 5'UTRS, and as a repressor of translation, by recruiting the CCR4-NOT complex to target mRNAs. However the mechanism as to how eIF4A2 selects its transcripts has never been uncovered.

eIF4A2 has been shown to play an additional crucial role in the formation of stress granules (Jongjitwimol et al, 2016). In response to stress, cytoplasmic bodies known as stress granules are formed, containing translational machinery that has been stalled upon an mRNA to allow for a reduction activate protein synthesis and to allow for re-programming of the translational machinery (Jongjitwimol et al, 2016). eIF4A2 was shown to be modified

by sumoylation at a single residue (K226), which involves the covalent attachment of SUMO groups to a target protein (Jongjitwimol et al, 2016). Sumoylation can regulate protein localisation, activity and protein-protein interactions. Inhibition of eIF4A2 sumoylation was found to impair stress granule formation, suggesting a new role for sumoylation in the regulation of eIF4A2 function, and a new role for eIF4A2 in the regulation of stress granule formation (Jongjiwimol et al, 2016).

However a paper that has been published since the completion of this thesis laboratory work has shown that eIF4A2 is highly expressed in CRC tumours and is an independent predictor of progression free survival. The same study showed eIF4A2 inhibition resulted in a significant reduction colorectal cancer cell migration and sphere formation, in addition to inhibiting lung metastasis in an *in vivo* model (Chen et al, 2019). Therefore the expression and role of eIF4A2 in malignancy appears to be tumour specific.

1.14 Project Aims

As described in within this introduction, the protein synthesis machinery undergoes a global adaptive response to hypoxia to allow for the continued translation of proteins crucial for the stress response to hypoxia. This is in part regulated by *cis* and *trans* acting factors present within the 5'UTR of target transcripts. Transcripts with highly structured 5'UTRs are more dependent on eIF4A to be efficiency translated. However eIF4A2 has generally been ignored in the literature, with the majority of the work focusing on eIF4A1. This thesis aims to identify eIF4A2 as a key regulator of normoxic and hypoxic tumour cell survival and growth and to investigate the mRNAs whose translation is repressed or activated by eIF4A2. In addition this thesis aims to determine that high eIF4A2 protein expression is associated with worse patient outcome and hypoxia in colorectal cancer patient.

Specifically this thesis will address the following:

1. To determine a role for eIF4A2 in tumour cell growth and survival in normoxia and hypoxia in CRC
2. To identify eIF4A2 bound mRNAs in normoxia and hypoxia and those whose translation is mediated by eIF4A2 directed translational activation
3. To determine the hypoxic co localisations and prognostic outcome of eIF4A2 protein expression in colorectal cancer

2.0 Methods and Materials

2.1 Cell Culture

2.1.1 Culture of Adherent Cells

All cell culture was performed in a Class II Microbiological Safety Cabinet (Walker, Glossop, UK). All colorectal cell lines, DLD-1, HCT116, LS174T, CCD 841 CoN and SW1222 were purchased from ATCC and routinely cultured in complete media consisting of Dulbecco's Modified Eagle's Medium high glucose (DMEM)(Sigma Aldrich, Poole, UK)) supplemented with 10% [v/v] fetal bovine serum and 1% [v/v] L-Glutamine (both Sigma Aldrich). Cell lines were grown at 37°C, in a humidified carbon dioxide atmosphere (5% CO_2).

Cell lines were routinely sub-cultured when they reached ~70% confluence in a T175cm^2 flask (Corning, Fisher Scientific, Loughborough, UK). Media was removed by aspiration and cells washed once with 1x sterile phosphate buffered saline (PBS (Sigma Aldrich)). Cells were detached from each other and the base of the culture flask with Trypsin-EDTA solution 1x (Sigma Aldrich) for 3-4 minutes at 37°C. Dissociation was aided by gently tapping the flask and was confirmed by microscopy. Trypsin was quenched with the appropriate amount of fresh media. Cells were then typically split 1:10 into fresh T175^2 flasks and dispersed evenly by gentle shaking.

2.1.2 Cryopreservation of Cells

Cells were grown to 70-80% confluence in T175^2 flasks and released from the adherent surface as described above, and pelleted by centrifugation at 250 x g for 8 minutes. Cell pellets were re-suspended in freezing down media (90% [v/v] FBS, 10% [v/v] dimethyl sulfoxide [DMSO]). The suspension was transferred into separate cryovials (Star Labs, Milton Keynes, UK). Vials were placed into a "Mr Frosty" freezing container (Thermo Scientific, Loughborough, UK) filled to the appropriate level with isopropanol (Sigma Aldrich) and frozen overnight at -80°C. Frozen vials were stored long term at -150°C in liquid N_2.

2.1.3 Cell Counting

Cells were counted using the BioRad Automated Cell Counter (BioRad). Cells were detached from tissue culture flasks and pelleted by centrifugation using the method as described above.

2.2 Hypoxic Culture Conditions

Cells were maintained under hypoxic conditions (0.5-1% O_2 and 37°C) using the Hypoxia Workstation Invivo$_2$ 400 (Baker Ruskinn, South Wales, UK). Cells were lysed inside the hypoxia chamber to prevent reoxygenation. Cells were typically exposed to 1% O_2 for 24,

48 or 72 hours unless stated otherwise. Normoxic conditions used in this thesis were 20% O_2.

2.3 Western Blot

2.3.1 Protein Extraction

Media was removed and cells washed in 1x ice cold phosphate buffered saline (PBS). 1x RIPA buffer (Abcam, Cambridge, UK) supplemented with protease inhibitor cocktail (Sigma Aldrich) was added to each dish. To visual HIF transcription factors 4M urea buffer was used, lysis buffer components are detailed in the appendix. Dishes were scraped using a cell scraper (Greiner Bio One, Stonehouse, UK), collected into the bottom of the dish and transferred to a 1.5mL centrifuge tube. Lysates were cleared via centrifugation for 10 minutes at 2,500 x g at 4°C. Protein samples were stored at -80°C.

2.3.2 Protein Quantification – Bradford Assay

Protein samples were quantified using a Bradford Assay. A stock solution of bovine serum albumin 50mg/ml (BSA (Santa Cruz Biotechnology, Texas, USA)) was created by dissolving BSA powder in distilled H_20. The stock solution was added to 1x PBS to create a top concentration of 4000 µg/mL. Serial dilutions were performed to achieve the following concentrations: 2000 µg/mL, 1000 µg/mL, 500 µg/mL, 250 µg/mL, 125 µg/mL, 62.5 µg/mL, 31.25 µg/mL, 15.625 µg/mL, 1x PBS was used as a negative control. Experimental samples were diluted 1 in 10 with PBS. For use with 4M urea buffer, samples were diluted 1:20 in in dH_20. Bradford reagent (BioRad) was diluted 1 in 5 with distilled H_20. Samples were run in triplicate in a 96 well plate, 1x Bradford reagent was added to each well. The plate was read using a spectrophotometer at 620nm (Infinite®F5 (Tecan, Reading, UK)). The raw data file was exported to Microsoft Excel for further analysis.

2.3.3 Gel Electrophoresis

Samples were prepared for western blot with 4 x Laemmli (BioRad) working solution used in the ratio of 1 part Laemmli to 3 parts sample. 4x Laemmli working solution consisted of 900µl of 4 x Laemmli containing 100µl of β-mercaptoethanol (Sigma Aldrich). Typically 40-50ug of protein were loaded for western blotting. Samples were boiled at 95°C for 5 minutes.

Samples were separated via electrophoresis based on their size through a 4-20% gradient pre-cast gel (Mini-PROTEAN®TGX (BioRad)) using the Mini-PROTEAN Tetra Cell 1-D vertical gel electrophoresis set up (BioRad). Protein ladder was run to allow for identification of protein weights (Precision Plus Protein™ Dual Colour Standard (BioRad)). Gels were run at a constant 100 v.

2.3.4 Gel Transfer

Resolved proteins were transferred onto a nitrocellulose membrane (0.45 µM pore size (BioRad)) using the Trans-Blot®Turbo™Transfer System (BioRad). Depending on the predicted molecular weight of the protein, proteins were transferred using either: 1) mixed molecular weight programme, 1.3 A, 25 v, for 7 minutes 2) high molecular weight programme, 1.3 A, 25 v for 12 minutes. Turbo Transfer Buffer (BioRad) was made according to the manufacturer's instructions. See appendix for buffer details. Membranes were blocked in 5% BSA [w/v] Tris Buffered Saline (TBS) (Sigma Aldrich)) for 1-2 hours at room temperature aided by gentle rocking. The membrane was then incubated in primary antibody diluted 1:1000 in 5% BSA [w/v] TBS-T 0.5% [v/v] at 4°C overnight with gentle rocking (see appendix for primary antibody details used for Western Blot). All primary antibodies were used at 1:1000 dilution unless stated otherwise. B-actin was used as a loading control for all samples. The membrane was then washed three times in TBS-T 0.1% [v/v] for 5 minutes per wash with gentle rocking. The membrane was then incubated with 5mL of secondary antibody (IRDye®, LI-COR Biotechnology, Cambridge, UK) diluted 1:15000 in 5% BSA [w/v] TBS-T 0.5% [v/v] for 60 minutes at room temperature protected from light with gentle rocking. Secondary antibodies were used at 1:15000 dilution unless stated otherwise. The membrane was washed a further 3 times before imaging. Membranes were imaged using the Odyssey FC Imaging System (LI-COR) and signal intensity values exported to Microsoft Excel for further analysis.

2.4 Co-immunoprecipitation of Endogenous Proteins

Media from experimental plates was aspirated off the cells followed by two washes in ice cold PBS; protein was extracted and quantified as previously described in section. Samples were passed five times through a 21 gauge needle prior to centrifugation as previously described. Details of the lysis buffer (IP Buffer) and Wash Buffer used for Co-IP experiments can be found in the appendix. Complete IP Buffer refers to the lysis buffer with the addition of protease and phosphatase inhibitors. 1.5 mg of protein per pull down was used, additional controls included for each experiment included an IgG negative control and 15 µg of input (sample that had not undergone immunoprecipitation).

1.5mg of lysate was incubated with the recommended dilution of primary antibody, samples were made up to a final volume of 500 uL in Complete IP Buffer (found in appendix). Lysate and primary antibody were incubated overnight at 4°C aided by end over rotation. The following day 100 uL of bead slurry per pull down was washed twice in Wash

Buffer and twice in IP Buffer. Beads were engaged on a magnetic rack, IP Buffer removed and pre-cleaned beads re-suspended in the lysate: antibody complexes from the previous step. Lysate, antibody and beads were incubated together at 4°C for 4 hours with end over rotation. Beads were washed five times with cold wash buffer, on the final wash the bead slurry was transferred to a fresh tube. Proteins were eluted from the beads in 40 µl of 2X Lamelli and boiled for 5-10 minutes at 95°C. Eluted proteins were then separated via gel electrophoresis as previously described.

2.5 RNA Extraction

Media was removed by aspiration, TRI Reagent® (Sigma Aldrich) was added per 10cm^2 dish, and 500 µl of TRI Reagent® per each well of a 6 well plate. Samples were incubated for 5 minutes at room temperature. 200 µl of chloroform (Fisher Scientific) was added to each sample, shaken thoroughly by hand to distribute the chloroform through the sample and centrifuged at 12,000 x g for 15 minutes. 400 µL of the aqueous supernatant was removed and transferred to a fresh centrifuge tube containing 500 µL isopropanol (Fisher Scientific). Samples were centrifuged at 12,000 x g for 15 minutes to form a pellet. The supernatant was removed and pellets washed with 800 µL of 70% ethanol. Samples were centrifuged a final time at 12,000 x g for 5 minutes. Ethanol was removed by aspiration and the pellet dissolved in 20 µL of ultra-pure water. RNA samples were stored at -80°C. RNA samples were quantified using the Nanodrop 2000c (Thermo Scientific, Loughborough, UK).

2.6 cDNA Synthesis

cDNA synthesis was carried out from 2 µg of good quality total RNA using the High Capacity cDNA Reverse Transcription Kit (Applied Biosystems, Fisher Scientific). cDNA master mix was prepared according to the table below by multiplying the volumes of individual reagents required per reaction.

Table 2. Master mix components per sample for cDNA synthesis

Component	**Volume (µL)**
10x RT Buffer	2.0
25x dNTP Mix (100uM)	0.8
10x RT Random Primers	2.0
Ultra-Pure Water	4.2
MultiScribe Reverse Transcriptase	1.0
Total Volume for 1 Reaction	**10**

Samples were placed into a thermal cycler (Veriti (Applied Biosystems)), see appendix for thermal cycle programme details. cDNA was placed directly onto ice upon completion of programme and stored at -20°C. cDNA samples were diluted 1 in 10 in ultra-pure water prior to qPCR.

2.7 Quantitative PCR

Quantitative PCR (qPCR) was performed using the LightCycler®480 II thermal cycler (Roche Diagnostics Ltd, Burgess Hill, UK). Reactions were prepared using the LightCyler® 480 SYBR Green I Master Mix. All samples were run in triplicate in a 96 well plate format (LightCycler® 480 Multiwell white plate, (Roche)). A separate master mix for every primer set was prepared according to the table below by multiplying the reagent volumes by the number of samples required:

Table 2.1. Master mix components per sample for qRT-PCR.

Reagent	**Volume (uL)**
Forward Primer (10uM working solution)	1
Reverse Primer (10uM working solution)	1
Ultra-pure Water	6
Master Mix	10
cDNA	2
Total Volume per Reaction	**20**

Primers were purchased from either Eurofins Genomics (Ebersberg, Germany) or Sigma Aldrich (see appendix for primer sequences and details). All samples were probed for actin to act as an house keeping gene, PCR grade water was used as a negative control. See appendix for thermal cycling programme. Upon completion of the programme Ct values and melting curves were generated using the built in LightCyler® 480 II software. C_t values were exported to Microsoft Excel for further analysis using the $\Delta\Delta C_t$ method (Livak and Schmittgen, 2001) .

2.8 Nucleic Acid Transfection of Adherent Cells

2.8.1 Oligofectamine siRNA Reverse Transfection

siRNA was introduced to cell lines using lipofection, in these cases Oligofectamine® (Invitrogen (Thermo Fisher) and a reverse transfection method was used. See appendix for details of siRNA sequences and controls used. For each transfection sample complexes were prepared in sterile 0.5 ml centrifuge tube. Oligofectamine® reagent was diluted in OPTI-MEM® Reduced Serum Media (Gibco®, Thermo Scientific), mixed gently and

incubated at room temperature for 5-10 minutes. 10µL of 20uM stock siRNA was diluted in 175µL of OPTI-MEM® and mixed gently. Oligonucleotide and Oligofectamine solutions were combined and incubated at room temperature for 15-20 minutes. Complexes were pipetted into their corresponding wells and cell suspensions were pipetted directly on top of the complexes. Cells counts were obtained using the method as previously described, it was ensured to re-suspended cell pellets in OPTI-MEM®. 45,000 cells were seeded per well of a 6 well plate. Cells and siRNA: Oligofectamine® complexes were incubated at 37°C for 6 hours. OPTI-MEM® and siRNA: Oligofectamine® complexes were aspirated off the cells and replaced with complete media. Cells were assayed for gene knockdown via qPCR/Western Blot as previously described 24-48 hours post transfection.

2.9 Assessment of Cell Survival

2.9.1 Clonogenic Assay

Clonogenic assays were conducted in a $T75^2$ flask (Corning), cells were harvested and counted using the method as previously described Cells were typically seeded a concentration of 2000 cells/flask containing complete media with two flasks seeded per condition to obtain average colony counts. Colonies were allowed to form over 2 weeks; during this time it was ensured the flasks were left untouched. Extra flasks were seeded to check on the growth of colonies during this time. Media was aspirated from the flasks and colonies were fixed and stained with 1% methylene blue (Sigma Aldrich) for 60 minutes at room temperature. Working methylene blue solution was made by dissolving 1g of methylene blue powder in 100mL 70% ethanol diluted with PBS. Methylene blue was aspirated from the flasks, flasks were rinsed once in tap water and a further two times by submerging the flasks in tap water. Flasks were allowed to dry overnight and colonies were counted using a cell counter and a grid overlay to avoid double counting.

2.10 Generation of eIF4A2 Inducible Knockdown Cell Line

Sigma MISSION® custom lentiviral shRNA services was used to generate Isopropyl β-D-1-thiogalactopyranoside (IPTG) inducible lentiviral transduction particles for this study using the pLKO-puro-IPTG 3xLacO inducible vector. (See Figure 2 for plasmid information) The service included shRNA cloning, sequence verification, DNA quantitation and tier determination. Two separate shRNA sequences were used to generate eIF4A2 knockdown cell lines (Clone ID TRCN0000051**69** and TRCN0000369**84**,) which will be referred to as sh69 and sh84. To generate a control knockdown cell line, cells were transduced with MISSION 3x LacO Inducible Non-Target shRNA Control Transduction Particles (Sigma MISSION®, Sigma Aldrich) which will be referred to as shCTL. Dioxane free IPTG was

purchased from FORMEDIUM (Norfolk, UK) and a working solution of 0.1 M was made. IPTG aliquots were stored at -20°C and freeze thaw cycles avoided. Cells were incubated with 1 mM IPTG in cell culture media for 3-4 days, with fresh IPTG containing media added daily, prior to assessing knockdown or experimental manipulation.

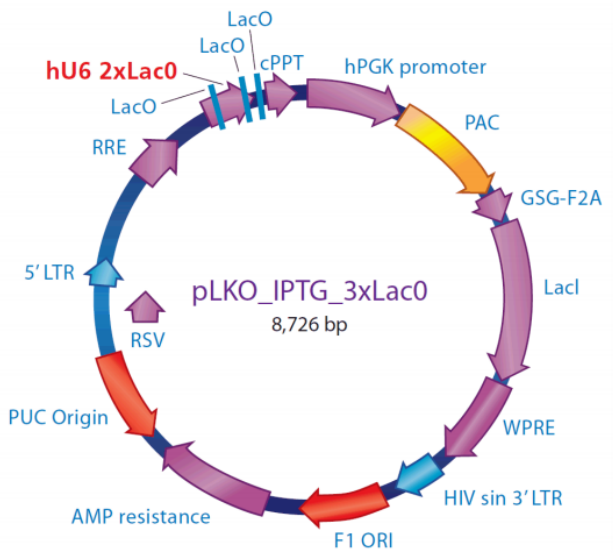


Figure 2. Structure of the pLKO-puro-IPTG-3xLacO inducible vector. Lentiviral particles were obtained using Sigma MISSION ® Inducible shRNA Vector service. Figure taken from Sigma, 2019.

2.10.1 Transduction of Lentiviral Particles

Cells were pelleted, counted and re-suspended using the method as previously described. Lentiviral transductions were performed in 48 well plates. 400,000 cells were incubated with the corresponding lentiviral particles at a multiplicity of infection (MOI) of 5 at 37°C for 24 hours. Hexadimethrine bromide (Polybrene (Sigma Aldrich)), a cationic polymer was used to overcome the charge difference between the viral particles and the cell and was used at a final concentration of 6 µg/mL. 3 wells of a 48 well plate for each shRNA sequence (shCTL, sh69, sh84) were transduced. Following 24 hour incubation virus was aspirated off the cells and cells were washed 3 times in complete media. The following day transduced cells were split into a 6 well plate; puromyocin selection (HCT116 8 µg/mL, LS174T 4 µg/mL,) began once the cells had reached 70-80% confluence in a 6 well plate. The appropriate puromycin concentration for selection had been previously obtained by performing a kill curve for both cell lines. Briefly, 35,000 cells were seeded in each well of a

6 well plate with the following puromycin concentrations: 10 µg/mL, 8 µg/mL, 6 µg/mL, 4 µg/mL, 2 µg/mL, and 0 µg/mL. Plates were visually assessed for cell death. Transduced pools were grown under selection up to a $T175^2$ flask (Corning) and assessed for knockdown at both the RNA and protein level using the methods as previously described.

2.10.2 Single Cell Clonal Selection

Single cell clonal selection was performed to obtain clones with the highest percentage of knockdown from transduced pools. Cells were harvested and counted as previously described. A fresh cell suspension containing $<10^6$ cell/mL was created before counting cells and further diluted to make a 1:100 dilution. To seed one 96 well plate, a fresh suspension of 10 mL of a 5 cell/mL solution was made. The new cell suspension was plated out into 96 well plates, two plates per shRNA condition. After 7 days wells were checked for the presence of individual colonies. Any wells containing multiple colonies were excluded. Single colonies were then expanded up to $T175^2$ flasks (Corning) and frozen down as previously described and assessed for knockdown at both the RNA and protein level using the methods as previously described.

2.10.3 Generation of CRISPR Cell Lines

HCT116 and LS174T HIF1α and HIF2α knockout cell lines were generated using the CRISPR-Cas9 Genome Engingering Edit-R™ Inducible Lentiviral Cas9 Nuclease (Dharmacon) to allow for the inducible expression of the Cas9 nuclease following the addition of doxycycline to the system. HCT116 and LS174T cells underwent lentiviral transduction of the Cas9 nuclease followed by blasticidin selection. Stably transduced pools then underwent clonal cell isolation and expansion followed by lentiviral transduction of a modified sgRNA against HIF1α and HIF2α (Sigma). Cells underwent futher selection and expansion with puromycin. Cell lines were then validated for knockout at both the protein and RNA level following doxycycline induction via q-RT-PCR and immunoblot. Tammy Potgeier, a PhD student in the McIntyre Laboratory, carried out this laboratory work.

2.11 Immunocytochemical Staining

Cells were fixed in 4 % paraformaldehyde (PFA) for 10 minutes at room temperature followed by three washes in PBS 0.1% Tween [v/v]. Cells were permeabilised in 1x PBS 0.2% Triton X 100 [v/v] for 5 minutes at room temperate followed by 3 washes in 1x PBS 0.1% Tween [v/v]. Cells were blocked for 1 hour at room temperature in 1% BSA [w/v] in 1x PBS containing 0.1% Triton X 100 [v/v]. Cells were again washed three times in 1x PBS 0.1% Tween [v/v]. Cells were incubated with the recommended primary antibody dilution in 1% BSA [w/v] 1x PBS containing 0.1% Triton X 100 [v/v] overnight at 4°C. Cells were washed

three times in 1x PBS 0.1% Tween [v/v]. Cells were incubated with the appropriate secondary antibody in 1% BSA [w/v] in 1x PBS containing 0.1% Triton X 100 [v/v] for 40 minutes at room temperature protected from light. Cells underwent a final wash in 1x PBS 0.1% Tween [v/v] and coverslips were mounted onto microscopy slides using ProLong™ Gold Antifade Mountant with DAPI (Invitrogen™). Cells were imaged using the Leica Confocal TCS SPE (Wetzlar, Germany).Details of primary and secondary antibodies used can be found in the appendix.

2.12 3D Cell Culture

2.12.1 Formation of Spheroids

Cells were harvested and counted as previously described. A fresh cell suspension was prepared containing enough cells to seed individual wells of an ultra-low attachment 96 well plate (Corning® Costar®) at 10,000 cells/well with the addition of 5 µL/well of Matrigel® in a final volume of 100 µl according to Vinci et al, 2012 method (Vinci et al, 2012). It was ensured to keep both Matrigel® and the cell suspension containing Matrigel® on ice at all times, and that all plasticware was pre-chilled to avoid polymerisation of the gel. Plates were spun at 300 x g for 10 minutes. The following day a further 100 µL of complete media was added to each well. Spheroids were grown for 7-14 days with media changes occurring every other day. Media changes involved the aspiration of 100 µl of media from each well and replacement with 100 µl of fresh media. Spheroids grown in the presence of IPTG had fresh 1 mM IPTG containing media replaced every day.

2.12.2 Preparation of Spheroids for Immunohistochemistry

Spheroids were aspirated from the 96 well plate and transferred to a 15mL centrifuge tube. Remaining media was aspirated and spheroids were fixed in 5-10 mL of 1x neutral buffered formalin (NBF (Sigma Aldrich)). Spheroids were fixed for a minimum period of overnight. For long term storage spheroids were kept in 70% ethanol at 4°C.

It was necessary to embed spheroids in an intermediate mould of 2% [w/v] agarose gel (Sigma Aldrich). Again using a p1000 pipette tip with the end cut off, 5-6 spheroids were transferred into the mould. Excess NBF was aspirated and replaced with ~200 µL of 2% [w/v] agarose. Agarose was allowed to set for 5 minutes, and the agarose domes containing spheroids were transferred into a labelled tissue cassette. Samples were submerged in 50% [v/v] methanol (Sigma Aldrich) to prevent spheroids from drying out.

Spheroids underwent a 14 hour tissue processing programme using a TP1020 Semi-enclosed Benchtop Tissue Processor (Leica Biosystems, Milton Keynes, UK). Samples were

embedded in paraffin wax and chilled using an EG1160 embedding working station (Leica Biosystems). Once cooled, excess wax was removed using a Paratrimmer™ (Thermo Fisher Scientific). Paraffin blocks were mounted onto a rotary microtome (RM2135, Leica Biosystems) and sectioned to produce ribbons that were 4 µM in thickness. Paraffin ribbons were floated onto a water bath (Thermo Fisher Scientific) and individual sections gently separated using tweezers. Paraffin sections were mounted onto polylysine coated microscopy slides (Thermo Fisher Scientific) and allowed to air dry overnight.

2.13 Immunohistochemistry

Sectioned samples were baked at 60°C for 10 minutes. Xylene (Fisher Scientific) was used to deparaffinise sections, 100% methanol (Sigma Aldrich) was used to rehydrate samples. Samples were taken through the following steps:

Table 2.3. Reagents, time in minutes and number of washed performed to perform rehydration of immunohistochemical samples.

Reagent	Time (minutes)	Number of Washes
Xylene	5	2
100% Methanol	5	2
Tap Water	5	1

Heated mediated antigen retrieval was performed at 95°C for 30 minutes in 1 mM EDTA. Samples were allowed to cool followed by equilibration in 1x PBS. Slides were removed and marked with a hydrophobic barrier pen (ImmEdge PAP Pen (Vector Laboratories, Peterborough, UK)). Sections were incubated with 50 µL of primary antibody for 60 minutes a humidified chamber at room temperature (see the appendix for details of primary antibodies). Sections were washed for 5 minutes in 1x PBS. Sections were incubated with 100 µL of secondary antibody for 60 minutes in a humidified chamber (see the appendix for details for secondary antibodies). Sections were washed for 5 minutes in PBS. Countering staining was performed using the DAB (3, 3-diaminobenzidine tetrahydrochloride) two component enhanced Liquid Substrate System (Sigma Aldrich). Sections were incubated with 100 µL working DAB solution for 7 minutes. Sections were washed in 1x PBS for 5 minutes. Sections were stained with 100µL filtered haematoxylin (Sigma Aldrich) for 3 minutes and washed in running tap water for 5 minutes. Samples were dehydrated by submerging them in glass troughs through the sequence listed in the table below.

Table 2.4. Reagents, time in minutes and number of washed performed to perform dehydration of immunohistochemical samples.

Reagent	Time (minutes)	Number of Washes
100% Methanol	1	3
Xylene	3	2

Samples were mounted with glass coverslips (Menzel-Glaser, Thermo Scientific) using DPX (Sigma Aldrich) and allowed to dry in a fume hood overnight.

2.14 eIF4A2 Human Colorectal Cancer Tissue Micro Array

Human colorectal cancer Tissue Microarrays (TMA) were obtained from the Nottingham and Health Sciences Biobank and were covered by the North West 7 Research and Ethics Committee number 15/NW/0685. TMAs were stained using the standard histological techniques as previously described with the exception of undergoing an additional blocking stage in 3% hydrogen peroxide [v/v] for 30 minutes prior to heat mediated antigen retrieval to block endogenous peroxidase activity. Stained TMAs were scanned and recorded using the Ventana DP 200 Slide Scanner (Roche). Images were H-scored by Hannah Bolland and scores reviewed by and independent pathologist for agreement.

2.15 RNA Immunoprecipitation

RNA-immunoprecipitations were performed using the Magna RIP™ RNA-Binding Protein Immunoprecipitation Kit (Merk Millipore, Massachusetts, USA). Throughout the protocol all precautions were taken to minimise RNase contamination. Lysates were prepared from experimental dishes by first washing twice with 10mL of ice cold PBS. Cells were then scraped in 1 mL of 1x PBS into a 1.5 mL centrifuge tube. Cells were collected by centrifugation at 250 x g for 5 minutes at 4°C, the supernatant was discarded. Cell pellets were resuspended in the appropriate amount of Complete RIP Lysis Buffer required which consisted of the following reagents as supplied by the manufacturer:

Table 2.5. Components per sample for RIP lysis buffer.

Reagent	Volume(µL) for one reaction
RIP Lysis Buffer	100
Protease Inhibitor Cocktail	0.5
RNase Inhibitor	0.25

Lysates were incubated on ice for 5 minutes and stored at -80°C. Stock Magnetic Beads Protein A/G were re-suspended by gentle pipetting before use, 50 µL of bead slurry was

used for each individual pull down. Beads were separated using a magnetic separator, supernatant was removed and beads washed two times in 0.5 mL RIP Wash Buffer and brief vortexing. Beads were resuspended in 100 µL of RIP Wash Buffer along with 6 µg of the antibody of interest. Beads and primary antibody were incubated with rotation for 30 minutes at room temperature. Tubes were briefly centrifuged, placed on the magnetic separator and supernatant discarded. Beads were washed twice with RIP Wash Buffer as previously described.

RIP Immunoprecipitation Buffer was prepared using the reagents as follows:

Table 2.6. Components per sample for RIP Immunoprecipitation Buffer.

Reagent	Volume(µL) for one reaction
RIP Wash Buffer	860
0.5M EDTA	35
RNase Inhibitor	5

Beads were placed on the magnetic separator and resuspended in 900 µL of RIP Immunoprecipitation Buffer. Lysates were quickly thawed and centrifuged at 3,000 x g for 10 minutes at 4°C. 100 µL of the supernatant was removed and added to each beads:antibody complex in RIP Immunoprecipitation Buffer. The final volume of the immunoprecipitation reaction was 1 mL. 10 µL of lysate supernatant was removed and placed into a new tube to be stored at -80°C and used at the 'input'. Beads:antibody complex and lysate were incubated together overnight at 4°C with rotation. Tubes were briefly centrifuged, placed on a magnetic separator and supernatant discarded. Beads were washed for a total of six times with cold RIP Wash Buffer as previously described.

Proteinase K Buffer was prepared using the reagents as follows:

Table 2.7. Components per sample for Proteinase K Buffer.

Reagent	Volume(µL) for one reaction
RIP Wash Buffer	117
10% SDS	15
Proteinase K	18

Reagents were added in the order as stated in the table above to reduce the risk of denaturation of proteinase K by the addition of concentrated SDS. Each immunoprecipitate was re-suspended in 150 µL of Proteinase K Buffer. Input samples were thawed and underwent the same treatment. Tubes were incubated at 55°C for 30 minutes with shaking

to digest the protein. Tubes were placed on a magnetic separator and supernatant transferred to a fresh tube. 250 µL of RIP Wash Buffer was added to each tube containing the supernatant. 400 µL of phenol:chloroform:isoamyl alcohol was added to each tube, vortexed for 15 sections and centrifuged at 3,000 x g for 10 minutes at room temperature to separate the phases. 350 µL of the aqueous phase was removed and placed into a new tube containing 400 µL of chloroform. Tubes were centrifuged at 3,000 x g for 10 minutes at room temperature. 300 µL of the aqueous phase was removed and placed into a new tube. To each tube the following reagents were added: 50 µL Salt Solution 1, 15 µL Salt Solution II, 5 µL Precipitate Enhancer and 850 µL of absolute ethanol. Samples were mixed and kept at -80°C overnight to precipitate the RNA.

Samples were centrifuged at 3,000 x g for 30 minutes at 4°C and supernatant carefully discarded. Pellets were washed once with 80% ethanol and centrifuged at 3,000 x g for 15 minutes at 4°C. Supernatant was discarded and pellets air dried. Pellets were resuspended in 11 µL of RNase free water and placed on ice. For long term storage RNA was stored at -80°C.

For analysis of enriched transcripts by qPCR, the total volume of precipitated RNA and 1% input was reverse transcribed and cDNA prepared as previously described. qPCR analysed was then carried out as previously described.

2.16 RIP-qPCR Data Analysis

In order to calculate fold enrichment and percentage input for immunoprecipitated RNAs the following calculations were used:

i. Each RIP RNA fraction Ct value was normalized was the Input RNA fraction Ct value for the same qPCR assay to account for RNA sample preparation differences

$$\Delta Ct\ [normalized\ RIP] = (Ct\ [RIP] - (Ct\ [Input] - Log_2\ (Input\ Dilution\ Factor)))$$

Where, input dilution factor is the fraction of the input RNA saved.

ii. Average the normalized RIP Ct values for each replicate samples

iii. Calculate the % input for each RIP fraction (linear conversion of the normalised RIP ΔCt)

$$\% \ Input = 2^{(-\Delta Ct \ [normalised \ RIP])}$$

iv. Adjust the normalised RIP fraction Ct value for the normalised background [non-specific (NS) antibody] fraction Ct value (first ΔΔCt)

$$\Delta\Delta Ct[RIP/NS] = \Delta Ct \ [normalised \ RIP] - \Delta Ct \ [normalised \ NS]$$

v. Calculate the assay site IP fold enrichment above the sample specific background (linear conversion of the first *ΔΔCt)*

$$Fold \ Enrichment = 2^{(-\Delta\Delta Ct \ [RIP/NS])}$$

2.17 RNA Immunoprecipitation Sequencing (RIP-SEQ)

2.17.1 Sample Collection and Preparation

eIF4A2 RNA immunoprecipitations were performed as previously described. Immunoprecipitated and input mRNA were resuspended in 10 µl of ultrapure water. Experimental mRNA was subjected to illumina mRNA sequencing (150 pair end, 20 million reads) with the following steps performed by Novogene (China).

2.17.2 RNA Quality Control

RNA degradation and contamination was assessed using 1% agarose gels. RNA purity was checked using the NanoPhotometer® spectrophotometer (Implen, CA, USA). RNA integrity and quantitation was assessed using the RNA Nano 6000 Assay Kit of the Bioanalyzer 2100 system (Agilent Technologies, CA, USA).

2.17.3 Library Preparation

A total amount of 1 µg RNA per sample was used as input material for the RNA sample preparations. Sequencing libraries were generated using NEBNext® Ultra™RNA Library Prep Kit for Illumina (NEB, USA) following manufactures recommendations, index codes were added to attribute sequences to each sample. Briefly mRNA was murified from total RNA using poly-T oligo attached magnetic beads. Fragmentation was carried out using divalent cations under elevated temperature in NEBNext First Strand Synthesis Reaction Buffer (5X). First strand cDNA was synthesis using random hexamer primer and M-MuLV Reverse Transcriptase (RNase H-). Second strand cDNA synthesis was subsequently performed using DNA Polymerase I and RNase H. Remaining overhands were converted into blunt ends via exonuclease/polymerase activities. After adenylation of 3’ ends of DNA fragments,

NEVNext Adaptor with hairpin loop structure were ligated to prepare for hybridization. In order to select cDNA fragments of 150-200 bp in length, the library fragments were purified with AMPure XP System (Beckman Coluter, Beverly, USA). Subsequently 3 µl of USER Enzyme (NEB,USA) was used with size selected, adaptor ligated cDNA at 37°C for 15 minutes followed by 5 minutes at 95°C before PCR. PCR was performed with PHusion high Fidelity DNA polymerase, Universal PCR primers and Index (X) Primer. PCR products were then purified using the AMPure Xp System. Library concentrations were assessed using the Qubit 2.0 fluorometer (Life technologies) and diluted to 1 ng/µl before check insert sizes using the Agilent Bioanalyzer 2100 system.

2.17.4 Clustering and Sequencing

Clustering of index coded samples were performed on cBot Cluster Generation System using PE Cluster Kit cBot-HS (Illumina) according to the manufacturer's instructions. Following cluster generation, library preparations were sequenced on an Illumina platform and 125bp/150 bp paired-end reads were generated.

2.17.5 Data Analysis

Raw reads of FASTQ format were first processed through in-house pearl scripts. Clean reads were obtained by discarding the following reads: 1) reads with adaptor contamination 2) reads where uncertain nucleotides constitute more than 10% of either read 3) reads where low quality nucleotides (base quality <20) constitute more than 50% of the read. All downstream analysis was based on clean data with high quality reads.

Reference genome and gene model annotation files were downloaded from genome website directly. An index of the reference genome was built using Bowtie v2.2.3 and paired-end clean reads were aligned to the reference genome using TopHat v2.0.12.

HTSeq v0.6.1 was used to count the reads mapped to each gene. The Fragments per Kilobase of transcript per Million mapped reads (FPKM) of each gene was calculated based on the length of the gene and reads count mapped to this gene.

Differential expression analysis of 2 conditions/2 biological repeats per condition was performed using the DEseq R package (1.18.0). DESeq provide statistical routines for determining differential expression in digital gene expression data using a model based on the negative binomial distribution. The resulting P-values were adjusted using the Benjamini and Hochberg's approach for controlling the false discovery rate. Genes with an adjusted P-value <0.05 found by DEseq were assigned as differentially expressed.

2.17.8 GO and KEGG Analysis of Differentially Expressed Genes

Gene Ontology (GO) enrichment analysis of differentially expressed genes was performed using the GOseq R package, in which gene length bias was corrected for. GO terms with corrected P-values of <0.05 were considered significantly enriched by differential expressed genes. KEGG is a database resource for understand high level functions and utilities of the biological system such as the cell, organism and ecosystem from molecular level information, particularly large scale molecule datasets generated by genome sequencing. KOBAS software was used to test the statistical enrichment of differentially expressed genes in KEGG pathways.

2.18 Xenograft Experiments

HCT116 shCTL, HCT116 sh69 and HCT116 sh84 were luciferase labelled and taken forward into a xenograft experiment using CD-1 female mice, 6-7 weeks old and injected via an intra-peritoneal or sub cutaneous route ($2x10^6$ cells/mL). Tumour growth was measured via IVIS imaging for luciferase reporter expression or via the use of callipers to measure the length, width and height of tumour every 3 days. Images were taken directly after implantion and then on a weekly basis. 10mM IPTG was provided in the drinking water and given ad-libitum to all groups with the addition of Ribena to mask flavours. An optical post-mortem was used to identify spread into surrounding organs and tumour were split 50:50 into neutral buffered formalin for fixation or snap frozen. All animal work was carried out under a Home Office Licence, project number P435A9CF8.

2.19 Statistical Analysis

Statistical analysis and graphs were performed using GraphPad Prism v6.0 (GraphPad, La Jolla, CA, USA). Results are plotted as mean values with standard error. Statistical tests and the number of repeats are described in the figure legends. Students t-test was used for two sample analyses and normal distributions were assumed. No samples or experimental repeats were excluded from analysis. All expeirments are three separate experimental repeats unless stated otherwise. *p<0.05, **p<0.01, ***p<0.001. n=3.

3.0 eIF4A2 Hypoxic Expression and Regulation in Colorectal Cancer

3.1 Introduction

3.2Regulation of Gene Expression under Hypoxic Conditions

The transcriptional response to hypoxic stress is orchestrated by the family of HIF transcription factors (Dengler et al, 2015). As previously described in the introduction chapter of this thesis, under hypoxic conditions, the enzymatic activity of the oxygen dependent PHDs are inhibited, the ODD of HIF1α is not hydroxylated, and thus stabilized. HIF1α translocates to the nucleus where it dimerises with HIF1β and associates with its cofactors CBP/p300 (Majmundar et al, 2010). This HIF heterodimer then binds to the hypoxic response elements (HRE) in the promoter region of hypoxia response genes leading to upregulation of the target gene (Majmundar et al, 2010). Genes that are transcriptionally activated by HIF are essential for cell survival as they regulate phenotypic changes that allow for adaptation and survival under hypoxic stress. These adaptive processes include encompass many of the hallmarks of cancer including metabolism, pH regulation, angiogenesis, invasion, metastasis and evasion of apoptosis (Semenza, 2003).

Key examples of HIF dependent transcripts are those central to the metabolic re-wiring observed in hypoxic cancer cells include the upregulation of glucose transporters such as glucose transporter 1 and 3 (*GLUT1, GLUT3*) and glycolytic enzymes aldolase A (*ALDOA*), enolase 1 (*ENO1*) hexokinase 1 (*HK1*) and lactate dehydrogenase (*LDHA*) (Semenza, 2003). A consequence of increased glycolysis in hypoxic cells leads is the accumulation of its metabolic end products lactic acid and CO_2, in order to prevent acidification of the intracellular environment hypoxic cells also upregulate key genes involved in the regulation of pH (Sedlakova et al, 2014). *CA9*, a transmembrane zinc metalloenzyme that catalyses the reversible hydration of CO_2 to bicarbonate and proton ions is a notable example of this (Sedlakova et al, 2014). Similarly to the glucose transporters, upregulation of CA9 under hypoxic conditions occurs so reliably in hypoxic cells and is seldom expressed in normal tissues, it is now regarded as the most promising endogenous marker for hypoxia (Kaluz et al, 2009). Additional HIF dependent transcripts that are reliably and consistently upregulated under hypoxic conditions that promote cell survival include the master regulator of angiogenesis, the pro-angiogenic vascular endothelial growth factor A (VEGF-A) and its receptor VEGFR-1 (Semenza, 2003).

3.3 Transcriptional Co-operation with HIF

However transcriptional regulation by hypoxia is not always dependent solely on the HIF transcription factors alone (Villar et al, 2012). HIF transcriptional activation is dependent on the activity of its binding with additional co-factors which are recruited together with HIF1α and HIFβ to form an active complex, this process is mediated by the transactivation domains present within the C-terminus of the HIF proteins (Villar et al, 2012). HIF has been shown to functionally cooperate with a variety of transcription factors including p300/CBP, SRC-1, TIF-2, STAT3, Ets-1 and AP1 (Loboda et al, 2010) (Pawlus et al, 2014) (Elvert et al, 2003). As an example, STAT3 activates HIF1α target genes by binding to HIF1α target gene promoters, recruiting coactivators such as CBP and p300 to form enhanceosome complexes (Pawlus et al, 2014). These higher order complexes bind cooperatively to a promoter region and are necessary for the fine tuning of transcriptional activation (Pawlus et al, 2014). Both STAT3 and USF2 were shown to bind to the promoter region of HIF target genes and recruit histone acetylases p300 and CBP (Pawlus et al, 2013). Furthermore many other transcription factors have been shown regulate gene expression in response to hypoxia including: NFkβ, STAT3, C/EBP, SMAD3, Elk1, AP-1, p53, c-MYC, and GATA binding factor (Cummins and Taylor, 2005). As such, it is important to identify additional transcription factors that may be cooperating with HIF or, preceding HIF binding, in order to fine tune the gene regulation of eIF4A2 under hypoxic conditions.

3.4 RNA Helicase Gene Expression under Hypoxic Conditions

RNA helicases regulate a variety of processes including RNA metabolism, RNA export, translation initiation, translation termination, ribosome biogenesis, mRNA degradation and the formation of the spliceosome (Linder et al, 2006). As described earlier in the introduction section of this thesis, RNA helicases have been demonstrated to be over expressed in a variety of cancers and associated with poor patient outcome.

As previously described, the upregulation of a gene under hypoxic conditions demonstrates a potential requirement for that gene to promote hypoxic cell survival. With regards to eIF4A1 and eIF4A2, it is important to note that in the literature there is a lack of research distinguishing the distinct roles of eIF4A1 and eIF4A2 with the majority of research focusing on eIF4A1 (Raza et al, 2015). It is important to note that previous studies have demonstrated that eIF4A1 remains unaffected by hypoxia in HCT116 cells exposed to either 16 or 40 hours 1% O_2 (Lai et al, 2016). An additional study also confirmed that eIF4A1 was not found to accumulate to the hypoxic polysome of HEK293 cells following exposure to 1% 0_2 for 9 hours (Chen et al, 2019). In comparison to eIF4A1, eIF4A2 seems to have been

neglected in the literature. Particularly in hypoxia, a literature search reveals only 1 paper published on eIF4A2 in hypoxia. The paper demonstrated that eIF4A2 mRNA was upregulated under both hypoxic and acidosis conditions and additionally, simultaneous acidosis and hypoxia, a feature commonly found in solid tumours. This effect was observed across a panel of 5 different human squamous carcinoma cell lines. However the paper only investigates eIF4A2 expression and the mRNA level and provides no further investigation into the role of eIF4A2 in hypoxia (Sorensen et al, 2015).

In additional to its role in translation initiation, eIF4A2 has been demonstrated to be the only component of the eIF4F complex required for miRNA mediated translation repression (Meijer et al, 2013). It has been demonstrated that only eIF4A2 co-immunoprecipitates with CNOT7, a component of the CCR4-NOT complex (Meijer et al, 2013). Furthermore the same study uncovered a correlation between the degree of 5'UTR secondary structure and the presence of miRNA target sites within their 3'UTR. An additional conclusion from the same study was that transcripts with short unstructured 5'UTRs are unaffected by miRNA mediated regulation (Meijer et al, 2013). This paper supports the notion that eIF4A2 may possess dual roles in translation, acting as both an activator of translation, via unwinding of complex 5'UTRS, and as a repressor of translation, by recruiting the CCR4-NOT complex to target mRNAs (Meijer et al, 2013). However the mechanism as to how eIF4A2 selects its transcripts has never been uncovered. Furthermore, this work was performed using the HeLa cell line and does not investigate the binding of eIF4A2 to CNOT7 in a malignant cell nor under hypoxic conditions.

Despite emerging as a promising anti-cancer target as described in the introduction section of the thesis, very few papers have investigated the expression and role of RNA helicases under hypoxic conditions. In fact a literature search revealed only 4 RNA helicases with experimental evidence linking their expression and regulation to hypoxia and regulation via HIFs. DEAD-box polypeptide 3 (DDX3) mRNA was significantly increased 2 fold under hypoxic conditions relative to normoxic controls at 8, 12 and 24 hours exposure to hypoxia (1% O_2) in the MCF-7 breast cancer cell line (Botlagunta et al, 2011). Furthermore shRNA knockdown of HIF1α and lead to a reduction in the mRNA and protein expression of DDX3 after 12 hours exposure to 200uM $CoCl_2$. YTH domain containing (YTHDC2), a member of the DExD/H-box family of RNA helicases is a target of HIF1α, furthermore, YTHDC2 itself was shown to promote only the translation, not transcription of HIF1α and Twist1 mRNA under hypoxic conditions in HCT116 cell lines following shRNA knockdown of YTHDC2 and exposure to 6,12, and 24 hours 1% O_2 (Tanabe et al, 2016). DEAD-box RNA helicase 6

(DDX6) has been demonstrated to act as a *trans*-acting factor in the IRES dependent translation of VEGF mRNA under hypoxic conditions in cytoplasmic extracts and the MCF-7 breast cancer cell line (de Vries et al, 2013). DDX28 was found to directly interact with HIF2α and act as its negative regulator by preventing its interaction with the hypoxic isoform of eIF4E, eIF4E2, and leading to a subsequent reduction in eIF4E2 direction translation in glioblastoma cell lines (Evaelou et al, 2019). DDX28 expression was found to be significantly downregulated under hypoxic conditions in U87 cells exposed to hypoxia (1% O_2) for 24 hours) (Evaelou et al, 2019). Such evidence supports the hypothesis that RNA helicases play a crucial role in the hypoxic cell survival.

In the following chapter, the hypoxic expression, regulation and binding partners of eIF4A2 in colorectal cancer cells was investigated and the following hypothesis tested.

I hypothesise that eIF4A2 will be upregulated at the RNA and protein level following exposure to hypoxic (1% O_2) conditions and this is due to the presence of a HRE within the promoter region of the eIF4A2 sequence. Furthermore I hypothesise that eIF4A1 will remain unaffected by hypoxic conditions. Secondly I hypothesis that eIF4A2 and not eIF4A1 will be under the transcriptional control of either HIF1α or HIF2α. Finally I hypothesis that eIF4A2 displays increased binding to the CCR4-NOT complex under hypoxic conditions and binds to novel protein binding partners under hypoxic conditions that may begin to investigate how eIF4A2 selects its target transcripts.

I will test the hypothesis using the following aims:

1- Investigate eIF4A1 and eIF4A2 mRNA expression following exposure to a normoxia and hypoxia time course (1% O_2) measured via qPCR.
2- Investigate eIF4A1 and eIF4A2 protein expression following exposure to a normoxia and hypoxia time course (1% O_2) measure via immunoblot.
3- Investigate the impact of HIF1α and HIF2α inhibition on the transcriptional regulation of eIF4A1 and eIF4A2 via siRNA knockdown of HIF1α and HIF2α in a colorectal cancer cell line following exposure to 24 hours normoxia and hypoxia (1% O_2) measured via qPCR
4- Investigate the predicted transcription factor binding partners of eIF4A1 and eIF4A2 using *in silico* analysis of the genomic sequence of eIF4A1 and eIF4A2 promoter region.

5- Investigate the transcriptional regulation of eIF4A1 and eIF4A2 by HIF1α and HIF2α via siRNA knockdown of HIF1α and HIF2α in a colorectal cancer cell line following exposure to 24 hours normoxia and hypoxia (1% O_2) measured via immunoblot.
6- Demonstrate expression of eIF4A2 within the hypoxic core or peri-necrotic regions of colorectal 3D tumour spheroids via immunohistochemistry.
7- Investigate the interaction between eIF4A2 and CNOT7, a component of the CCR4-NOT complex in a colorectal cancer cell line, which has previously been demonstrated to bind in HeLa cells via co-immunoprecipitations and immunoblot.

3.5 Expression of eIF4A1 and eIF4A2 under Hypoxic Conditions in Colorectal Cancer Cells

3.5.1 eIF4A1 and eIF4A2 Hypoxic mRNA Expression

In order to first characterise the hypoxic expression of eIF4A1 and eIF4A2 mRNA, a panel of colorectal cancer cell lines (HCT116, LS174T, HT29, DLD1, SW620) were exposed to hypoxia (1% O_2) or normoxia (20% O_2) for 24, 48 and 72 hours and eIF4A1/2 mRNA expression analysed via qRT-PCR. eIF4A2 was significantly upregulated under hypoxic conditions when compared against the corresponding normoxic control time point across all colorectal cell lines tested (HCT116; 24hr $p<0.01$. 48hr $p<0.001$, LS174T; 24,48,72hrs $p<0.001$, HT29; 48,72hrs $p<0.01$, DLD1; 48hr $p<0.05$, SW620; 48hr $p<0.05$) as shown in Figure 3.1. HCT116 (Figure 3.1, A) and LS174T (Figure 3.1, B) cell lines displayed the highest induction of eIF4A2 under hypoxic conditions, demonstrating an 8 fold (HCT116 48hr) and 5 fold (LS174T 72hr) increase compared to the normoxic control respectively. Interestingly HCT116 eIF4A2 mRNA expression falls down to levels similar to the normoxic control at 72 hours (Figure 3.1,A).

In contrast, eIF4A1 was not upregulated at the mRNA by hypoxia and in some cases was significantly down regulated under hypoxic conditions (HCT116; 72hrs $p<0.05$, HT29; 24,48hrs $p<0.05$, 72hrs $p<0.01$, DLD1; 24, 48, 72hrs $p<0.001$) as shown in Figure 3.2.

The mRNA expression of *CA9* was used a positive control throughout the experiments to confirm the cells were hypoxic as shown in Figure 3.3. As described into the introduction section of this results chapter, *CA9* is a well-known HIF1α target gene found to be consistently and reliably upregulated at the mRNA and protein level under hypoxic conditions. *CA9* was significantly upregulated in all cell lines across all hypoxic time points tested (HCT116; 24hr $p<0.05$, 48hrs, $p<0.01$, 72hrs $p<0.001$, LS174T; 24,48,72hrs $p<0.001$, HT29; 24,48,72hrs $p<0.001$, DLD1; 24,48,72hrs $p<0.001$, SW620 24,48.72hrs $p<0.001$) as shown in Figure 3.3

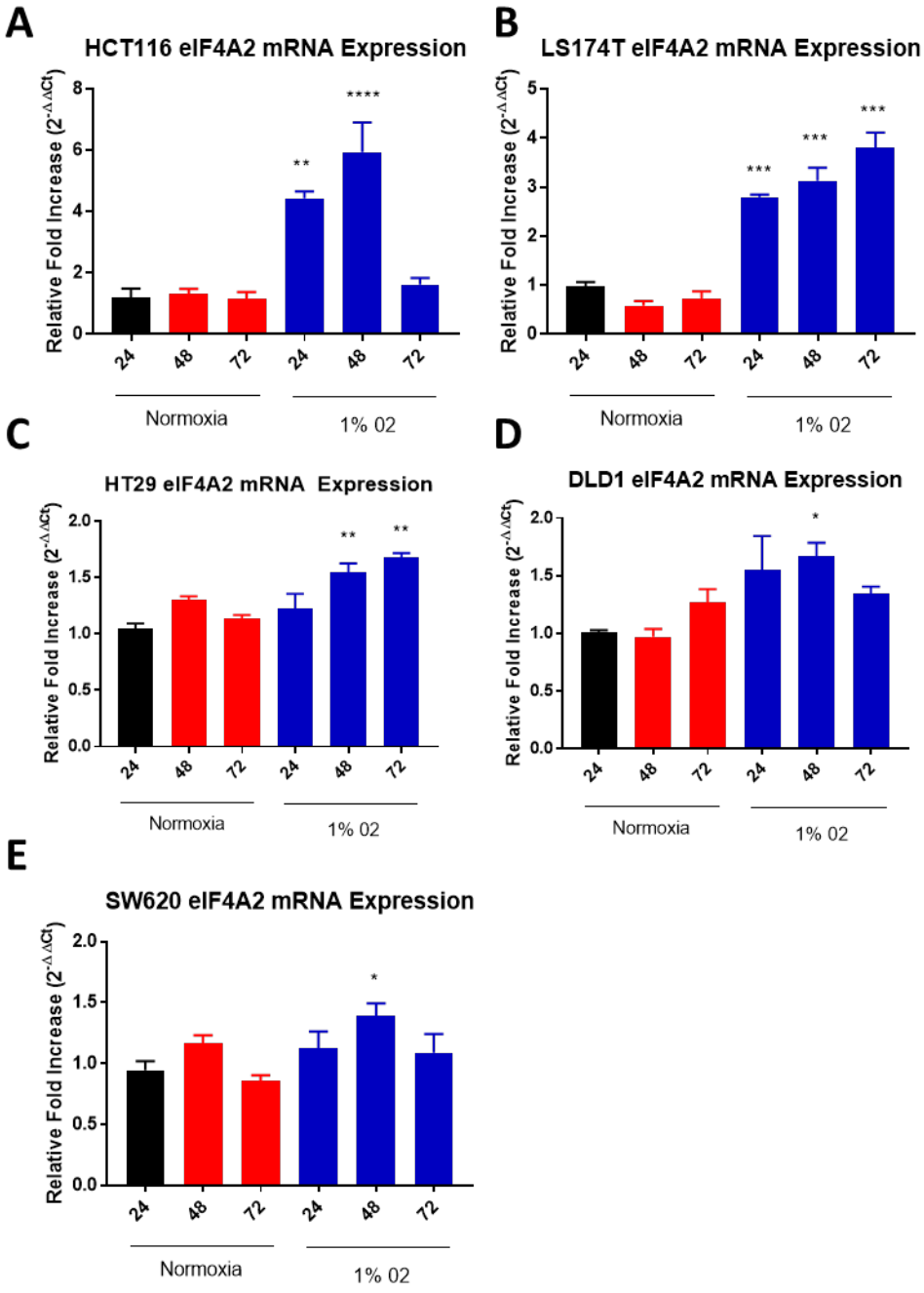


Figure 3.1 eIF4A2 mRNA expression under hypoxic conditions across a panel of colorectal cancer cell lines. eIF4A2 mRNA expression was measured via qRT-PCR following exposure to 24,48,72 hours normoxia (20 % O_2) or hypoxia (1% O_2). (A) HCT116 (B) LS174T (C) HT29 (D) DLD1 (E) SW620. Error bars indicate ± SEM. Data were analysed for significance by t-test comparing each hypoxic time point against its normoxic control time point. *p<0.05, **p<0.01, ***p<0.001. n=3.

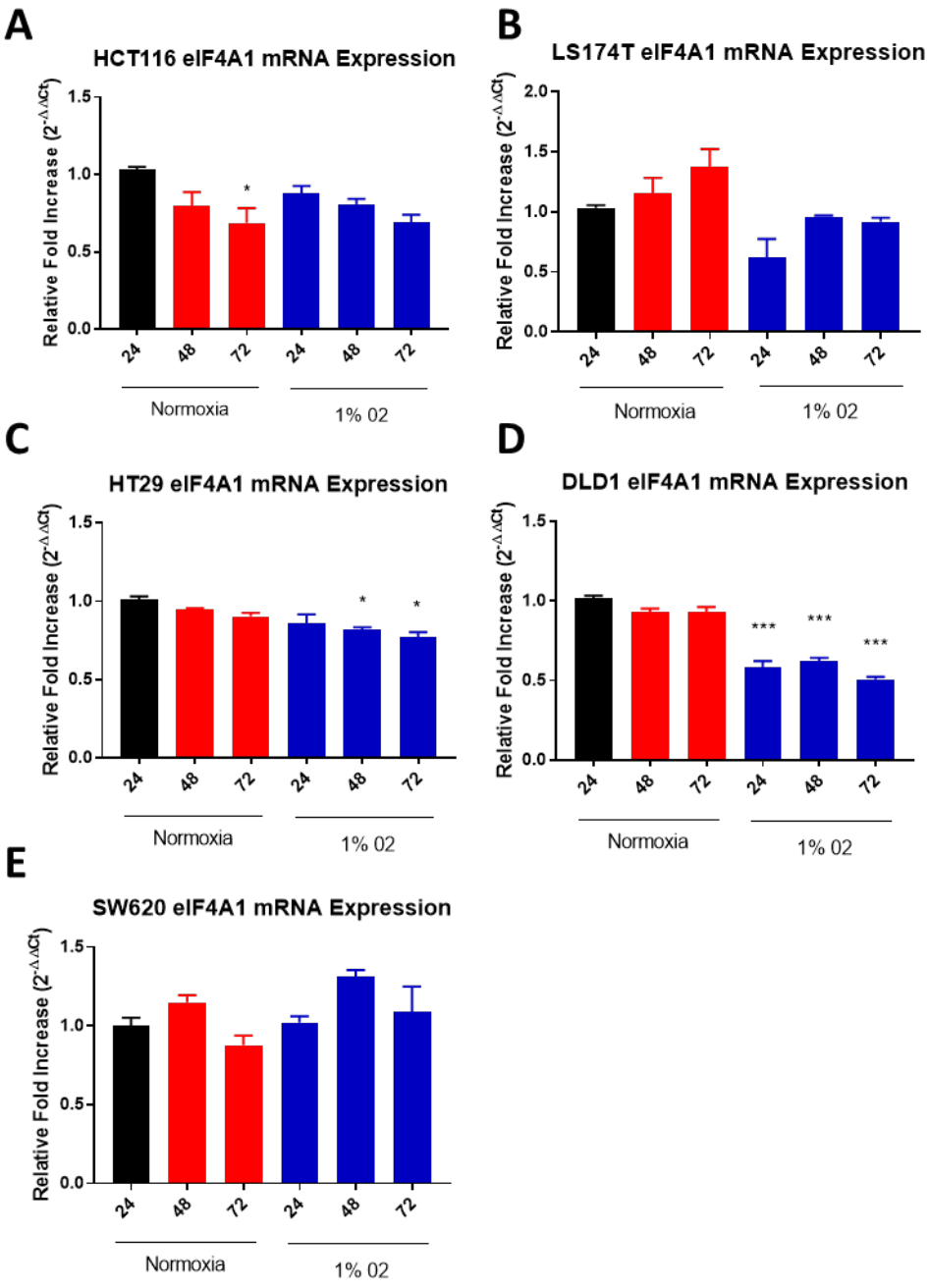


Figure 3.2. eIF4A1 mRNA expression under hypoxic conditions across a panel of colorectal cancer cell lines. eIF4A1 mRNA expression was measured via qRT-PCR following exposure to 24,48,72 hours normoxia (20 % O_2) or hypoxia (1% O_2). (A) HCT116 (B) LS174T (C) HT29 (D) DLD1 (E) SW620. Error bars indicate ± SEM. Data were analysed for significance by t-test comparing each hypoxic time point against its normoxic control time point. *p<0.05, **p<0.01, ***p<0.001. n=3.

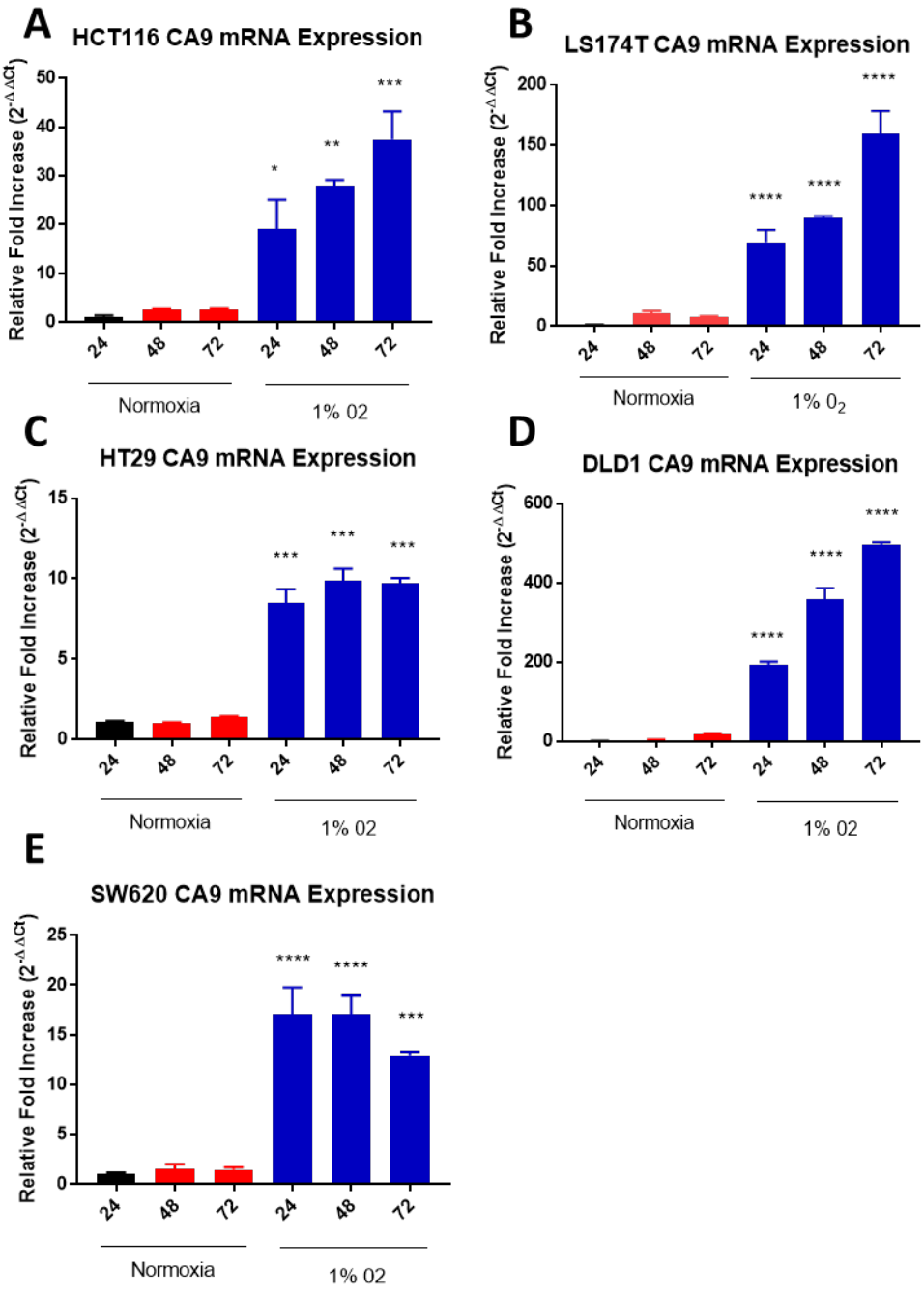


Figure 3.3. CA9 mRNA expression under hypoxic conditions across a panel of colorectal cancer cell lines. CA9 mRNA expression was measured via qRT-PCR following exposure to 24,48,72 hours normoxia (20% O_2) or hypoxia (1% O_2). (A) HCT116 (B) LS174T (C) HT29 (D) DLD1 (E) SW620. Error bars indicate ± SEM. Data were analysed for significance by t-test comparing each hypoxic time point against its normoxic control time point. *p<0.05, **p<0.01, ***p<0.001. n=3.

3.5.2 eIF4A1 and eIF4A2 Hypoxic Protein Expression

In order to characterise the hypoxic expression of eIF4A1 and eIF4A2 protein, a panel of colorectal cancer cell lines (HCT116, LS174T, HT29, DLD1, SW620) were exposed to hypoxia (1% O_2) or normoxia (20% 0_2) for 24, 48 and 72 hours and eIF4A1/2 mRNA expression analysed via immunoblot as previously described as shown in Figure 3.4. eIF4A2 was not seen to be significantly upregulated under hypoxic conditions, however a slight increasingly trend was observed at 24 hours and 48 hours hypoxia in comparison to the normoxic control. Despite the lack of significant upregulation, eIF4A2 was seen to be maintained and slightly increased under hypoxic conditions, suggesting that it may still play an important role in hypoxic cell survival. In contrast, eIF4A1 was seen to follow a generally decreased trend in expression with increasing duration under hypoxic conditions. In particular, eIF4A1 expression was shown to decrease specifically at 48 hours 1% O_2 in LS174T cells.

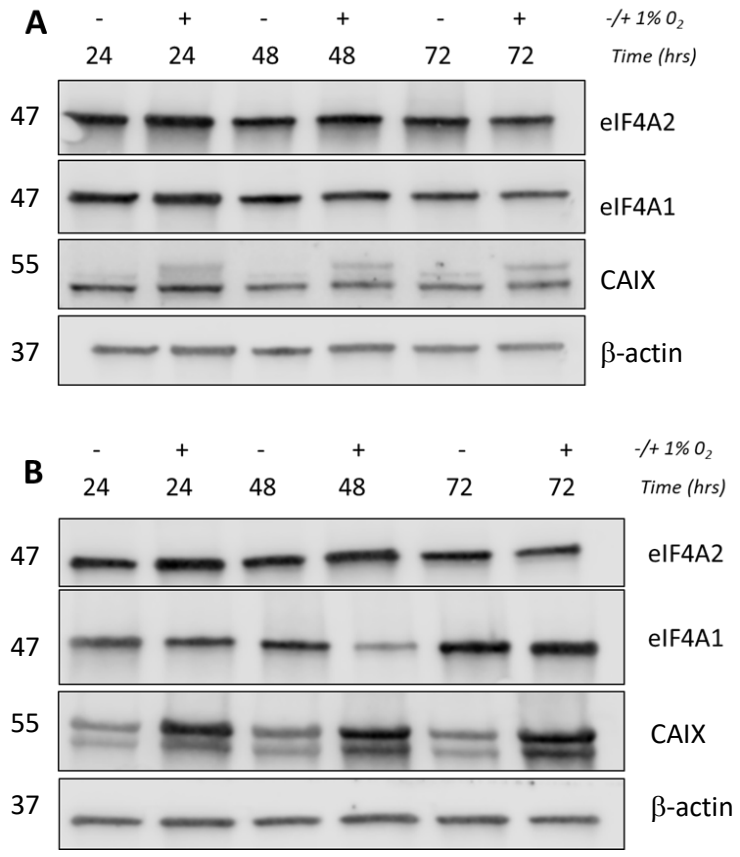


Figure 3.4. Representative immunoblot images of eIF4A1 and eIF4A2 protein expression following hypoxic time course. Cells were exposed to 24, 48 or 72 hours normoxia (20% O_2) or hypoxia (1% O_2). eIF4A2, eIF4A1, CAIX, and β-actin were analysed via immunoblot. (A) HCT116 (B) LS174T. Molecular weights in kDa are displayed on the left of the blot. n=3.

3.5.3 eIF4A1 and eIF4A2 Hypoxic Localisation

Despite the lack of significant upregulation of eIF4A2 under hypoxic conditions, it is possible that eIF4A2 displays differential localisation within the cell under hypoxic conditions. Differential localisation of eIF4A1/2 may be indicative of a different function under hypoxic conditions. LS174T cells were plated onto glass coverslips, exposed to 24 hours normoxia (20% 0_2) and hypoxia (1% 0_2) and underwent immunofluorescent staining of eIF4A1 and eIF4A2. Nuclei were stained using DAPI.

As displayed in Figure 3.6, under normoxic conditions eIF4A2 was found to be localised to the cytoplasm as expected. However under hypoxic conditions eIF4A2 was observed to localise to granular structures within the cytoplasm as highlighted by the white arrow. As described in the introduction section of this thesis, the SUMOylation status of eIF4A2 has previously been shown to be a crucial component of stress granule formation; however these experiments had only been performed following heat shock, ionising radiation and arsenite treatment, and not in hypoxia. The observation that eIF4A2 is localised to these cytoplasmic structures under hypoxic conditions is suggestive of stress granule formation. However further staining with a specific marker of stress granules such as TAI-1 would be required to draw this conclusion.

As displayed in Figure 3.5, eIF4A1 was found to be localised to the cytoplasm but in contrast did not display differential localisation nor localisation to cytoplasmic granules as seen with eIF4A2, upon exposure to hypoxic conditions.

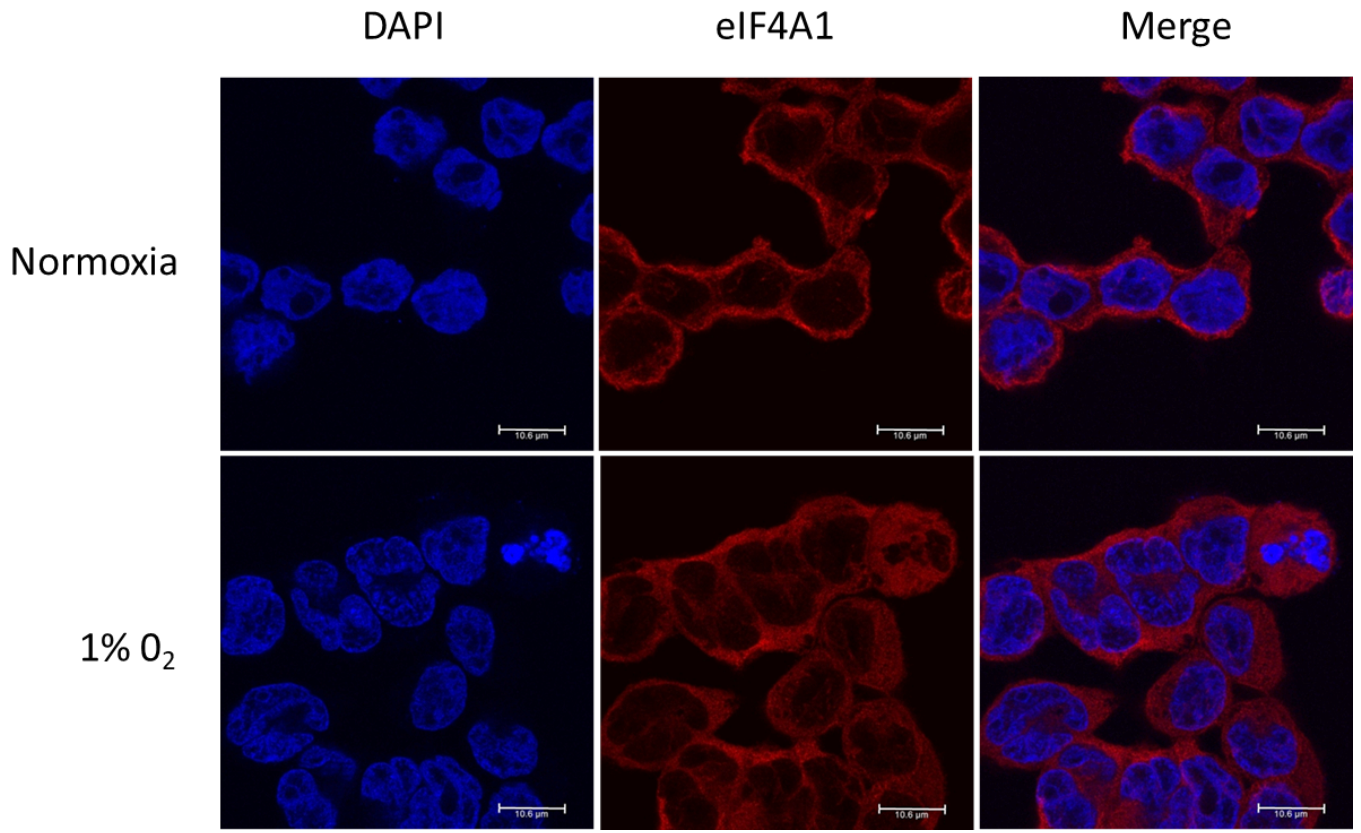


Figure 3.5. Representative images of hypoxic localisation of eIF4A1 protein in colorectal cancer cells. LS174T cells were exposed to 24 hr normoxia (20% O_2) or hypoxia (1% O_2) and stained for eIF4A1 expression using immunofluorescent techniques. Nuclei were staining using DAPI. Images were taken at 40x magnification. Scale bar represents 100µm.

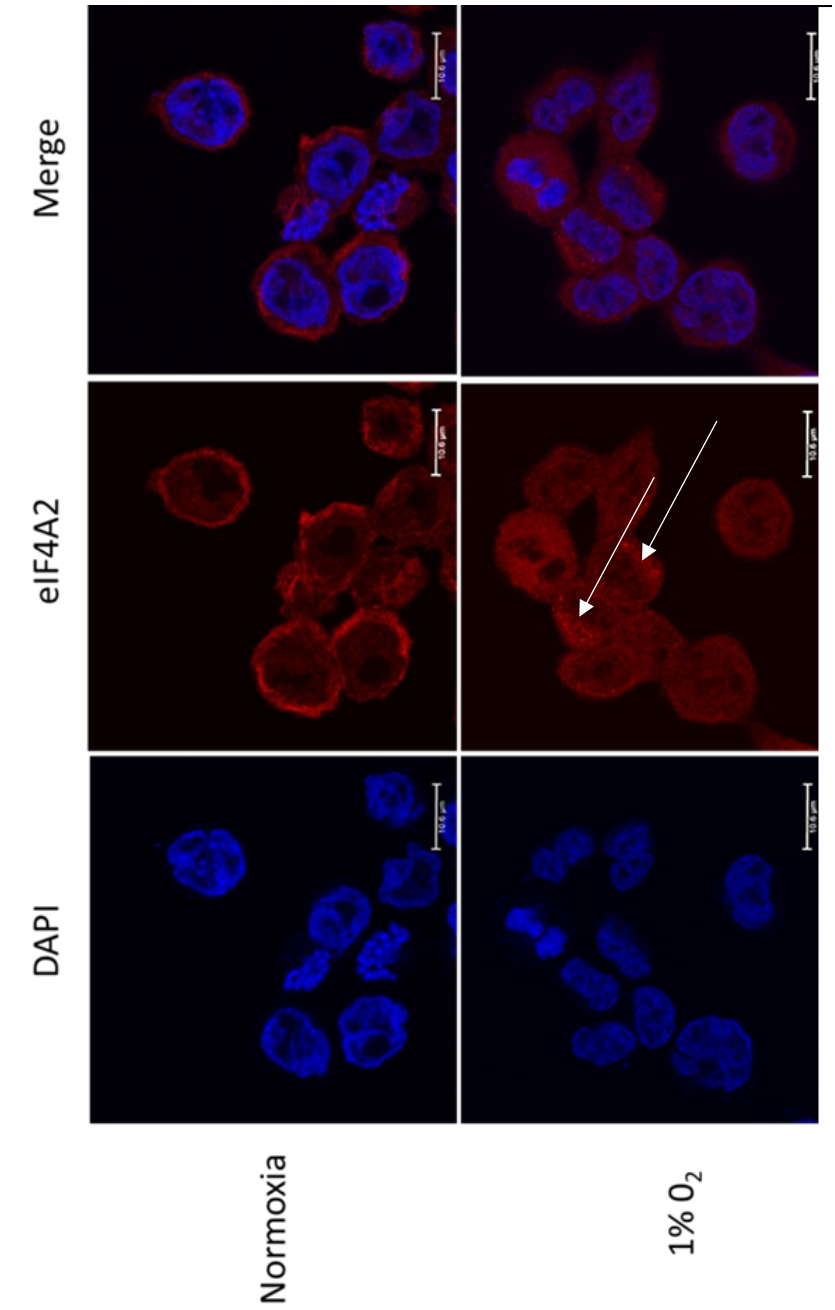


Figure 3.6 Representative images of hypoxic localisation of eIF4A2 protein in colorectal cancer cells. LS174T cells were exposed to 24 hr normoxia (20% O_2) or hypoxia (1% O_2) and stained for eIF4A2 expression using immunofluorescent techniques. Nuclei were staining using DAPI. Images were taken at 40x magnification. Scale bar represents 100µm.

3.5.4 eIF4A2 Expression in Colorectal Cancer Spheroids

Spheroids were used to investigate eIF4A2 expression as they have previously been demonstrated to better recapitulate and mimic the physiological gradients in oxygen and pH, ATP, lactate and glucose distribution in comparison to onvential 2D cell culture (Edmondson et al, 2014). Spheroids were generated using the ultra-low attachment microplates (ULA-plates) originally established by Vinci et al and described earlier in this

thesis (Vinci et al, 2012). Spheroids were then stained for eIF4A2 and CA9 protein expression using standard immunohistochemical techniques.

Spheroids generated were stained with H&E and Ki67 (data not shown) and displayed typical spheroid morphology i.e.: a necrotic core with dividing cells located along the periphery. As expected eIF4A2 was found to be localised to the cytoplasm as demonstrated in previous immunofluorescence experiments and in previously published literature, but unexpectedly found to be expressed across the whole of the spheroid with regions of more intense staining scattered across smaller areas of the spheroid toward the periphery as shown in Figure 3.7, A,B). This pattern of staining does not mimic typical hypoxic regulated proteins such as CAIX which shows more conventional perinecrotic staining found around the hypoxic core (Figure 3.7, C)

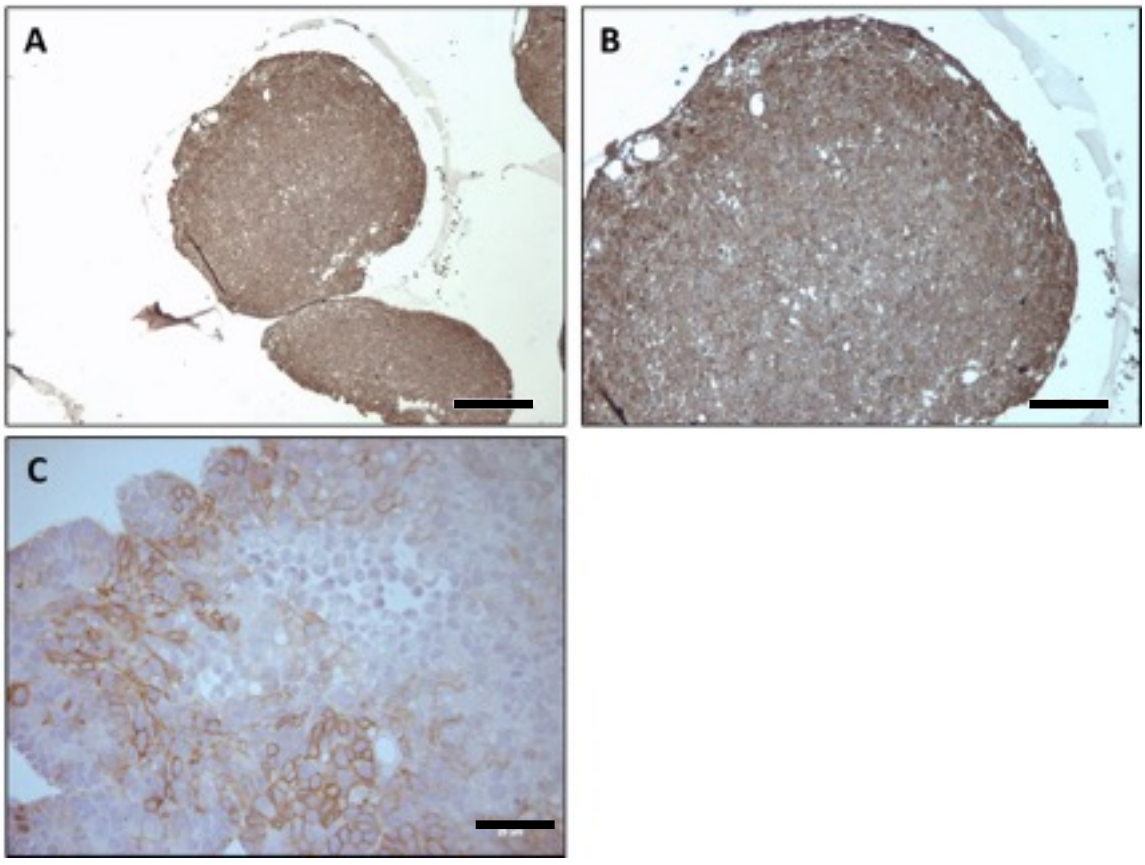


Figure 3.7 eIF4A2 and CAIX staining and localisation of colorectal cancer spheroids. eIF4A2 and CA9 staining are represented by the dark brown stain. (A) HCT116 eIF4A2 staining x10 magnification (B) HCT116 eIF4A2 staining x20 magnification. Scale bars represent 100um (C) HCT116 CAIX staining x20 magnification, scale bar represents 25um. Images are representative of 3 experimental repeats. n=3.

3.5.6 Regulation of eIF4A1 and eIF4A2 by HIF1α and HIF2α

In order to determine the transcriptional regulation of eIF4A2 by HIF1α or HIF2α, first the eIF4A2 genomic sequence was interrogated for the presence of a HRE. Retrospective motif analysis was performed by obtaining the promoter sequence and CDS from Genome Browser (Human Dec. 2013 GRCh38/hg38) and manually searching for the HRE 5'-RCGTG-3' where R denotes either A or G. The eIF4A2 genomic sequence possesses 1 HRE within the 3' exon and 7 within the main coding sequence. As the HRE is located in the 3'exon this suggests eIF4A2 is unlikely to be directly regulated by HIF. In contrast, the eIF4A1 genomic sequence, possesses two HREs in the promoter regions and 1 in the main coding sequence.



Figure 3.8. Flow diagram representing steps followed to indentify hypoxic response element sequence in the promoter and coding sequence of genomic sequences of interest. Retrospective motif analysis was performed by obtaining the promoter sequence and CDS from Genome Browser (Human Dec. 2013 GRCh38/hg38) and manually searching for the HRE 5'-RCGTG-3' where R denotes either A or G. Figure made using BioRender.

Subsequently, knockout of HIF1α and HIF2α was then performed using CRIPSR/CAS9 (HCT116 and LS174T cell lines) of either HIF1α or HIF2α and were generated by another member of the laboratory (Tammy Potgieter, Hypoxia and Acidosis Research Group). HCT116 and LS174T HIF1α and HIF2α KO cell lines were exposed to 24 hours normoxia (20% O_2) or hypoxia (1% 0_2). Knockout was validated at the mRNA level via qRT-PCR as shown in Figure 3.8. Significant knockdown was achieved for both HCT116 HIF1α ($p<0.001$) (Figure 3.8, A) and HIF2α ($p<0.001$) (Figure 3.8, C) and LS174T HIF1α ($p<0.001$) (Figure 3.8, B) and HIF2α ($p<0.001$) (Figure 3.8, D) at the mRNA level in comparison to the non-targeting control. *CA9* was again used as a positive control to ensure the cells were hypoxic and also as a known HIF target gene. Significant *CA9* inhibition was achieved at the mRNA level following knockout of either HIF1α or HIF2α in both HCT116 ($p<0.001$) (Figure 3.8, E) and LS174T ($p<0.001$) (Figure 3.8, F).

Interestingly, opposing effects were observed in the regulation of eIF4A1 and eIF4A2 between HCT116 and LS174T cell lines as shown in Figure 3.9. A significant increase in eIF4A1 mRNA expression was observed in HCT116 following both HIF1α ($p<0.001$) and

HIF2α ($p<0.001$) knockout (Figure 3.9, A). The same significant increase in eIF4A2 expression was also observed following knockout of both HIF1α ($p<0.001$) and HIF2α ($p<0.001$) (Figure 3.9, B). In contrast, the opposite effects were observed for LS174T cells, a significant reduction in eIF4A1 and eIF4A2 mRNA expression was observed following HIF2α inhibition. This suggests that eIF4A1 and eIF4A2 mRNA expression is under the control specifically of HIF2α only in LS174T cell lines.

An additional interesting observation was the observed effect of HIF expression upon knockdown of the opposing HIF isform in HCT116 cells. An increase (nonsignificant) in HIF1α was observed in HIF2α KO cells (Figure 3.8 A), and conversely, a significant increase in HIF2α expression was observed in HIF1α KO cells (Figure 3.8 C). In LS174T cells, a significant increase in HIF1α expression was observed in HIF2α KO cell lines.

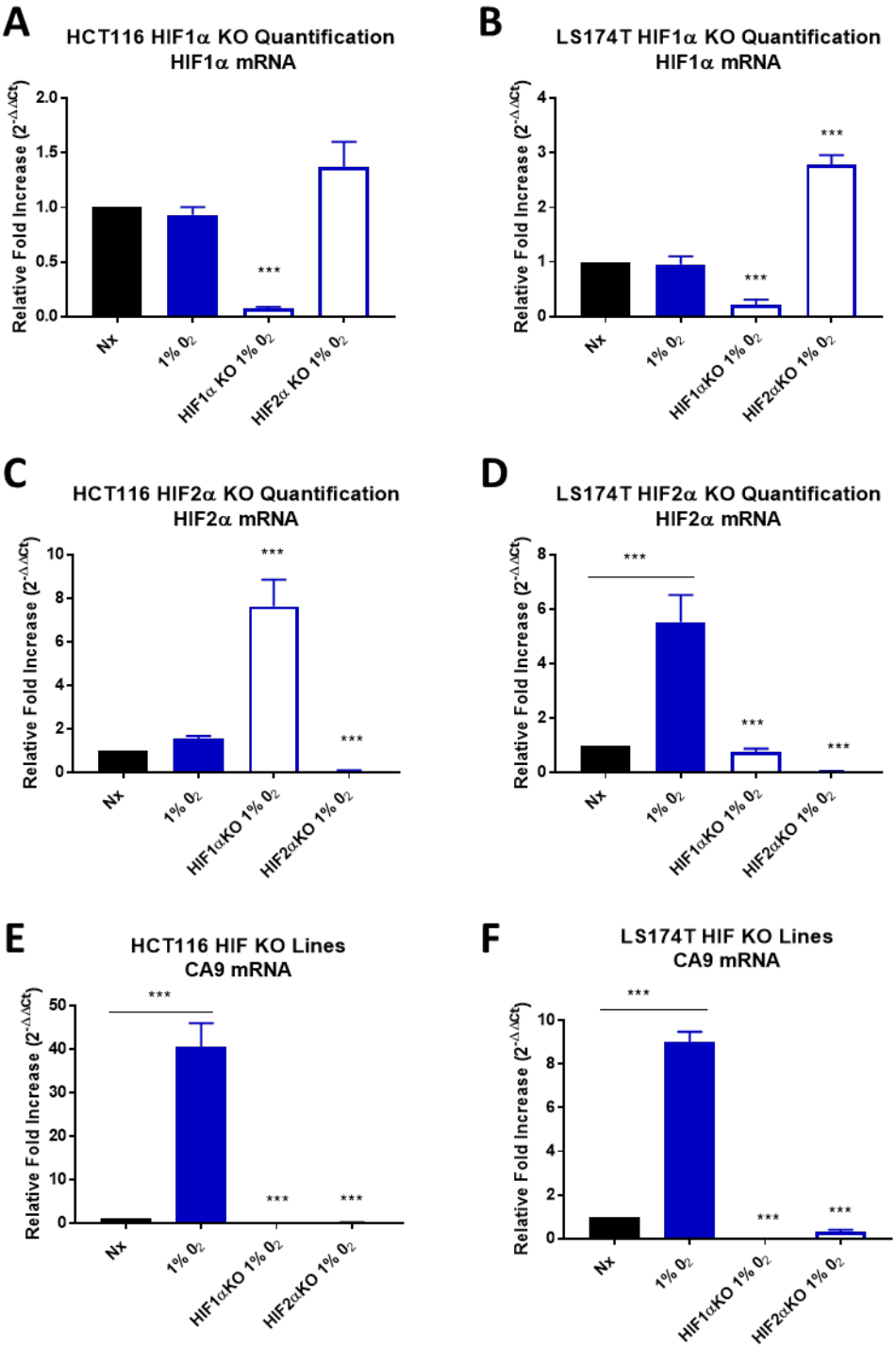


Figure 3.8. Validation of HIF1α, HIF2α knockout of HCT116 and LS174T cell lines at the mRNA level. HIF1α, HIF2α and CA9 mRNA expression was measured via qRT-PCR following exposure to 24 hours normoxia (20% O_2) or hypoxia (1% O_2). (A) HCT116 HIF1α expression (B) LS174T HIF1α expression (C) HCT116 HIF2α expression (D) LS174T HIF2α expression (E) HCT116 CA9 expression (F) LS174T CA9 expression. Error bars indicate ± SEM. Data were analysed for significance by one way ANOVA. *p<0.05, **p<0.01, ***p<0.001. n=3.

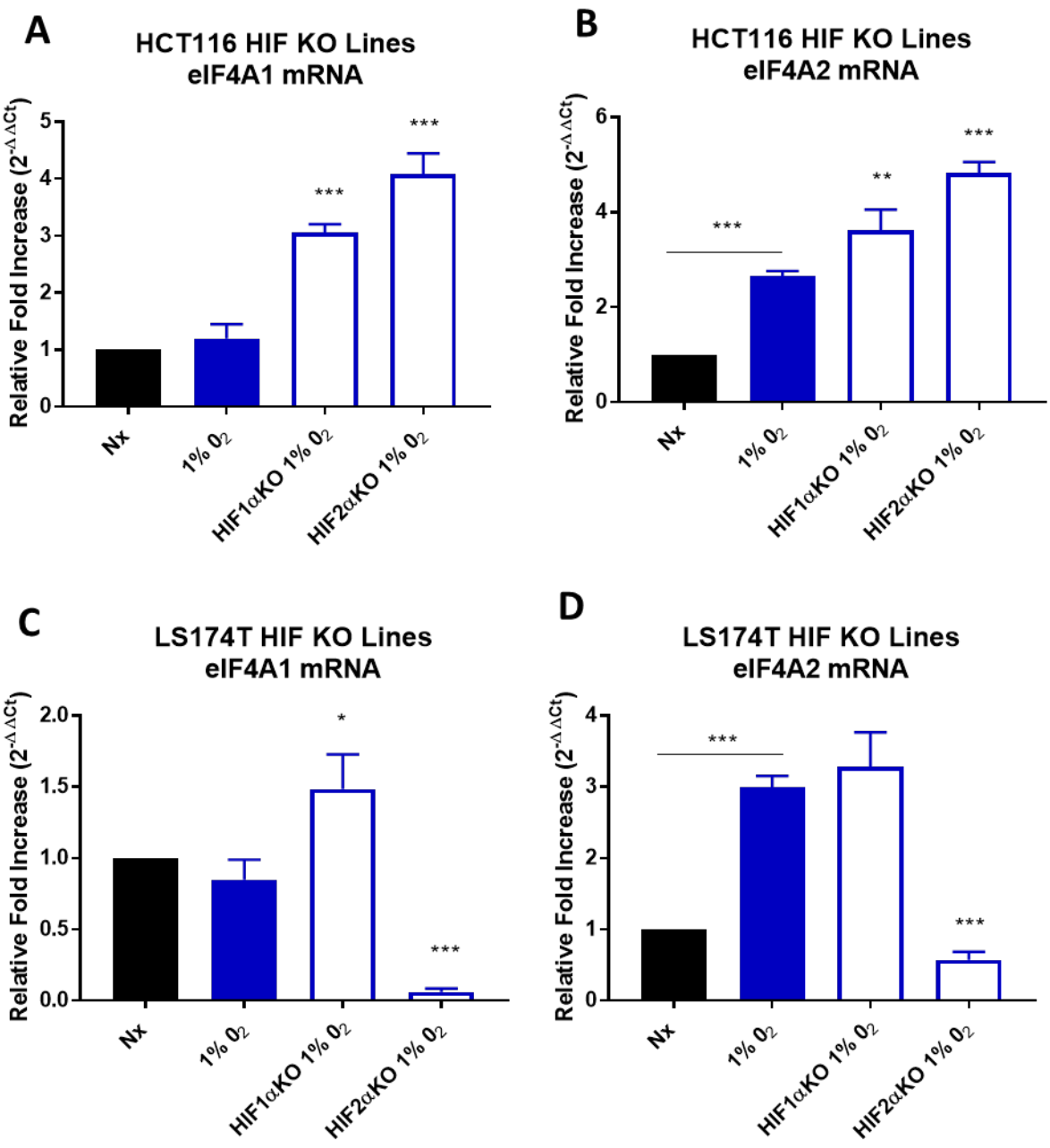


Figure 3.9. eIF4A1 and eIF4A2 mRNA expression following HIF1α or HIF2α knockout in HCT116 and LS174T cell lines. eIF4A1 and eIF4A2 mRNA expression was measured via qRT-PCR following exposure to 24hours normoxia (20% O_2) or hypoxia (1% O_2). (A) HCT116 eIF4A1 expression (B) HCT116 eIF4A2 expression (C) LS174T eIF4A1 expression (D) LS174T eIF4A2 expression. Error bars indicate ± SEM. Data were analysed for significance by one way ANOVA. *p<0.05, **p<0.01, ***p<0.001. n=3.

In order to investigate subsequent protein expression of eIF4A2 following knockout of HIF1α and HIF2α, HCT116 and LS174T KO cell lines were exposed to 24 hours normoxia f(20% O_2) or hypoxia (1% O_2) and protein expression of eIF4A2, HIF1α, HIF2α, CA9 and actin measure via immunoblot as shown in Figure 3.10; HCT116 Figure 3.10 panel A, B, LS174T Figure 3.10, panel C, D. No significant differences were observed in eIF4A2 protein expression following knockout of either HIF1α or HIF2α in HCT116 which in in agreement with previous published literature. A significant reduction in eIF4A2 protein expression was observed in LS174T cells following knockout of only HIF2α ($p<0.01$).

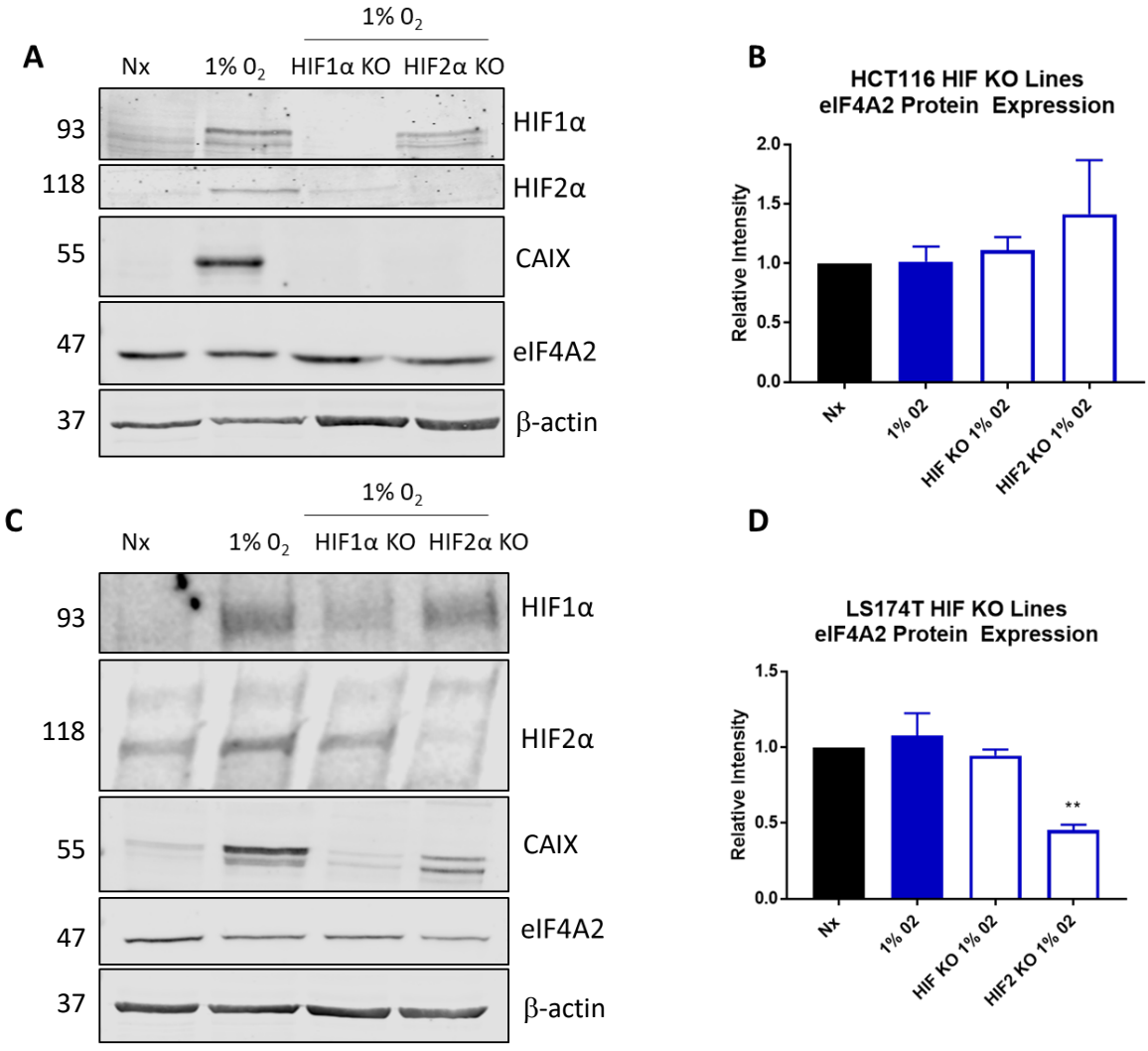


Figure 3.10. eIF4A2 protein expression following HIF1α and HIF2α KO in HCT116 and LS174T cell lines. eIF4A2, HIF1α, HIF2α, CAIX and actin protein expression was measured via immunoblot following exposure to 24hours normoxia (20% O_2) or hypoxia (1% O_2). (A) HCT116 representative blot (B) HCT116 eIF4A2 protein quantification (C) LS174T representative blot (D) LS174T eIF4A2 protein quantification. Error bars indicate ± SEM. Data were analysed for significance by one way ANOVA. *p<0.05, **p<0.01, ***p<0.001. Representative images of 3 experimental repeats of immunoblots. Molecular weights in kDa are displayed on the left hand side of the blot. n=3.

3.5.7 in silico Analysis of eIF4A1 and eIF4A2 Promoter Regions

As previously described in the introduction section of this results chapter, transcriptional regulation by hypoxia is not always dependent solely on the HIF transcription factors. HIF has been shown to functionally cooperate with a variety of transcription factors including p300/CBP, SRC-1, TIF-2, STAT3, Ets-1 and AP1 (Loboda et al, 2010) (Pawlus et al, 2014) (Elvert et al, 2003) (Laderoute, 2005). Based on the opposing effects of HIF1α and HIF2α knockdown on eIF4A1 and eIF4A2 mRNA expression between HCT116 and LS174T cell lines, it was decided to investigate additional potential transcription factor binding sites that may explain such differences in regulation.

To identify potential DNA binding consensus sequences for specific transcription factors within the eIF4A1 and eIF4A2 promoter region, an *in silico* transcription factor binding motif analysis was performed using the Genomatix MatInspector online software. The software compares the genomic nucleotides sequences with known transcription factor binding motifs. The algorithm then assigns a "matrix similarity" score between 0 and 1.00 for any putative binding site matches reflecting the similarity between the genomic sequence and the transcription factor binding motif. A score of 1.00 indicates a perfect match between the genomic DNA sequence and prediction factor binding motif. A score above 0.8 is considered a "good score" with a few nucleotide discrepancies. The tables below display matches for the eIF4A1 and eIF4A2 promoters only with a score of 0.98 or above. This list of predicated transcription factor binding sites demonstrated for eIF4A2 are displayed in Table 3 and for eIF4A1 in Table 3.1 may represent additional transcription factors that are responsible for eIF4A1/2 transcriptional regulation under hypoxic conditions and that may warrant further investigation in the future. Such experiments will be discussed later in the thesis.

Table 3. *In silico* analysis of the eIF4A2 promoter for transcription factor binding sites. The eIF4A2 whole promoter sequence was analysed for transcription factor binding using the MatInspector software. A matrix similarity score of 1.00 is classed as a perfect match.

Transcription Factor	Matrix Sim.
Alternative splicing variant of FOXP1, activated in ESCs	1
Binding site for monomeric Meis1 homeodomain protein	1
Binding site for S8 type homeodomains	1
Cysteine-serine-rich nuclear protein 1 (AXUD1, AXIN1 up-regulated 1)	1
Modulator recognition factor 2 (MRF2, ARID5B)	1
Myc-interacting Zn finger protein 1, zinc finger and BTB domain containing 17 (ZBTB17)	1
Snail family transcriptional repressor 2	1
T-box gene 16 (tbx16) of zebrafish	1
TCF11/LCR-F1/Nrf1 homodimers	1
Transcription factor II B (TFIIB) recognition element	1
Transcription factor Kaiso, ZBTB33	1
Multifunctional c-Abl src type tyrosine kinase	0.997
Meis homeobox 1	0.995
CCAAT/enhancer binding protein (C/EBP), epsilon	0.993
Homeodomain factor Nkx-2.5/Csx	0.993
Myeloid zinc finger protein MZF1	0.992
Sox-5	0.992
Basic leucine zipper transcription factor, ATF-like	0.991
MyT1 zinc finger transcription factor involved in primary neurogenesis	0.991
Smad3 transcription factor involved in TGF-beta signaling factor PU.1	0.99
AREB6 (ZEB1)	0.988
Kruppel-like zinc finger protein 219	0.988
SRY (sex determining region Y)-box 6	0.987
Caudal type homeobox transcription factor 2	0.986
c-Rel	0.986
v-Myb, AMV v-myb	0.986
Mammalian achaete scute homolog 1 (Ascl1)	0.985
Elk-1	0.984
Hepatocyte nuclear factor 3beta (FOXA2)	0.983
Kruppel-like factor 3 (basic)	0.983
Transcription factor Jun-B	0.982
CCAAT/enhancer binding protein (C/EBP), delta	0.981
Heat shock factor 2	0.981
Distal-less homeobox 3	0.98
Homeodomain transcription factor Gsh-2	0.98

Table 3.1. *In silico* analysis of the eIF4A1 promoter for transcription factor binding sites. The eIF4A1 whole promoter sequence was analysed for transcription factor binding using the MatInspector software. A matrix similarity score of 1.00 is classed as a perfect match.

Transcription Factor	Matrix Sim.
Pleomorphic adenoma gene 1	1
Homeo domain factor Nkx-2.5/Csx, tinman homolog, high affinity sites	1
Nuclear factor of activated T-cells	1
Zinc finger with KRAB and SCAN domains 3	1
Sterol regulatory element binding transcription factor	1
Alternative splicing variant of FOXP1, activated in ESCs	1
Zinc finger with KRAB and SCAN domains 3	1
T-cell acute lymphocytic leukemia 1, SCL	0.996
Smad3 transcription factor involved in TGF-beta signaling	0.995
MAX binding protein	0.994
KRAB-containing zinc finger protein 300	0.994
Zinc finger and BTB domain containing 3	0.994
Ribonucleoprotein associated zinc finger protein MOK-2 (human)	0.992
Zinc finger / POZ domain transcription factor	0.992
GATA-binding factor 3	0.991
Ets variant 1	0.991
Polyomavirus enhancer A binding protein 3, ETV4 (Ets variant gene 4)	0.99
MAX binding protein	0.989
Nuclear factor of activated T-cells	0.989
Human zinc finger protein ZNF35	0.989
X-linked zinc finger protein	0.986
TCF/LEF-1, involved in the Wnt signal transduction pathway	0.986
Gut-enriched Krueppel-like factor	0.986
Modulator recognition factor 2 (MRF2, ARID5B)	0.986
Hepatocyte nuclear factor 3 (alpha, beta) (FOXA1, FOXA2)	0.986
Mammalian achaete scute homolog 1 (Ascl1)	0.985
Human zinc finger protein ZNF35	0.985
Myelin regulatory factor	0.985
Spermatogenic Zip 1 transcription factor	0.984
Human zinc finger protein ZNF35	0.983
Non-palindromic nuclear factor I binding sites	0.983
E2F transcription factor 1	0.983
TEA domain family member 4, TEF-3	0.982
Basic helix-loop-helix protein known as Dec2, Sharp1 or BHLHE41	0.982
NMP4 (nuclear matrix protein 4) / CIZ (Cas-interacting zinc finger protein)	0.982

3.5.8 Investigation of eIF4A2 Hypoxic Binding Partners

eIF4A2 has previously been demonstrated to interact with the CNOT7 component of the CCR4-NOT complex and to be the only component of the eIF4F complex required for miRNA mediated repression (Meijer et al, 2013). However this work did not investigate modulation of this interaction under hypoxic conditions. In order to investigate if eIF4A2 binds to CNOT7 in colorectal cancer cells and whether this binding is modulated by hypoxia, LS174T cells were exposed to 48 hours normoxia (20% O_2) and hypoxia (1% O_2) followed by immunoprecipitation of CNOT7 as previously described. CNOT7 bound proteins were separated via gel electrophoresis and probed for the presence of eIF4A2.

Figure 3.11 displays a western blot of CNOT7 eluted proteins, probed with an eIF4A2 antibody with the eIF4A2 band highlighted by the black arrow. Figure 3.11 displays the following conditions: Lane 1) ladder, lane 2) 10 µg total protein before IP as input, lane 3) IgG control, lane 4) CNOT7 normoxia pull down, lane 5) CNOT7 hypoxia pull down. It was revealed that CNOT7 binds to eIF4A2 under normoxic conditions in LS174T colorectal cancer cell lines. However under hypoxic conditions this binding was reduced, however was still present as indicated by the very faint double band present in the CNOT7 hypoxic pull down condition which is indicative of eIF4A2. The same double band was not present in the IgG negative control.

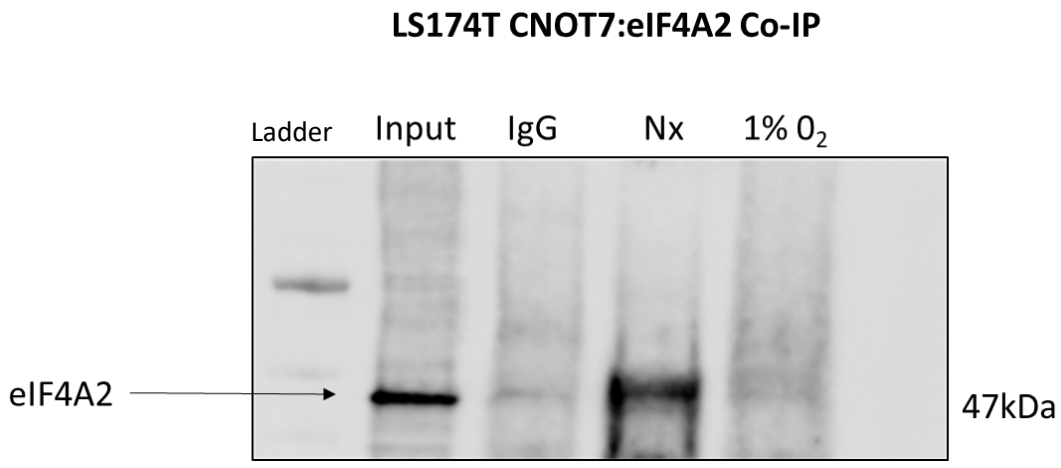


Figure 3.11. Representative image of CNOT7 interaction with eIF4A2 in colorectal cancer cells. LS174T cells were exposed to either 48 hours normoxia (20% O_2) or hypoxia (1% O_2) following by immunoprecipitation of the CNOT7 protein. CNOT7 bound proteins were then separated via gel electrophoresis and membranes probed for the presence of eIF4A2. Representative image from three experimental repeats. n=3.

3.5.9 eIF4A2 Expression in Human Colorectal Patient Samples

In order to assess the association between eIF4A2 protein expression and patient outcome, 1000 human colorectal cancer patient samples and their matched normal tissue counterparts were stained for eIF4A2 and CAIX expression using standard immunohistochemical techniques. eIF4A2 and CA9 staining intensity was assessed using a semi-quantitative approach by assigning a H-score for the entirety of the tissue core for nuclear, cytoplasmic and infiltrating cellular compartments. The staining intensity scores ranged from; 0=no staining, 1+=weak staining, 2+=strong staining. The percentage of cells at each staining intensity level is then calculated and assigned a H-score using the following formula with H-values ranging from 0-200:

H-score calculation = [0x (% cells 0+) + 1x (% cells 1+) + 2x (% cells 2+)]

eIF4A2 protein displayed an unexpected pattern of expression in comparison to that observed in the colorectal spheroids. eIF4A2 staining within spheroids was found to be strictly cytoplasmic, with no nuclear staining observed. However in the colorectal TMA, many cores displayed strong nuclear eIF4A2 staining. It in addition it was possible to observe infiltrating inflammatory cells staining highly positive for eIF4A2 expression, which was also observed in the lymph control cores included in the TMA. Preliminary results suggest increased eIF4A2 nuclear expression and increased staining of infilitrating cells in colorectal tumour samples compared to matched tissue controls. Figure 3.12 displays representative images of 0, 1+, 2+ nuclear staining for normal tissue cores, eIF4A2 protein expression is represented by the dark brown stain in all images. Figure 3.13 displays representative images of 0, 1+, 2+ nuclear staining for colorectal cancer cores. Figure 3.14 displays representative images of 0, 1+, 2+ cytoplasmic staining for colorectal cancer cores. Figure 3.15 displays representative images of 0,1+, 2+ cytoplasmic staining for normal tissue cores. Figure 3.16 displays representative images of 0, 1+, 2+ for infiltrating cells.

In addition, TMA cores and their matched normal controls were assessed for the level of co-localisation between eIF4A2 and CAIX staining intensity. Co-localisation of CAIX and eIF4A2 staining for all TMA cores is currently being assessed. Figure 3.17 and 3.8 displays representative example images of colorectal tumour tissue and their matched normal controls for both CAIX and eIF4A2 staining. Prelimary results suggest no co-localisation between eIF4A2 and CAIX staining in colorectal tumour samples or matched tissue controls.

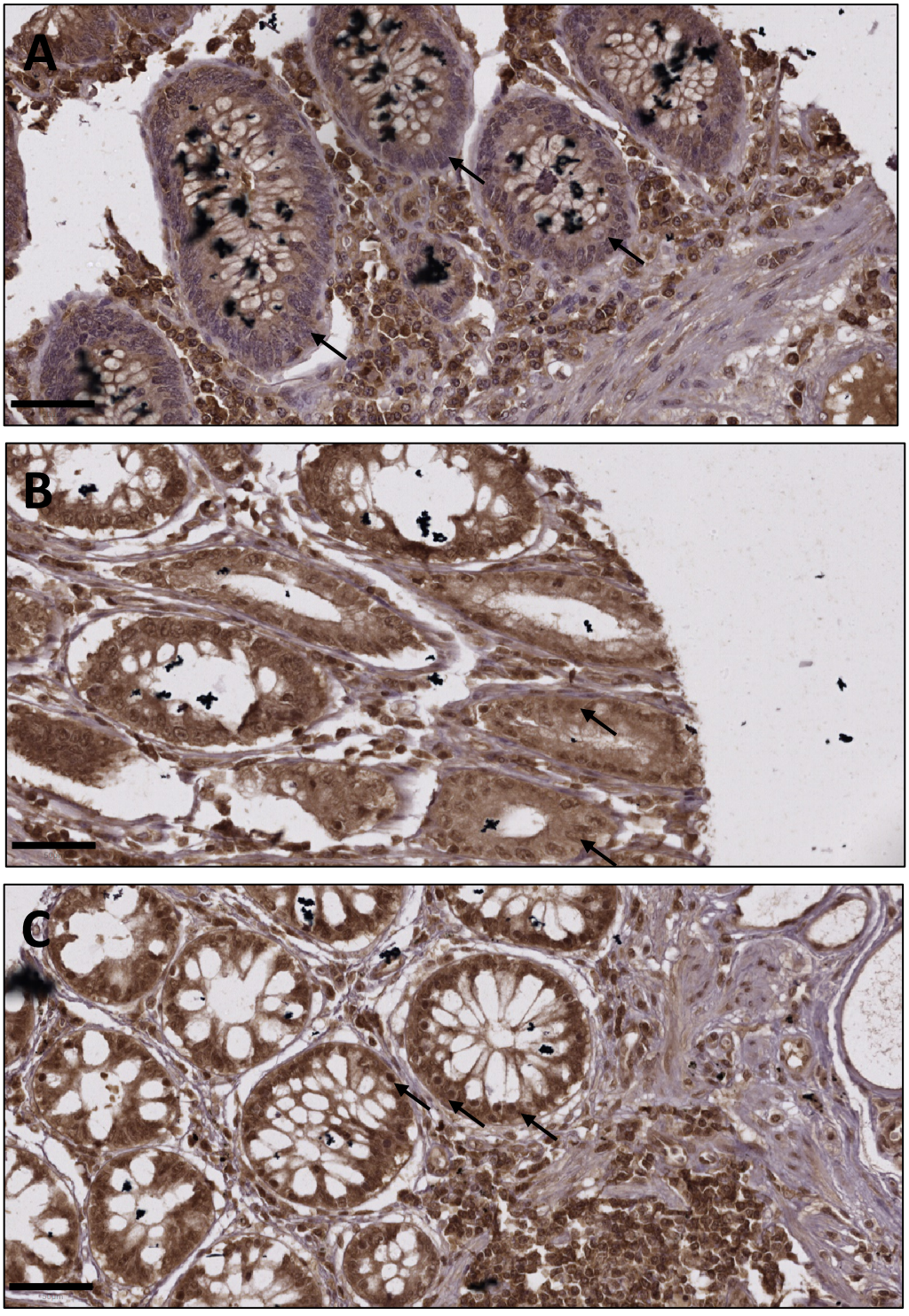


Figure 3.12. Representative images of eIF4A2 nuclear staining intensities of normal tissue cores. (A) 0 nuclear staining (B) 1+ nuclear staining (C) 2+ nuclear staining. Images taken at x23.44. eIF4A2 stain can be observed as a dark brown stain. Scale bar represents 50 µm.

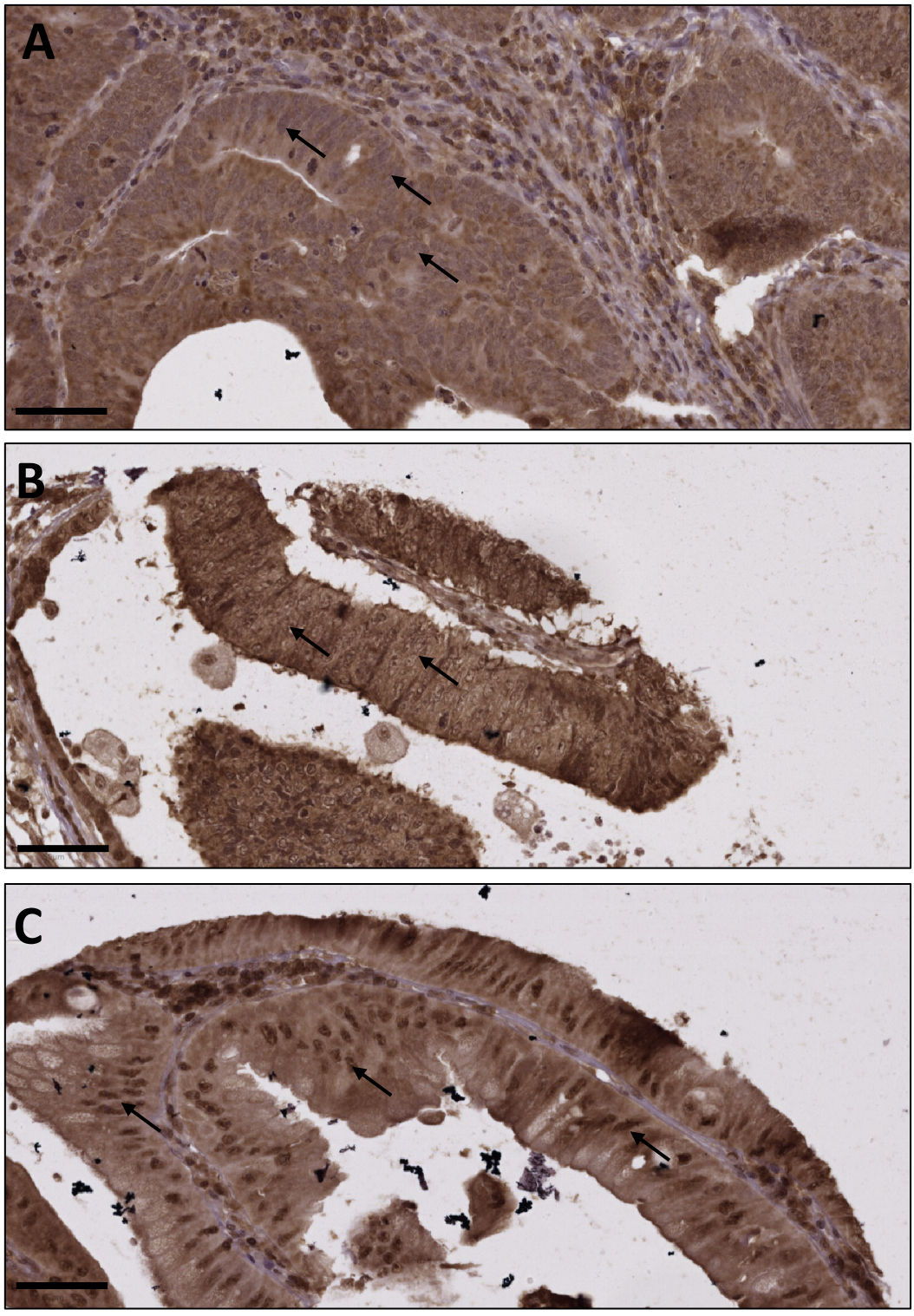


Figure 3.13 Representative images of eIF4A2 nuclear staining intensities of colorectal cancer tissue cores. (A) 0 nuclear staining (B) 1+ nuclear staining (C) 2+ nuclear staining. Images taken at x20. Scale bar represents 50 µm.

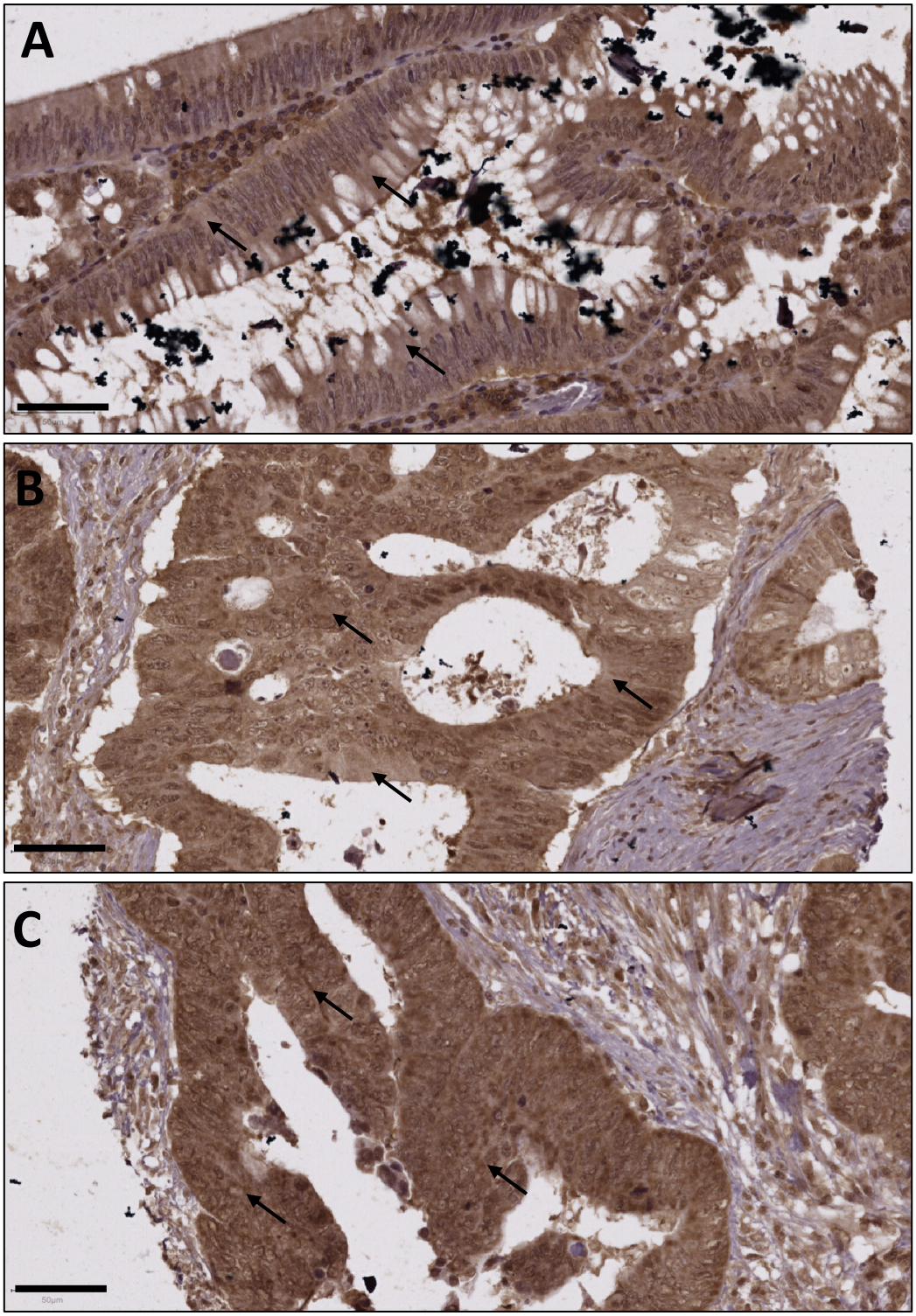


Figure 3.14 Representative images of eIF4A2 cytoplasmic staining intensities of colorectal cancer tissue cores. (A) 0 cytoplasmic staining (B) 1+ cytoplasmic staining (C) 2+ cytoplasmic staining. Images taken at x10. Scale bar represents 50 µm.

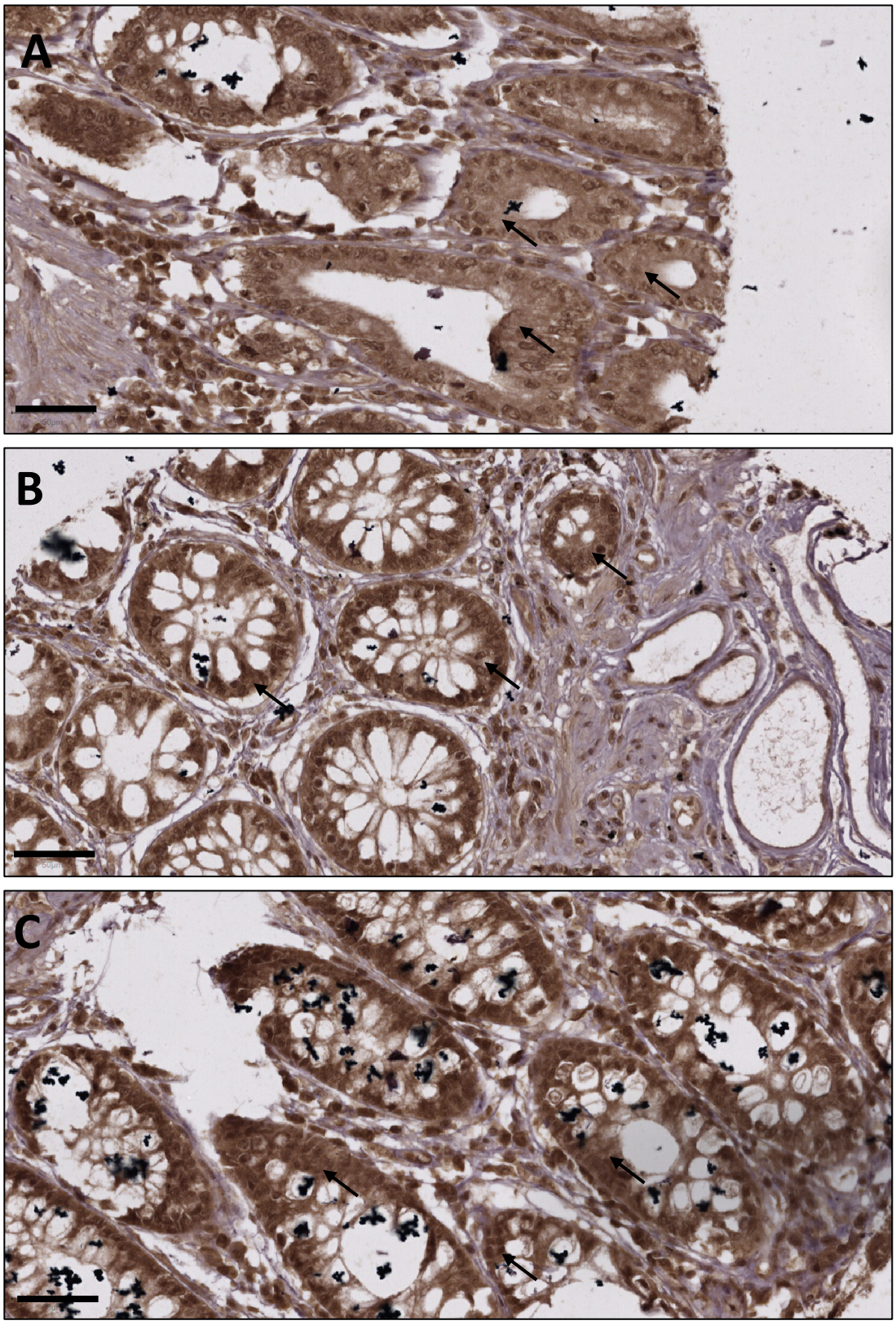


Figure 3.15 Representative images of eIF4A2 cytoplasmic staining intensities of normal matched tissue cores. (A) 0 cytoplasmic staining (B) 1+ cytoplasmic staining (C) 2+ cytoplasmic staining. Images taken at x10. Scale bar represents 50 µm.

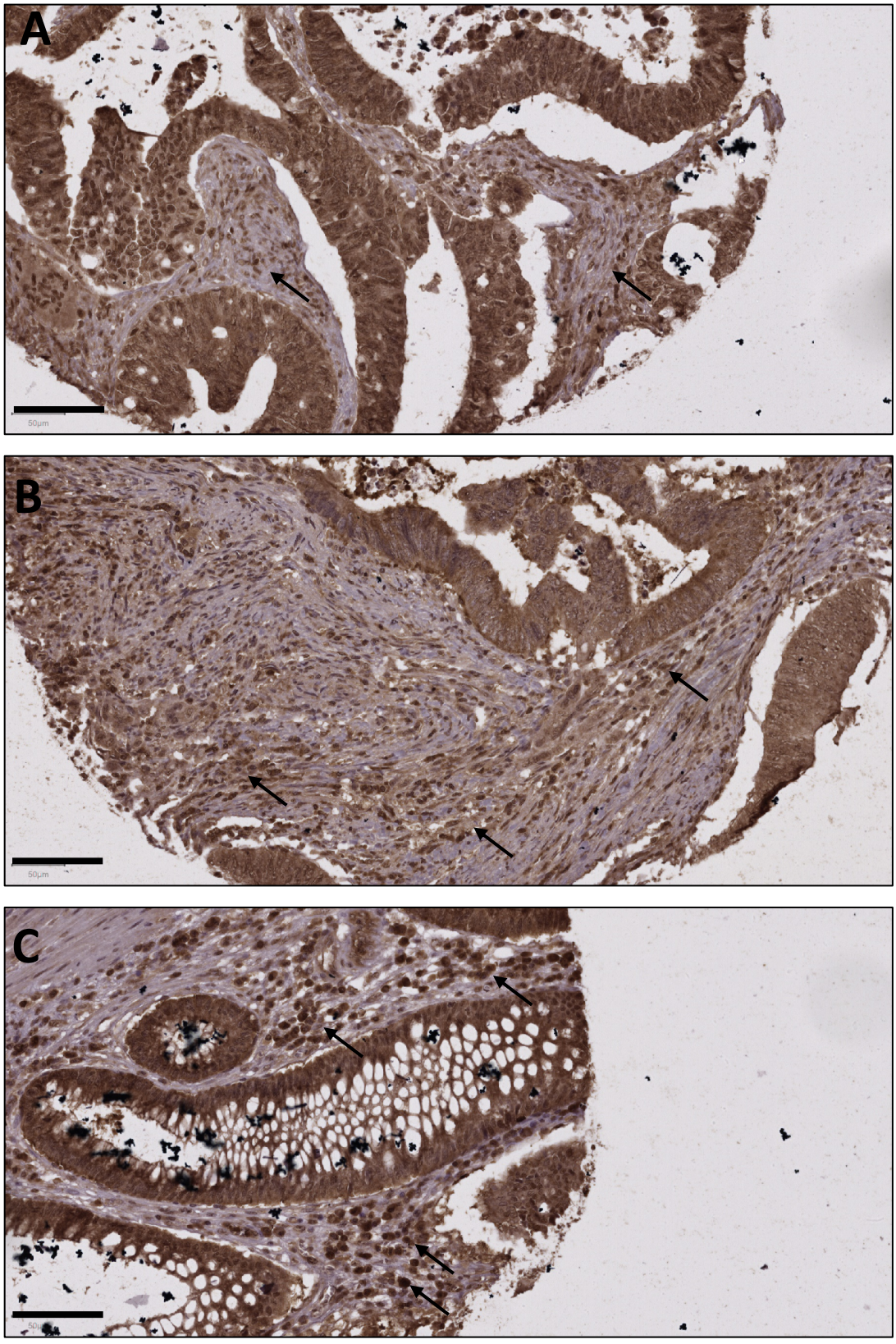


Figure 3.16 Representative images of eIF4A2 infiltrating cells staining intensities. (A) 0 infiltrate staining (B) 1+ infiltrate staining (C) 2+ infiltrate staining. Images taken at x10. Scale bar represents 50 µm.

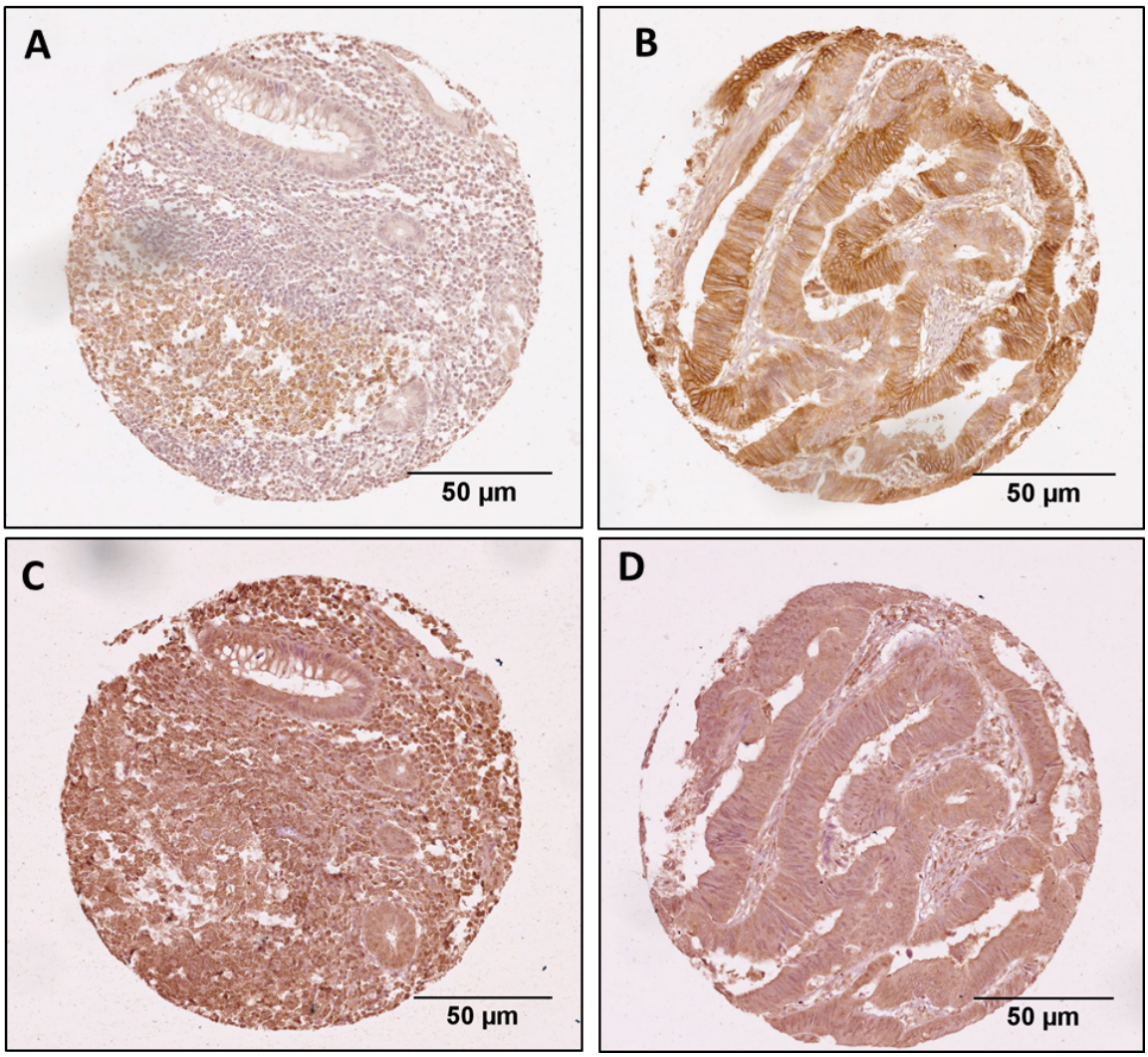


Figure 3.17 Representative images of CAIX and eIF4A2 co-localisation of colorectal tumour and matched normal tissue controls of core 68 (A) normal tissue CAIX staining (B) colorectal tumour CAIX staining (C) normal tissue eIF4A2 staining (D) colorectal tumour eIF4A2 staining. Images taken at x10. Scale bar represents 50 µm.

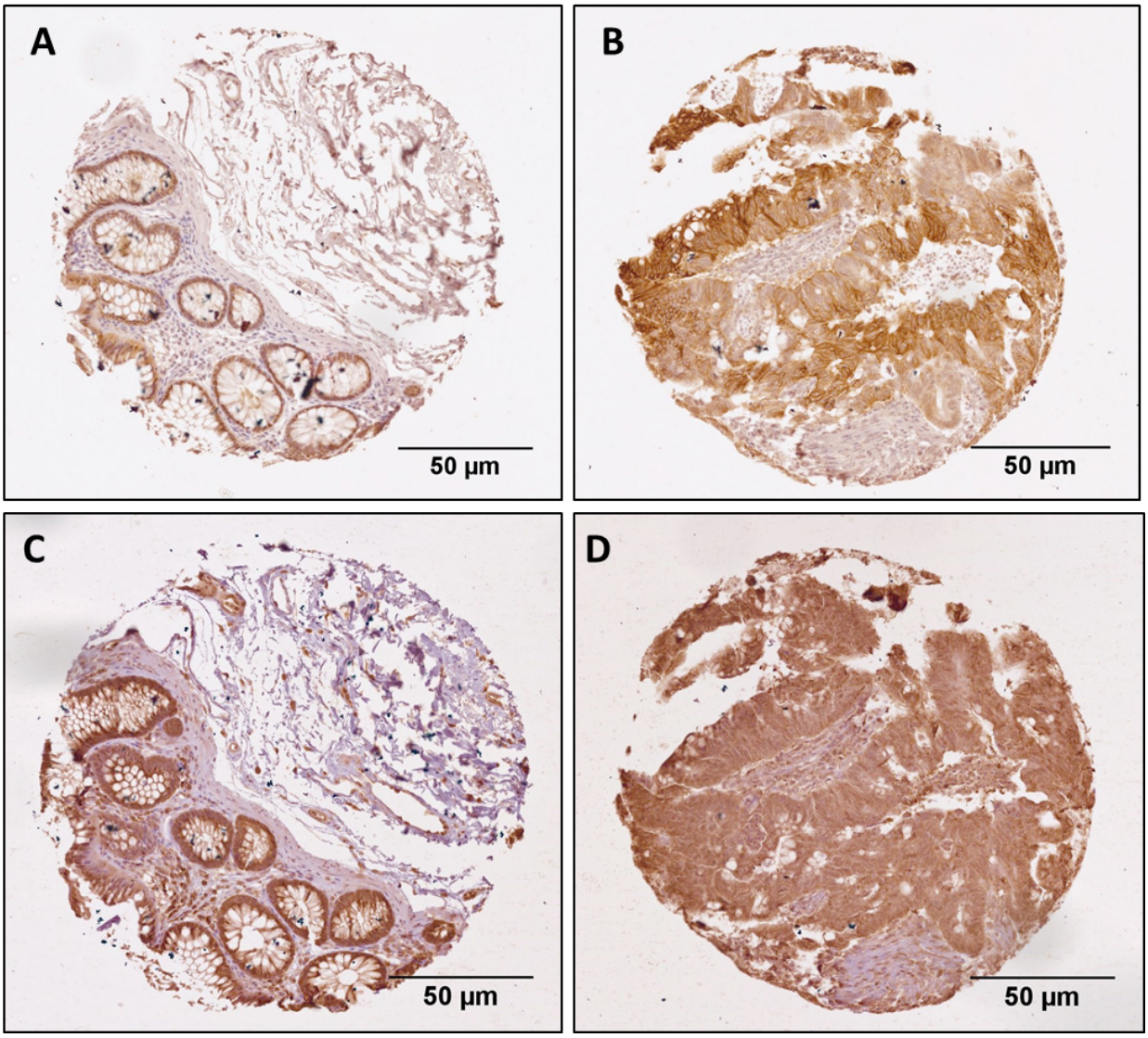


Figure 3.18 Representative images of CAIX and eIF4A2 co-localisation of colorectal tumour and matched normal tissue controls of core 128 (A) normal tissue CAIX staining (B) colorectal tumour CAIX staining (C) normal tissue eIF4A2 staining (D) colorectal tumour eIF4A2 staining. Images taken at x10. Scale bar represents 50 µm.

3.6 Discussion

We hypothesised that eIF4A2 expression would be upregulated under hypoxic conditions at both the mRNA and protein level and that this would be due to the presence of a HRE within the eIF4A2 promoter region which concurred transcriptional regulation by HIF1α and HIF2α. Hypoxic time course experiments identified a significant upregulation of eIF4A2 mRNA but not protein under hypoxic conditions. This mechanism behind the lack of upregulation of eIF4A2 protein under hypoxic conditions remains to be elucidated, but possible mechanisms will be discussed in the following sections. In addition, *in silico* analysis of the eIF4A2 genomic sequence identified several predicted HRE elements which provided the rational for performing knockout experiments of HIF1α and HIF2α to assess their role in the transcriptional regulation of eIF4A1/2 at both the mRNA and protein level.

Knockout of only HIF2α in LS174T cells, lead to a significant reduction of eIF4A2 mRNA and protein expression, demonstrating that eIF4A2 is under the control specifically of HIF2α. The opposite effect was observed in HCT116 cell line. Additionally eIF4A2 was found to bind to CNOT7 in LS174T cells, however this binding was unexpectedly reduced under hypoxic conditions. An additional unexpected result was the expression of eIF4A2 protein being observed across the entirety of the spheroid as opposed to localised to hypoxic or peri necrotic regions as hypothesised. In addition, infiltrating cells and the nucleus stained highly for eIF4A2 protein expression, in addition to cytoplasmic expression as hypothesised.

3.6.1 Regulation of eIF4A2 at the Transcriptional Level

One mechanism by which eIF4A2 mRNA may be upregulated under hypoxic conditions is through the presence of a HRE within the DNA promotor region of the eIF4A2 gene. *in silico* analysis of the eIF4A2 genomic sequence did predict the presence of several HRE however, none were found within the promoter region. The eIF4A2 genomic sequence was shown to possess one HRE within the 3'exon and its mRNA and protein expression were shown to be specifically under control of HIF2α only in LS174T cell lines. Interestingly and in contrast to previous data, eIF4A1 was found to possess several HREs within its promoter region and its mRNA expression shown to be under the control of HIF2α but only in LS174T cell line. The opposite effect was observed in HCT116 cells, with a significant increase in eIF4A1 and eIF4A2 mRNA expression observed following knockdown of either HIF1α or HIF2α.

Despite the predicted HRE within the eIF4A2 genomic sequence existing far from the promoter region, previous genome wide ChIP experiments have shown that HIF binding sites exist at distances far from gene promoters, indeed HREs have been located in the 5'UTR, 3'UTR, intronic and exonic regions (Schodel et al, 2011). Such genome wide

experiments demonstrated differences in the distribution of binding sites between HIF1α and HIF2α isoforms. The same study demonstrated that in MCF-7 cells, 40% of HIF1α binding sites were located within 2.5kb of the transcription start site (TSS), and only 20% of HIF2α binding sites located within 2.5kb of the TSS. HIF2α binding sites were demonstrated to be more widely distributed across a transcript (i.e.: distal to the TSS within promoter regions) (Schodel et al, 2011).

Previous DNase-seq experiments have revealed that HIF itself is not a "pioneer" transcription factor (i:e: it is not the first transcription factor to bind to the HRE). Instead HIF was shown to binds to enhancers that have been defined by other transcription factors (Schodel et al, 2011). The same study also revealed that only a small proportion of HREs were actually occupied by HIF, suggesting that additional transcription factors are required to enable HIF binding (Schodel et al, 2011). As such, the *in silico* analysis presented in this chapter goes some way into highlighting potential transcription factors that may be required for the hypoxic induction of eIF4A2 at the transcriptional level. Since the completion of the practical work for this thesis, a paper was published highlighting the role of the transcription factor ZNF143 in the transcriptional regulation of eIF4A2 in colorectal cancer cells which was experimentally validated (Chen et al, 2019). ZNF143 is a chromatin looping factor, it is responsible for occupying distal regulatory sites upon the chromatin, known as chromatin interaction anchors, and binding or looping them directly to the promoter region (Bailey et al, 2015). This poses an interesting possible mechanism by which ZNF143 occupies the chromatin upon the site of the HRE within the eIF4A2 3'exon, looping it back to the promoter region and promoting hypoxic transcription of eIF4A2. However experiments performed by Chen et al were only performed under normoxic conditions, ZNF143 remains to be identified as possessing a role in the hypoxic transcriptional regulation of eIF4A2. The *in silico* analysis presented in this chapter is in agreement with these findings by Chen et al, 2019, both ATF and ZBTB33 binding sites were predicted to be located in the eIF4A2 promoter with a core matrix similarity of 1. Additional transcription factor binding sites with a matrix similarity of 1 include: FOXP1, Meis1, AXUD1, ARID5B, ZBTB17, SNAIL2, TCF11 and TFIIB. Such predicted transcription factors may represent additional mechanism through via eIF4A2 is regulated at the transcriptional level and would require further investigation under both normoxic and hypoxic conditions.

An increase (nonsignificant) in HIF1α mRNA expression was observed in HIF2α KO cells (Figure 3.8 A), and conversely, a significant increase in HIF2α mRNA expression was observed in HIF1α KO cells (Figure 3.8 C). In LS174T cells, a significant increase in HIF1α

expression was observed in HIF2α KO cell lines. It has previously been demonstrated that endogenous HIF2α was unable to compensate for HIF1α function during hypoxia (Park et al, 2003). However more recent studies demonstrated that upon stable knockout of HIF1α and HIF2α lead to a compensatory increase in expression of the opposing isoform in HepG2 tumour spheroids and conclude that both isoforms regulate eachother. The athours hypothesised that knockout of HIF2α, which regulate the expression of SOD and catalase, would lead to an increase in ROS expression, stabilising HIF1α leading to increased expression (Menrad et al, 2010). The same effect has been observed in glioma cells (Anelli et al, 2008). One explantion for the differences between HCT116 and LS174T with regards to HIF regulation of eIF4A2 and differences in HIF expression following knockdout of either α isform may be their genetic background. Both possess the same PI3KCA mutation (H1047R). Both HCT116 and LS174T are wild type for p53, PTEN and BRAF, however they differ with regards to KRAS mutation (G13D and G12D respectively). In addition, HCT116 was found to be positive for the methylation status of CIMP 1 and 2 panel of genes, in contrast LS174T was found to be negative for both these panels of genes. CIMP panel 1 is based on previous work by Issa, 2004 and include the genes *CDKN2Q, MINT1, MINT31* and *MLH1* (Issa, 2004). CIMP panel 2 is based on previous work by Weisenberger et al, 2006 and includes the genes *CACNA1G, IGF2, NEUROG1, RUNX3* and *SOCS1* (Weisenberger et al, 2006).

An additional observation was the increase of eIF4A2 at the mRNA level under increasing time spent under hypoxic conditions, but this effect was not reflected at the protein level. One explaination for this could be that eIF4A2 is required for an ischemia/reperfusion response or a cycling hypoxia response. Having a pool of eIF4A2 mRNA present in the cell would allow for rapid translation of eIF4A2 upon restoration or increase in oxygen levels.

3.6.2 Regulation of eIF4A2 at the Protein Level

Under hypoxic conditions a global downregulation in transcription and protein synthesis as observed, therefore the post-transcriptional regulation of the existing pool of mRNAs is crucial in determining protein output under hypoxic conditions (Ho et al, 2016. Such post transcriptional mechanisms include mRNA turnover and translational control, such processes are regulated by RBPs and non-coding RNAs such as miRNAs as described in the introduction section of this thesis (Hentze et al, 2018). The data presented in this thesis does not demonstrate a significant upregulation of the eIF4A2 protein under hypoxic conditions, only that the eIF4A2 protein expression is maintained. However the fact that

the eIF4A2 protein is maintained and not downregulated under hypoxic conditions still suggests a requirement for eIF4A2 under hypoxic conditions.

Despite a lack of significant upregulation of eIF4A2 at the protein level, eIF4A2 mRNA and protein expression was shown to be under the control of HIF2α in LS174T cells. One explanation is due to the direct binding of HIF2α and HIF1β to the HRE within the eIF4A2 3'exon. An additional mechanism comes from further inspection of the supplementary data from the Uniacke 2012 paper. On inspection of the supplementary data associated with the Uniacke et al paper investigating the HIF2α:RBM4:eIF4E2 complex, eIF4A2 and not eIF4A1 was identified as being present following a HIF2α/RBM4 PAR-CLIP experiment (HIF2α immunoprecipitation following by excision of the RBM4 band) (Uniacke et al, 2012). This data demonstrates that eIF4A2 mRNA interacts with the HIF2α:RBM4:eIF4E2 protein complex, highlighting a possible mechanism for its preferential translation or maintenance of translation during hypoxia. Uniacke et al demonstrated that mRNAs recruited by the HIF2:RBM4:eIF4E2 complex contain an RNA hypoxic response element (rHRE) which share commonality with the CGG RBMF binding motif (Uniacke et al, 2012). In addition, using PAR-CLIP experiments, Uniake identified a CGG motif within the 3'UTR of transcripts that interacts with RBM4 (Uniacke et al, 2012). Upon retrospective analysis of the eIF4A2 3'UTR mRNA sequence, 4 CGG repeats were found as highlighted in Figure 3.20. Such data strengthens the argument that eIF4A2 is under the control of HIF2α under hypoxic conditions.

5'AATGCAAAAACTGCAGGCTGAAGCACCACATATTGTTGTTGGTACACC**CGG**GAGAGTGTTTGATATGTTA
AACAGAAGATACCTTTCTCCAAAATGGATCAAAATGTTTGTTTTGGATGAAGCAGATGAAATGTTGAGCCG
TGGTTTTAAGGATCAAATCTATGAGATTTTCCAAAAACTAAACACAAGTATTCAGGTTGTGTTGCTTTCTGC
CACAATGCCAACTGATGTGTTGGAAGTGACCAAAAAATTCATGAGAGATCCAATTCGAATTCTGGTGAAAA
AGGAAGAATTGACCCTTGAAGGAATCAAACAGTTTTATATTAATGTTGAGAGAGAGGAATGGAAGTTGGA
TACACTTTGTGACTTGTACGAGACACTGACCATTACACAGGCTGTTATTTTTCTCAATACGAGGCGCAAGGT
GGACTGGCTGACTGAGAAGATGCATGCCAGAGACTTCACAGTTTCTGCTCTGCATGGTGACATGGACCAG
AAGGAGAGAGATGTTATCATGAGGGAATTC**CGG**TCAGGGTCAAGTCGTGTTCTGATCACTACTGACTTGTT
GGCTCG**CGG**GATTGATGTGCAACAAGTGTCTTTGGTTATAAATTATGATCTACCTACCAATCGTGAAAACTA
TATTCACAGAATTGGCAGAGGGGGTCGATTTGGGAGGAAAGGTGTGGCTATAAACTTTGTTACTGAAGAA
GACAAGAGGATTCTTCGTGACATTGAGACTTTCTACAATACTACAGTGGAGGAGATGCCCATGAATGTGGC
TGACCTTATTTAATTCCTGGGATGAGAGTTTTGGATGCAGTGCTCGCTGTTGCTGAATAGGCGATCACAAC
GTGCATTGTGCTTCTTTCTTTGGGAATATTTGAATCTTGTCTCAATGCTCATAA**CGG**ATCAGAAATACAGATT
TTGATAGCAAAGCGACGTTAGTCGTGAGCTCTTGTGAGGAAAGTCATTGGCTTTATCCTCTTTAGAGTTAG
ACTGTTGGGGTGGGTATAAAAGATGGGGTCTGTAAAATCTTTCTTTCTTAGAAATTTATTTCCTAGTTCTGTA
GAAATGGTTGTATTAGATGTTCTCTATCATTTAATAATATACTTGTGGACTAAAAGATATAAGTGCTGTATAAA
ATCAGCCAATTATGTTAAACTAGCATATCTGCCTTTATTGTGTTTGTCATTAGCCTGAGTAGAAAGGCCTTTA
AAATTTTTTTAGAAAGCATTTGAATGCATTTTGTTTGGTATTGTATTTATTCAATAAAGTATTTAATTAGTGCT
AAGTGTGAACTGGACCCTGTTGCTAAGCCCCAGCAAGCAATCCTAGGTAGGGTTTAATCCCCAGTAAAATT
GCCATATTGCACATGTCTTAATGAAGTTTGAATGTTAAATAAATTGTATATTCACTTTAAA'3

Figure 3.20 eIF4A2 3'UTR mRNA sequence. eIF4A2 3'UTR sequence was obtained from BioMart Ensemble and manual inspected for the presence of the RBM4 binding motif CGG. 4 RBM4 binding motifs are highlighted in red.

Uniacke et al concluded that RBM4 first binds to specific regions in the 3'UTR of mRNAs that recruit HIF2 to induce hypoxic translation and that these RNA sequence share commonality with RBM4 binding sites (Uniacke et al, 2012). The fact that the eIF4A2 3'UTR contains 4 RBM4 binding sites represents a possible exciting novel mechanism in how eIF4A2 protein expression is maintained under hypoxic conditions specifically through HIF2α binding.

Upon exposure to stress conditions components of the translational machinery are known to be localised and sequestered into stress granules; this stalls the translation machinery in order to allow for the re-programming of protein synthesis machinery. This additionally allows for mRNAs to be sorted and sent for storage, degradation or translation (Decker and Parker, 2012). Stress granules are then able to fuse with other cytoplasmic structures known as P-bodies with contain the mRNA decay machinery (Decker and Parker, 2012). Stress granules have been shown to contain translation initiation factors, small ribosomal sub unit, miRNAs and long non-coding RNAs (Decker and Parker, 2012). Previous studies undertaken by Jongjitwimol et al, has demonstrated eIF4A2 is recruited to stress granules following arsenite treatment and ionising radiation and that SUMOylation of eIF4A2

correlates with its recruitment to stress granules (Jongjitwimol et al, 2016). Hippuristanol, an eIF4A inhibitor was found to prevent the recruitment of eIF4A2 to stress granules (Jongjitwimol et al, 2016). However this work was performed on HeLa cells and failed to investigate the role of eIF4A2 in stress granule formation in response to hypoxia. The data presented in Figure 3.6 demonstrates that under hypoxic conditions eIF4A2 is observed to localise into granules within the cytoplasm, suggestive of stress granule formation. This suggests a role for eIF4A2 in the regulation of translation under stress response, but more importantly in the regulation of the sorting of stalled mRNAs for storage, degradation or translation. In order to prove the structures observed in Fig 3.5, 3.6 are stress granules, a stress granule specific marker such as TIA-1 could have been used to stain the same samples (Gilks et al, 2004). eIF4A2 has previously been shown to interact with CNOT7, a component of the CCR4-NOT complex (Meijer et al, 2013). Stress granules have been shown to fuse with P-bodies which contain miRNA translational repression machinery including the CCR4-NOT complex (Decker and Parker, 2012). This could present a mechanism by which eIF4A2 is recruited to stress granules and directly interacts with the CCR4-NOT complex under stress conditions via the fusion of stress granules and P-bodies, delivering the mRNAs which eIF4A2 has selected for degradation.

3.6.3 Investigation of eIF4A2 Hypoxic Binding Partners

Previous research undertaken by Meijer et al, demonstrated that eIF4A2 is the only component of the eIF4F required for miRNA translational repression via its direct interaction with CNOT7, a component of the CCR4-NOT complex (Meijer et al, 2013). However this work was performed on HeLa cells and failed to investigate the role of eIF4A2 in stress granule formation in response to hypoxia. We hypothesised that eIF4A2 would show increased binding to CNOT7 under hypoxic conditions. The results presented in Figure 3.11 demonstrate eIF4A2 binding to CNOT7 under normoxic conditions, however this binding was unexpectedly observed to be reduced under hypoxic conditions. Under hypoxic conditions, a global downregulation of protein synthesis is observed alongside an increase in the formation of stress granules and P-bodies to cope with the increase in stalled components of translational machinery (Mahboubi and Stochaj, 2017). If eIF4A2 is being recruited to stress granules under hypoxic conditions, why do we see a reduction in CCR4-NOT complex binding under hypoxic conditions? One explanation for this could be explained using the results from the following piece of previous research. Since the completion of the laboratory work for this thesis a paper by Meijer et al demonstrated that eIF4A2 and the RNA helicase DDX6, both bind and are recruited to the CRR4-NOT complex,

and that incorporation of eIF4A2 into the CCR4-NOT complex inhibits CNOT7 deadenylation activity, in contrast, binding of DDX6 to the CCR4-NOT complex enhances CNOT7 deadenylation activity (Meijer al, 2019). Meijer et al also identified 107 proteins via mass spectrometry analysis bound to the eIF4A2:CCR4-NOT complex. The same paper also identified a novel RBP, TAB182 that selects which helicase is incorporated into the CCR4-NOT complex, thereby governing the fate of target mRNAs (Meijer et al, 2019). The paper concluded that the fate of a target mRNA is dependent on whether eIF4A2 or DDX6, governed by TAB182, is incorporated into the CCR4-NOT complex. If eIF4A2 is incorporated into the CCR4-NOT complex, the mRNA poly (A) tail remains intact, if DDX6 is incorporated into the CCR4-NOT complex, the mRNA can be deadenylated (Meijer et al, 2019). This may represent a possible mechanism by which either eIF4A2 or DDX6 are preferentially loaded into the CCR4-NOT complex under hypoxic conditions within stress granules; however this remains to be elucidated. H

3.6.4 Concluding Statements

The first hypothesis presented in this chapter stated that eIF4A2 would be upregulated at the protein and RNA level under hypoxic conditions, this hypothesis was found to be true only at the mRNA level, not the protein. In addition the hypothesis that eIF4A2 would contain a HRE within its promoter region was disproved, as it was found to contain one within the 3'UTR region. Thirdly, it was hypothesised that eIF4A2 would be under the control of either HIF1α or HIF2, this was found to be true, but eIF4A2 was found to be HIF2α and this effect was cell line specific. Finally it was hypothesied that eIF4A2 would bind to CNOT7 under hypoxic conditions in colorectal cancer cells, this hypothesis was interestingly disproved as eIF4A2 was found to display decreased binding to CNOT7 udner hypoxic conditions.

4.0 Functional Consequences of eIF4A2 Inhibition

4.1 Introduction

4.1.1 Inhibition of Components of Protein Synthesis Machinery

Deregulated protein synthesis and translational control is now a well-recognized characteristic of tumour cells (Bhat et al, 2015). It is therefore not surprising that targeting translation, direct components of the translation machinery (RBPs, eIFs, and RNA helicases) and molecules upstream of the translational machinery has received increasing attention and demonstrated anti-cancer activity in recent years (Bhat et al, 2015). Compounds that target molecules upstream of the eIF4F complex include the allosteric inhibitors of mTORC1 (Rapamycin, Temsirolimus, Everolimus and Ridaforolimus (Rapalogues)), dual inhibitors of PI3K and mTOR, inhibitors of the active site of mTOR (INK128, Torin1) and indirect inhibitors of mTOR (Metformin) (Pal et al, 2019). Despite Rapalogues gaining FDA approval as a single use agent for the treatment of renal cell carcinoma and neuroendocrine tumours, single agent clinical trials do not demonstrate therapeutic benefit, nor do they extend survival for a handful of cancer patients (Benjamin et al, 2011)(Fruman and Rommel, 2014). Therefore the discovery of novel drug targets and development of their inhibitors is required to oversome said resistance. Furthermore resistance to active site mTOR inhibitors is determined by the eIF4E:4EBP ratio, which is commonly observed in advanced tumours (Alain et al, 2012). Due to the evidence supporting the notion that targeting signalling molecules upstream of the eIF4F complex (mTOR, PI3K) commonly leads to treatment resistance, there has been much work developing small molecule inhibitors that directly target components of the eIF4F complex. These include inhibitors of eIF4E (4Ei-1), inhibitors of the eIF4E-eIF4G interaction (4EGI-1), inhibitors of eIF2α dephosphorylation (Salubrinal) and the eIF4A inhibitors as described earlier (Bhat et al, 2015). Antisense oligonucleotides inhibiting eIF4E have shown promising anti-cancer effects in breast and prostate xenograft models with minimal toxicity along with a subsequent reduction in pro survival eIF4E sensitive mRNAs (Graff et al, 2007).

4.2 Pre-Clinical Inhibitors of eIF4A

In 2004 the Pelletier group performed an in vitro high throughput bicistronic mRNA assay to screen more than 90,000 compounds to identify novel inhibitors of cap dependent translation and translation elongation and termination in addition to identifying compounds that bind to a specific motif within the 5'UTR that inhibit ribosome scanning (Novac et al, 2004). The screen identified 36 compounds, with the most notable from the screen are the three listed below.

4.2.3 Silvestrol

Isolated from the species of the *Aglaia* genus of plants, Silvestrol is the most studied of the three eIF4A inhibitors and belongs to a class of compounds known as rocaglamides (RocA) which belong to a class of natural products known as flavaglines (Pan et al, 2015). iCLIP experiments have revealed that Silvestrol inhibits eIF4A by increasing its affinity for a polypurine motif within the 5'UTR of the mRNA causing it to clamp shut, preventing the catalytic helicase cycle even in the presence of ATP, directly blocking scanning by the 43SPIC (Cencic et al, 2009) Silvestrol shows striking anti-cancer activity in vitro in a broad range of cancer cell line including B-cell leukemia, breast, prostate and lymphoma (Lucas et al, 2009) (Alinari et al, 2012) (Cencic et al, 2009). In chronic lymphocytic leukemia (CLL) cell lines Silvestrol possess an LC50 of 6.9 nM at 72 hours (Lucas et al, 2009). In a Eu-Myc/eIF4E mouse model of lymphoma, Silvestrol plus doxorubicin proved more effective than rapamycin plus doxorubicin ($p<0.001$) (Bordeleau et al, 2008). The combination of Silvestrol plus doxorubicin also produced longer tumour free survival that either agent on its own, with all animals achieving remission that lasted up to 25 days (Bordeleau et al, 2008). In comparison in the same tumour setting, rapamycin plus doxorubicin only achieved remission in 60% of animals lasting only 4 days (Bordeleau et al, 2008). In a PTEN+/- Eu Myc mouse model of lymphoma where these tumours exhibit increases of phosphorylated Akt and S6 kinase; Silvestrol also synergized with doxorubicin, with all animals achieving remission lasting up to 16 days ($P<0.001$) (Bordeleau et al, 2008). Furthermore Silvestrol treatment is effective as a single agent treatment in a murine model of T-cell acute lymphoblastic leukemia (KOPT-K1 tumour bearing NOD/SCID mice); 0.5mg/kg treatment for 6 days induced apoptosis, cell cycle arrest and inhibited tumour growth ($p<0.001$) (Wolfe et al, 2014).

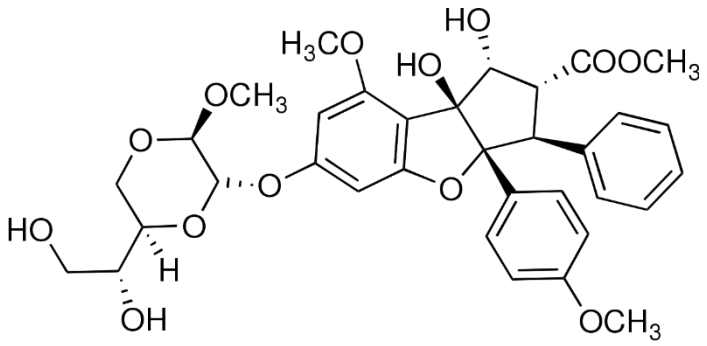


Figure 4. Structural formula of the natural product Silvestrol ($C_{34}H_{38}O_{13}$).

4.2.4 Hippuristanol

A natural compound, Hippuristanol is isolated form the coral *Isis hippuris* and is a selective inhibitor of both eIF4A1 and eIF4A2 (Cencic and Pelletier, 2016). Its mechanism of action is via the binding to residues 237-406 within the C-terminal domain of eIF4A1 and eIF4A2 adjacent to the ATP binding and away from the RNA binding site, acting as an allosteric inhibitor (Lindqvist et al, 2008). More recent studies using single molecule FRET demonstrated that Hippursitanol inhibits eIF4A1 activity by locking it in a closed conformation that inhibits RNA unwinding (Sun et al, 2014). When used in an $Tsc2^{+}$/Eμ Myc transgenic mouse model, Hippuristanol (10 mg/kg) inhibited translation *in vivo*, significantly inhibited tumour growth rates and re-sensitized tumours to chemotherapeutic agents (Galicia-Vazquez et al,2012). However this effects was eIF4A1 specific. Hippuristanol additionally inhibited the proliferation of T-cell leukemia cell lines via the induction of apoptosis through the inhibition of Bcl-xL and XIAP, and via induction of cell cycle arrest in the G1 phase via the reduction in expression of CDK6, cyclin D1 and cyclin D2 (Tsumuraya et al, 2011).

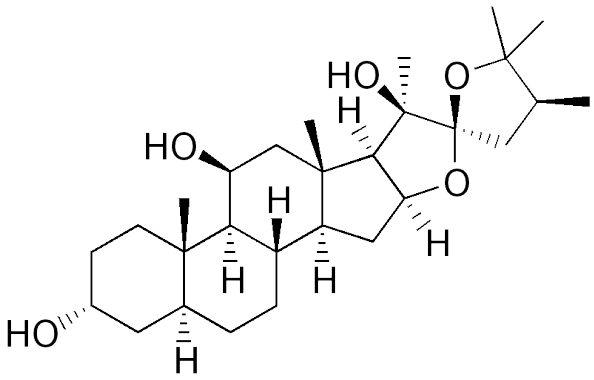


Figure 4.1. Structural formula of the natural product Hippuristanol ($C_{24}H_{46}0_5$).

4.2.5 Pateamine A

Another natural compound, Pateamine A is derived from the sea sponge *Mycale hentscheli*; it inhibits eIF4A by increasing the affinity of eIF4A for ATP and RNA by inducing dimerization, allowing for non-specific interactions between eIF4A and RNA and sequestering it from the eIF4F complex (Low et al, 2014). At the time of the original

characterisation of Pat A, isoform specific antibodies of eIF4A isoforms were not available and so it was not possible to determine the specific isoform inhibited by Pat A (Bordeleau et al, 2005). A synthetic analogue of Pat A, DMDA-Pat A inhibits xenograft growth rates in both LOX and MDA-MB-435 melanoma models and inhibits growth rate across a broad panel of 32 human cancer cell lines *in vitro* (Kuznestov et al, 2008).

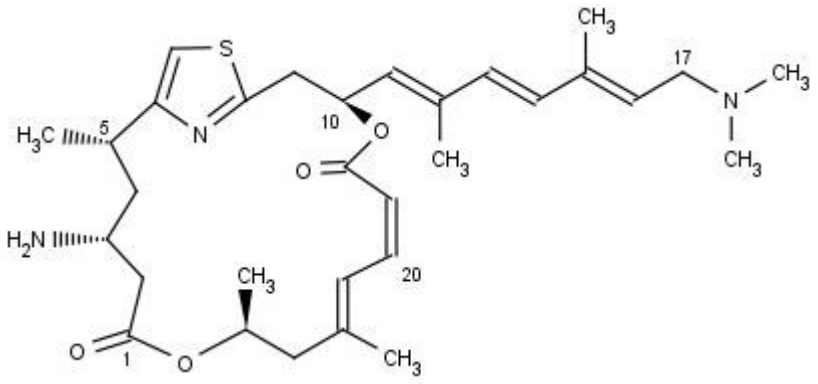


Figure 4.2. Structural formula of the natural product Pateamine A ($C_{31}H_{45}N_30_4S$).

Despite showing promising anti-cancer properties *in vivo*, eIF4A inhibitors are yet to be taken forward into phase I clinical trials. One reason for this is due to a mechanism of acquired resistance mediated by the over expression of the drug transporter ABCB1 (Gupta et al, 2011). Studies have shown that chronic exposure to Silvestrol in ALL cell lines lead to the upregulation of ABCB1 mRNA levels resulting in low bioavailability of the drug when administered orally; siRNA inhibition of ABCB1 re-sensitised ALL cell lines to Silvestrol (Gupta et al, 2011). In order to overcome this barrier, the same research group are working to develop nanoparticle mediated delivery of Silvestrol to overcome the ABCB1 mediated resistance mechanism (Gupta et al, 2011). There are currently no specific eIF4A2 inhibitors, nor are there any papers that investigate the role of eIF4A2 in hypoxic colorectal cancer cell survival.

It is hypothesised that eIF4A2 binds to and regulates the translation of a subset of mRNAs required for hypoxic cell survival, Data presented in chapter 1 of this thesis supports the notion that the eIF4A2 protein is maintained in hypoxia and therefore may play a more important role in hypoxic cell survival. Therefore by inhibiting eIF4A2, one should observe a reduction in cell survival, specifically in hypoxia. It is important to note that housekeeping

genes such as actin and GAPDH have previously been shown to be refractory to eIF4A inhibition by Silvestrol due to the lack of RNA-Quadruplexes and complex secondary structures within their 5'UTR (Wolfe et al, 2015).

I hypothesise that eIF4A2 inhibition will lead to a reduction in colorectal cancer cell survival in both normoxia and hypoxia, with an enhanced effect being observed specifically under hypoxic conditions. Furthermore I hypothesise this effect to be tumour specific as demonstrated by the lack of inhibition on cell survival in a normal colon epithelial cell line. Secondly I hypothesise eIF4A2 inhibition to lead to a reduction in colorectal 3D spheroid growth alongside an observation in the increase in tumour necrosis, an increase in the number of apoptotic cells and a decrease in the number of proliferating cells. Thirdly I hypothesise that eIF4A2 knockdown will lead to a reduction in xenograft tumour growth rate alongside an increase in necrotic cells within sheIF4A2 knockdown xenograft tumours.

I will test the hypothesise using the following aims and methodology:

1- To demonstrate that eIF4A2 knockdown with lead to significant reduction in colorectal cancer cell survival in normoxia with the effect being enhanced in hypoxia. This will be tested using siRNA knockdown of eIF4A2 followed by a clonogenic assay and exposure to 72 hours normoxia or hypoxia (1% O_2).
2- To demonstrate that the reduction in cell survival following eIF4A2 is tumour specific via siRNA inhibition of eIF4A2 followed by clonogenic assay and exposure to 72 hours normoxia or hypoxia (1% O_2) using a normal colon epithelial cell line.
3- To demonstrate that eIF4A2 inhibition leads to a reduction in 3D colorectal spheroid growth rates using an IPTG inducible sheIF4A2 cell line and immunohistochemical analysis of markers of interest.
4- To demonstrate that eIF4A2 knockdown will lead to a reduction in xenograft growth rates and an increase in xenograft tumour necrosis using an IPTG inducible sheIF4A2 knockout cell line and immunohistochemical analysis of tumours.

4.3 Results

4.3.1 siRNA inhibition of eIF4A2 and its effects on cell survival

siRNA knockdown of eIF4A2 was performed as previously described followed by clonogenic assay in HCT116, LS174T and CCD 841 CON cell lines. Cells were exposed to either 72 hours normoxia (20% O_2) or 72 hours hypoxia (1% 0_2) following plating, returned to normoxia and allowed to form colonies for 2 weeks. Colonies were stained and analysed as previously described. Data presented in Figure 4.3 demonstrates the results from the clonogenic assay following siRNA inhibition of eIF4A2 on HCT116 (Figure 4.3, A), LS174T (Figure 4.3, B) and CCD 841 CON (Figure 4.3, C). Following siRNA knockdown of eIF4A2 in HCT116 cells a significant reduction in cell survival was observed under normoxic conditions ($p<0.01$), and under hypoxic conditions ($p<0.001$). A significant difference was observed in the reduction of cell survival between normoxia and hypoxia in HCT116 cells ($p<0.01$) with a more significant reduction being observed under hypoxic conditions. Following siRNA knockdown of eIF4A2 in LS174T cells a significant reduction in cell survival was observed under normoxic conditions ($p<0.001$), and under hypoxic conditions ($p<0.001$). A significant difference was observed in the reduction of cell survival between normoxia and hypoxia in LS174T cells ($p<0.01$) with a more significant reduction being observed under hypoxic conditions. Interestingly the same reduction in cell survival was not observed following siRNA knockdown of eIF4A2 in the CCD 841 CON normal colonic epithelial cell line. Figure 32, C shows a significant increase ($p<0.01$) in cell survival following siRNA knockdown of eIF4A2 under hypoxic conditions. No significant difference in cell survival was observed in the control groups between normoxia and hypoxia for any of the cell lines tested. This data supports the hypothesis that eIF4A2 is required for both normoxic and hypoxic cell survival in colorectal cancer cells, with the observed effected enhanced under hypoxic conditions and this effect is tumour specific.

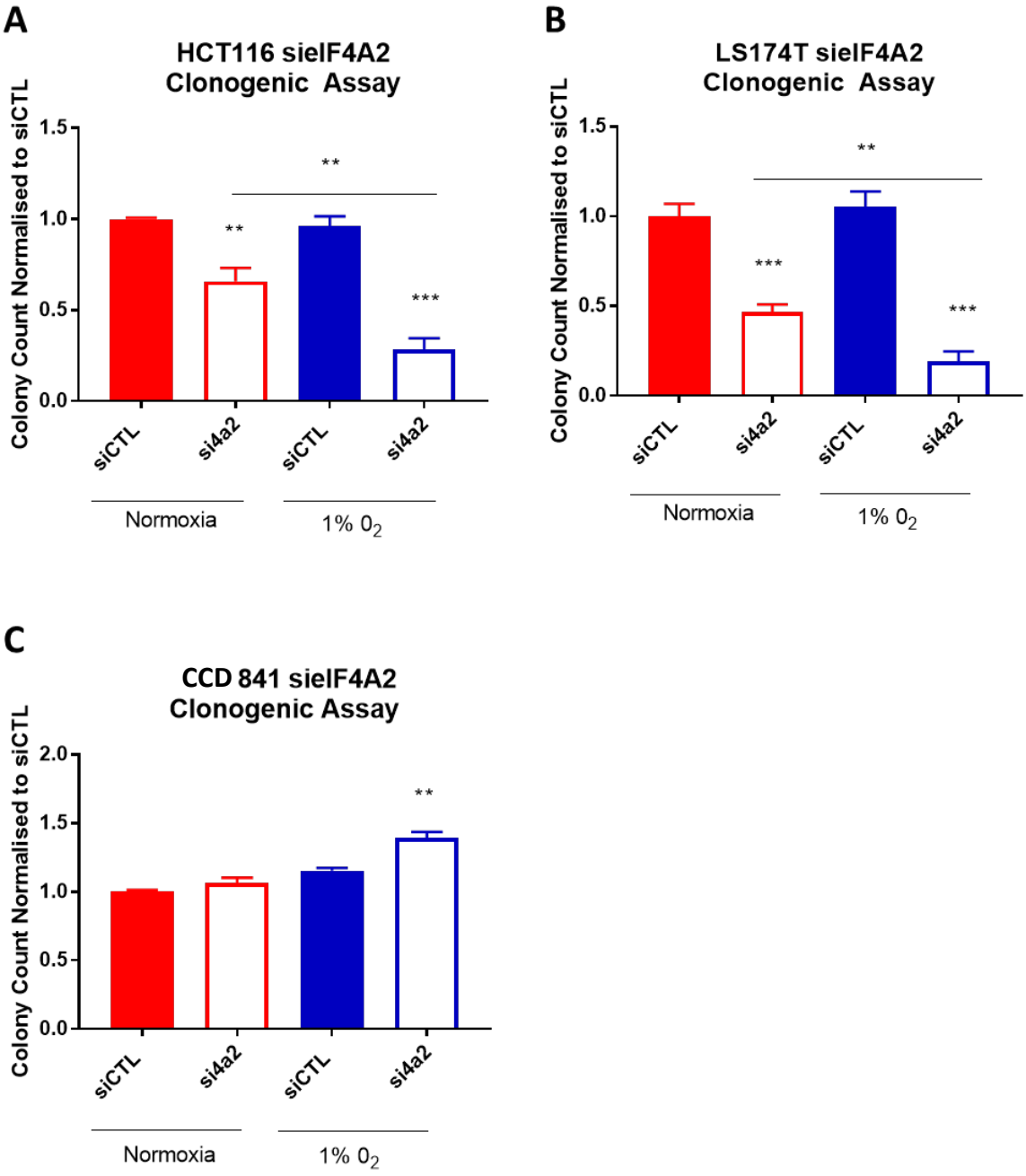


Figure 4.3. siRNA knockdown of eIF4A2 on cell survival. siRNA knockdown of eIF4A2 was performed as previously described and cell survival measured via clonogenic assay after 72 hours exposure to either normoxia (20% O_2) or hypoxia (1% O_2). (A) HCT116 (B) LS174T (C) CCD 841 CON. Error bars indicate ± SEM. Data were analysed for significance by one way ANOVA. *p<0.05, **p<0.01, ***p<0.001. n=3.

4.3.2 Generation of an IPTG inducible sheIF4A2 colorectal cancer cell line

Sigma MISSION® custom lentiviral shRNA services were used to generate IPTG inducible lentiviral transduction particles for this study using the pLKO-puro-IPTG 3xLacO inducible vector. Transduction of lentivrial particles and single cell clonal selection were performed as previously described. In order to validate the extent of eIF4A2 knockdown cells were plated and incubated with 1 mM IPTG for 3 or 4 days to induce shRNA expression with media changes containing fresh IPTG occurring every day. Due to the cell lines being derived from a single clone and are therefore an isogenic cell line, lysates were generated with and without IPTG incubation to determine the effect of IPTG alone on the cell lines.

4.3.4 qPCR validation of sheIF4A2 cell lines

HCT116 and LS174T shCTL, sh69 and sh84 were plated, incubated with 1mM IPTG for 3 or 4 days and eIF4A2 expression analysed via qPCR as previously described. The results presented in Figure 4.4 display knockdown validation of eIF4A2 mRNA for HCT116. Figure 4.4,A presents eIF4A2 knockdown following 3 day induction, Figure 4.4,B presents eIF4A2 knockdown following a 4 day induction. Knockdown of eIF4A2 with sh69 resulted in a significant reduction in eIF4A2 expression following induction with 1 mM IPTG under both normoxic ($p<0.001$) and hypoxic conditions ($p<0.001$). Knockdown of eIF4A2 with sh84 resulted in a significant reduction in eIF4A2 expression following induction with 1 mM IPTG under both normoxic ($p<0.001$) and hypoxic conditions ($p<0.001$). Identical results were obtained following a 4 day 1 mM IPTG induction as displayed in Figure 4.4, B. Therefore for HCT116 cells a 3 day 1 mM IPTG induction protocol was followed for all future experiments.

The results presented in Figure 4.6 display knockdown validation of eIF4A2 mRNA for LS174T. Figure 4.6,A presents eIF4A2 knockdown following 3 day induction, Figure 4.6,B presents eIF4A2 knockdown following a 4 day induction. Knockdown of eIF4A2 with sh69 resulted in no significant reduction in eIF4A2 under normoxic or hypoxic conditions following a three day 1 mM IPTG incubation. Knockdown of eIF4A2 with sh84 resulted in a significant reduction in eIF4A2 expression under both normoxic ($p<0.01$) and hypoxic conditions ($p<0.01$). Knockdown of eIF4A2 with sh69 following 4 days 1 mM IPTG incubation resulted in a significant reduction in eIF4A2 levels in both normoxic ($p<0.01$) and hypoxic conditions ($p<0.01$). Knockdown of eIF4A2 with sh68 following 4 days 1mM IPTG incubation resulted in a significant reduction in eIF4A2 levels in both normoxic ($p<0.001$) and hypoxic conditions ($p<0.001$). It was therefore decided to use a 4 day 1 mM induction protocol for LS174T cells going forward for all future experiments. There was no significant

difference in eIF4A2 mRNA expression in the shCTL line following 1mM IPTG induction in either cell line tested.

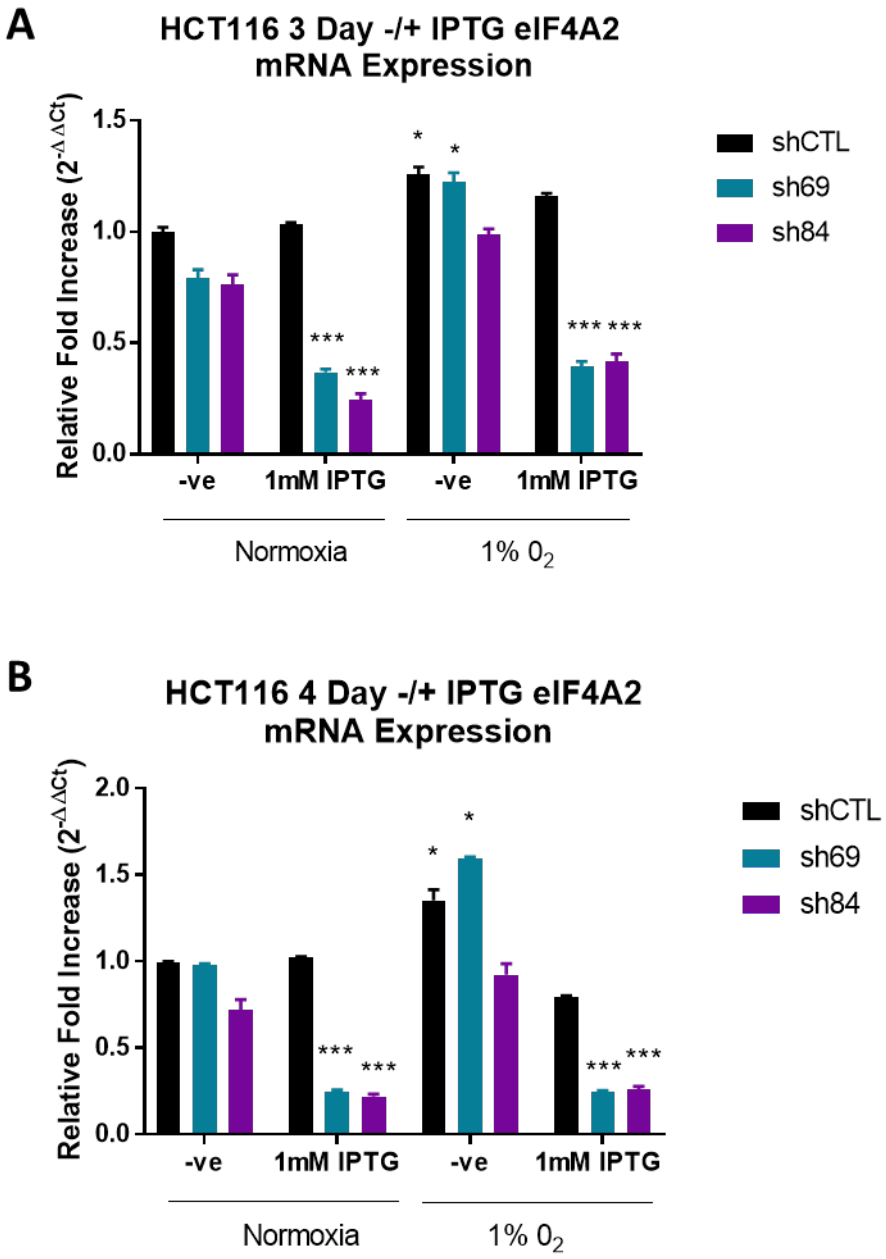


Figure 4.4. Validation of eIF4A2 IPTG inducible system at the RNA level in HCT116 cells. HCT116 shCTL, sh69 and sh84 cells were cultured with 1 mM IPTG for 3 or 4 days followed by exposure to 24 hours hypoxia (1% O_2). eIF4A2 mRNA was analysed via qRT-PCR. (A) 3 day 1mM IPTG induction (B) 4 day 1 mM IPTG induction. Error bars indicate ± SEM. Data were analysed for significance by one way ANOVA. *p<0.05, **p<0.01, ***p<0.001. n=3.

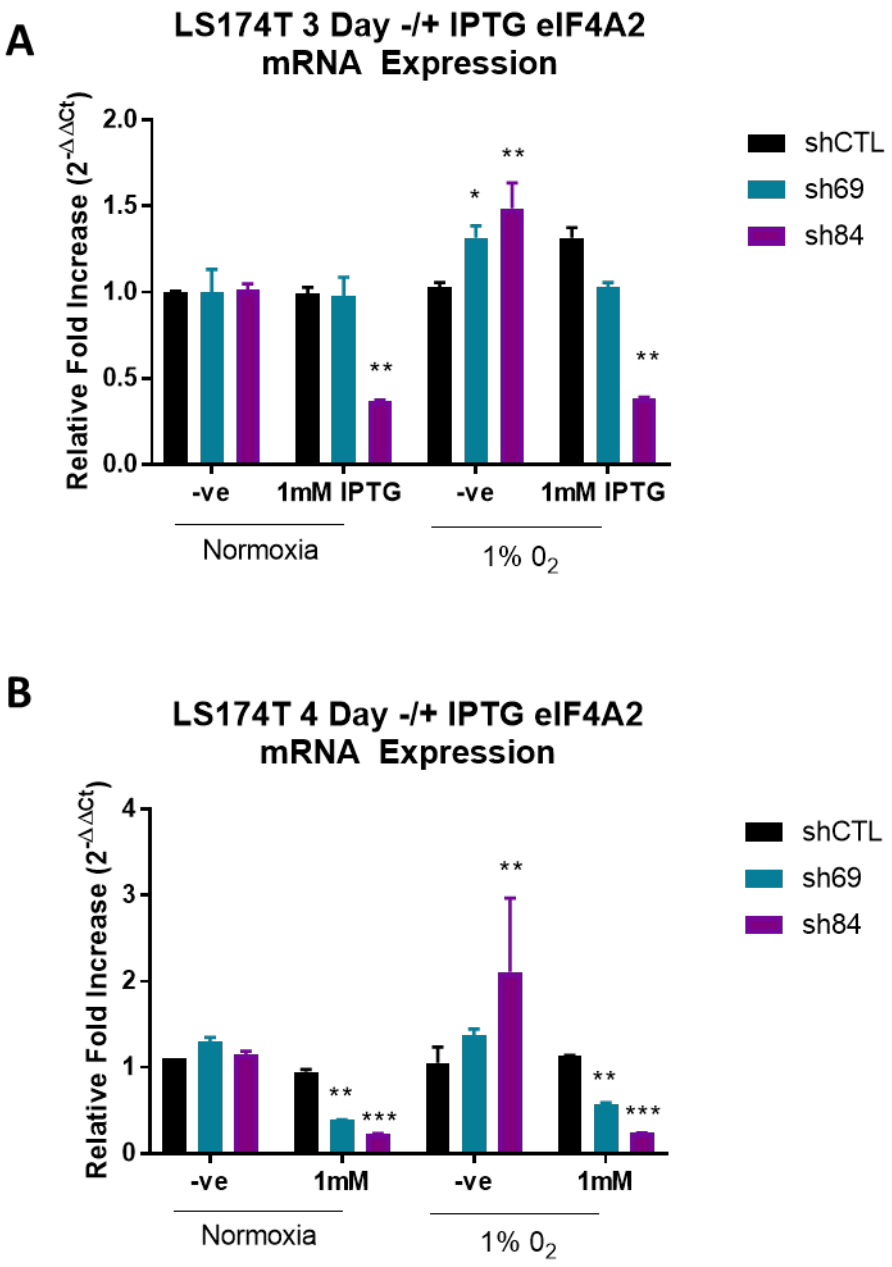


Figure 4.5. Validation of eIF4A2 IPTG inducible system at the RNA level in LS174T cells. LS174T shCTL, sh69 and sh84 cells were cultured with 1mM IPTG for 3 or 4 days followed by exposure to 24 hours hypoxia (1% O_2). eIF4A2 mRNA was analysed via qRT-PCR. (A) 3 day 1 mM IPTG induction (B) 4 day 1 mM IPTG induction. Error bars indicate ± SEM. Data were analysed for significance by one way ANOVA. *p<0.05, **p<0.01, ***p<0.001. n=3.

4.3.5 Immunoblot validation of sheIF4A2 cell lines

In order to validate knockdown of eIF4A2 at the protein level, HCT116 and LS174T (data not shown) were cultured with 1mM IPTG for 3 days exposed to normoxia (20% 0_2) or hypoxia (1% 0_2) for 24 hours and eIF4A2 expression analysed via immunoblot. Figure 4.6 presents validation of eIF4A2 knockdown at the protein level for HCT116 cells for the sh69 clone (Figure 4.6, A) and the sh84 clone (Figure 4.6, B). Similar results were also obtained for LS174T knockdown validation for eIF4A2 at the protein level.

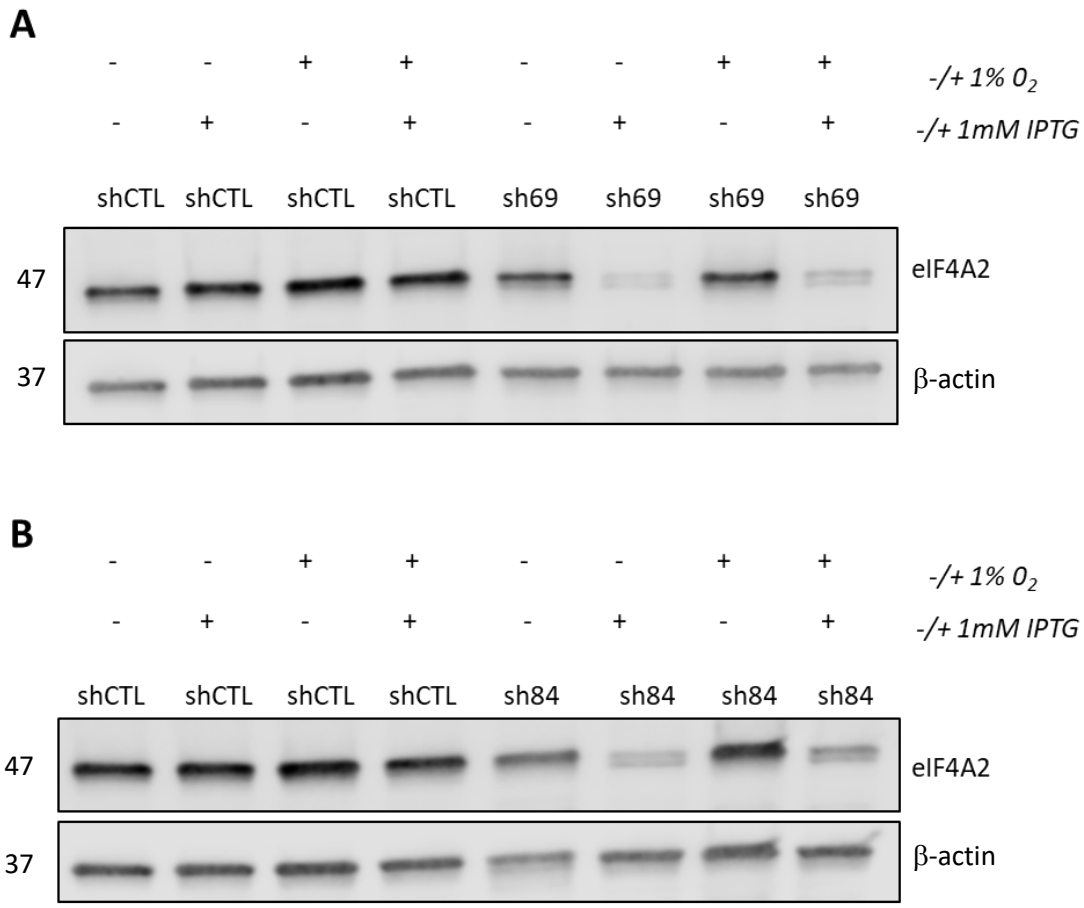


Figure 4.6. Validation of eIF4A2 IPTG inducible system at the protein level in HCT116 cells. HCT116 shCTL, sh69 and sh84 cells were cultured with 1mM IPTG for 3 days followed by exposure to 24 hours hypoxia (1% 0_2). eIF4A2 protein was analysed via immunoblot. (A) Validation of sh69 sequence (B) validation of sh84 sequence. Molecular weights in kDa are displayed on the left of the blot. n=3.

4.3.6 Effect of eIF4A2 Inhibition on Cell Growth

To assess the effect of eIF4A2 inhibition on short term cell growth, as opposed to more long term cell survival which is determined via clonogenic assay; sheIF4A2 HCT116 and LS174T cells were induced for 3/4 days with 1mM IPTG as previously described. 10,000 cells were seeded per well of a 6 well plate and exposed to 24, 48 and 72 hours normoxia (20% O_2) or hypoxia (1% O_2). At each time point cells were washed once with PBS and counted using Trypan Blue inclusion/exclusion to determine viable cells. Cells counts are expressed relative to 24 hour shCTL normoxic control. Figure 4.7 displays the results of cell counts following sheIF4A2 in HCT116 cells in normoxia (Figure 4.7, A) and hypoxia (Figure 4.7,B). A significant reduction in cell growth was observed following sheIF4A2 for both HCT116 sh69 and sh84 cell lines in comparison to shCTL under normoxic (Figure 4.7,A, $p<0.001$) and hypoxic conditions (Figure 4.7,B, $p<0.01$). Similar effects were observed for sheIF4A2 LS174T cells; a significant reduction in cell growth was observed following sheIF4A2 for both LS174T sh69 and sh84 cell lines in comparison to shCTL under normoxic (Figure 4.7,C,$p<0.01$) and hypoxic conditions (Figure 4.7,D,$p<0.05$)

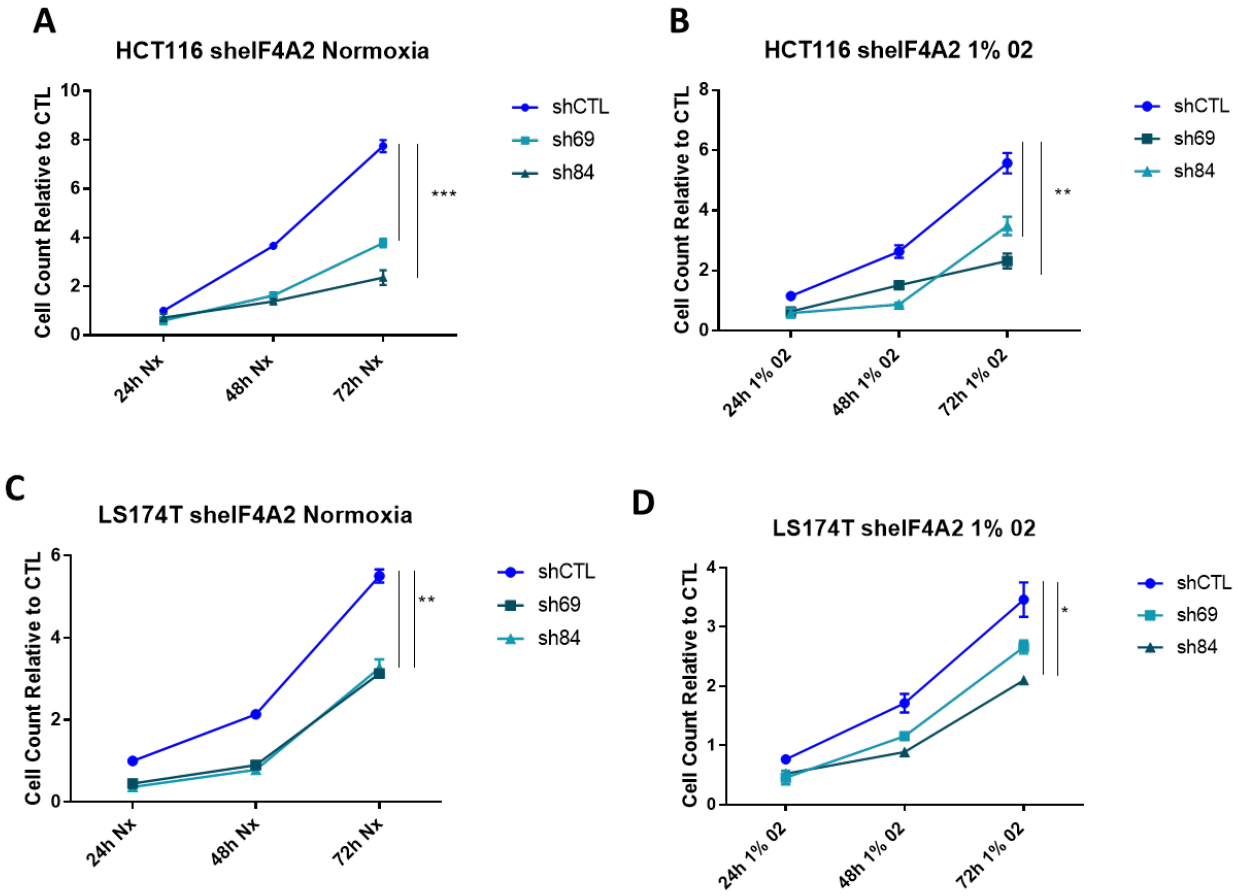


Figure 4.7. Effect of sheIF4A2 on cell growth in HCT116 and LS174T cells under normoxic and hypoxic conditions. Knockdown of eIF4A2 was induced as previously described, followed by exposure to 24, 48 or 72 hours normoxia (20% O_2) or hypoxia (1% O_2) followed by counting using Trypan Blue inclusion/exclusion criteria. (A) HCT116 sheIF4A2 normoxic (B) HCT116 sheIF4A2 hypoxia (C) LS174T sheIF4A2 normoxia (D) LS174T sheIF4A2 hypoxia. Error bars indicate ± SEM. Data were analysed for significance by t-test. *p<0.05, **p<0.01, ***p<0.001. n=3.

4.3.7 sheIF4A2 and its effects on 3D spheroid culture

In order to investigate the effects of eIF4A2 knockdown on 3D spheroid growth rates, sheIF4A2 cell lines were taken forward to generate tumour spheroids. Spheroids were formed from HCT116 and LS174T shCTL, sh69 and sh84 cells as previously described. In order to determine if IPTG alone had any effect on spheroid growth, all cell lines were grown in either the absence of presence of 1mM IPTG. The day of spheroid initiation, i.e.: plate centrifugation, is termed day 1. Spheroids had compacted by day 3 and images were taken every day for further analysis from day 3 onwards. Spheroids underwent media changes containing fresh 1 mM IPTG every other day. Spheroids were fixed as previously described on day 11 and underwent immunohistochemical analysis as previously described. Figure 4.9 presents spheroid volumes following eIF4A2 knockdown in HCT116 shCTL, sh69 and sh84 spheroids without (Figure 4.9,A) and with 1 mM IPTG induction (Figure 4.9, B). No significant difference was observed between any cell lines tested in the absence of 1mM IPTG as displayed in Figure 4.9, A. It was important to determine that these isogenic lines did not different in their growth rates without IPTG induction. Upon the addition of 1 mM IPTG and eIF4A2 knockdown, a significant reduction was found in spheroid volume (Figure 4.9,B. sh69;$p<0.05$, sh84;$p<0.01$). Figure 4.10 displays representative images from HCT116 sheIF4A2 spheroids across the duration of the culture period. With regards to LS174T, knockdown of eIF4A2 prevented the formation of spheroids. Following induction with 1 mM IPTG spheroids displayed a diffuse and abnormal morphology, distinct from that of the LS174T shCTL cell line as shown in Figure 4.8. Upon attempts to fix and embed the LS174T sheIF4A2 spheroids, they were observed to disintegrate and were unable to maintain their integrity as spheroid structures.

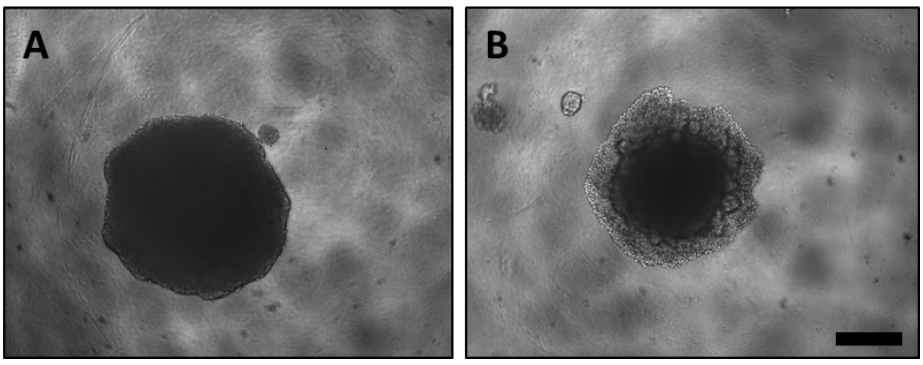


Figure 4.8. Representative images of LS174T sheIF4A2 spheroids failing to form. (A) LS147 shCTL (B) LS174T sh84. Images taken at x10 magnification. Scale bar represents 200μm.

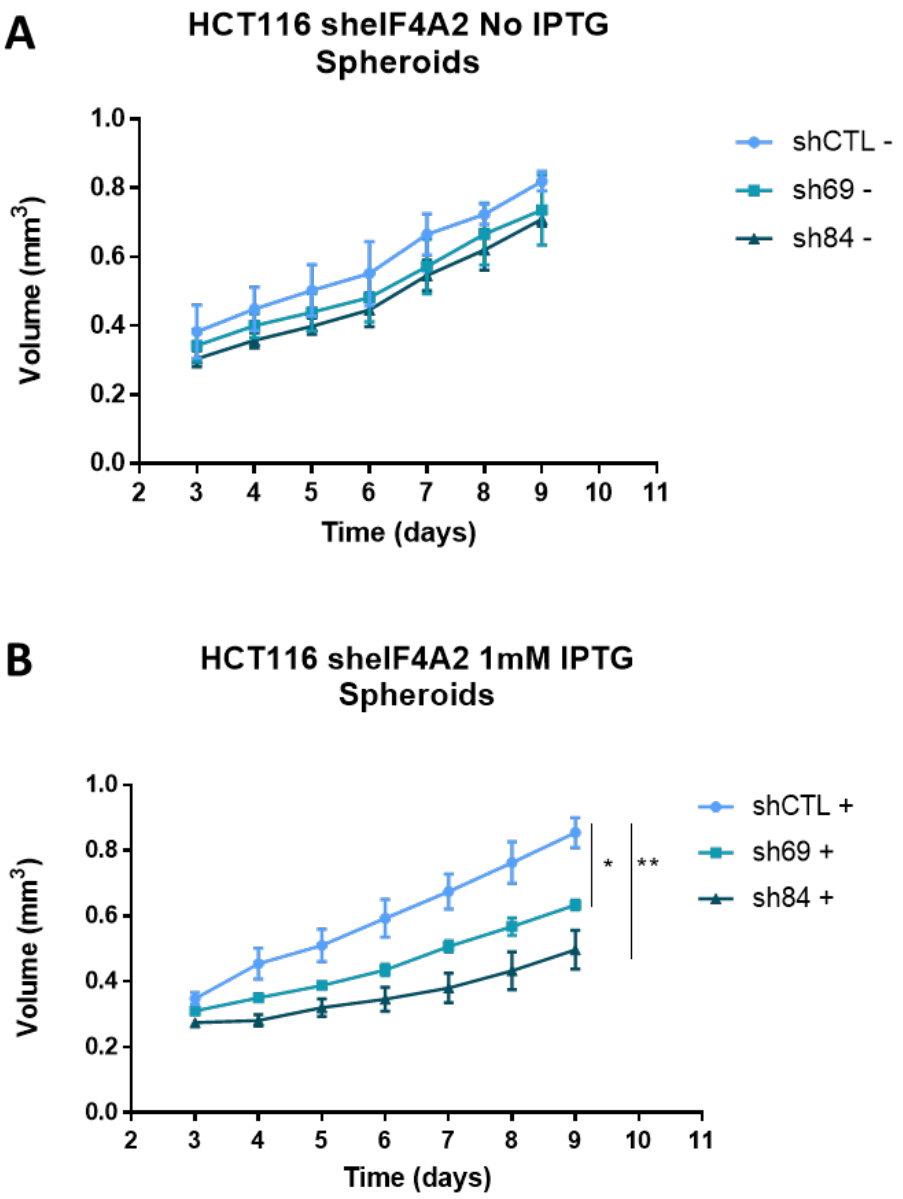


Figure 4.9. HCT116 sheIF4A2 spheroid growth rates. Spheroids were formed from HCT116 shCTL, sh68 and sh84 cell lines with and without 1mM IPTG induction. Photos were taken every day for 11 days and used to calculate spheroid volume (A) HCT116 sheIF4A2 lines without 1mM IPTG induction (B) HCT116 sheIF4A2 cells with 1 mM IPTG induction. . Error bars indicate ± SEM. Data were analysed for significance by t-test. *p<0.05, **p<0.01, ***p<0.001. n=3.

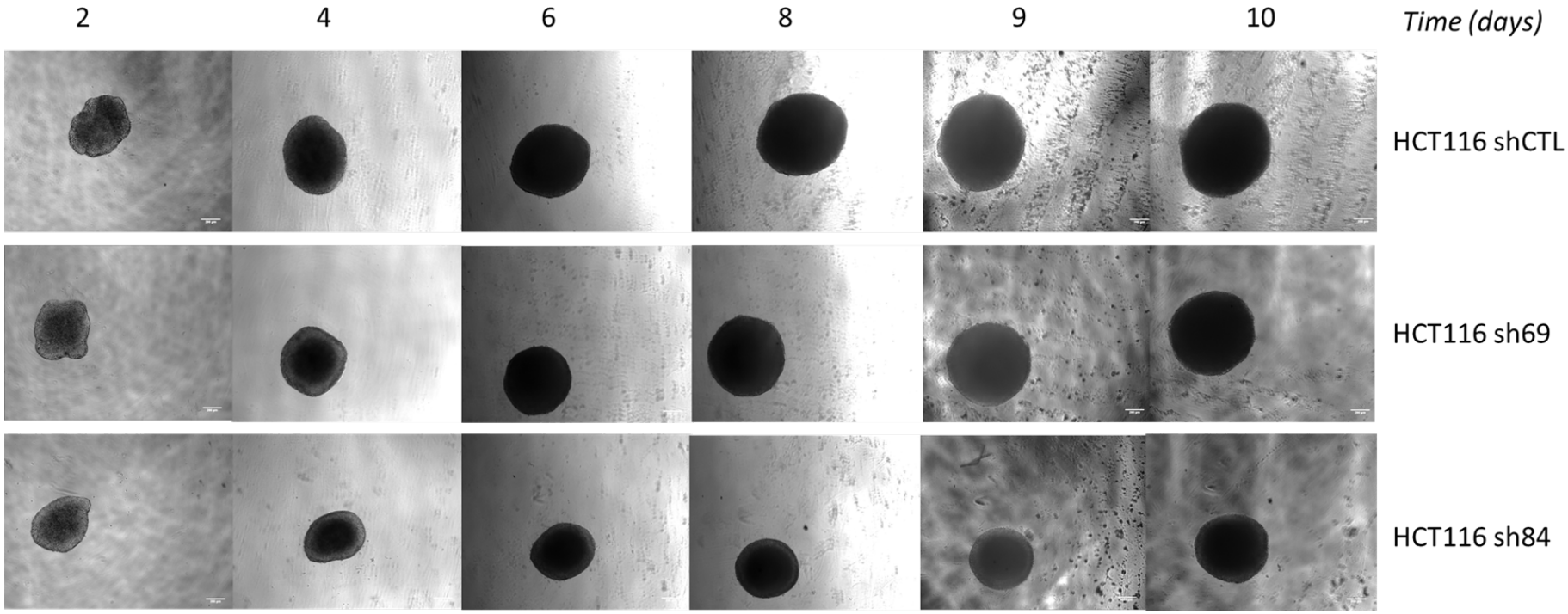


Figure 4.10. Representative images of HCT116 sheIF4A2 knockdown spheroids. Spheroids were grown as previously described from HCT116 shCTL, sh69 or sh84 cell lines. Images are representative from 3 experimental repeats of cell lines in the presence of 1mM IPTG. Scale bar represents 100 µm. Images taken at x10 magnification.

4.3.8 Immunohistochemical analysis of sheIF4A2 knockdown spheroids

It was first important to confirm successful knockdown of eIF4A2 within the spheroids; Figure 44 displays representative images of HCT116 sh84 without IPTG (Figure 4.11, A) versus HCT116 sh84 with 1mM IPTG (Figure 4.11, B) spheroids stained for eIF4A2 expression. eIF4A2 can be seen as a dark brown stain across the entirety of the spheroid, it is apparent that there is some reduction in eIF4A2 expression in the sheIF4A2 spheroids. It is important to consider the limitations of inducible knockdown cell lines used for spheroid formation; there may be issues with penetration of IPTG into the core of the spheroid as they continue to grow, leading to a reduced efficiency of eIF4A2 knockdown.

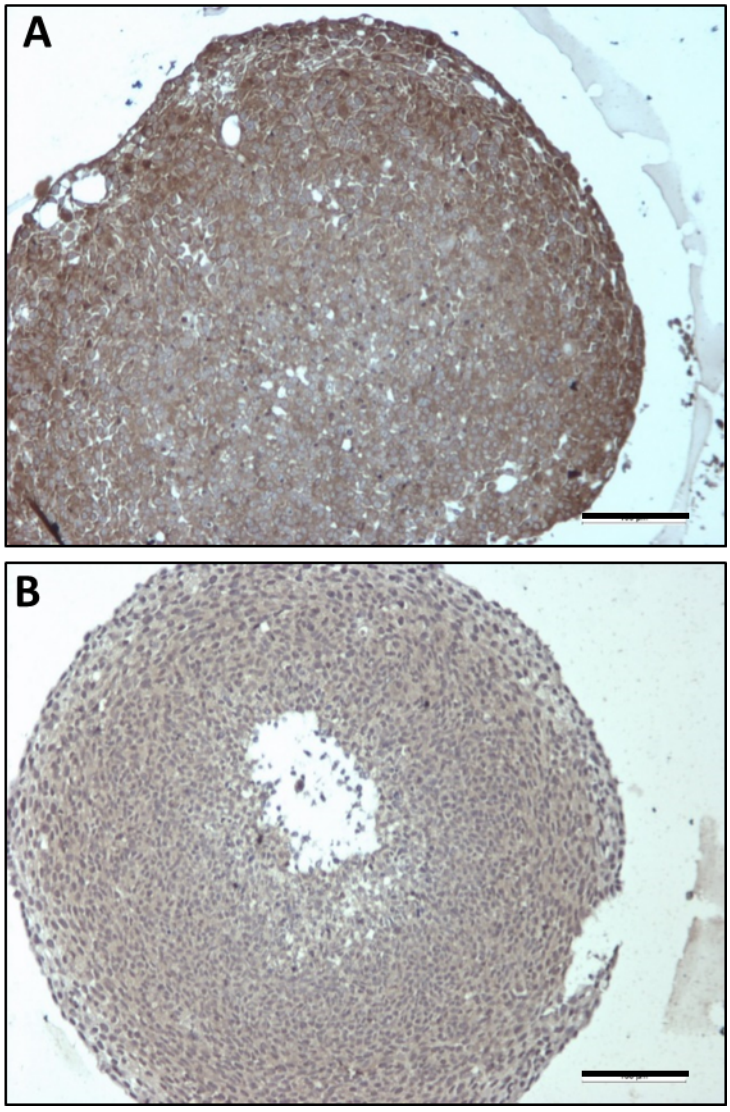


Figure 4.11. Representative images of eIF4A2 knockdown in HCT116 spheroids. (A) HCT116 sh84 no IPTG induction (B) HCT116 sh84 with 1 mM IPTG induction. eIF4A2 can be observed as a dark brown stain localised to the cytoplasm. Scale bar represents 100 µm. Images taken at x20 magnification.

4.3.9 sheIF4A2 Spheroid Necrosis

HCT116 sheIF4A2 spheroids underwent haematoxylin and eosin (H&E) staining to assess general morphology and levels of necrosis within the spheroids. Figure 4.12 displays representative images of central necrosis of HCT116 sheIF4A2 cells; Figure 4.12,A displays HCT116 shCTL spheroids, Figure 4.12,B displays HCT116 sh69 spheroids and Figure 4.12,C displays HCT116 sh84 spheroids all with 1 mM IPTG induction. Levels of central necrosis was observed to be increased in the HCT116 sh69 and sh84 sheIF4A2 conditions following 1 mM IPTG incubation. HCT116 sh69 and sh84 knockdown spheroids appeared to display differing patterns of necrosis; with HCT116 sh69 knockdown spheroids displaying a more diffuse necrosis across the whole of the spheroids and appearing very loosely packed (Figure 4.13,A,C,E) whilst sh84 knockdown spheroids appear to display more typical, central necrosis (Figure 4.13 B,D,F). This may be explained in part due to each cell line being derived from a single clone, and so it is expected that they may different slightly in growth rates and morphology to some extent. This data supported the decision to take the sheIF4A2 cell lines forward into an *in vivo* xenograft model in order to assess the effect of eIF4A2 knockdown on tumour growth rates.

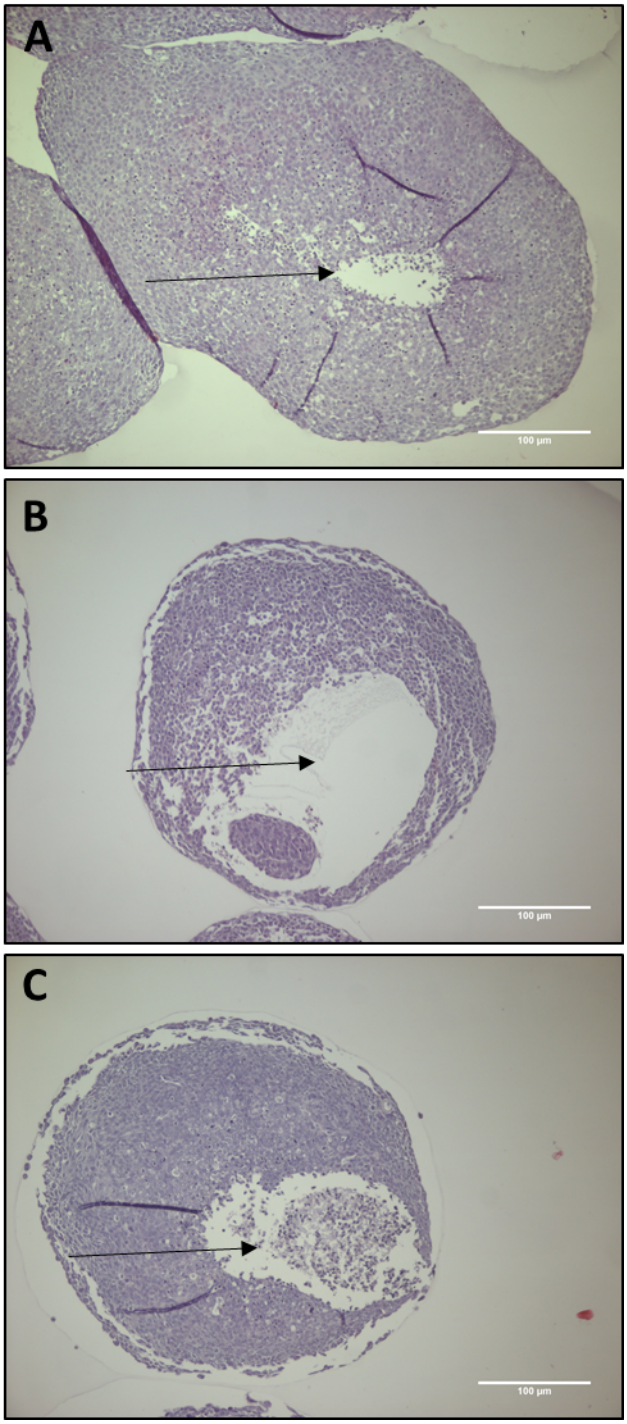


Figure 4.12. Representative images of sheIF4A2 HCT116 necrotic cores. HCT116 shCTL, sh69, sh84 spheroids were formed as previously described and stained with H&E to visually assess the levels of necrosis. (A) HCT116 shCTL (B) HCT116 sh69 (C) HCT116 sh84. Central necrosis is highlighted by the black arrows. Scale bar represents 100 µm. Images taken at x10 magnification. Representative images of 3 experimental repeats.

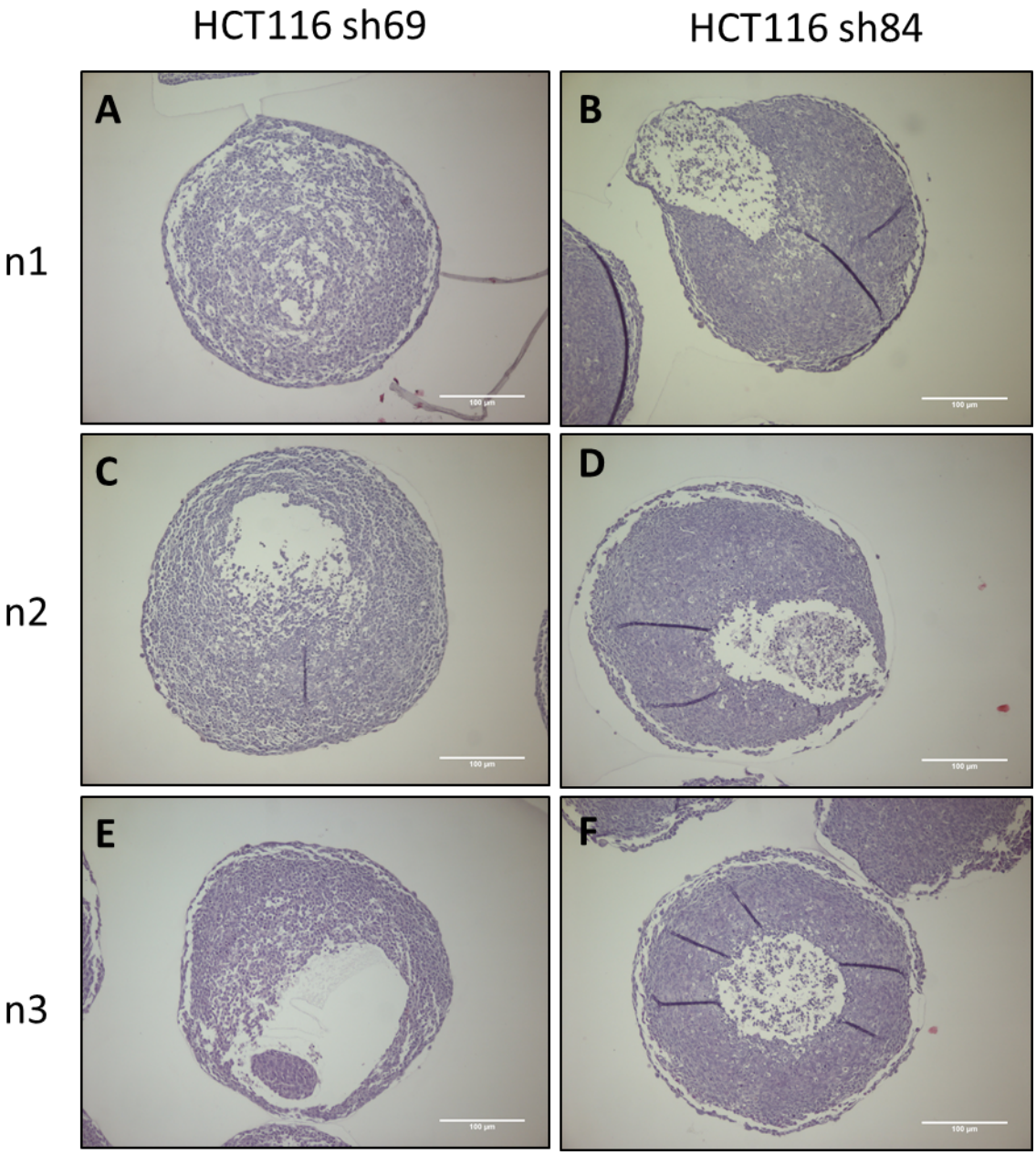


Figure 4.13. Representative images of differing patterns of necrosis between HCT116 sh69 and HCT116 sh94 cells. HCT116 sh69 and HCT116 sh84 spheroids were formed as previously described and stained with H&E to assess necrosis. (A, C, E) HCT116 sh69 representative images from each experimental repeat (B, D, and F) HCT116 sh84 representative images from each experimental repeat. Scale bar represents 100 µm. Images taken at x10 magnification.

4.3.10 HCT116 sheIF4A2 xenograft

In order to determine the role of eIF4A2 knockdown in an *in vivo* setting, HCT116 shCTL, HCT116 sh69 (sheIF4A2 (1)) and HCT116 sh84 (sheIF4A2 (2)) were luciferase labelled and taken forward into a xenograft experiment using CD-1 female mice, 6-7 weeks old and injected via an intra-peritoneal route ($2X10^6$ cells/mL). Tumour growth was measured via IVIS imaging for luciferase reporter expression. Images were also taken directly after implantation and then on a weekly basis. 10mM IPTG was provided in the drinking water and given ad-libitum to all groups with the addition of Ribena to mask flavours. An optical post mortem was used to identify spread into surround organs and tumours were split 5-:50 into neutral buffered formalin fixation and snap freezing. All animal work was carried out under a Home Office License, project license number P435A9CF8. Table 4 displays the groups used for the xenograft experiment (CSU1774).

Table 4. HCT116 sheIF4A2 experimental groups for xenograft (CSU1774).

Group	**Treatment**	**n**
Grp1 HCT116 shCTRL	+ IPTG	9
Grp2 HCT116 sheIF4A2 (1)	+ IPTG	9
Grp3 HCT116 sheIF4A2 (2)	+ IPTG	9

Figure 4.14, A displays the results of the HCT116 sheIF4A2 xenograft combined luciferase signal (ventral and dorsal orientation) for each experimental group. Figure 4.14,B displays the mean body weights for each experimental group. Upon analysis neither eIF4A2 knockdown group were statistically significant in comparison to the control group (shCTL vs sh69 p=0.297)(shCTL vs sh84 p=0.0954). No significant difference was observed in body weight. Upon post mortem analysis for tumour spread, in the shCTL experimental group, 5 out of 9 mice displayed visible tumour spread, sh69 experimental group, 2 out of 9 mice displayed visible tumour spread, and in the sh84 experimental group, 5 out of 9 mice displayed visible tumour spread.

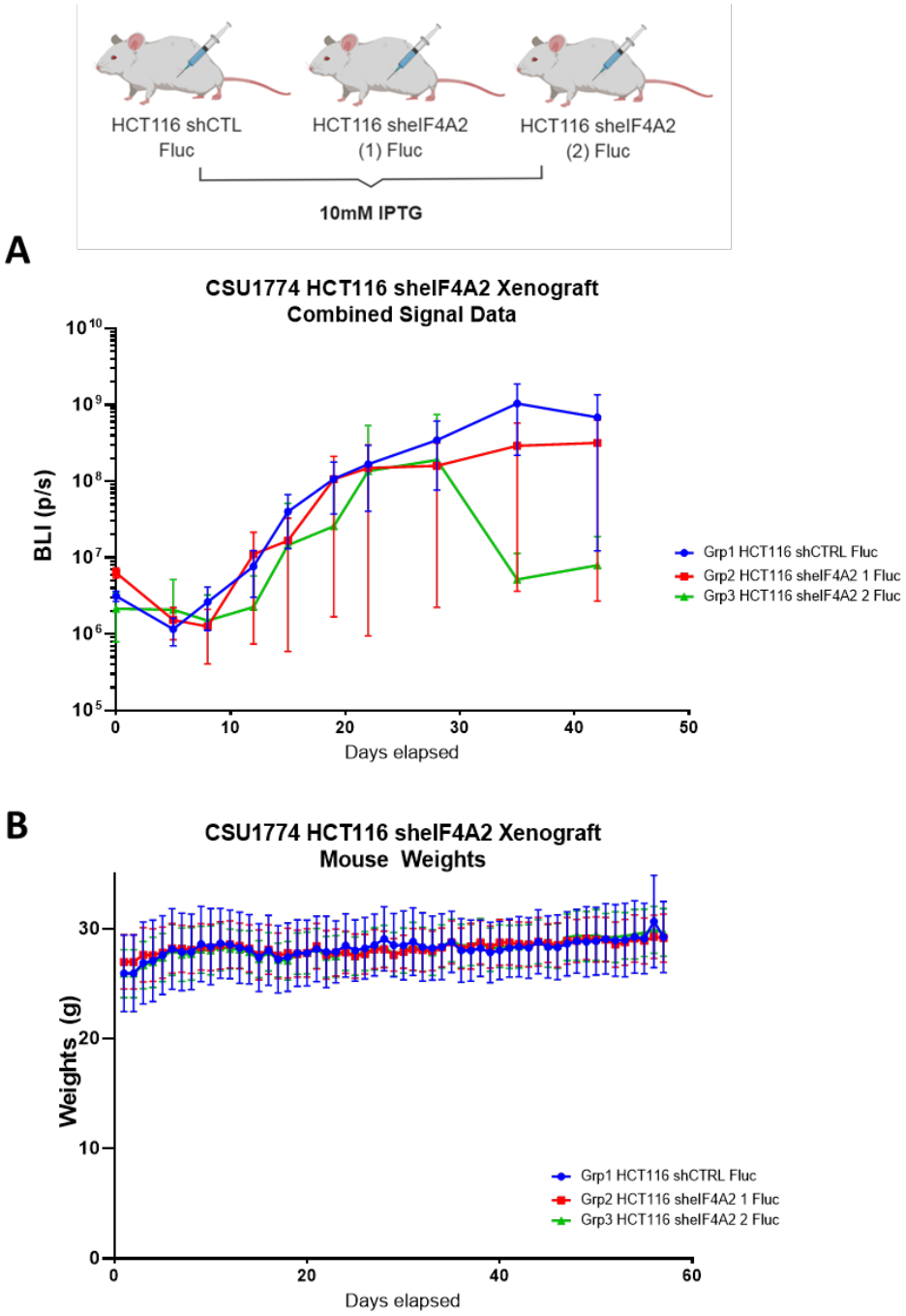


Figure 4.14. sheIF4A2 xenograft growth rates and average body weights. (A)Bioluminescent imaging (BLI) measured in photon emission (p/s) of HCT116 shCTRL (blue), sheIF4A2 1 Fluc (red) and HCT116 sheIF4A2 2 Fluc (green) xenograft tumours following 1mM IPTG induction (B) Body weights of HCT116 shCTRL (blue), sheIF4A2 1 Fluc (red) and HCT116 sheIF4A2 2 Fluc (green) bearing mice. Errors bar indicate ± SD. n=9

There were some concerns regarding the lack of tumour establishment following i.p implantation of HCT116 cell lines when compared to previous xenograft data of the same wild type cells (HCT116) implanted via the same route as shown by the additional growth curve in pink, overlaid onto the HCT116 sheIF4A2 data in Figure 4.15. Therefore due to the lack of tumour establishment it was decided to perform a short pilot study to determine if we could successfully grow the wild type cells in the strain of mice used, in addition to assessing if a sub cutaneous method of injection would be more successful. The pilot study consisted of HCT116 and LS174T wild type cells that had no undergone transduction with a control shRNA plasmid nor a luciferase plasmid. Both cell lines were injected sub-cutaneous into the flank of CD-1 female mice aged 6-7 weeks and measured via callipers every 3 days. 3 mice per group were used. All animal work was carried out under the project license number P435A9CF8.

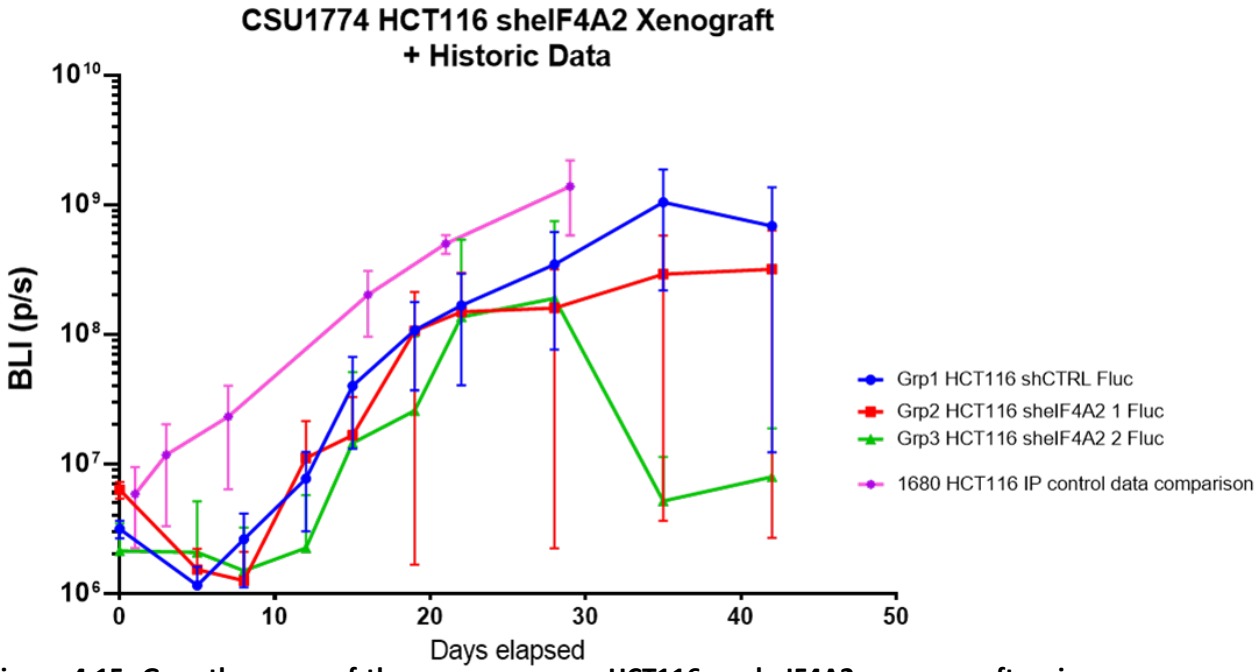


Figure 4.15. Growth curves of the HCT116 sheIF4A2 xenograft in comparison to historical data from HCT116 wild type cells of the same administration route. Bioluminescent imaging (BLI) measured in photon emission (p/s) of HCT116 shCTRL (blue), sheIF4A2 1 Fluc (red) and HCT116 sheIF4A2 2 Fluc (green) and SCU160 HCT116 wild type historical data (pink) xenograft tumours. Errors bar indicate ± SD. n=9



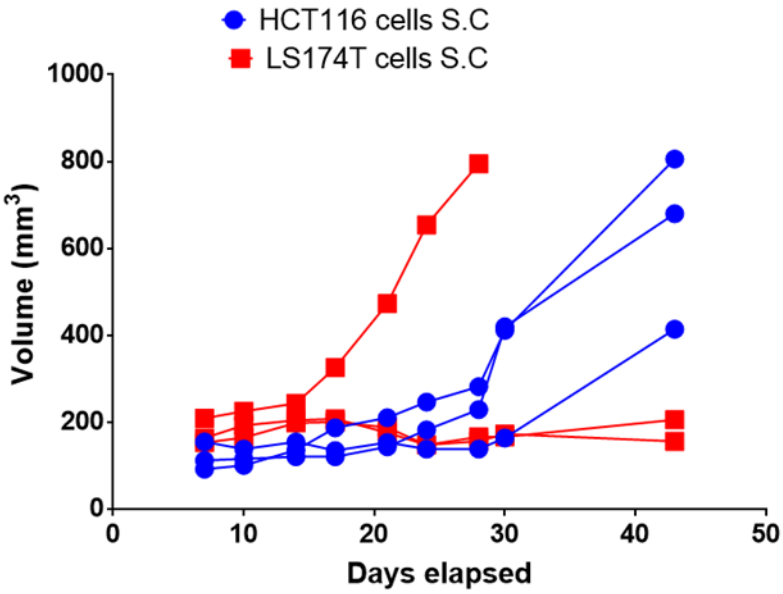


Figure 4.16. Pilot study of HCT116 and LS174T wild type cells. HCT116 and LS174T wild type cells were administered sub cutaneous into the flank of CD-1 nude female mice. Tumour height, width and length were measured via callipers every 3 days. Data displayed represents tumour volume (mm^3). n=3.

Figure 4.16 demonstrates successful tumour establishment for all mice bearing HCT116 wild type cells, however only one mouse bearing LS174T wild type cells showed successful tumour establishment even after 40 days following implantation. It was therefore decided to repeat the sheIF4A2 HCT116 xenograft experiment but this time using cells that had not undergone transduction with a luciferase reporter plasmid in addition to using a sub cutaneous route of administration.

The second improved xenograft study based on the data from the first xenograft and pilot study involved the use of, HCT116 shCTL cells with and without 1mM IPTG induction and HCT116 sh84 cells (sheIF4A2 (1)) with and without 1 mM IPTG induction. Cells were administered via a sub-cutaneous route into CD-1 female mice, 6-7 weeks old. Tumour growth was measured with the use of callipers to measure the length, width and height of

tumours every 3 days. 10 mM IPTG was provided in the drinking water and given ad-libitum to all groups requiring IPTG induction with the addition of Ribena to mask flavours. An optical post mortem was used to identify spread into surround organs and tumours were split 50:50 into neutral buffered formalin fixation and snap freezing. All animal work was carried out under the project license number P435A9CF8. Table 5 displays the groups used for the xenograft experiment (CSU1784).

Table 4.1. HCT116 sheIF4A2 experimental groups for xenograft (CSU 1784).

Group	**Treatment**	**n**
HCT116 shCTRL	+ IPTG	7
HCT116 shCTRL	-IPTG	7
HCT116 sheIF4A2 (1)	+ IPTG	7
HCT116 sheIF4A2 (1)	-IPTG	7

Figure 4.17 displays the results of the mean tumour volume (Figure 4.17,A), mean tumour diameter (Figure 4.17,B) and mean body weights (Figure 4.17,C) of the HCT116 sheIF4A2 sub-cut xenograft study. A significant difference in body weights was observed between shCTL + IPTG and HCT116 sh84 + IPTG ($p<0.05$). Raw values for both tumour volumes and tumour diameters were Log transformed to enable generation of growth curves in order to assess statistical differences between the groups. Log transformed growth curves of mean tumour volume are presented in Figure 4.18 and diameters Figure 4.19. Differences in growth rates were analysed using an unpaired student's t-test. Unfortunately no statistically significant differences were found between shCTL + IPTG and sh84 + IPTG in either tumour volume ($p=0.3429$) or tumour diameter ($p=0.3213$).

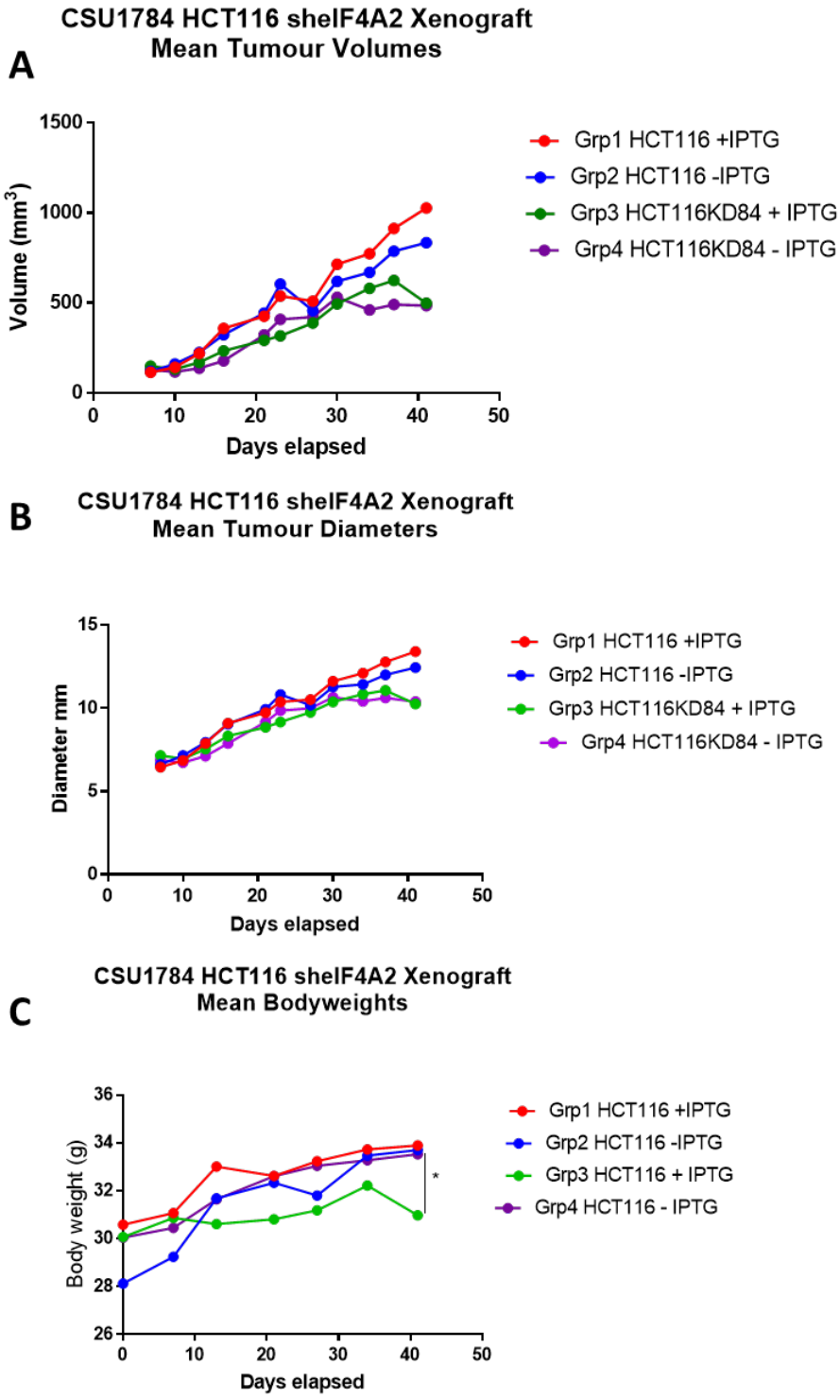


Figure 4.17. Tumour growth rates of HCT116 sheIF4A2 xenografts (CSU1784). HCT116 shCTL with (red) and without 1mM IPTG (blue) and HCT116 sh84 with (green) and without 1mM (purple) IPTG xenograft tumours. Tumour height, width and length were measured via callipers every 3 days. (A) HCT116 sheIF4A2 xenograft mean tumours volumes displayed as volume (mm3) (B) HCT116 xenograft mean tumour diameters (mm) (C) HCT116 sheIF4A2 mean bodyweights. Data were analysed via unpaired t-test. *p<0.05. n=7.

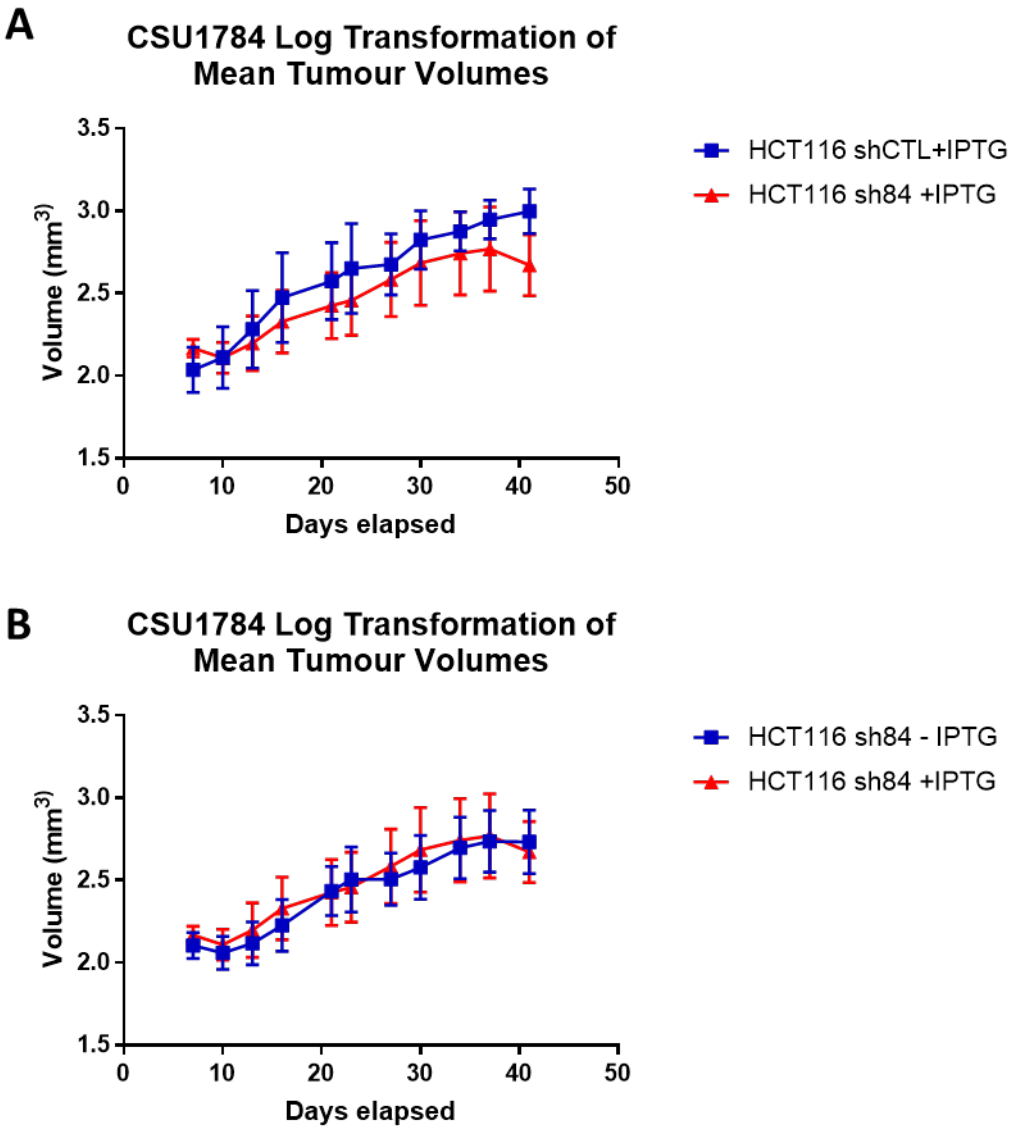


Figure 4.18. Log transformation of HCT116 sheIF4A2 xenograft tumour volumes. (A) Log transformation of HCT116 shCTL + IPTG xenografts (blue) and HCT116 sh84 + IPTG xenograft volume (red) (B) Log transformation of HCT116 sh84 - IPTG xenografts (blue) and HCT116 sh84 + IPTG xenograft (red) volumes. Error bars ± SD. Data were analysed via unpaired student's t-test. n=7.

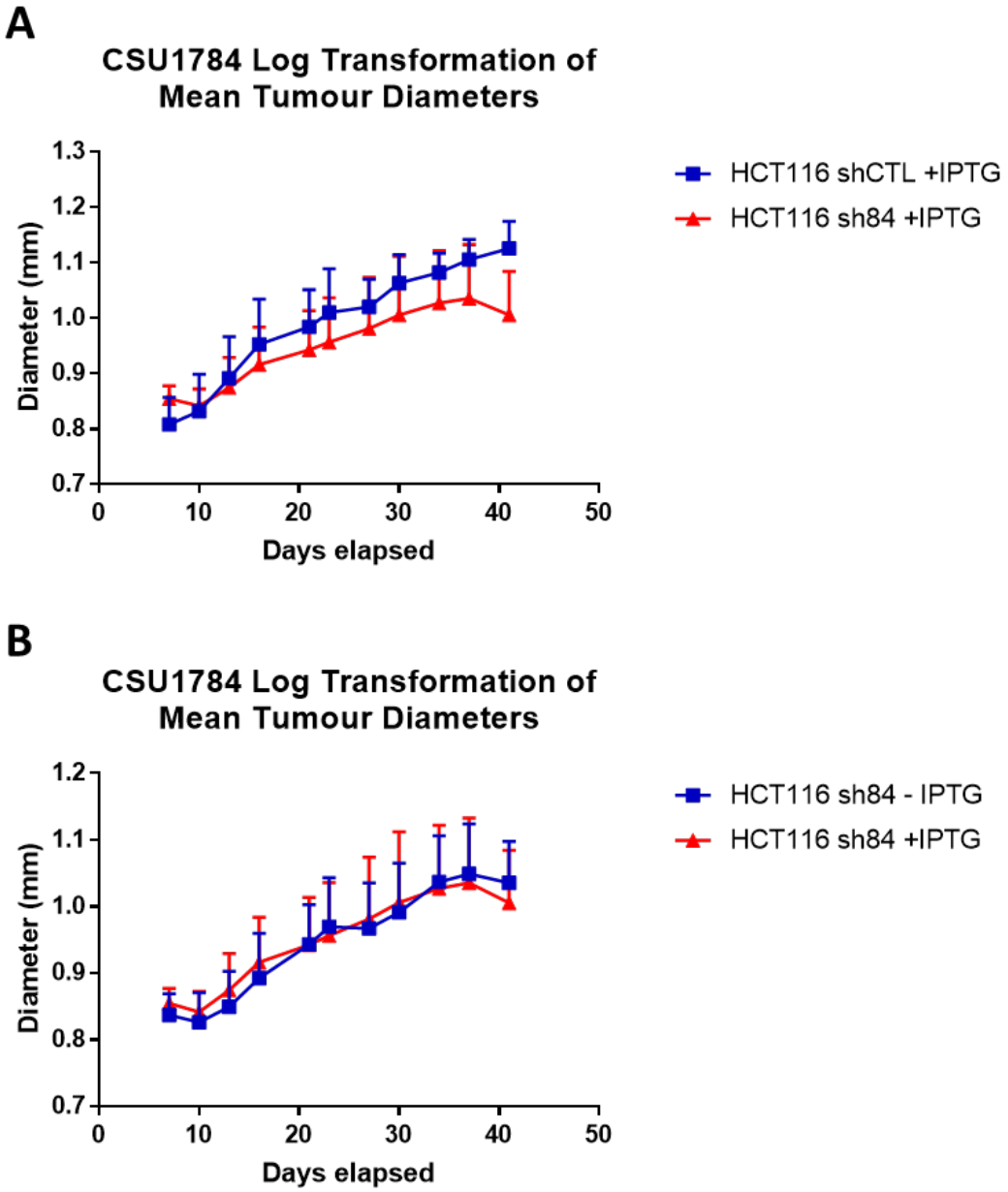


Figure 4.19. Log transformation of HCT116 sheIF4A2 xenograft tumour diameters. (A) Log transformation of HCT116 shCTL + IPTG xenografts (blue) and HCT116 sh84 + IPTG xenograft diameter (red) (B) Log transformation of HCT116 sh84 - IPTG xenografts (blue) and HCT116 sh84 + IPTG xenograft (red) diameters. Error bars ± SD. Data were analysed via unpaired student's t-test. n=7.

4.3.11 Immunohistochemical Analysis of HCT116 sheIF4A2 Xenografts

HCT116 shCTL +IPTG and HCT116 sh84 + IPTG xenografts were stained with H&E in order to first assess the amount of necrosis present in each tumour. Necrotic cells display the following common morphological features: organelle swelling, dilation of nuclear membrane, translucent cytoplasm, and condensation of chromatin in irregular patches, cytoplasmic vacuoles and loss of cell membrane integrity (Vandenabeele et al, 2010). Figure 4.20 and 4.21 display H&E staining of HCT116 shCTL + IPTG for each mouse, each figure displays a scan of the whole tissue slice (not to scale) alongside a magnification box of the necrotic tissue from each mouse taken at x20 magnification. Figure 4.22 and 4.23 display H&E staining of HCT116 sh84 + IPTG for each mouse.

With regards to the amounts of necrosis within the HCT116 sh84 + IPTG samples, with the exception of mouse 21 (Figure 4.23, E, F), all sheIF4A2 xenograft tumours can be characterised by large amounts of central necrosis. In particular mouse 17 (Figure 4.22, C, D), mouse 18 (Figure 4.22, E, F), mouse 18 (Figure 4.23, A, B) and mouse 20 (Figure 4.23, C, D), almost the entirety of the tumour was comprised of necrotic tissue as highlighted by the green boxes.

Figure 4.24 displays the quantification of necrotic cells between the shCTL and sheIF4A2 xenograft tumours, a significant increase in necrosis was observed in the sheIF4A2 xenograft tumours in comparison to the control ($p<0.05$).

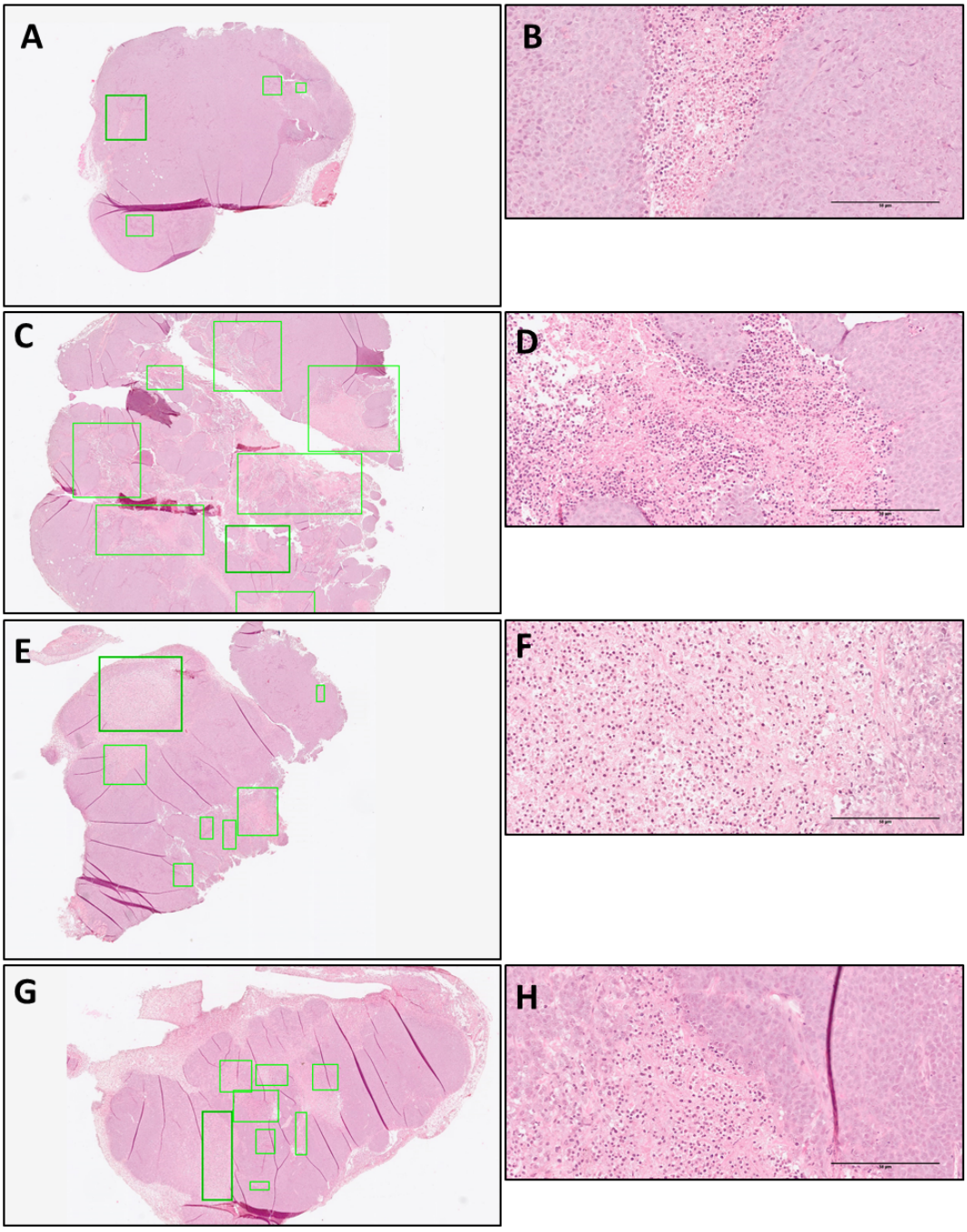


Figure 4.20. H&E staining of HCT116 shCTL + IPTG xenograft samples (CSU1784). H&E staining of tumours excised from each mouse. For each mouse there is displayed a scan of the whole tissue section (not to scale) alongside a magnification box displaying a representative image of necrotic tissue. Necrotic tissue across the whole tissue sample is highlighted by the green boxes. (A,B) mouse 9 (C,D) mouse 9 (E,F) mouse 10 (G,H) mouse 11. Scale bar represents 50 µm. Magnification box images taken at 20x.

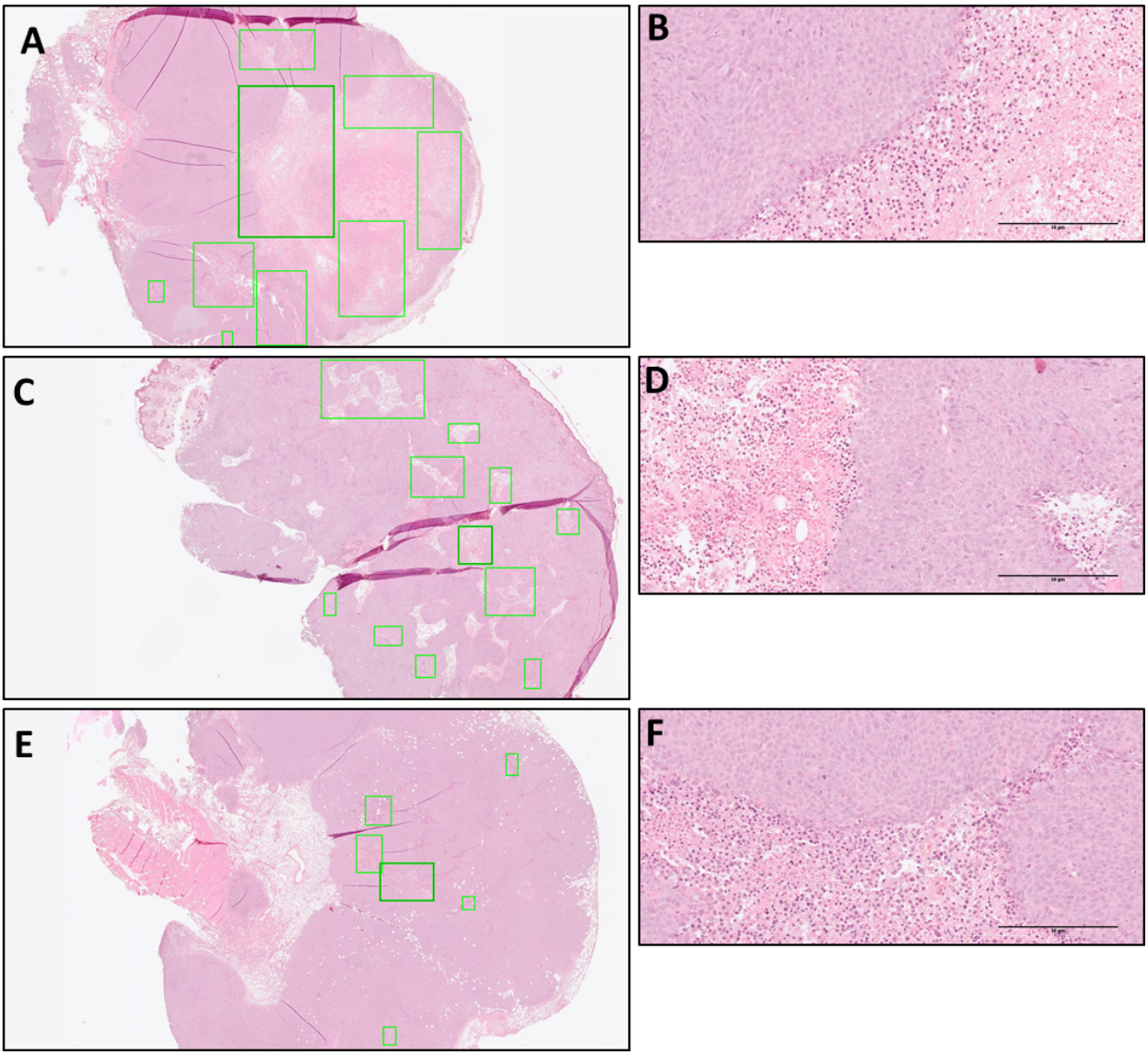


Figure 4.21. H&E staining of HCT116 shCTL + IPTG xenograft samples (CSU1784). H&E staining of tumours excised from each mouse. For each mouse there is displayed a scan of the whole tissue section (not to scale) alongside a magnification box displaying a representative image of necrotic tissue. Necrotic tissue across the whole tissue sample is highlighted by the green boxes. (A,B) mouse 12 (C,D) mouse 13 (E,F) mouse 14. Scale bar represents 50 µm. Magnification box images taken at 20x.

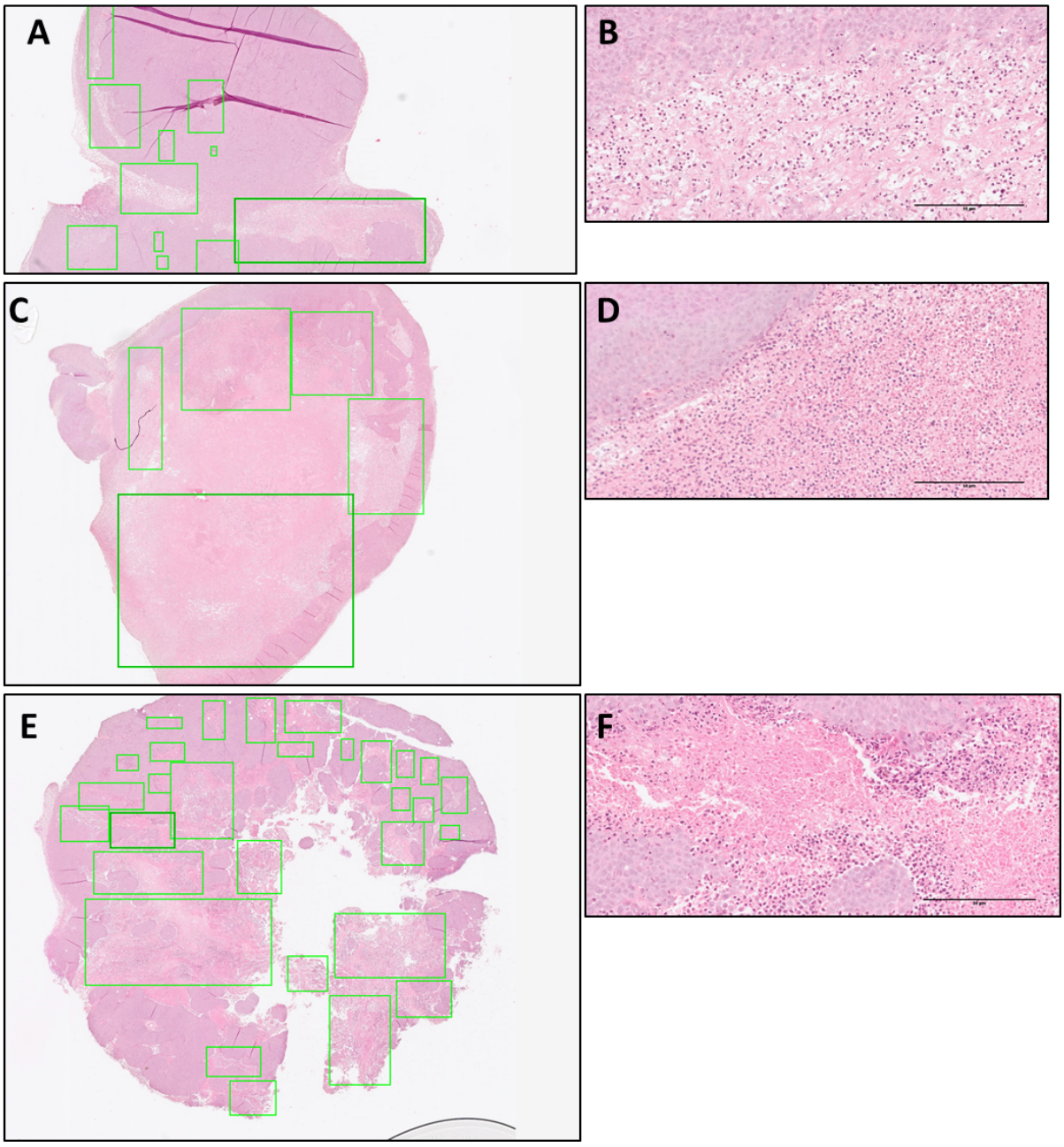


Figure 4.22. H&E staining of HCT116 sh84 + IPTG xenograft samples (CSU1784). H&E staining of tumours excised from each mouse. For each mouse there is displayed a scan of the whole tissue section (not to scale) alongside a magnification box displaying a representative image of necrotic tissue. Necrotic tissue across the whole tissue sample is highlighted by the green boxes. (A,B) mouse 15 (C,D) mouse 17 (E,F) mouse 18. Scale bar represents 50 µm. Magnification box images taken at 20x.

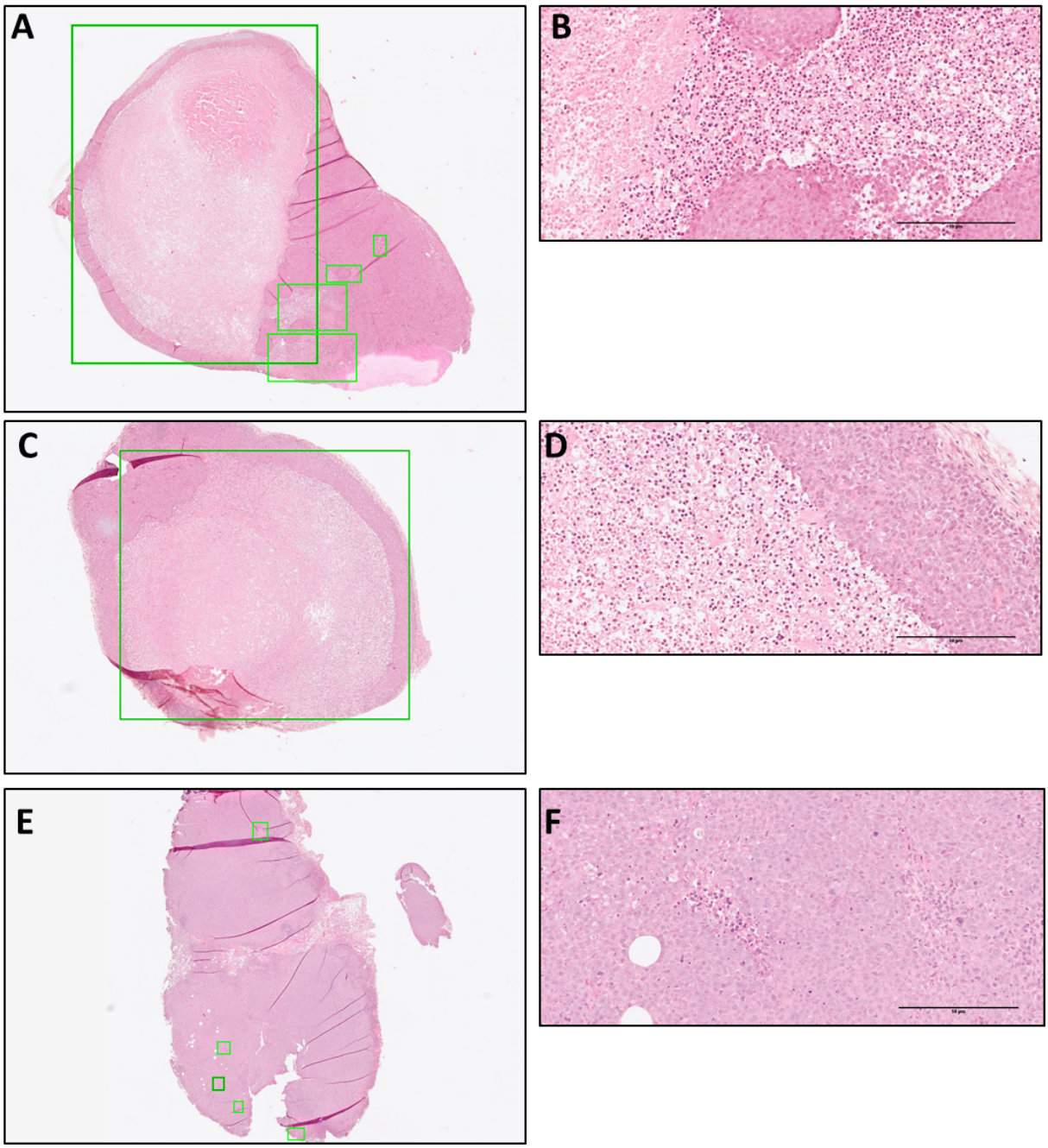


Figure 4.23. H&E staining of HCT116 sh84 + IPTG xenograft samples (CSU1784). H&E staining of tumours excised from each mouse. For each mouse there is displayed a scan of the whole tissue section (not to scale) alongside a magnification box displaying a representative image of necrotic tissue. Necrotic tissue across the whole tissue sample is highlighted by the green boxes. (A,B) mouse 19 (C,D) mouse 20 (E,F) mouse 21. Scale bar represents 50 µm. Magnification box images taken at 20x.

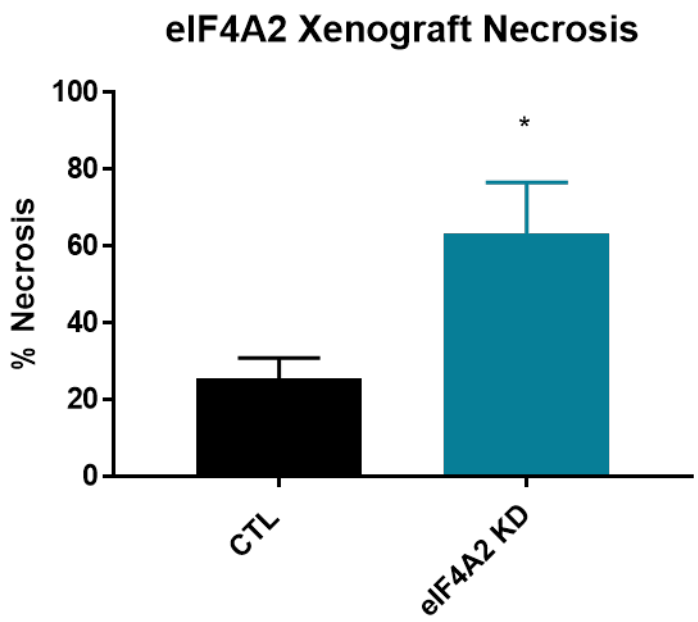


Figure 4.24. Quantification of necrosis in shCTL and sheIF4A2 xenograft tumours (CSU1784). shCTL and sheIF4A2 knockdown paraffin embedded tumours were stained with H&E and visually scored for percentage of necrosis. Error bars ± SD. Data were analysed via unpaired student's t-test. *p<0.05, **p<0.01, ***p<0.001. n=7.

4.4 Discussion

The data presented in this chapter demonstrates that inhibition of eIF4A2 significantly inhibits colorectal cancer cell survival in normoxia, with an enhanced effect being observed in hypoxia. Furthermore this effect was observed to be tumour specific as for the first time no negative effect of eIF4A2 knockdown was observed in a normal colon epithelial cell line. Due to the negative effects of eIF4A2 inhibition on long term cell survival, an IPTG inducible shRNA methodology was selected as the most appropriate to carry out future experiments with. sheIF4A2 lead to a significant reduction in spheroid growth rates in HCT116 cells; and an increase in central necrosis was observed within such spheroids. In addition HCT116 sheIF4A2 xenografts failed to show a significant reduction in tumour volume however tumours from sheIF4A2 bearing cells displayed a significant increase in necrosis as demonstrated by H&E staining.

4.4.1 The effect of eIF4A2 inhibition of colorectal cancer cell survival

siRNA knockdown of eIF4A2 was shown to lead to a significant reduction in cell survival in both HCT116 and LS174T colorectal cell lines and demonstrated via clonogenic assay as displayed in Figure 4.3. In addition there was a significant decrease in cell survival under hypoxic conditions in comparison to normoxic conditions following eIF4A2 knockdown. This

data suggests that colorectal cancer cells are more dependent on eIF4A2 for their survival in normoxic conditions, but more so under hypoxic conditions. This highlights the value of developing eIF4A2 inhibitors in order to specifically target the hypoxic fraction of tumour cells in the future. The data displayed in Figure 4.3 in in agreement with previous literature demonstrating that eIF4A inhibitors possess potent anti-cancer properties (Novac, 2004). It is hypothesised that this is due to a subsequent reduction in eIF4A2 hypoxic dependent transcripts that are yet to be identified. Such transcripts based on previous literature identifying the eIF4A translatome (Wolfe et al, 2014)(Rubio et al, 2014)(Modelska et al, 2015) would likely be enriched for pro-survival proteins enriched for metabolism, angiogenesis, pH regulation, apoptosis and other hallmarks of cancer and processes required for continued survival under hypoxic conditions. The result observed in the normal colon epithelial cell line (Figure 4.3, C) is a promising one; suggesting that if a specific eIF4A2 inhibitor were to be developed, normal cells would remain unaffected. However one question remains, what is the effect of total knockout of eIF4A2 on the normal colon epithelial phenotype *in vitro* and *in vivo* if eIF4A2 is required for the translation of proteins required for cellular homeostasis, as it is required for all transcripts translated via cap-dependent translation. Furthermore, a significant increase in cell survival was observed following eIF4A2 knockdown in CCD 841 CON cells, specifically under hypoxic conditions. This poses the question, would this increase in cell survival eventually give rise to a hyper proliferative state in the normal colon epithelium leading to an increase risk of an adenocarcinoma developing? Further studies such as eIF4A2 knockout in normal colon epithelial cells followed by long term culture, perhaps as spheroids or organoids in order to study the long term effects of eIF4A2 knockdown on the normal colon epithelium.

4.4.2 The generation of an inducible sheIF4A2 line and its effects on colorectal spheroid growth

shRNA knockdown of eIF4A2 was found to significantly reduce spheroid volume as shown in Figure 4.9 and representative images in Figure 4.10. HCT116 shCTL, sh69 and sh89 spheroids did not significantly differ in their growth rates in the absence of 1 mM IPTG. Cells were induced with 1 mM IPTG for 3 days before the formation of spheroids; both sh69 ($p<0.05$) and sh84 ($p<0.01$) spheroids displayed significantly reduced growth rates as represented by spheroid volume in comparison to the shCTL spheroids. sh84 spheroids displayed the most significant reduction in spheroid volume in comparison to shCTL spheroids ($p<0.01$). This reduction in spheroid growth rate is again hypothesised to be due to the reduction in eIF4A2 dependent transcriptions following eIF4A2 knockdown, such transcripts remain to be identified. H&E staining of sheIF4A2 spheroids revealed an

increase in central necrosis in sh69 and sh84 spheroids in comparison to shCTL spheroids as shown in Figure 4.12 and 4.13. This data supports the fact that eIF4A2 knockdown leads to a reduction in colorectal spheroid growth rates and an increase in spheroid necrosis which has previously never been published before.

4.4.3 eIF4A2 knockdown and its effects on xenograft growth rate

Despite seeing a significant reduction in spheroid growth rate following eIF4A2 inhibition, no significant decrease in xenograft tumour volume or diameter was observed following shRNA knockdown of eIF4A2 when compared against the non-targeting control shRNA. Despite this, a significant increase in xenograft tumour necrosis was observed in the sheIF4A2 xenograft tumours. This is a promising result but would need to be investigated further via immunohistochemical staining for markers of apoptosis such as cleaved caspase 3. One reason for a lack of statistical difference in xenograft growth rates may be due to the lack of eIF4A2 knockdown within the xenografts. To combat this possibility, eIF4A2 knockdown was induced with 1 mM IPTG for 3 days prior to injection into mice to ensure adequate eIF4A2 knockdown. However, due to the mice being supplied with IPTG *ad libitum* in drinking water, it is possible some xenografts may have lost shRNA induction and therefore did not maintain eIF4A2 knockdown.

Unfortunately mice were sacrificed after the completion of this thesis, and as such due to supply issues, it was only possible to stain the xenograft with H&E. In the future, xenograft samples will be stained by a PhD student continuing in the laboratory with cleaved caspase 3 in order to quantify necrosis, and eIF4A2 to assess the extent of eIF4A2 knockdown. Only after it has been confirmed that there was a significant reduction in eIF4A2 protein expression in the xenograft tumours can these results be compared against previously xenografts performed in the literature using eIF4A inhibitors.

4.5 Concluding Remarks

In conclusion the data presented in this chapter supports the hypothesis presented at the start of this result chapter. eIF4A2 knockdown inhibits colorectal cancer cell survival, and the fact this negative impact on cell survival was not observed in a normal colon epithelial cell line suggest this is tumour specific. Furthermore, sheIF4A2 resulted in a significant reduction in colorectal cancer spheroid growth, short term colorectal cancer cell survival, with sheIF4A2 spheroids displaying increased regions of central necrosis. Both findings are supportive of hypothesis one, that eIF4A2 knockdown will lead to a reduction in colorectal tumour cell survival. Unfortunately HCT116 sheIF4A2 xenografts failed to show a significant difference in comparison to HCT116 shCTL xenografts, however xenografts from sheIF4A2

bearing mice displayed increased levels of necrosis in comparison to controls. This finding partly supports hypothesis two presented at the start of this results chapter. Perhaps with alternative and improved methodlogy with regards to eIF4A2 KO in a mouse model, this hypothesis will be proved correct in the future.

5.0 Identification of hypoxic eIF4A2 bound mRNAs in Colorectal Cancer Cells using a RIP-SEQ Approach

5.1 Introduction

5.1.1 The eIF4A Dependent Translatome

Three major studies have attempted to uncover the eIF4A dependent translatome, however all use Silvestrol, which non-specifically inhibits both eIF4A1 and eIF4A2 or have used siRNA inhibition of eIF4A1. These studies are invaluable in uncovering eIF4A1 dependent transcripts and their characteristics but none investigate the differences between the 2 isoforms with regards to the transcripts they regulate. This is an important distinction to make as eIF4A1 and eIF4A2 have been demonstrated to possess different functions. Modelska et al, demonstrated eIF4A1 as an independent predictor of poor patient outcome in ER-negative breast cancer (Modelska et al, 2015). Polysome profiling following eIF4A1 siRNA knockdown revealed such transcripts were enriched for structural protein families including serine-threonine protein kinases and G-protein a sub units. Gene ontology analysis of the same data set revealed enrichment for biological processes such amino acid phosphorylation and chromatin modification (Modelska et al, 2015). Characteristics of eIF4A1 dependent transcripts included those that were GC rich and those whose 5'UTR contained the $GC(GGC)_3G$ repeat motif which have previously been predicted to form G-quadruplexes (Modelska et al, 2015).

Selective targeting of G-quadruplexes using a selective small molecule inhibitor CM03 633.34 whose mechanism of action is to increase the thermodynamic stability of the G-quadruplex, preventing it from behind unwound, resulting in inhibition of the transcript. CM03 633.34 treatment demonstrated anti-proliferative activity against a prostate cancer cell line *in vitro* and in a PDAC xenograft model with a mean decrease in tumour volume of 73% being observed (Marchetti, Zyner, Ohnmact et al, 2018). CM03 633.34 treatment led to the downregulation of genes containing G-quadruplexes that were enriched for transcripts involved in Hippo pathway signalling, mTOR signalling, and endocytosis (Marchetti, Zyner, Ohnmact et al, 2018).

The second notable study investigating the eIF4A translatome was performed by Wolfe et al, who utilized ribosome footprinting following Silvestrol treatment (25 nM) in KOPT-K1, a T-cell acute lymphoblastic leukemia cell line (Wolfe et al, 2014). The study uncovered that transcripts in the translationally downregulated group following Silvestrol treatment were enriched for the presence of a $(CGG)_4$ motif within their 5'UTR. This motif was not found to be present in the 5'UTR of transcripts who displayed an increase in translation following Silvestrol treatment (Wolfe et al, 2014). This $(CGG)_4$ motif has been computationally predicted to form a G-quadruplex and demonstrated that eIF4A is the limiting factor for the translation of mRNAs containing G-quadruplexes in their 5'UTRs (Wolfe et al, 2014). The study also found transcripts in the translationally down regulated group following Silvestrol were also enriched for longer 5'UTRs (Wolfe et al, 2014). Such transcripts were identified as transcription factors and oncogenes including *MYC*, *NOTCH1*, *MYC*, *CDK6*, *MDM2*, *BCL2*, *RUNX1* and *ETS1* and their inhibition at the protein level following Silvestrol treatment was confirmed by immunoblot (Wolfe et al, 2014). Housekeeping genes β-actin, α-tubulin and GAPDH were unaffected by Silvestrol treatment due to their short and unstructured 5'UTRs. However it is interesting to the note that contained within the supplementary data by Wolfe et al, eIF4A2 and not eIF4A1 was shown to be the predominantly expressed isoform at the mRNA level in t-cell acute lymphoblastic leukemia (Wolfe et al, 2014).

The final study contributing toward the mechanism of eIF4A dependent translation was undertaken by Rubio et al, again utilising ribosome footprinting following Silvestrol treatment but in MDA-MB-231 breast cancer cell lines (Rubio et al, 2014). Deep sequencing of ribosome protected fragments following 1 or 2 hours of 25nM Silvestrol treatment, 284 transcripts were shown to be translationally down regulated and enriched for genes involved in the regulation of cell cycle, morphology, migration, survival, proliferation and growth. CONTRAfold prediction software was used to analyse the 5'UTR of Silvestrol sensitive and insensitive transcripts and revealed a significant difference in free energy values ($p=2.53x10^{-67}$), Silvestrol sensitive transcripts possessed longer 5'UTRs ($p=1.39x10^{-133}$) and possessed lower GC content ($p=1.02x10^{-47}$) (Rubio et al, 2014). Free energy values are the is the amount of free energy required to unwind the RNA strand; the more negative the value the more thermodynamically stable the RNA strand is (Zhang et al, 2019). Rubio et al additionally demonstrated that Silvestrol sensitive transcripts showed an increased prevalence of alternative transcript start sites (TSSs) or 5'UTR introns and were distinct from the subset of mRNAs regulated by mTOR containing 5'TOP sequences (Rubio et al, 2014). These 3 key studies support the hypothesis that eIF4A binds to and regulates a key

subset of transcripts essential for cell survival in malignant cells. However these studies have not been expanded out to study the eIF4A2 dependent translatome specifically.

G-quadruplexes have been used as an example in this introduction section as a complex secondary structure within the 5'UTR that regulates translation efficiency (Fay et al, 2017). However there are additional elements of the 5'UTR that would confer more dependence on eIF4A to be efficiently unwound. There are canonical and non-canonical ways in which bases can pair, allowing RNA duplexes to form a variety of secondary structures such as exterior loops, hairpin loops, bulge loops, interior loops and multi loop branches (Hinnebusch et al, 2016). Figure 5 displays the 5'UTR of MYC, known to be Silvestrol sensitive and dependent on eIF4A1 for its translation. The 5'UTR of MYC is known to be long, complex and GC rich and figure presents some of the key RNA secondary structures as aforementioned. Recent studies using eIF3 PAR-CLIP and SHAPE-seq have identified a stem loop present in the 5'UTR of transcripts recognised by eIF3 and targeting mRNAs for translational activation or repression (Lee et al, 2015). This subset of mRNAs recruited by eIF3 are enriched for transcripts involved in apoptosis, cell cycle and cell differentiation (Lee et al, 2015). The thermodynamic stability of an RNA can be predicted using computer algorithms which predict the most thermodynamically stable and likely combination of base pairings between nucleotides. This allows for the prediction of a "minimum free energy" value; this is the amount of free energy required to unwind the RNA strand; the more negative the value the more thermodynamically stable the RNA strand is (Zhang et al, 2019). However such computer algorithms are not able to predict the formation of more complex structures such as pseudo knots and RNA G-quadruplexes.

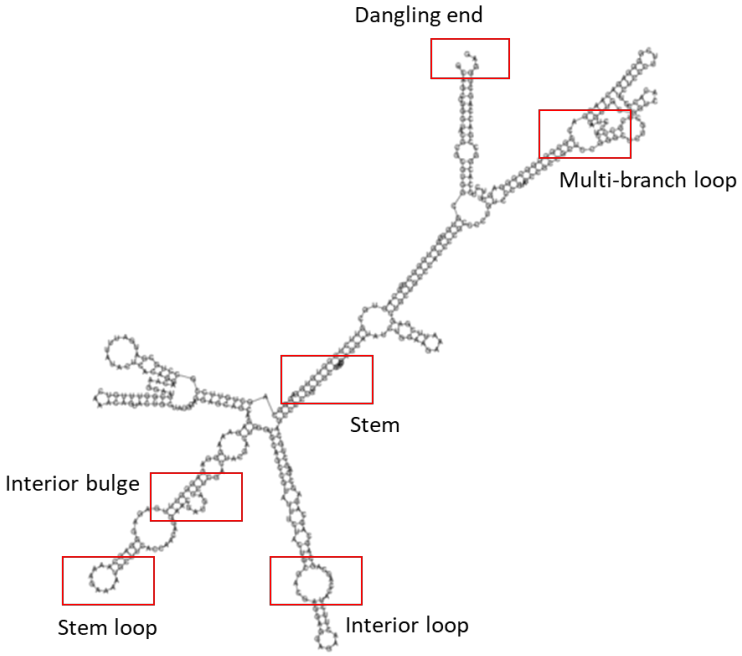


Figure 5. c-MYC 5'UTR secondary structure. Minimum free energy (MFE) diagram displaying examples of secondary structures within the c-MYC 5'UTR. MFE plots were obtained by entering the 5'UTR sequence of c-MYC into the RNAfold web server which is based on the programming algorithm introduced by Zuker and Stiegler, 1981.

No work has previously been undertaken to identify eIF4A2 specific bound transcripts in colorectal cancer cells, nor has this been performed to investigate the differences in eIF4A2 bound transcripts between normoxia and hypoxia. I hypothesise that eIF4A2 binds to a unique subset of transcripts specifically under hypoxic conditions and that such eIF4A2 bound transcripts encode for pathways crucial for cell survival in order to support their hypoxic translation that currently remain unknown. Secondly, I hypothesise that inhibition of eIF4A2 bound transcripts will lead to a reduction in colorectal cancer cell survival with the observed effect being enhanced under hypoxic conditions. Thirdly I hypothesise that upregulated hypoxic eIF4A2 bound transcripts will possess significantly longer and more complex 5'UTRs in comparison to transcripts that are downregulated when bound to eIf4A2 under hypoxic conditions.

I will test the hypothesis using the following aims and methodology:

1- I will identify novel eIF4A2 bound transcripts in normoxia and hypoxia in colorectal cancer cells and demonstrate those that are upregulated under hypoxic conditions when bound to eIF4A2 in comparison to normoxia. This will be achieved using an RIP-SEQ approach in LS174T cells following exposure to 48 hours hypoxia (1% O_2).

2- I will indentify whether there are novel pathways regulated by eIF4A2 under hypoxic conditions via KEGG analysis of eIF4A2 bound transcripts upregulated under hypoxic conditions.
3- I will demonstrate that inhibition of hypoxic eIF4A2 bound transcripts leads to a reduction in colorectal cancer cell survival as demonstrated by siRNA inhibition of selected top targets identified from the RIP-SEQ followed by clonogenic assay and exposure to 72 hours normoxia (20% O_2) and hypoxia (1% O_2).
4- I will demonstrate that eIF4A2 bound transcripts upregulated under hypoxic conditions possess longer and more complex 5'UTRs via bioinformatics analysis of 5'UTR sequence and predicted minimum free energy using the Ensemble database and Vienna RNAfold server package.

5.2 Results

5.2.1 eIF4A2 binds to a Distinct Subset of mRNAs Under Hypoxic Conditions

In brief, LS174T cells were exposed to either 48 hours normoxia (20% O_2) or hypoxia (1% O_2) followed by eIF4A2 immunoprecipitation as previously described in the Materials and Methods section. mRNA obtained from immunoprecipitations underwent illumina mRNA sequencing (20 million reads, 150 PE) provided as a service by Novogene. Bioinformatics analysis including classification of reads, mapping to reference genome, differential gene expression analysis, cluster analysis, Gene Ontology and KEGG pathway analysis was also provided as a service by Novogene. Samples sent for mRNA sequencing included 3 separate experimental repeats of each condition and included both a normoxic and hypoxic input, which consisted of total mRNA that had not undergone immunoprecipitation, also exposed to 48 hours normoxic or 1% O_2 to. IgG pull downs were also performed at the same time and cDNA reverse transcribed as previously described to act as a negative control for use in qRT-PCR at a later date. IgG pull downs were not sent for library preparations, as the IgG ultimately pulls down a very small amount of non-specific noise and as a result would produce a low complexity library likely with a large number of PCR duplicates/artefacts. Hence why using the normoxic and hypoxic input was selected as a more appropriate control to use as it also allowed for the normalisation of each transcript to the total amount of RNA. Instead cDNA was reverse transcribed from the RNA obtained from the IgG pull downs as previously described and used as a control for qPCR validation of the selected targets.

5.2.2 Cluster Analysis of Differentially Expressed Genes

Cluster analysis is used to find genes with similar expression patterns under different experimental conditions. In hierarchical clustering, areas of different colours denote different groups (clusters) and genes, and genes within each cluster may have similar functions or take part in the same biological process allowing correlations in the data to become visible (Vidman et al, 2019). Figure 5.1 displays the overall results of FPKM cluster analysis, clustered using the $\log_{10}$(FPKM+1) value of the 4 experimental conditions whereby the row tree represents the gene, the column tree represents the treatments and the colours from red to blue represents the $\log_{10}$(FPKM+1) value from large to small of the underlying gene expression data. Hierarchical clustering uncovered several distinct clusters of transcripts based on their binding to eIF4A2 in normoxia and hypoxia. Cluster 1 represents transcripts that display the highest expression only when bound to eIF4A2 in hypoxic conditions. Such transcripts display miminal changes in expression when bound to eIF4A2 in normoxia, or input hypoxia and decreased expression when not bound to eIF4A2 in normoxia. Transcripts in cluster 1 likely represent those that are only translated when bound to eIF4A2 only under hypoxic conditions and not normoxic conditions. Such transcripts also do not show increased expression in the input hypoxia and so their increase in expression in the hypoxia RIP is not merely because they are upregulated under hypoxic conditions. Cluster 2 represent transcripts that display decreased expression in both input normoxia and hypoxia, increased expression when bound to eIF4A2 in normoxia and a further increase in expression when bound to eIF4A2 in hypoxia. These likely reflect transcripts required for cell survival in normoxia that require eIF4A2 for translation, but even more so under hypoxic conditons. Cluster 3 represents transcripts that display the highest expression when bound to eIF4A2 in normoxic conditons, less so under hypoxic conditions when bound to eIF4A2 and decreased expression in both input normoxia and hypoxia. It is likely that these transcripts are required for normoxic cell survival, less so for hypoxic cell survival but both require eIF4A2 for efficient translation. Cluster 4 represents transcripts with the highest expression under normoxic conditons and the largest decrease in expression when bound to eIF4A2 under hypoxic conditions suggest they do not bind to eIF4A2 under hypoxic conditions but are expressed in normoxic cells. Interestingly cluster 5 represent transcripts that show the highest expression when bound to eIF4A2 in normoxic conditions alone, suggesting that these are the transcripts required for normoxic cell survival and require eIF4A2 for efficient translation. Cluster 6 transcripts display the highest expression only in the input 1% O_2 condtion, likely reflecting hypoxia response genes that do not require eIF4A2 for transltion. Finally cluster 7 transrcripts display the highest

expression under normoxic conditions and decreased expression when bound to eIF4A2 under both normoxic and hypoxia conditons suggesting these are transcripts required for normal cell survival that do not require eIF4A2 for translation.

Upon analysis of differentially expressed genes within the 1% O_2 input condition, these genes were confirmed as commonly observed hypoxia response genes which included the significant up regulation of the following genes and adjusted p-values; *CA9* (p=3.0x10-6), *BNIP3* (p=3.0x10-42), *VEGFA* (p=9.0x10-8) and *LDHA* (p=2.0x10-9).

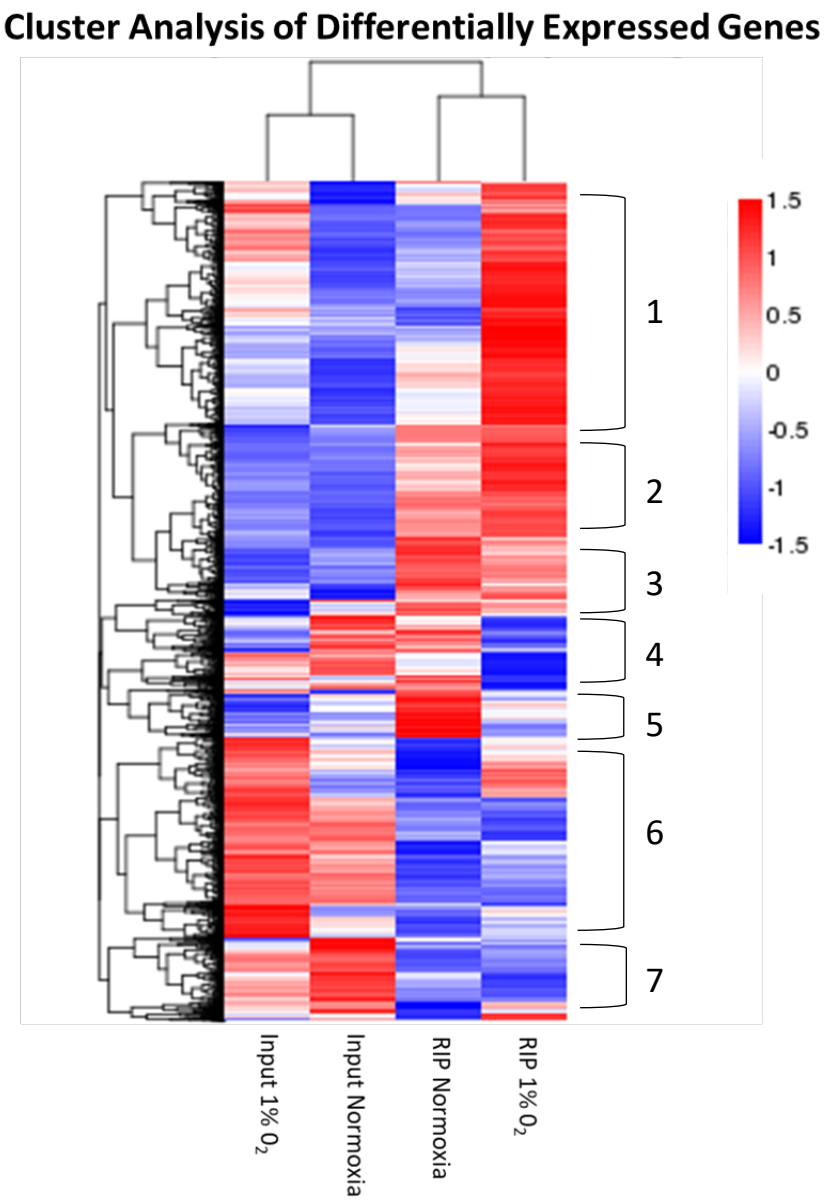


Figure 5.1. Overall results of FPKM cluster analysis from eIF4A2 RIP-SEQ experimental conditions. Differential gene expression was clustered using the log_{10}(FPKM+1) value. Red denotes high read counts, blue denotes low read counts. n=3.

5.2.3 Screening of Differentially Expressed Genes

Figure 5.2 displays volcano plots for each comparison between experimental groups and is used to infer the overall distribution of differentially expressed genes. Figure 5.2 displays the experimental groups compared and the number of differentially expression genes either upregulated of downregulated; (A) eIF4A2 1% O_2 RIP vs eIF4A2 normoxic RIP (3640 upregulated, 3589 downregulated), (B) eIF4A2 1% O_2 RIP vs input normoxia (4983 upregulated, 4684 downregulated), (C) input 1% O_2 vs input normoxia (1827 upregulated, 1353 down regulated) and (D) eIF4A2 normoxic RIP vs input normoxia (3943 upregulated, 4174 downregulated).

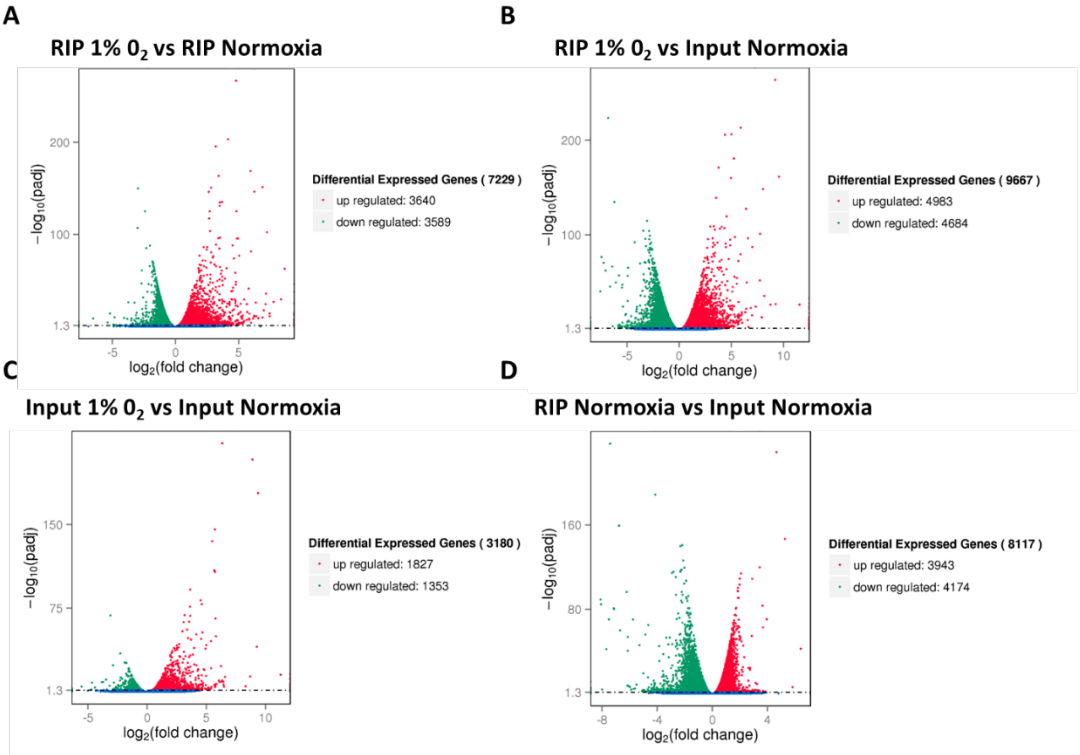


Figure 5.2. Volcano plots showing overall distribution of differentially expressed genes from the eIF4A2 RIP-SEQ. Dots in green denote differentially expresses downregulated genes, dots in red denote differentially expressed upregulated genes. Genes that did not display differentially expression between groups are highlighted by the blue dots. The x-axis displays the log_2 fold change in genes expression plotted against the statistical significance in $-log_{10}$ (padj). n=3.

5.2.4 Co-expression Analysis of Differentially Expressed Genes

Figure 5.3 displays the results of co-expression analysis that is the number of transcripts co-expressed between experimental conditions and reveals the number of genes that are uniquely expressed and shared between conditions. The comparison of particular interest to this project is that between the normoxic and hypoxic RIP (Figure 5.3 ,A); when comparing eIF4A2 1% O_2 RIP and eIF4A2 normoxic RIP, 1237 transcripts were found to be unique to the eIF4A2 1% O_2 RIP, 242 unique to the eIF4A2 normoxic RIP and 12146 transcripts shared by both pull downs. The transcripts shared by both pull downs represent the transcripts that are bound to eIF4A2 and are likely to be those transcripts regulated by eIF4A2 in tumorigenesis however not involved in the adaptation to hypoxia. As shown in Figure 5.3,B, 1629 transcripts were found to be unique to eIF4A2 1% O_2 RIP, 549 unique to the input normoxia and 11754 transcripts shared by both conditions.

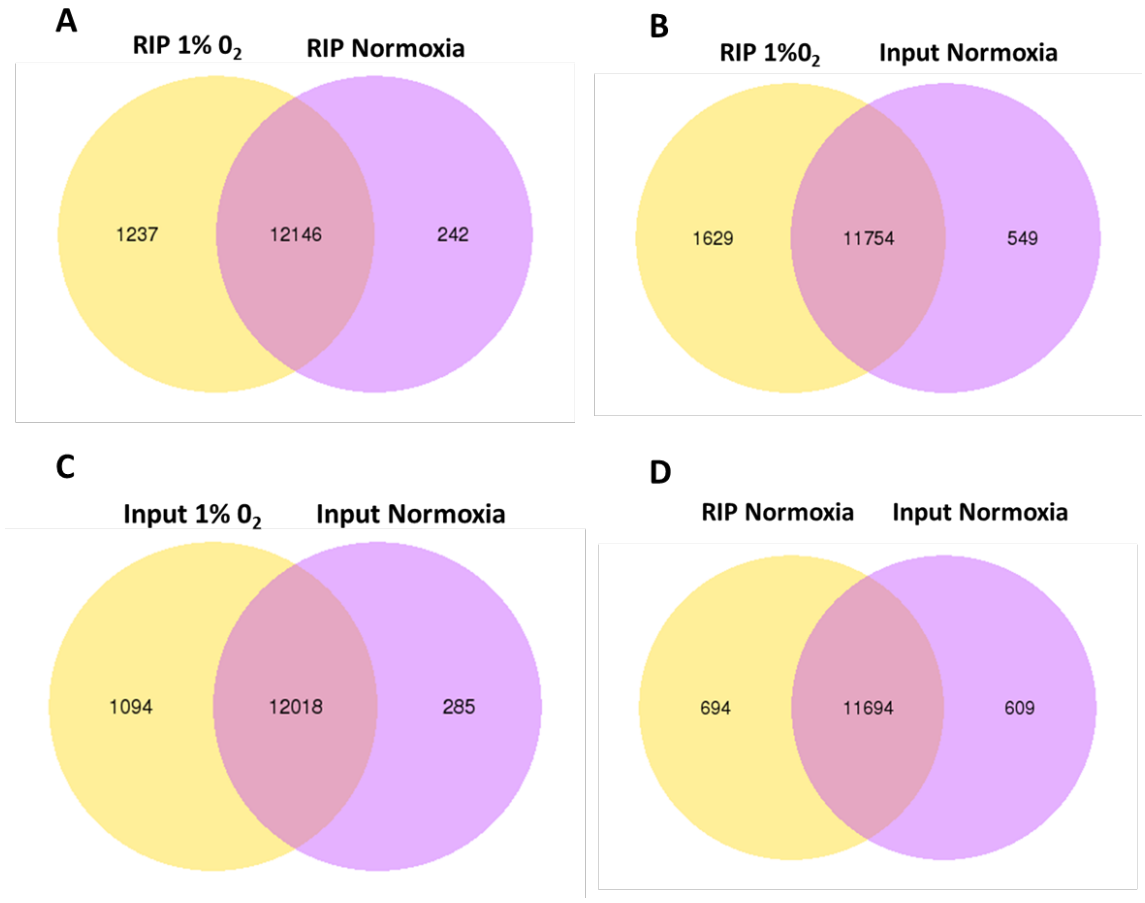


Figure 5.3. Co-expression of differentially expressed genes from eIF4A2 RIP-SEQ. The sum of the numbers in each circle represents the total number of genes expressed within a sample, the overlap represents the genes that are commonly expressed between groups. n=3.

5.2.5 KEGG Pathway Analysis

In order to direct future downstream experiments, it was important to identify pathways enriched within the differentially expressed genes found between the eIF4A2 1% O_2 RIP

and eIF4A2 normoxic RIP. KEGG is a database containing information regarding genomes, biological pathways and chemical substances used in bioinformatics analysis to identify metabolic and signalling pathways that are enriched in a gene list more than would be expected by chance when compared to the whole genome background (Kanehisa et al, 2017). Figure 5.4 and Figure 5.5 displays a scatter diagram representing the KEGG enrichment analysis results for eIF4A2 1% 0_2 RIP vs eIF4A2 normoxic RIP upregulated and downregulated genes. In these scatter plots the degree of KEGG enrichment can be measured through the Rich factor, Q value and gene counts enriched in this pathway. The Rich Factor is the ratio of differentially expressed gene counts annotated in a pathway term to all gene numbers annotated in the pathway term. The higher the Rich factor, the higher the degree of enrichment. The Q-value represents the adjusted p-value following multiple hypothesis testing and the values ranges from 0-1. The closer the Q-value is to 0, the more significant the enrichment is. Statistical significance was assessed using a Fisher's exact test followed by Benjamini and Hochberg post-hoc test.

KEGG pathway analysis of differentially expressed upregulated genes in the eIF4A2 1% 0_2 RIP vs eIF4A2 normoxic RIP (those genes that have increased binding to eIF4A2 under hypoxic conditions) uncovered novel pathways and associated transcripts that eIF4A2 may contribute toward the regulation of through it directly binding to such transcripts and directing them for translational activation or translational repression. The top 5 most significantly enriched pathways and their associated corrected p-value for differentially expressed upregulated genes in the eIF4A2 1% 0_2 RIP vs eIF4A2 normoxic RIP include: 'metabolic pathways' ($4.0x10^{-25}$), endocytosis ($7.0x10^{-14}$), 'carbon metabolism' ($1.0x10^{-11}$), 'focal adhesion' ($5.0x10^{-9}$) and 'lysosome' ($9.0x10^{-10}$) along with many other pathways in line with the major changes in hypoxia. The most enriched metabolic pathway aside from the general 'metabolism' category was uncovered as 'biosynthesis of amino acids' ($3.7x10^{-7}$). KEGG plots for eIF4A2 bound transcripts upregulated in hypoxia are displayed in Figure 5.4. Individual gene names for the top 5 enriched pathways for each pathway found to be enriched within the differentially expressed upregulated genes in the eIF4A2 1% 0_2 RIP vs eIF4A2 normoxic RIP can be found in the following tables: endocytosis (Table 5), carbon metabolism (Table 5.1), biosynthesis of amino acids (Table 5.2), focal adhesion (Table 5.3) and lysosome (Table 5.4).

KEGG pathway analysis of differentially expressed downregulated genes in the eIF4A2 1% 0_2 RIP vs eIF4A2 normoxic RIP (those genes that were found to be downregulated in the eIF4A2 1% 0_2 RIP when compared to the eIF4A2 normoxic RIP) uncovered pathways and

transcripts that eIF4A2 may not be as important in the regulation of under hypoxic conditions. The top 5 most significantly enriched pathways and their associated corrected p-value include: 'ribosome' ($2.0x10^{-63}$), 'metabolic pathways' ($5.0x10^{-62}$), 'Huntington's disease' ($1.0x10^{-28}$), 'Alzheimer's disease' ($7x10^{-27}$) and 'oxidative phosphorylation' ($1.0x10^{-26}$). KEGG plots for eIF4A2 bound transcripts downregulated in hypoxia are displayed in Figure 5.5.

It is also important to consider the data generated from the normoxic and input samples as they represent the total mRNA before eIF4A2 immunoprecipitation and so can be used as a data set to investigate the response at the transcriptional level to hypoxia in colorectal cancer cells. The top 5 most significantly enriched pathways and their associated corrected p-value that were found to be upregulated under hypoxic conditions include: 'metabolic pathways' ($7.0x10^{-12}$), 'HIF1 signalling pathways' ($7.0x10^{-10}$), 'pathways in cancer' ($5.0x10^{-8}$), 'glycolysis/gluconeogenesis' ($8.0x10^{-8}$) and 'fructose and mannose metabolism' ($4.0x10^{-8}$). In addition to many other pathways that are in line with the major adaptions occurring under hypoxic conditions. The top 5 most significantly enriched pathways and their associated corrected p-value that were found to be downregulated under hypoxic conditions displayed include: 'metabolic pathways' ($6.0x10^{-44}$), 'oxidative phosphorylation' ($7.0x10^{-20}$), 'cell cycle' ($3.0x10^{-13}$), 'spliceosome' ($1.0x10^{-12}$) and 'DNA replication' ($3.0x10^{-12}$). This data again is in line with the major processes that are downregulated under hypoxic conditions and act as a useful control for this experiment. It is well known that under hypoxic conditions we see a shift away from oxidative phosphorylation toward a more anaerobic method of energy production, glycolysis in a phenomenon known as the "Warburg effect".

Table 5. Differentially bound upregulated genes in the eIF4A2 1% O_2 RIP vs eIF4A2 20% 0_2 RIP enriched for the endocytic pathway. Table displays transcripts that were found to be upregulated under hypoxic conditions when bound to eIF4A2 in comparison when bound to eIF4A2 under normoxic conditions. Such transcripts were then found to be enriched for endocytosis genes, individual gene names are displayed. Alongside log2 fold change, adjusted p-value and average read counts. Data are sorted from highest to lowest log2fold upregulation in comparison to eIF4A2 normoxic RIP. Statistical significance was assessed using a Fisher's exact test followed by Benjamini and Hochberg post-hoc test. n=3.

Gene Name	log2FoldChange	padj	Read Count 1% 02 RIP	Read Count Nx RIP
IL2RG	4.56	5.46E-43	994.01	42.27
EHD2	3.13	0.000748	15.15	1.73
ACAP1	2.05	6.91E-62	1330.19	321.66
PIP5KL1	1.97	7.89E-12	332.78	84.99
PSD4	1.70	1.57E-23	1109.38	340.71
EHD1	1.19	1.34E-15	501.62	219.78
WASH5P	1.13	6.44E-16	636.30	291.57
IGF2R	1.11	1.68E-12	404.79	188.03
KIT	1.07	1.97E-08	220.87	104.94
KIF5B	1.04	6.13E-23	4754.43	2316.92
CHMP6	1.03	2.98E-05	710.25	347.97
PARD6A	1.01	0.002676	2149.94	1065.54
EGFR	0.89	1.17E-08	400.01	216.46
GRK5	0.84	0.014839	64.34	35.96
GBF1	0.82	9.36E-07	322.02	182.11
PLD2	0.78	4.55E-05	234.69	137.00
ARRB1	0.78	6.71E-10	1000.29	583.96
TRAF6	0.77	0.033481	59.31	34.86
CLTB	0.75	1.44E-12	7141.94	4257.40
CBLC	0.74	1.88E-05	818.11	489.72
RAB11FIP5	0.73	5.94E-05	249.76	150.83
CYTH2	0.72	1.66E-07	642.79	389.82
MET	0.70	5.55E-09	1215.42	748.40
FAM21EP	0.69	0.010093	114.21	71.01
EEA1	0.68	0.000834	197.30	123.04
ASAP2	0.65	3.70E-06	585.10	371.75
ARF3	0.65	0.000156	325.89	208.30
HLA-K	0.64	0.005449	201.80	129.24
FAM21C	0.63	0.000485	298.77	193.58
CLTC	0.62	0.02447	645.11	419.58

USP8	0.62	4.86E-06	781.57	510.27
PML	0.61	0.027857	100.47	65.96
SH3KBP1	0.60	0.000107	417.38	275.65
NEDD4L	0.60	2.23E-05	610.51	403.29
WIPF2	0.59	0.019455	280.86	186.48
FAM21A	0.58	0.000684	306.66	204.80
CBL	0.56	0.022704	139.31	94.41
ZFYVE9	0.52	0.040378	290.02	202.53
CCDC53	0.52	5.83E-06	2348.93	1642.18
ACAP3	0.50	0.000149	922.52	651.00
STAM2	0.50	0.036029	133.99	94.76
DNM2	0.50	2.93E-05	1489.81	1054.25
BIN1	0.49	0.017363	1328.23	943.86
PARD3	0.49	0.004011	348.12	247.56
VPS28	0.47	2.51E-05	3157.66	2273.91
HSPA1B	0.46	0.023335	439.55	318.79
ARF6	0.46	0.002821	3892.55	2825.84
SMAD2	0.45	0.000376	1182.39	863.28
PDCD6IP	0.44	0.005768	404.60	298.36
PARD6B	0.44	0.033261	250.28	184.94
RAB22A	0.42	0.000915	1518.28	1133.62
VPS26B	0.42	0.001717	949.61	711.40
ARFGEF2	0.41	0.007441	534.44	400.93
PIP5K1C	0.41	0.008527	554.82	418.96
IST1	0.40	0.00165	1240.31	942.08
AGAP1	0.39	0.005065	771.26	588.10
SH3GLB1	0.38	0.004671	975.82	749.57
CHMP2A	0.37	0.001435	3797.20	2935.52
SNF8	0.35	0.010345	1165.43	917.11
ARPC1B	0.33	0.048639	4474.14	3549.53
AGAP3	0.33	0.013762	1258.34	998.84
RUFY1	0.31	0.047229	539.72	433.89
VPS4A	0.31	0.036411	889.63	716.97

Table 5.1. Differentially bound upregulated genes in the eIF4A2 1% O_2 RIP vs eIF4A2 20% 0_2 RIP enriched for the carbon metabolism pathway. Table displays transcripts that were found to be upregulated under hypoxic conditions when bound to eIF4A2 in comparison when bound to eIF4A2 under normoxic conditions. Such transcripts were then found to be enriched for carbon metabolism genes, individual gene names are displayed. Alongside log2 fold change, adjusted p-value and average read counts. Data are sorted from highest to lowest log2fold upregulation in comparison to eIF4A2 normoxic RIP. Statistical significance was assessed using a Fisher's exact test followed by Benjamini and Hochberg post-hoc test. n=3.

Gene Name	log2FoldChange	padj	Read Count 1% 02 RIP	Read Count Nx RIP
PKM	2.04	4.35E-13	14655.18	3567.39
SHMT2	2.00	1.31E-53	7505.18	1870.24
PGK1	1.92	5.34E-10	10894.07	2870.15
AGXT	1.92	1.68E-12	295.20	78.16
ALDOA	1.92	1.69E-41	43968.94	11650.31
HK1	1.90	1.30E-37	802.38	215.58
ALDOC	1.89	3.64E-10	674.64	181.50
FBP1	1.72	1.36E-14	181.02	54.80
HKDC1	1.64	1.54E-13	336.49	107.98
ENO2	1.62	2.17E-42	1467.98	476.22
ENO1	1.46	2.50E-10	15378.34	5576.69
PC	1.44	8.26E-19	386.40	142.18
HK2	1.35	6.27E-13	251.21	98.83
ENO3	1.28	5.88E-08	458.08	189.10
MTHFR	1.07	1.07E-06	153.22	72.83
PFKP	1.03	4.51E-15	773.58	379.50
GPI	0.99	1.40E-20	3766.28	1898.80
HADHA	0.73	4.20E-09	948.16	571.09
IDNK	0.72	2.54E-06	432.94	263.36
PGLS	0.70	0.000499	1499.93	922.78
SUCLA2	0.65	3.20E-07	897.71	570.44
TPI1	0.65	5.66E-07	64646.51	41178.68
ACADS	0.64	3.77E-07	1047.68	671.63
ME1	0.63	1.22E-07	1443.29	931.90
PGAM1	0.60	8.86E-09	12532.98	8257.94
ACO1	0.55	0.006738	189.09	128.96
ACSS1	0.54	0.000865	372.68	257.10
SDHA	0.52	4.77E-06	2468.92	1727.35
CAT	0.44	0.001328	741.50	548.00

IDH2	0.41	0.002213	2428.50	1825.29
PHGDH	0.41	0.002671	1732.20	1303.46
GPT2	0.39	0.002762	1386.28	1059.89
IDH3G	0.38	0.003322	1204.07	925.92
IDH3B	0.33	0.005548	2778.44	2210.09
TKFC	0.32	0.044431	642.46	513.44

Table 5.2. Differentially bound upregulated genes in the eIF4A2 1% O_2 RIP vs eIF4A2 20% O_2 RIP enriched for the biosynthesis of amino acids pathway. Table displays transcripts that were found to be upregulated under hypoxic conditions when bound to eIF4A2 in comparison when bound to eIF4A2 under normoxic conditions. Such transcripts were then found to be enriched for biosynthesis of amino acid genes, individual gene names are displayed. Alongside log2 fold change, adjusted p-value and average read counts. Data are sorted from highest to lowest log2fold upregulation in comparison to eIF4A2 normoxic RIP. Statistical significance was assessed using a Fisher's exact test followed by Benjamini and Hochberg post-hoc test. n=3.

Gene Name	log2FoldChange	padj	Read Count 1% 02 RIP	Read Count Nx RIP
CTH	2.25	3.47E-66	1109.32	232.62
PKM	2.04	4.35E-13	14655.18	3567.39
SHMT2	2.00	1.31E-53	7505.18	1870.24
PGK1	1.92	5.34E-10	10894.07	2870.15
ALDOA	1.92	1.69E-41	43968.94	11650.31
ALDOC	1.89	3.64E-10	674.64	181.50
ENO2	1.62	2.17E-42	1467.98	476.22
ENO1	1.46	2.50E-10	15378.34	5576.69
PC	1.44	8.26E-19	386.40	142.18
GPT	1.33	0.027112	26.18	10.38
ENO3	1.28	5.88E-08	458.08	189.10
PFKP	1.03	4.51E-15	773.58	379.50
ALDH18A1	0.69	1.88E-07	697.67	431.68
TPI1	0.65	5.66E-07	64646.51	41178.68
PGAM1	0.60	8.86E-09	12532.98	8257.94
ACO1	0.55	0.006738	189.09	128.96
BCAT1	0.55	8.30E-05	640.77	438.84
ASS1	0.54	2.89E-06	2413.98	1664.38
NAGS	0.43	0.038103	239.07	177.78
IDH2	0.41	0.002213	2428.50	1825.29
PHGDH	0.41	0.002671	1732.20	1303.46
GPT2	0.39	0.002762	1386.28	1059.89

IDH3G	0.38	0.003322	1204.07	925.92
IDH3B	0.33	0.005548	2778.44	2210.09

Table 5.3. Differentially bound upregulated genes in the eIF4A2 1% O_2 RIP vs eIF4A2 20% 0_2 RIP enriched for the focal adhesion pathway. Table displays transcripts that were found to be upregulated under hypoxic conditions when bound to eIF4A2 in comparison when bound to eIF4A2 under normoxic conditions. Such transcripts were then found to be enriched for focal adhesion genes, individual gene names are displayed. Alongside log2 fold change, adjusted p-value and average read counts. Data are sorted from highest to lowest log2fold upregulation in comparison to eIF4A2 normoxic RIP. Statistical significance was assessed using a Fisher's exact test followed by Benjamini and Hochberg post-hoc test. n=3.

Gene Name	log2FoldChange	padj	Read Count 1% 02 RIP	Read Count Nx RIP
SLC11A1	2.41	7.89E-37	669.48	126.29
CTSE	2.03	6.93E-31	357.45	87.60
CTSD	1.70	2.08E-50	2190.95	673.86
NAGLU	1.22	7.75E-08	535.67	230.23
GALNS	1.14	4.77E-10	270.13	122.70
IGF2R	1.11	1.68E-12	404.79	188.03
SMPD1	1.06	0.020769	161.32	77.46
ATP6V0D1	1.03	1.75E-19	2286.74	1116.55
NEU1	1.03	6.55E-08	2469.55	1211.97
ARSA	0.95	2.05E-09	393.45	203.15
SORT1	0.93	5.46E-12	685.41	358.86
HEXA	0.91	9.16E-06	184.71	98.10
TPP1	0.89	1.06E-09	506.55	273.33
AP3D1	0.82	7.50E-13	2060.31	1170.29
GBA	0.80	2.28E-07	417.10	239.09
ATP6V0A1	0.77	4.29E-05	232.60	136.73
CLTB	0.75	1.44E-12	7141.94	4257.40
NAPSA	0.70	0.047904	71.36	44.07
AP4E1	0.68	0.036455	83.90	52.41
HGSNAT	0.66	2.25E-05	620.13	392.18
ATP6AP1	0.66	2.06E-08	1652.34	1047.03
ACP2	0.65	0.006237	302.06	192.21
AP1G1	0.64	0.046659	198.17	126.74
ATP6V1H	0.63	8.29E-05	346.45	223.41

Table 5.4. Differentially bound upregulated genes in the eIF4A2 1% O_2 RIP vs eIF4A2 20% O_2 RIP enriched for the lysosome pathway. Table displays transcripts that were found to be upregulated under hypoxic conditions when bound to eIF4A2 in comparison when bound to eIF4A2 under normoxic conditions. Such transcripts were then found to be enriched for lysosome genes, individual gene names are displayed. Alongside log2 fold change, adjusted p-value and average read count. Data are sorted from highest to lowest log2fold upregulation in comparison to eIF4A2 normoxic RIP. Statistical significance was assessed using a Fisher's exact test followed by Benjamini and Hochberg post-hoc test. n=3.

Gene Name	log2FoldChange	padj	Read Count 1% 02 RIP	Read Count Nx RIP
LAMA3	3.31	2.88E-38	255.40	25.74
LAMB3	2.79	2.47E-70	653.01	94.75
ITGA5	2.67	3.23E-20	126.92	19.90
SHC2	2.66	4.10E-09	50.10	7.91
THBS2	2.51	6.98E-28	207.56	36.36
ITGA3	1.42	4.19E-17	346.71	129.39
LAMB2	1.35	5.38E-20	867.38	340.67
LAMC2	1.32	1.03E-11	231.04	92.83
ARHGAP35	1.29	2.22E-22	762.83	311.61
LINC01547	1.27	3.94E-13	296.88	123.24
FLNB	1.23	1.16E-13	575.39	244.73
ITGA6	1.22	3.41E-12	4081.16	1749.43
JUN	1.21	4.75E-10	228.36	98.56
ACTN4	1.17	1.33E-06	294.38	130.43
PIK3R1	1.16	0.001674	124.61	55.85
TLN1	1.05	1.32E-15	748.50	362.71
LAMC1	1.04	1.13E-07	206.76	100.61
CAPN2	1.01	5.59E-11	1148.27	571.29
ITGB4	1.00	8.31E-12	505.19	251.75
LAMA5-AS1	1.00	0.000969	86.33	43.11
ARHGAP5	0.98	8.34E-10	969.22	491.77
FLNA	0.95	3.25E-11	549.11	284.01
ROCK2	0.90	1.69E-06	1171.43	627.54
EGFR	0.89	1.17E-08	400.01	216.46

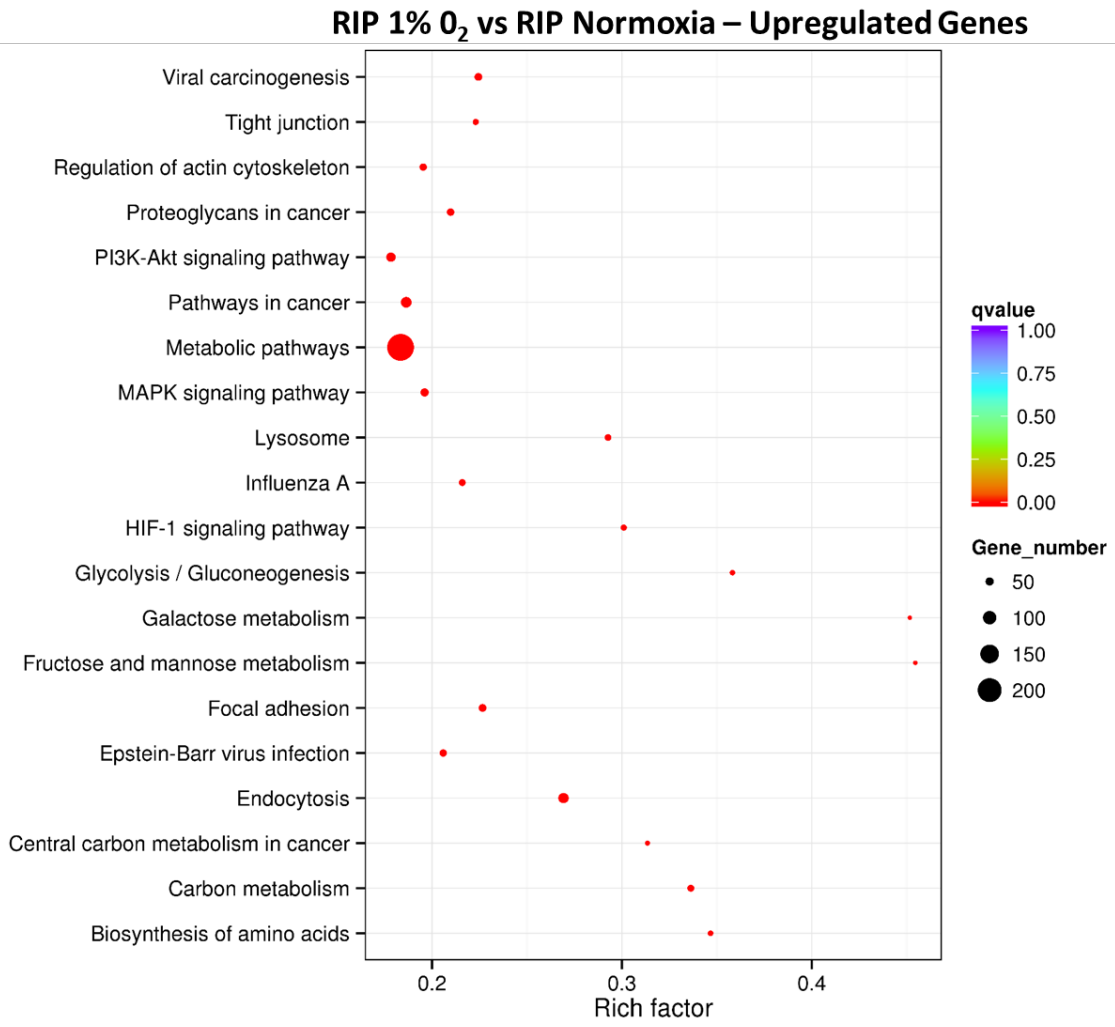


Figure 5.4 KEGG pathway analysis of differentially bound eIF4A2 1% O_2 bound upregulated genes in comparison to eIF4A2 20% 0_2 bound genes. The y-axis denotes the name of the pathway, the x-axis denotes the rich factor (ratio of DEG counts to this pathway in the annotated gene counts). Dot size represents the number of genes within that grouping and the colour indicates the q-value (adjusted p-value), the closer the value to 0, the more significant the enrichment. n=3.

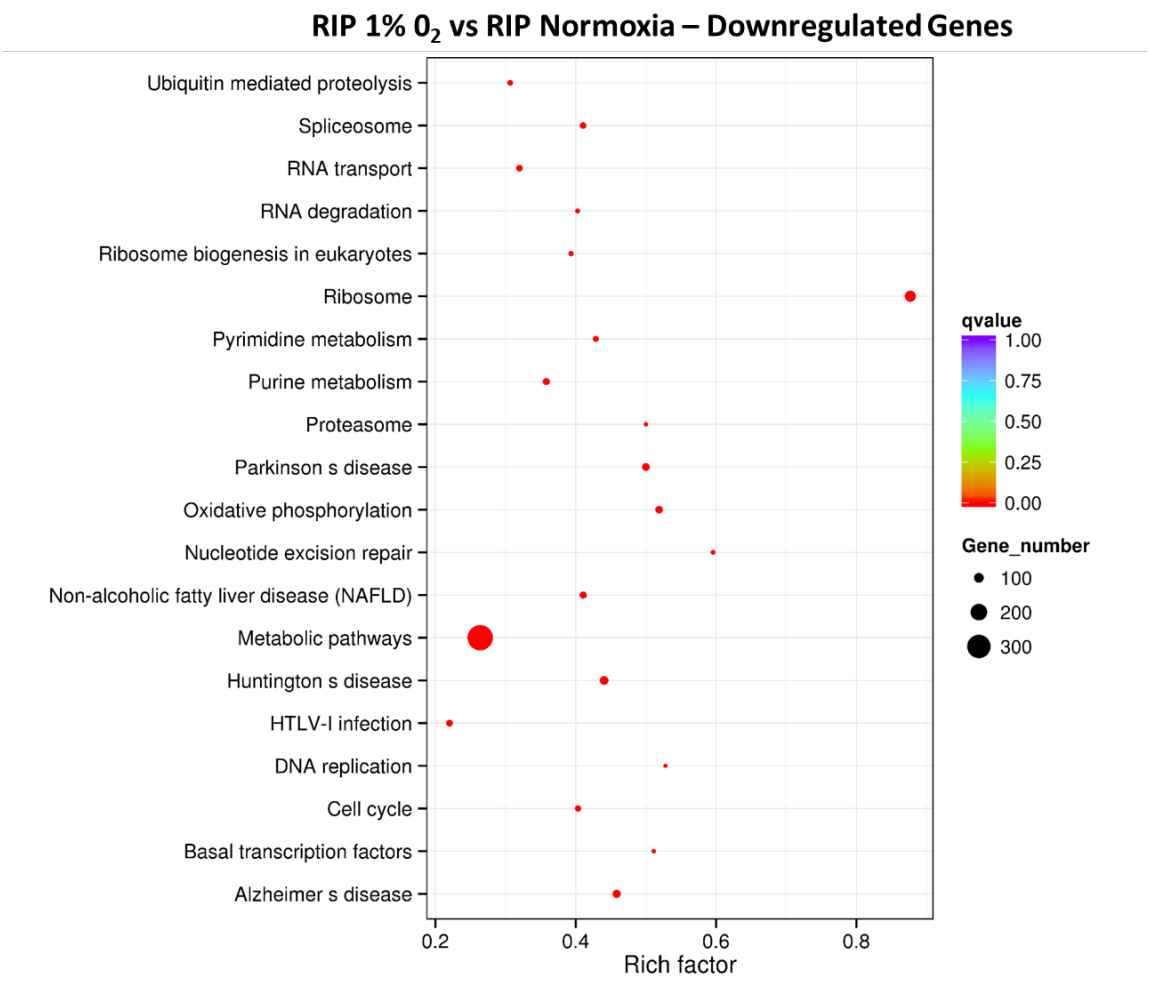


Figure 5.5. KEGG pathway analysis of differentially bound eIF4A2 1% 0_2 bound downregulated genes in comparison to eIF4A2 20% O_2 bound genes. The y-axis denotes the name of the pathway, the x-axis denotes the rich factor (ratio of DEG counts to this pathway in the annotated gene counts). Dot size represents the number of genes within that grouping and the colour indicates the q-value (adjusted p-value), the closer the value to 0, the more significant the enrichment. n=3.

5.2.6 qPCR validation of RIP-seq

Using the KEGG pathway analysis from the upregulated genes between the eIF4A2 1% O_2 RIP and eIF4A2 20% O_2 RIP as a guide to help select top candidates for further investigation, the top pathways selected for further analysis were 'biosynthesis of amino acids' and 'endocytosis'. These 2 pathways were selected for further validation as the most significantly enriched pathway from the eIF4A2 upregulated genes in hypoxia was found to be 'metabolism', however when this group was broken down, the most significantly enriched pathway within the metabolism group was found to be 'biosynthesis of amino acids'. In addition to this, endocytosis was found to be the second most significantly

enriched KEGG pathway within the eIF4A2 hypoxic bound upregulated genes and so was selected for further validation. cDNA generated from an additional 3 separate experimental repeats of eIF4A2 immunoprecipitations performed in LS174T cells as previously described, along with cDNA generated from IgG pull downs as a negative control were used for qPCR validation of selected top targets from the RIP-seq data set. qRT-PCR and fold change calculations were performed as previously described.

Figure 5.7 displays the results of qRT-PCR validation of selected transcripts from the RIP-SEQ data for biosynthesis of amino acids pathway displayed as fold enrichment over the IgG negative control. Such transcripts were selected as they represented the most significantly upregulated genes within the biosynthesis of amino acids pathway. Selected transcripts were phosphoglycerate dehydrogenase (*PDGDG*) (Figure 5.7,A), isocitrate dehydrogenase (*IDH2*) (Figure 5.7,B), phosphoglycerate kinase 1 (PGK1) (Figure 5.7,C), pyruvate kinase 1 (*PKM1*) (Figure 5.7,D), serine hydroxymethyltransferase (*SHMT2*) (Figure 5.7,E), and cystathionine gamma-lyase (*CTH*) (Figure 5.7,F). All transcripts showed a significant enrichment specifically under hypoxic conditions when bound to eIF4A2. In particular a significant difference between normoxic and hypoxic enrichment was observed for *IDH2* ($p<0.05$).

Figure 5.8 displays the results of qRT-PCR validation of selected transcripts from the RIP-SEQ data for carbon metabolism pathway displayed as fold enrichment over the IgG negative control. Such transcripts were selected as they represented the most significantly upregulated genes within the carbon metabolism pathway. Selected transcripts were enolase 1 (*ENO1*) (Figure 5.8, A), enolase 2 (*ENO2*) (Figure 5.8, B), aldolase A (*ALDOA*) (Figure 5.8, C), aldolase C (*ALDOC*) (Figure 5.8, D) and enolase 3 (*ENO3*) (Figure 5.8, E). All transcripts showed a significant enrichment specifically under hypoxic conditions when bound to eIF4A2. In particular a significant difference between normoxic and hypoxic enrichment was observed for *ALODA* and *ENO3* ($p<0.05$).

Figure 5.9 displays the results of qRT-PCR validation of selected transcripts from the RIP-SEQ data for the endocytosis pathway displayed as fold enrichment over the IgG negative control. Selected transcripts were phospholipase D2 (*PLD2*) (Figure 5.9, A), EH domain-containing protein 1 (*EHD1*) (Figure 5.9, B), kinesin family member 5B (*KIF5B*) (Figure 5.9, C), insulin-induced gene 2 protein (*INSIG2*) (Figure 5.9, D), eukaryotic translation initiation factor 3 subunit A (*eIF3a*) (Figure 5.9, E) and F-box only protein 2 (*FBX02*) (Figure 5.9, F). All

transcripts showed a significant enrichment specifically under hypoxic conditions when bound to eIF4A2.

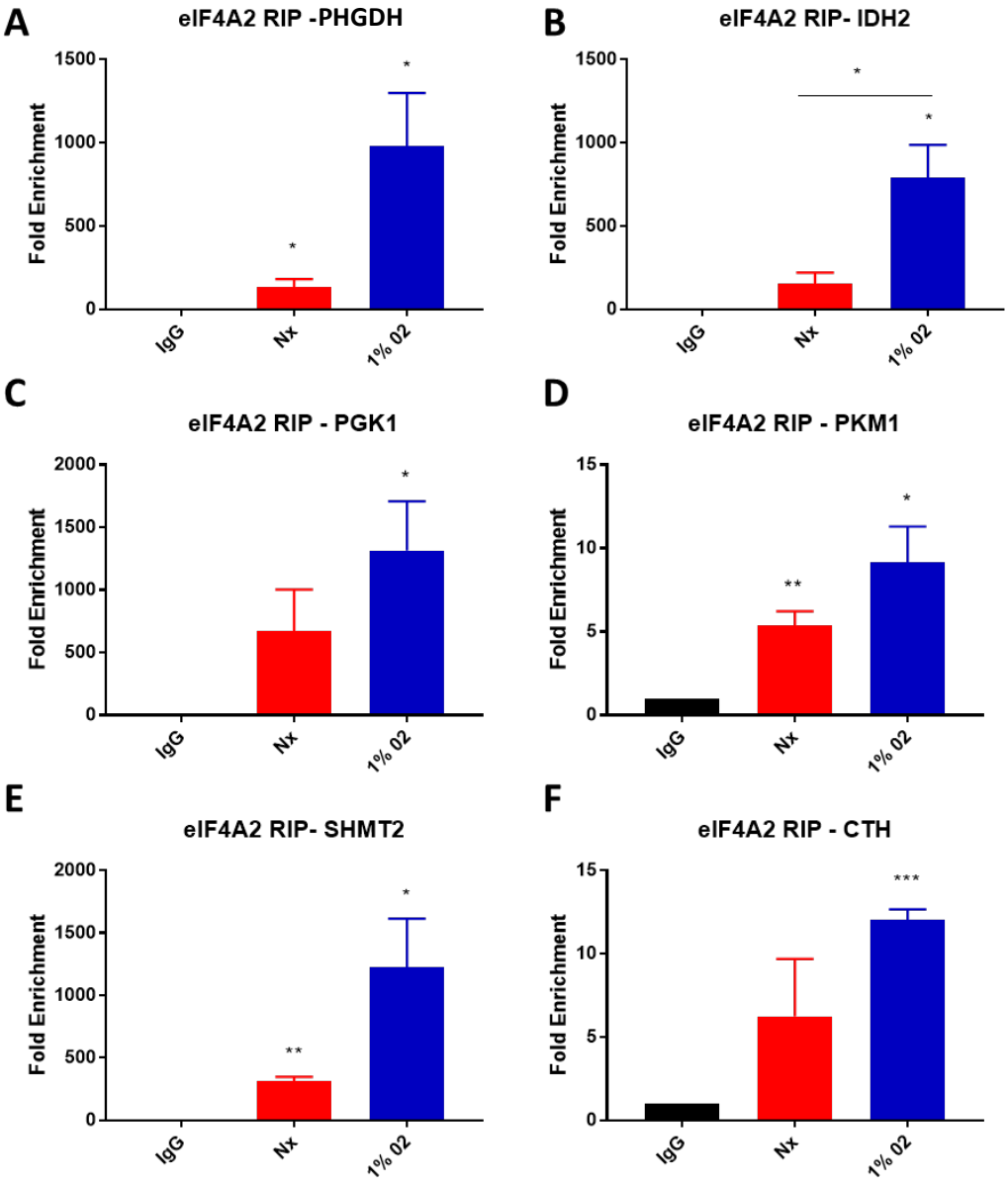


Figure 5.7. qRT-PCR validation of eIF4A2 normoxic and hypoxic RIP for biosynthesis of amino acid selected top transcripts. eIF4A2 RIP and cDNA synthesis was performed as previously described. mRNA expression was analysed via qRT-PCR. Data displayed as fold enrichment over IgG negative control. (A)*PDGDH* (B) *IDH2* (C) *PGK1* (D) *PKM1* (E) *SHMT2* (F) *CTH*. Error bars indicate ± SEM. Data were analysed for significance by one way ANOVA. *p<0.05, **p<0.01, ***p<0.001. n=3.

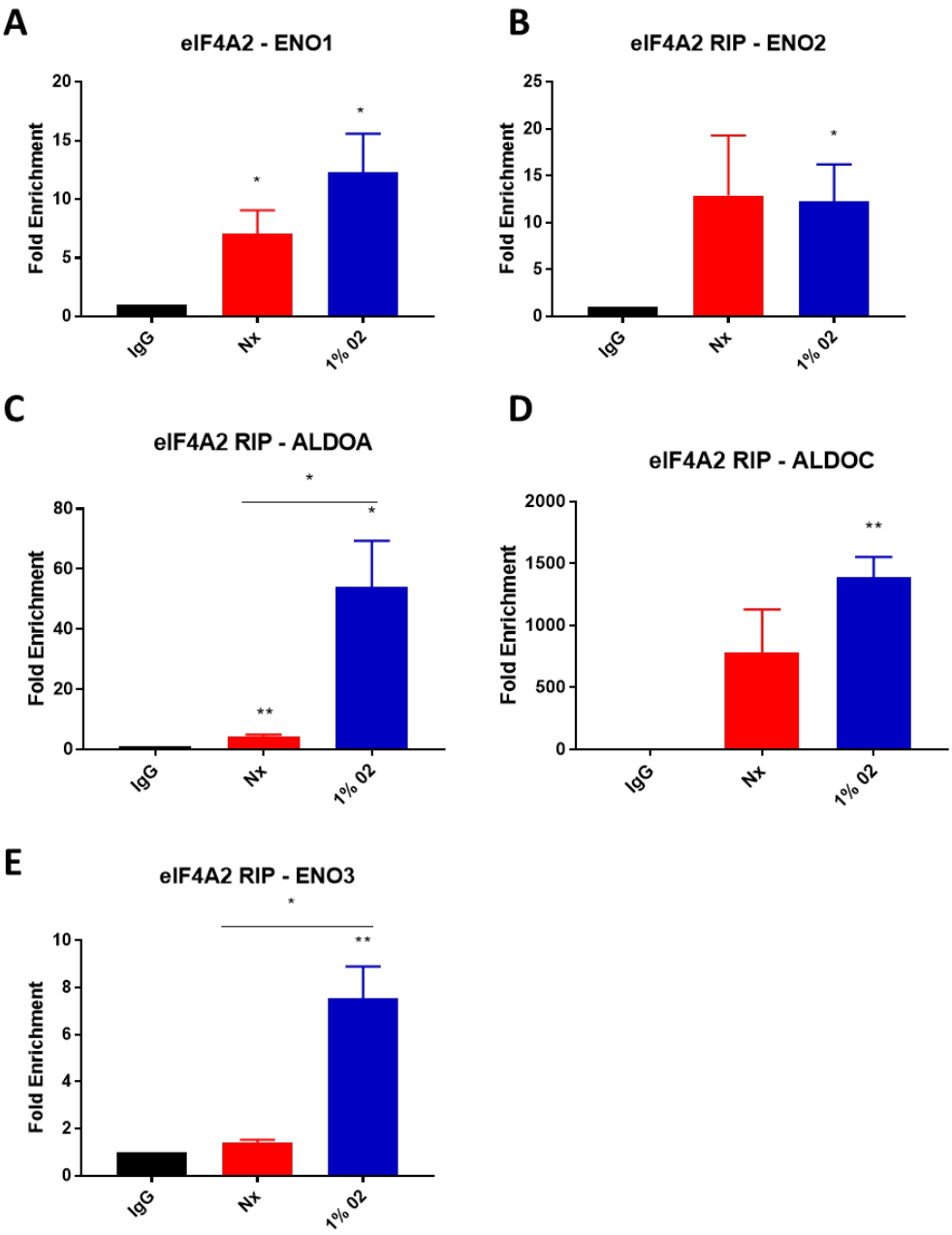


Figure 5.8. qRT-PCR validation of eIF4A2 normoxic and hypoxic RIP for carbon metabolism selected top transcripts. eIF4A2 RIP and cDNA synthesis was performed as previously described. mRNA expression was analysed via qRT-PCR. Data displayed as fold enrichment over IgG negative control. (A)*ENO1* (B) *ENO2* (C) *ALDOA* (D) *ALDOC* (E) *ENO3* Error bars indicate ± SEM. Data were analysed for significance by one way ANOVA. *p<0.05, **p<0.01, ***p<0.001. n=3.

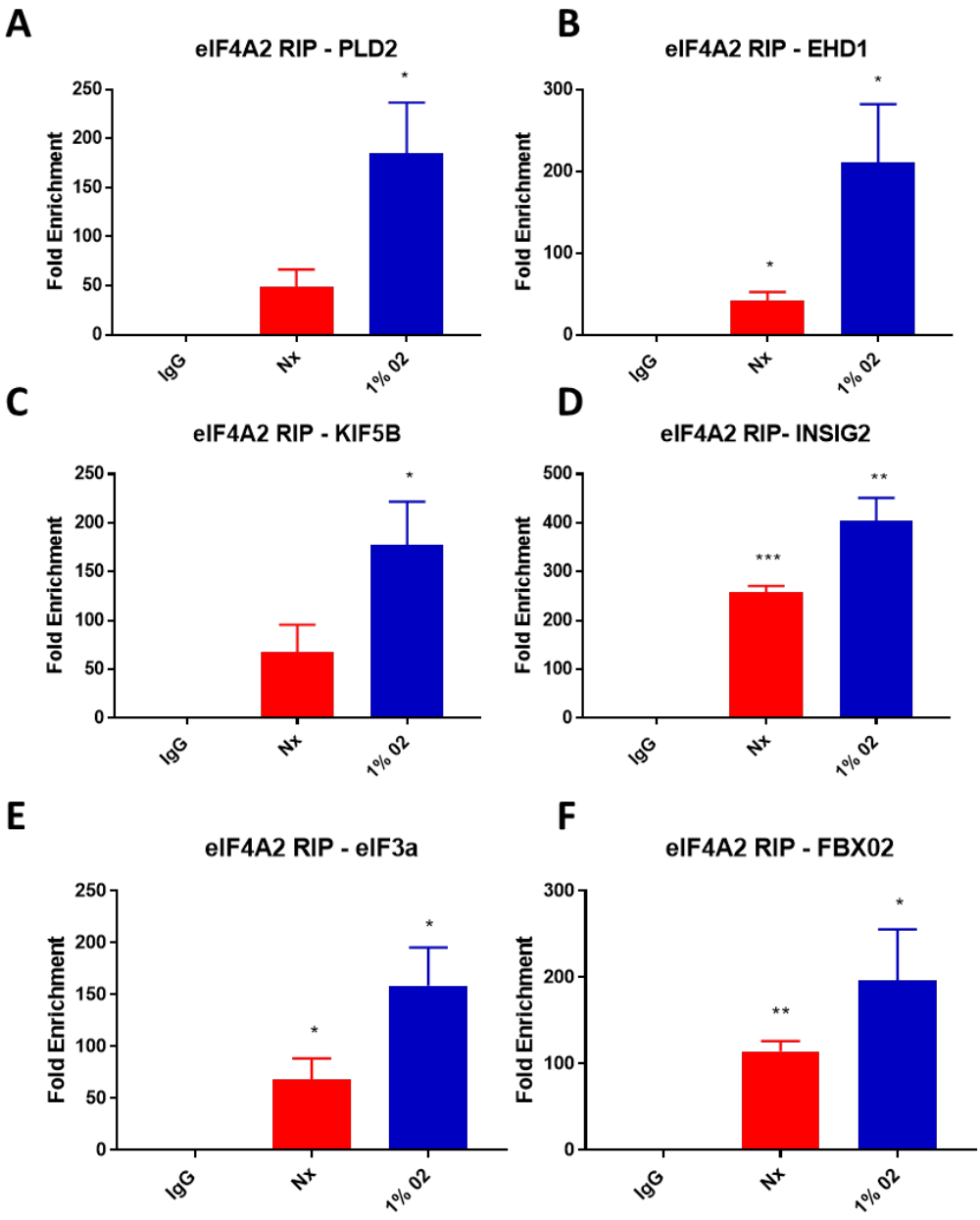


Figure 5.9. qRT-PCR validation of eIF4A2 normoxic and hypoxic RIP for endocytosis selected top transcripts. eIF4A2 RIP and cDNA synthesis was performed as previously described. mRNA expression was analysed via qRT-PCR. Data displayed as fold enrichment over IgG negative control. (A)*PLD2* (B) *EHD1* (C) *KIF5B* (D) *INSIG2* (E) *eIF3a* (F) *FBXO2.* Error bars indicate ± SEM. Data were analysed for significance by one way ANOVA. *p<0.05, **p<0.01, ***p<0.001. n=3.

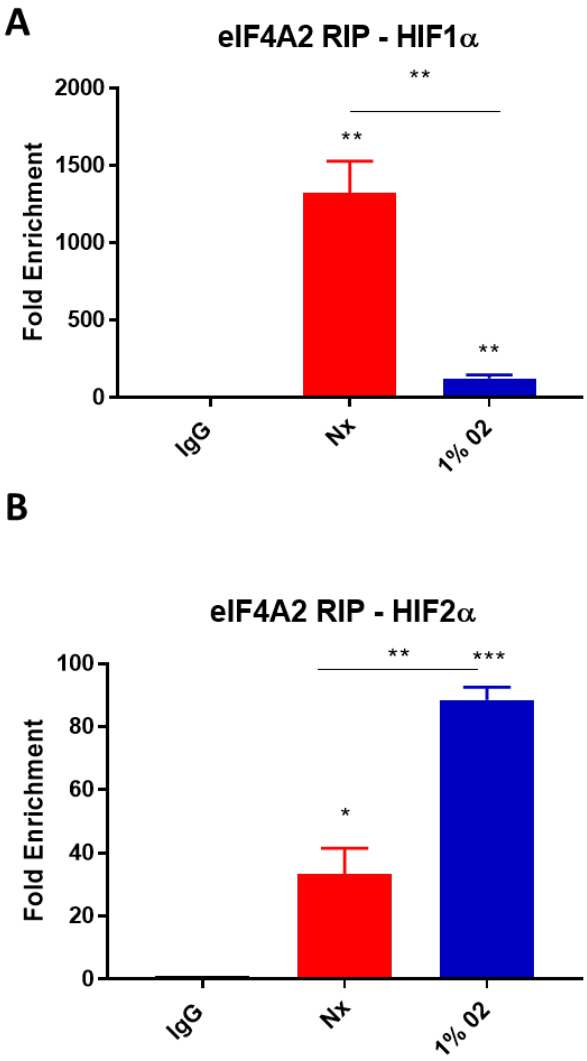


Figure 5.10. qRT-PCR validation of eIF4A2 normoxic and hypoxic RIP for HIF isoforms.. eIF4A2 RIP and cDNA synthesis was performed as previously described. mRNA expression was analysed via qRT-PCR. Data displayed as fold enrichment over IgG negative control. (A)*HIF1α* (B) *HIF2α*. Error bars indicate ± SEM. Data were analysed for significance by one way ANOVA. *p<0.05, **p<0.01, ***p<0.001. n=3.

Interestingly, data obtained from the eIF4A2 RIP-SEQ demonstrated increased binding of the eIF4A2 protein to the *HIF1α* transcript under hypoxic conditions (padj=4.0x10^{-10}) in addition to increased binding to the *HIF1β* sub-unit (padj=1.0x10^{-11}), *HIF2α* (padj=1.0x10^{-5}) and the *HIF1α* anti-sense RNA 2 (padj=2.0x10^{-9}). Figure 5.10 shows eIF4A2:*HIF2α* binding via qRT-PCR, with eIF4A2 displaying a significant increase in fold enrichment over the IgG control for both normoxic (p<0.05) and hypoxic (p<0.001) pull downs, with a statistically significant increase in hypoxic enrichment in comparison to normoxic enrichment (p<0.01).

However upon qRT-PCR validation of eIF4A2:*HIF1α* binding, the opposite effect was found than that obtained in the RIP-SEQ data. Instead a significant reduction in eIF4A2 binding to *HIF1α* was observed under hypoxic conditions ($p<0.01$) in comparison to normoxic pull downs. Yet both normoxic ($p<0.01$) and hypoxic ($p<0.01$) pull downs still displayed significant fold enrichment over the IgG control. This finding will be discussed in detail in the discussion section of this chapter.

5.2.7 Immunoblot Validation of RIP-SEQ Top Targets

The RIP-seq data identified a list of differentially expressed transcripts between the eIF4A2 1% O_2 RIP and eIF4A2 20% O_2 RIP, this is demonstrative of direct binding between eIF4A2 and its identified mRNA target. However, eIF4A2 possesses both translational activation effects due to its helicase function and translation repressive effects due to its interactions with the CCR4-NOT complex. Therefore the protein expression of the top targets identified was investigated via immunoblot following siRNA inhibition using 2 separately validated siRNA sequences both targeting eIF4A2 as previously described. LS174T cells underwent siRNA knockdown of eIF4A2 and were exposed to 1% O_2 for 48 hours. Immunoblot was performed as previously described and proteins investigated were as follows: FOSL2, JunB, JunD, LDHA, NOTCH1, SF3B4, EHD1, KIF5B, SHMT2, CTH. The additional proteins FOSL2, JunB, JunD, LDHA, NOTCH1 and SF3B4 were selected as they had previously been identified in preliminary RIP-SEQ experiments performed using Nanopore technology (data shown in appendix). A selection of proteins were also investigated following siRNA inhibition of eIF4A1 as performed as previously described to uncover if the identified targets were regulated specifically by eIF4A2 and not eIF4A1. A panel of proteins were also investigated at the protein level following siRNA inhibition of HIF to further elucidate its mechanism of hypoxic expression and whether it is dependent on eIF4A2 of HIF for its hypoxic expression. Figure 5.11 displays representative images of immunoblot from three experimental repeats following siRNA knockdown of eIF4A2 and probed for proteins of interested identified from the RIP-SEQ. A reduction in all proteins analysed was observed following eIF4A2 knockdown, suggesting the translational activation effects of eIF4A2 on these proteins.

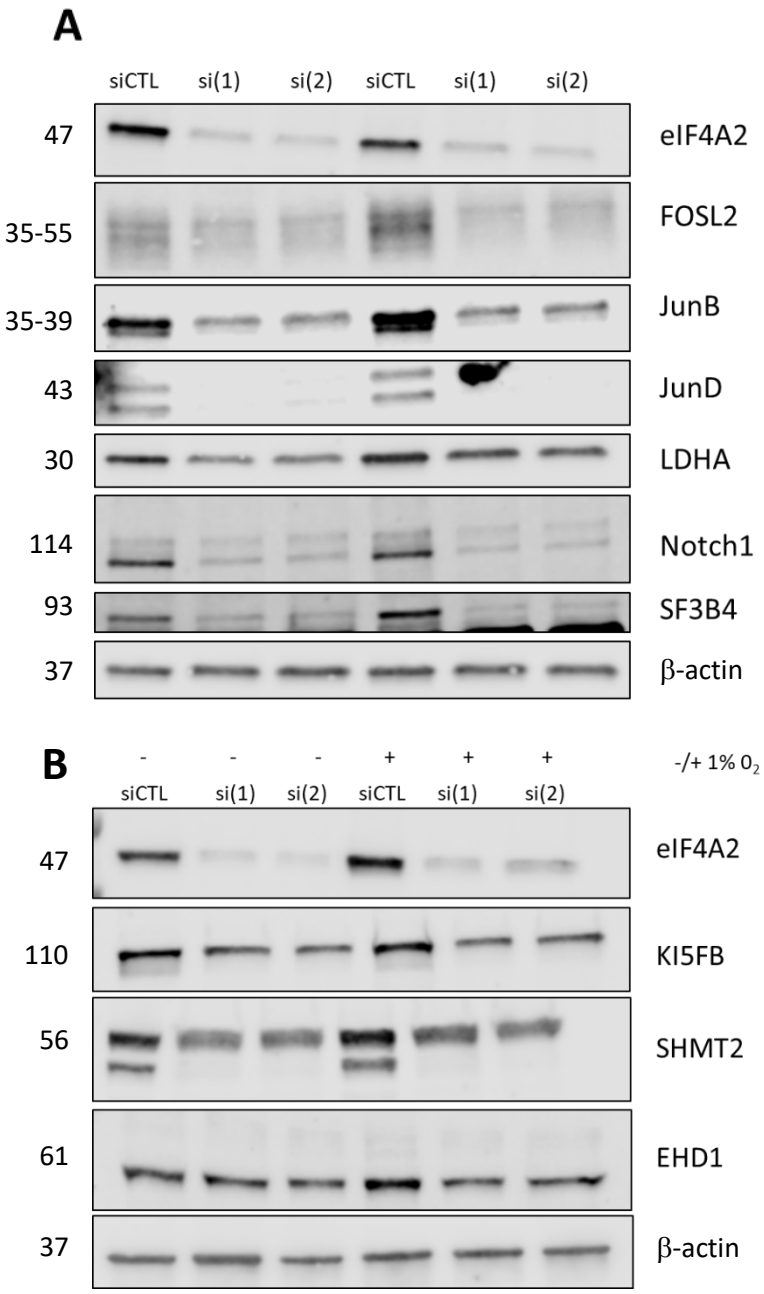


Figure 5.11. Representative images of immunoblot validation of eIF4A2 dependent transcripts identified from RIP-SEQ. LS174T cells underwent siRNA knockdown of eIF4A2 using 2 separately validated sequences and exposed to 24 hours normoxia (20% O_2) or hypoxia (1% O_2). Protein expression of (A) eIF4A2, FOSL2, JunB, JunD, LDHA, Actin (B) KIF5B, SHMT2, EHD1, β-actin was analysed via western blot as previously described. Molecular weights in kDa are displayed on the left of the blot. n=3.

The IPTG inducible sheIF4A2 cell line was also utilised to determine the translation effect of eIF4A2 on additional proteins of interest. LS174T cells incubated with 1 mM IPTG and protein expression of CTH analysed via immunoblot. Appropriate controls both with and without IPTG were included in the analysed to exclude any effect of the IPTG alone influencing protein expression or eIF4A2 knockdown. Figure 5.12 displays immunoblot results of CTH expression in the LS174T sheIF4A2 cell line following exposure to 48 hours normoxia (20% O_2) or hypoxia (1% O_2). A demonstrable reduction in CTH levels were obtained following eIF4A2 knockdown highlighting the translation activation role of eIF4A2 on CTH.

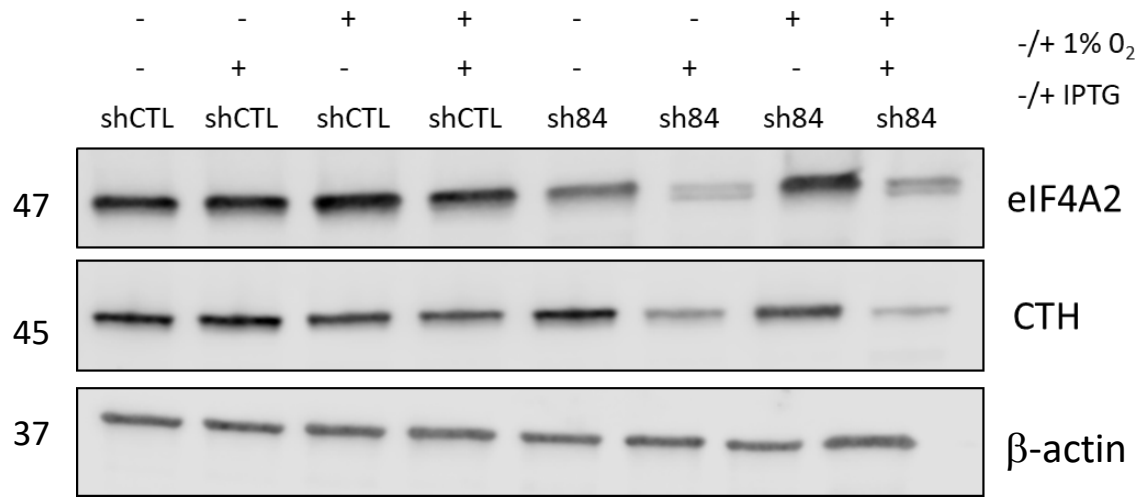


Figure 5.12. Representative images of immunoblot validation of eIF4A2 knockdown on CTH protein expression. LS174T eIF4A2 shRNA knockdown was induced with 1mM IPTG and cells exposed to either 24 hours normoxia (20% O_2) or hypoxia (1% O_2). Protein expression of eIF4A2, CTH and β-actin were analysed via immunoblot. Molecular weights in kDa are displayed on the left of the blot. n=3.

In order to determine that the reduction in protein expression observed was specific to the eIF4A2 isoform, siRNA knockdown of eIF4A1 was performed as cells again exposed to 24 hours normoxia (20% O_2) or hypoxia (1% O_2). Figure 5.13 displays protein expression of FOSL2, KIF5B, JunB, EHD1, SF3B4, LDHA and β-actin following eIF4A1 knockdown. Interestingly, the opposite effect was observed for the protein expression of FOSL2 following eIF4A1 knockdown in comparison to eI4A2 knockdown, suggesting the different eIF4A isoforms may have opposing roles in the regulation of FOSL2 under normoxic and hypoxic conditions. The same observation held true for both JunB, JunD and LDHA.

However eIF4A1 knockdown appeared to have similar effects on EHD1 reduction in comparison to eIF4A2 knockdown, suggesting EHD1 may be under the control of both eIF4A isoforms.

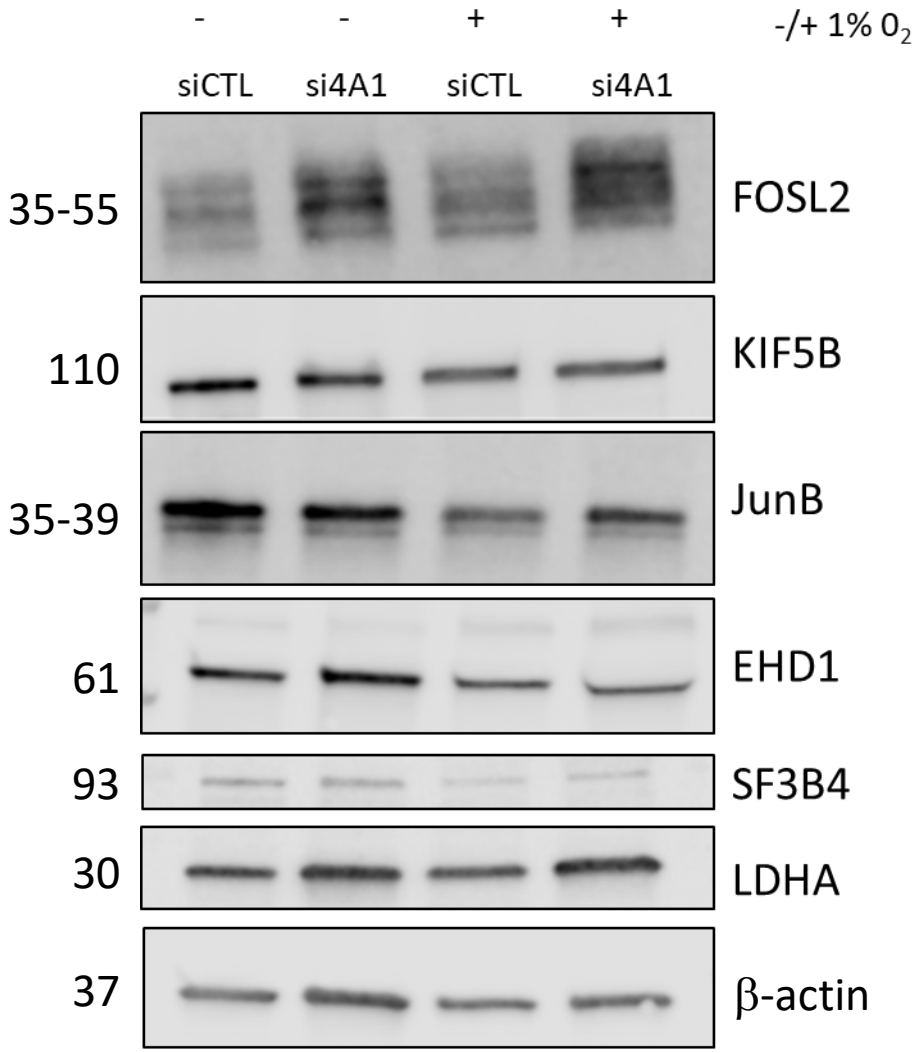


Figure 5.13. Representative images of immunoblot validation of eIF4A2 RIP-SEQ targets following eIF4A1 knockdown. LS174T eIF4A1 siRNA knockdown was performed as previously described and cells exposed to either 24 hours normoxia (20% O_2) or hypoxia (1% O_2). Protein expression of eIF4A2, FOSL2, KJF5B, JUND, JUNB, EHD1, SF3B4, LDHA and β -actin were analysed via immunoblot. Molecular weights in kDa are displayed on the left of the blot. n=3.

5.2.8 Functional Validation of RIP-SEQ Targets

In order to validate the functional effect of the top selected targets from the RIP-SEQ, siRNA knockdown of KIF5B, PLD2 and EHD1 were performed followed by clonogenic assay to investigate the effect of knockdown of endocytic genes on colorectal cancer cell survival in both normoxia and hypoxia as previously described. siRNA knockdown was confirmed via qPCR and immunoblot as previously described. Due to technical issues with the PLD2 antibody, only an extremely faint band was detectable, however this was enough to observe effective knockdown following siRNA knockdown of PLD2. Figure 5.14 displays siRNA knockdown efficiency at the RNA level for EHD1 (Figure 5.14, A), PLD2 (Figure 5.14, B) and KIF5B (Figure 5.14, C). Figure 5.14 also displays siRNA knockdown efficiency for the same targets at the protein level for EHD1 (Figure 5.14, D), PLD2 (Figure 5.14, E) and KIF5B (Figure 5.14, C). Significant knockdown was achieved at the RNA level for all targets in both normoxia and hypoxia (EHD1; normoxia $p<0.001$, hypoxia $p<0.001$) (PLD2; normoxia $p<0.01$, hypoxia $p<0.05$) (KIF5B; normoxia $p<0.001$, hypoxia ($p<0.001$). Figure 5.15 displays the results the clonogenic assay as measure of cell survival following siRNA knockdown of top endocytic genes identified from the eIF4A2 RIP-SEQ. There was no significant difference in cell survival in the siCTL condition between normoxia and hypoxia, demonstrating hypoxia alone does not negatively impact colorectal cancer cell survival. A significant reduction in cell survival under normoxic conditions was observed following siRNA inhibition of PLD2 ($p<0.001$), KIF5B ($p<0.001$) and EHD1 ($p<0.001$) in comparison to the siRNA normoxic control group. A significant reduction in cell survival under hypoxic conditions was observed following siRNA inhibition of PLD2 ($p<0.001$), KIF5B ($p<0.001$) and EHD1 ($p<0.001$) in comparison to the siRNA normoxic control group. A significant difference between normoxic and hypoxic cell survival was observed following inhibition of PLD2 ($p<0.01$). However no significant difference was observed between the reduction in normoxic and hypoxic cell survival for either KIF5B or EHD1. This demonstrates that knockdown of eIF4A2 bind endocytic genes leads to a reduction in colorectal cancer cell survival with the effect enhanced under hypoxic conditions only for PLD2.

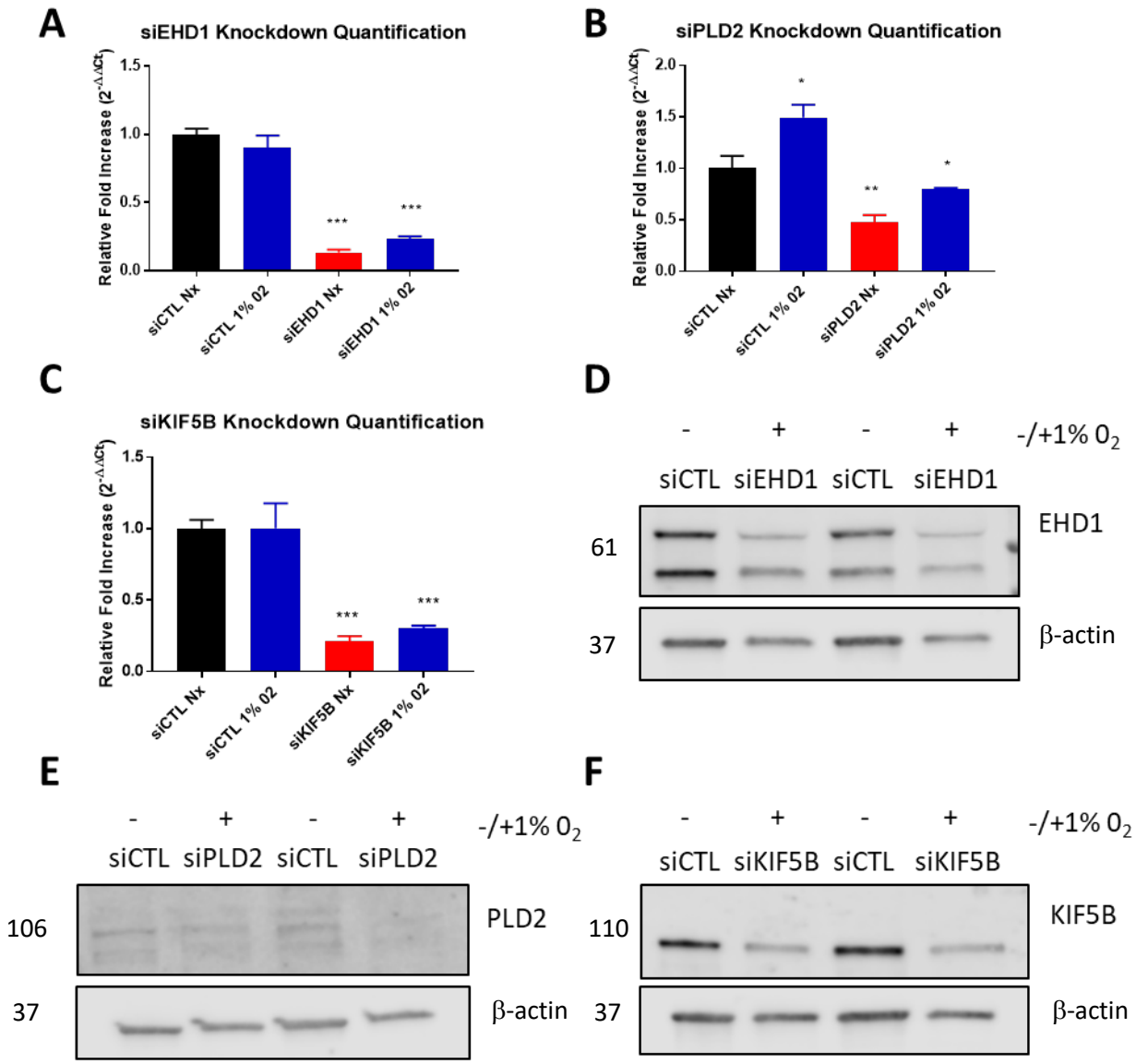


Figure 5.14. Representative images of immunoblot validation of eIF4A2 RIP-SEQ targets following eIF4A1 knockdown. LS174T siRNA knockdown of *EHD1, PLD2* and *KIF5B* was performed as previously described. EHD1, PLD2 and KIF5B mRNA was measured vis qRT-PCR and protein expression measured via immunoblot. Error bars indicate ± SEM. Data were analysed for significance by a t-test. Molecular weights in kDa are displated on the left of the blot. *p<0.05, **p<0.01, ***p<0.001. n=3.

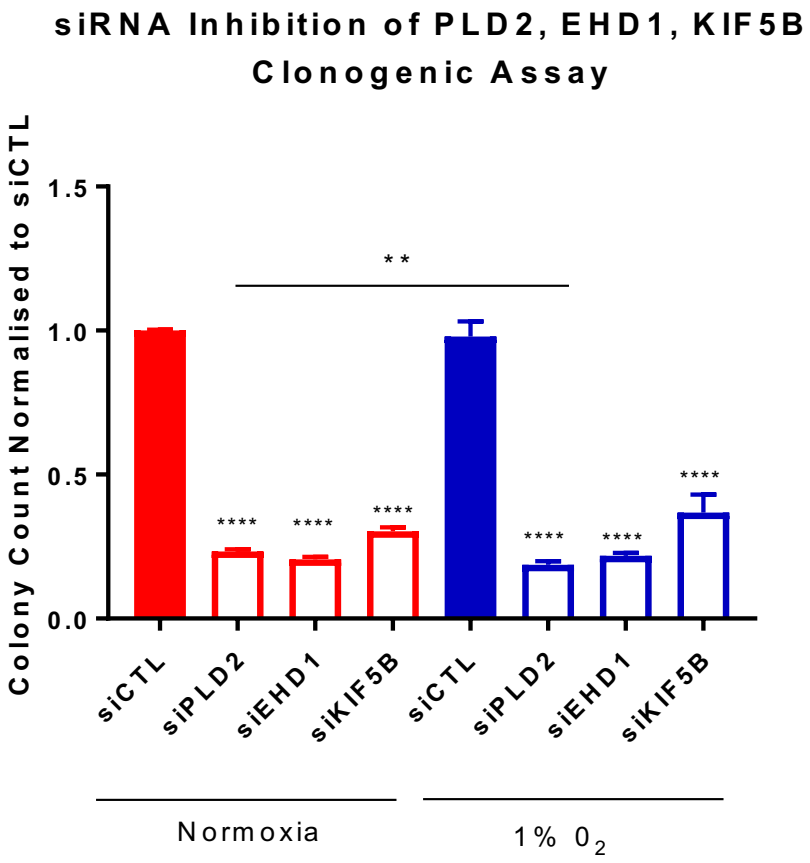


Figure 5.15. Cell survival of colorectal cancer cells following siRNA knockdown of endocytic genes identified from the eIF4A2 RIP-SEQ. siRNA knockdown of *PLD2*, *EHD1* and *KIF5B* was performed as previously described. Cell survival was measure via clonogenic assay and data presented as a percentage of colony counts normalised to the normoxic control. Error bars indicate ± SEM. Data were analysed for significance by a t-test. *p<0.05, **p<0.01, ***p<0.001. n=3.

5.2.9 5'UTR Analysis of eIF4A2 bound hypoxic transcripts

An additional hypothesis investigated in the chapter was that eIF4A2 bound transcripts that were upregulated under hypoxic conditions were possess longer and more thermodynamically stable transcripts. This hypothesis was formed based on the previous findings that long and complex 5'UTRs are inhibitory to ribosomal scanning, in addition to all 3 of the major studies investigating the eIF4A dependent translatome reporting that eIF4A dependent or Silvestrol sensitive transcripts also possess longer and more complex 5'UTRs (Wolfe et al, 2014)(Rubio et al, 2014) (Modelska et al, 2015).

Gene IDs were used to retrieve 5'UTR sequences Ensembl Biomart which included all unique transcripts associated with each gene ID. An in house pearl script was used to feed each 5'UTR sequence into "ovrnafold" and the FASTA header, 5'UTR length and predicted free energy was captured. This was performed for transcripts identified as being eIF4A2 bound under hypoxic conditions in both the upregulated and downregulated group. The average 5'UTR length and predicted free energy was then calculated for transcripts identified as upregulated and bound to eIF4A2 under hypoxic conditions and transcripts identified as downregulated under hypoxic conditions. This work was performed by a bioinformatician, Dr Keith Spriggs, School of Pharmacy. Figure 5.16 presents the average 5'UTR length (Figure 5.16, A) for transcripts bound to eIF4A2 when upregulated under hypoxic conditions and those which were downregulated when bound to eIF4A2 under hypoxic conditions. The data demonstrates a significant difference between the average 5'UTR length, with transcripts upregulated and bound to eIF4A2 under hypoxic conditions possessing on average longer 5'UTRs ($p<0.001$). Figure 5.16, B presents the average predicted free energy for the same transcripts and demonstrates a significant difference in predicted free energy, with transcripts with transcripts upregulated and bound to eIF4A2 under hypoxic conditions possessing on average a more negative predicted free energy ($p<0.001$). The more negative the value of predicted free energy, the more thermodynamically stable the transcript is predicted to be, and so the more energy will be required to unwind said transcripts. That said, transcripts with more thermodynamically stable 5'UTRs will depend more so on eIF4A2 to be unwound to allow for efficient translation. This data demonstrates that eIF4A2 bound transcripts upregulated under hypoxic conditions possess longer and more thermodynamically stable 5'UTRs.

In order to identify any physical characteristics present in eIF4A2 bound hypoxic transcripts that may confer a potential mechanism by which eIF4A2 recognises its targets, the MFE plot of the secondary structure of the 5'UTR sequence of selected transcripts was obtained from Vienna RNAFold web server. This investigation was based on previous data demonstrating that eIF3d acts as both a translation activator and repressor of a subset of transcripts and is able to target these transcripts through recognition and binding to a particular stem loop present in the 5'UTRs of such transcripts (Lee et al, 2016). As an initial investigation, transcripts with the highest log2fold change in both the upregulated and downregulated eIF4A2 bound groups were fed into the Vienna RNAfold web server to obtain representative example MFE diagrams depicting the predicted RNA secondary structure for that transcript.

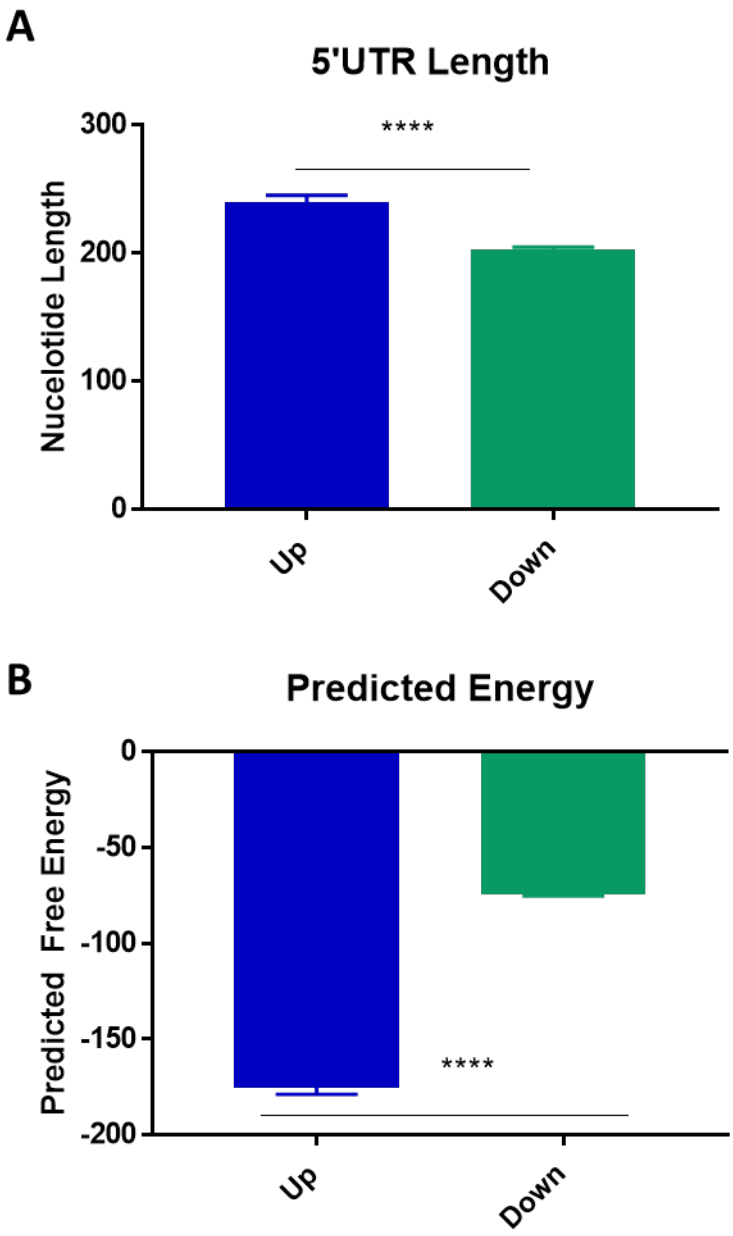


Figure 5.16. Average 5'UTR length and predicted free energy of eIF4A2 bound transcripts that were found to be upregulated or downregulated under hypoxic conditions identified from the eIF4A2 RIP-SEQ. An in house pearl script was used to feed each 5'UTR sequence into ovrnafold and the FASTA header, 5'UTR length and predicted free energy was captured. (A) Average nucleotide length for eIF4A2 bound transcripts upregulated and downregulated under hypoxic conditions (B) Average predicted free energy of eIF4A2 bound transcripts upregulated and downregulated under hypoxic conditions. Error bars indicate ± SEM. Data were analysed for significance by a t-test. *p<0.05, **p<0.01, ***p<0.001. n=3.

The 5’UTR secondary structure diagram was also obtained for beta-actin as an example of a transcript that has previously shown not to be dependent on eIF4A for its translation. Figure 5.17, A presents the secondary structure of the 5’UTR of beta-actin, with a nucleotide length of 84 and a predicted free energy of -15.5. It is apparent that this 5’UTR is generally short, unstructured with no complex secondary structures such as stem loops etc. Figure 5.17, B presents the secondary structure of SLC6A18, which had the highest log2fold change in the eIF4A2 bound downregulated group; with a nucleotide length of 97 and a predicted free energy of -36.9. Figure 5.17, C presents the secondary structure of NEURL3 which possessed the highest log2gold change of the eIF4A2 bound transcripts upregulated in hypoxia; with a nucleotide length of 712 and a predicted free energy of -350.2. It is apparent that the 5’UTR of NEURL3, as an example, possesses an extremely long and highly structured 5’UTR containing multiple stem loops, hairpin loops and interior bulges. Any one of these structures may represent a possible mechanism by which eIF4A2 recognises and binds to its target transcripts. Future work on these findings will be discussed later in this thesis.

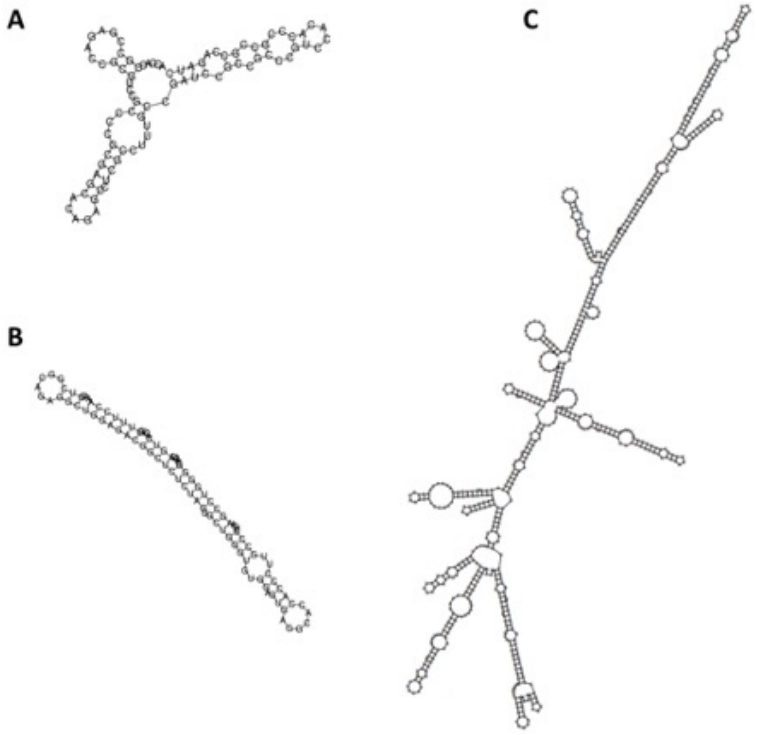


Figure 5.17. Representative MFE plots of the most upregulated and downregulated transcripts when bound to eIF4A2 under hypoxic conditions. (A) Actin (B) SLC6A18 (C) NEURL3. MFE plots display predicted secondary structure of 5’UTR sequences and were obtained by feeding the 5’UTR sequences into the Vienna RNAFold web server.

5.3 Discussion

The data presented in this chapter for the first time demonstrates the identification of novel eIF4A2 bound transcripts under hypoxic conditions and the differences in eIF4A2 bound transcripts between normoxia and hypoxia in colorectal cancer cells. This data presents the identification of 1237 unique transcripts bound to eIF4A2 specifically under hypoxic conditions that were not found in normoxia. This data has uncovered novel pathways enriched in the eIF4A2 bound hypoxic transcripts, many of which are in line with the major changes associated with low oxygen conditions. "Metabolic pathways" was the most enriched pathway (corrected p-value $4.0x10^{-25}$) and of these the most enriched metabolic pathway was "biosynthesis of amino acids" (corrected p-value $3.7x10^{-7}$). The most enriched pathways in the eIF4A2 bound hypoxic transcripts aside from metabolism was "endocytosis" (corrected p-value $7.0x10^{-14}$). The top transcripts selected for further investigation were validated via RIP-qPCR and immunoblot; eIF4A2 knockdown was shown to reduce the protein levels of identified targets. The data presented in this chapter also for the first time demonstrates that hypoxic eIF4A2 bound transcripts on average possess longer and more thermodynamically stable 5'UTRs.

5.3.1 eIF4A2 Dependent Pathways under Hypoxia: Possible Mechanisms

KEGG pathways analysis revealed the top 5 most significantly enriched pathways in the eIF4A2 bound transcripts upregulated under hypoxic conditions and their associated corrected p-value include: 'metabolic pathways' ($4.0x10^{-25}$), endocytosis ($7.0x10^{-14}$), 'carbon metabolism' ($1.0x10^{-11}$), 'pathways in cancer' ($4.0x10^{-10}$) and 'lysosome' ($9.0x10^{-10}$) along with many other pathways in line with the major changes in hypoxia. The most enriched metabolic pathway aside from the general 'metabolism' category was uncovered as 'biosynthesis of amino acids' ($3.7x10^{-7}$).

5.3.1.1 Endocytosis

Endocytosis was selected for further investigation as it was the second most enriched pathway identified in the KEGG analysis. Endocytosis involves the uptake, sorting and either recycling back to the plasma membrane or the degradation in lysosomes of internalised proteins from the extracellular environment; regulating nutrient uptake and display of adhesion molecules and ion channels (Mellaman and Yarden, 2013). Endocytosis is intrinsically linked to the propagation of intracellular signalling pathways that ultimately influence behaviours such as proliferation, migration and cellular adhesion (Mosesson, Gordon and Yarden, 2008). Many aspects of the endocytic pathway are often dysregulated in cancers such as; breakdown of cell-cell adherens and tight junctions preceding malignant

transformation, enhanced internalisation of junctional proteins (such as the degradation of e-cadherin), disruption of epithelial cellular polarity, endocytic mediated inactivation/long term modulation of growth factor receptors which can lead to increased receptor recycling and sustained cellular proliferation (Nanes and Kowalczyk, 2014) (Goh and Sorkin, 2013)(Mellaman and Yarden, 2013). A key example linking receptor regulation via endocytosis and proliferative signalling is that of the ErbB family of RTKs, which includes EGFR and HER2, that subsequently bind to a number of ligands containing the EGF motif (EGF, HB-EGF and TGFα). The overexpression of these RTKs in malignant cells provides a way to evade degradation and sustain pro-proliferative signalling; HER2 overexpression is present in 15-30% of invasive breast cancers, EGFR frequently overexpressed and mutated in a variety of cancers including breast, lung and glioblastoma (Iqbal et al, 2014) (Sigismund et al, 2018).

Endocytosis regulates and forms the basis of many processes that have been shown to support cancer cell survival and tumour progression. Previous research support the role of endocytic regulated processes such as autophagy in the hypoxic adaptation of cancer cells in order to aid their survival such stress conditions (Lai et al, 2016). Autophagy involves the degradation of dysfunctional organelles and proteins in order to maintain a nutrient supply during stress conditions such as hypoxia (Lai et al, 2016). Autophagy has previously been shown to be induced in a HIF1α dependent manner via the induction of BNIP3/BNIP3L and promoting tumour progression (Bellot et al, 2009). In addition, mitochondrial autophagy was shown act as an adaptive response to hypoxia in order to prevent increased levels of ROS leading to eventual cell death (Zhang et al, 2008). In addition to autophagy, cancer cells are able to take in and degrade extracellular components through the endocytic process known as micropinocytosis (Bloomfield and Kay, 2016).

A key study supporting the fact that colorectal cancer cells preferentially upregulate the hypoxic translation of autophagy/endocytic proteins was performed by Lai et al, 2016. The study exposed HCT116 cells to 1% 0_2 for 16 hours and performed polysome profiling coupled with cDNA microarray analysis to identify mRNAs preferentially translated specifically in the hypoxic polysome (Lai et al, 2016). KEGG analysis of such transcripts revealed enrichment for pathways including; lysosome, focal adhesion and glycan biosynthesis (Lai et al, 2016). The same KEGG pathways were found to be enriched in the eIF4A2 bound transcripts upregulated under hypoxic conditions presented in this thesis (Figure 5.4). Further validation revealed a significant increase in lysosome content and autophagy (via measurement of LC3: cleaved LC3 ratio) in HCT116 cells exposed to hypoxia

(Lai et al, 2016). Data presented in this thesis supports the statement that eIF4A2 binds to and regulates the expression endocytic proteins under hypoxic conditions, and whereby eIF4A2 may act as the master regulator of hypoxic adaptation via promoting the translation of lysosomal and endocytic transcripts.

Figure 5.18 shows the KEGG pathways for endocytosis with proteins in red representing the transcripts upregulated and bound to eIF4A2 under hypoxic conditions. It is clear that eIF4A2 binds to a variety of endocytic transcripts under hypoxia and may represent multiple ways in which eIF4A2 may promote tumour proliferation is via regulation of endocytosis. Whether this be via induction of autophagy, mitochondrial autophagy or other endocytic regulated processes remains to be uncovered.

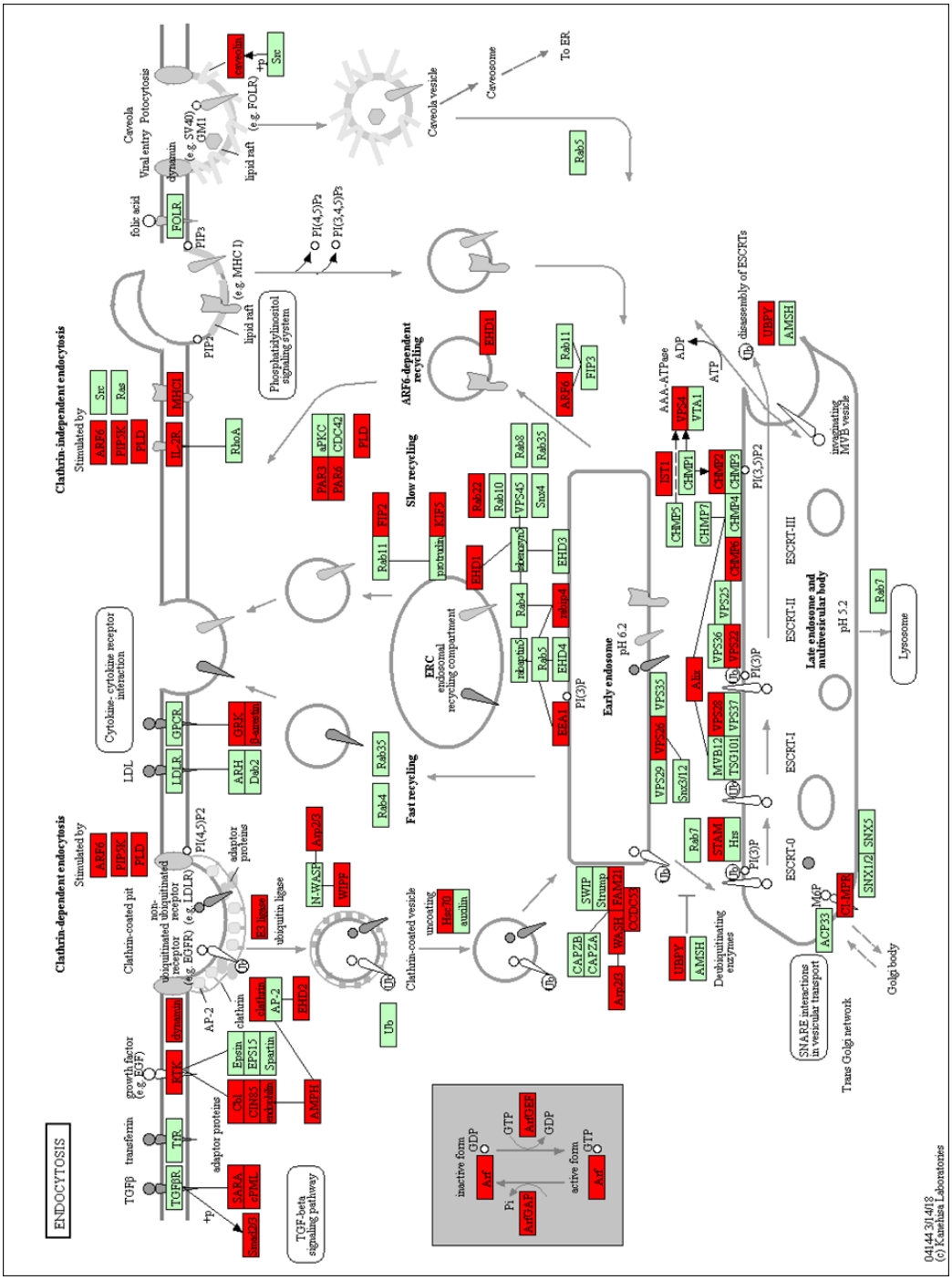


Figure 5.18. KEGG pathway of endocytosis, transcripts in red highlight eIF4A2 bound transcripts upregulated under hypoxic conditions. Endocytosis is process entailing the uptake, sorting and either recycling back to the plasma membrane or the degradation in lysosomes of internalised proteins from the extracellular environment; regulating nutrient uptake and display of adhesion molecules and ion channels.

KIF5B displayed a 2 fold increase (adjusted p-value $6.0x10^{-23}$) in transcript abundance when bound to eIF4A2 in hypoxia when compared bound to eIF4A2 in normoxia; the average read count for the *KIF5B* transcript (when bound to eIF4A2) in normoxia was 2316.10 compared to the read count observed in hypoxia at 4754.40. KIF5B is a member of the kinesin family, it is a microtubule dependent motor required for transportation of membrane bound organelles such as mitochondria, lysosomes and early endosomes (Liu, Gong and Huang, 2013). Additional roles include the regulation of centrosome and nuclear positioning during mitosis and it has recently been shown to play a role in clathrin mediated endocytosis via the removal of the clathrin coat from large clathrin coated vesicles to allow for subsequent rounds of endocytosis (Ni et al, 2018). In a transgenic mouse breast cancer model utilising liposome pull down followed by mass-spectrometry to identify PA bound proteins, KIF5B was shown to directly bind to phosphatidic acid (PA), signalling lipid which is generated by PLD2 (Wang et al, 2017).

PLD2 was also identified as having increased binding to eIF4A2 under hypoxic conditions, displaying a 1.4 fold increase (adjusted p-value $5.0x10^{-6}$) in transcript abundance when bound in eIF4A2 in hypoxia when compared bound to eIF4A2 in normoxia; the average read count for the *PLD2* transcript (when bound to eIF4A2) in normoxia was 137, compared to the read count observed in hypoxia at 234.70. PLD2 belongs to the phospholipase D family of enzymes and is localised to both the plasma membrane and endosomes, regulating membrane trafficking and cell motility (Bruntz, Lindsley and Brown, 2014). PLD2 expression is upregulated breast cancer, over expression is associated with enhanced proliferation and invasion, whereas knockdown of *PLD2* led to an inhibition of proliferation and invasion in a mouse xenograft model (Zhang et al, 2014) (Henkels et al, 2013). The binding of KIF5B to PLD2 generated PA in a transgenic mouse model of breast cancer was shown to be required for the plasma membrane localisation of membrane type 1 matrix metalloproteinase (MT1-MMP), invadopodia formation (required to invade into ECM) and invasion both *in vitro* and *in vivo* (Wang et al, 2017). MT1-MMP is a membrane tethered metalloproteinase responsible ECM breakdown and invasive tumour growth (Linder, 2015). Furthermore a KIF5B-RET fusion oncoprotein has been identified in 2% of NSCLC patients and has been shown to recruit additional kinases to form a signalling axis that activates a variety of RTKs to promote RAS/MAPK signalling and invadopodia formation (Das and Cagan, 2017). KIF5B and PLD2 are yet to be investigated in colorectal cancers, and are also yet to be investigated in the context of hypoxia. The same study by Wang et al also

demonstrated that EHD1 directly binds to PA in a transgenic mouse model of breast cancer (Wang et al, 2018).

EHD1 was also identified as having increased binding to eIF4A2 under hypoxic conditions displaying a 2.2 fold increase (adjusted p-value $1.34x10^{-15}$) in transcript abundance when bound in eIF4A2 in hypoxia when compared bound to eIF4A2 in normoxia; the average read count for the *EHD1* transcript (when bound to eIF4A2) in normoxia was 219.80, compared to the read count observed in hypoxia at 501.60. EHD1 is a member of the dynamin family and acts as an ATP and membrane binding protein that controls vesiculation of endocytic membranes, membrane trafficking of recycling endosomes and endocytic membrane fusion (Deo et al, 2018). EHD1 regulates β1 integrin endosomal transport and so effects proliferation, migration, metastasis and focal adhesions (Jovic et al, 2007). EHD1 overexpression has been identified and shown to promote EMT in NSCLC (Meng et al, 2017). As shown in Figure 76, EHD1 is associated with both arms of the endosomal recycling compartment; the slow recycling pathway and ARF6-dependent recycling. One possible explanation for how eIF4A2 translation activation of EHD1 promotes cell survival is that by increasing the rate at which receptors are recycled back to the plasma membrane via multiple pathways. Thereby inhibiting eIF4A2, we may prevent the recycling of key pro-proliferative signalling receptors to the plasma membrane, leading to receptor accumulation within the cell.

Previous RNA-SEQ studies undertaken by Marchetti, Zyner, Ohnmact et al using the compound CM03 633.34 to stabilise RNA G-quadruplexes and prevent the translation of such transcripts, identified transcripts containing RNA G-quadruplexes downregulated following treatment with CM03 633.34. Interestingly, KEGG analysis of such downregulated transcripts were also enriched for genes involved in endocytosis, which mirror the results found in this study (Marchetti et al, 2018). Following treatment of PANC-1 cells with 400nM of CM03, 44 transcripts enriched for endocytosis were identified. Interestingly, 18 identical endocytic transcripts found in the hypoxic eIF4A2 RIP-SEQ undertaken by Marchetii, Zyner and Ohnmact et al and the eIF4A2 RIP-SEQ in this thesis. Identical endocytic transcripts between the 2 studies include: *CHMP6, PIP5K1C, ARF6, HSPA2, ZFYVE9, WIPF2, AGAP1, EHD2, AGAP3, PARD6A, FAM21A, RUFY1, PSD4, RAB11FIP4, ARRB1, GRK5* (Marchetti et al, 2018). These identical targets may represent endocytic proteins conserved across cancer types required for hypoxic cell survival that additionally contain RNA- G-quadruplex as a mechanism to regulate their hypoxic translation.

5.3.2 RIP-Seq Methodology Limitations and Future Investigations

The use of RIP is a well-known and accepted RNA analogue of the more commonly known ChIP; whereby RBPs are immunoprecipitated using an antibody directed against the protein of interest, bound mRNAs are sequenced an identified (Wheeler et al, 2018). In comparison to the newly developed techniques being used to study RNA-protein interactions, RIP is a relatively old and outdated technique. Since the RNA-protein interactions are not stabilised by a crosslink, RNAs bound to the RBPs with low affinity may be lost in the washes and not recovered leading to false negatives, furthermore RBPs may dissociate from their targets and re-associate with other RNAs during harsh lysis conditions such as sonication (Wheeler et al, 2018). However a milder lysis condition was used for this RIP protocol which may have gone some way into minimising this potential effect. Despite its disadvantages, if RNA binding sites do not need to be determined, RIP is an easy methodology and does not require the use of any specialised lab equipment and for this thesis provided a relatively simple to perform genome wide screen of eIF4A2 bound mRNAs. All current global RNA-protein interaction techniques still incorporate an RNA immunoprecipitation step but include additional steps to improve RNA yield, signal to noise ratio (CLIP-seq, PAR-CLIP), identification of binding sites down to single nucleotide resolution (iCLIP, PIP-seq) and identification of transcripts being actively translated (TRAP-seq, RIBO-seq) (Lin and Miles, 2019). Such techniques incorporate a UV cross linking step (245nm) to generate the formation of a covalent bond between RNA and protein (Lin and Miles, 2019). However such strategies still require the use of high input of cell numbers to maximise the capture of RNA-protein interactions and still suffer from potential poor cross linking efficiency, low RNA-ribonucleoprotein complex abundance, poor antibodies, inefficient library preparation or a combination of all of the above (Ramanathan et al, 2019). Any further investigations into eIF4A2 bound RNAs would be improved by the use of a cross linking step to prevent any RBPs bound with low affinity to prevent the RBPs dissociating with their native RNA targets and binding to alternative RNAs in the lysis process; this would also allow for the identification for RBP binding sites on each target mRNA if this differs between normoxia and hypoxia. However it is important to note that RBP binding is a dynamic and transient process, making it difficult to determine what are the most important proteins bound to an RNA (Mitchell and Parker, 2014).

5.3.3 5'UTR Analysis Limitations and Future Investigations

The data presented in this chapter goes some way into beginning to investigate the characteristics of 5'UTRs of hypoxic eIF4A2 dependent transcripts. Said transcripts that were found to be upregulated when bound to eIF4A2 under hypoxic conditions possessed

longer and more thermodynamically stable 5'UTRs as represented by a more negative predicted free energy value as shown in Figure 5.16. There is a large body of evidence to support the fact that a longer and more complex 5'UTR impedes translation. This data is in line with previous published findings regarding the characteristics of 5'UTRs of eIF4A dependent transcripts (Wolfe et al, 2015)(Rubio et al, 2014)(Modelska et al, 2015). Previous findings by Wolfe et al using ribosomal footprinting techniques uncovered Silvestrol (an eIF4A inhibitor that inhibits both eIF4A1 and eIF4A2) sensitive transcripts; the same paper then demonstrated that those Silvestrol sensitive transcripts possessed significantly longer 5'UTRS (mean UTR length 368 nucleotides) and a $(CGG)_4$ motif within the 5'UTR which corresponding to the formation of an RNA G-quadruplex (Wolfe et al, 2015). Wolfe et al did not analyse predicted free energy of Silvestrol sensitive transcripts and so the data presented in this thesis is the first to present such findings specifically for the eIF4A2 isoform and the first to analysis these under hypoxic conditions.

It was not possible to perform motif enrichment nor prediction of RNA G-quadruplex formation for the data set generated in this thesis; this would pose an interesting bioinformatics analysis to perform in the future to establish if hypoxic eIF4A2 bound transcripts are enriched for a particular motif. The identification of such a motif may act as the sequence element, or structural element that eIF4A2 recognises in its target transcripts. Such research has previously been performed to investigate the mechanism of eIF3 directed translation. Through PAR-CLIP experiments, eIF3 was shown to bind to the 5'UTR of transcripts enriched for cell cycle progression and apoptosis; 2 such transcripts, c-JUN (promotes proliferation) and BTG1 (negative regulator of proliferation) were selected for further investigation as to why eIF3 would bind to 2 transcripts with opposing functions (Lee et al, 2015). Removal of the eI3 binding site from the 5'UTR of both transcripts led to a complete inhibition of c-JUN translation, in contrast, BTG1 translation was highly upregulated; thus demonstrating the opposing roles of eIF3 on translation of its target transcripts (Lee et al, 2015). The same study further investigated the full RNA elements required for eIF3 recognition using selective 2'-hydroxyl acylation analysed by primer extension (SHAPE), a methodology used to experimental determine secondary structure around the binding sites identified from PAR-CLIP (Lee et al, 2015). SHAPE analysis of the c-JUN and the BTG1 transcript revealed that eIF3 binding sites mapped to regions containing conserved RNA stem-loops. Furthermore single point mutation studies revealed that eIF3 binds to the stem loops of c-JUN to promote its translation, in contrast, eIF3 binding to the stem-loop of BTG1 required additional factors or modifications to repress its translation

(Lee et al, 2015). A similar scenario may also be the case for eIF4A2, Figure 5.7 panel A presents the secondary structure of the 5'UTR of beta-actin, with a nucleotide length of 84 and a predicted free energy of -15.5. Figure 5.7 panel B presents the secondary structure of SLC6A18, which had the highest log2fold change in the eIF4A2 bound downregulated group; with a nucleotide length of 97 and a predicted free energy of -36.9. Figure 5.7 panel C presents the secondary structure of NEURL3 which possess the highest log2gold change of the eIF4A2 bound transcripts upregulated in hypoxia; with a nucleotide length of 712 and a predicted free energy of -350.2. The 5'UTR of NEURL3 is extremely large and contains multiple complex secondary structures, including a number of stem-loops. This could potentially act as a structural element to regulate eIF4A2 binding, however, such investigations were beyond the scope of this thesis but would be extremely exciting for future investigations.

The 5'UTR analysis presented in the thesis does possess some limitations; the script used to extract 5'UTR sequences from Ensembl extracted all associated transcripts associated with each gene ID. This meant that a number of gene IDs were associated with multiple gene transcripts which may have led to underlying bias in the data. If such analysis were to be repeated, then only the main "canonical" isoform transcript for each gene ID would be taken forward for 5'UTR analysis.

5.3.4 Concluding Statements

The data presented in this chapter for the first time identifies novel eIF4A2 bound transcripts and the differences between normoxia and hypoxia in colorectal cancer cells. eIF4A2 bound transcripts that were upregulated under hypoxic conditions were found to be enriched for many of the pathways in line with the major changes that occur under hypoxic conditions. These finidngs are in support of hypothesis one presented at the start of this results chatper. For the first time eIF4A2 was shown to possess enriched binding to endocytic genes under hypoxic conditions, with siRNA knockdown of such eIF4A2 bound genes resulting in a significant reduction in colorectal cancer cell survival in both normoxia and hypoxia; supporting hypothesis two presented at the start of this results chapter. Such eIF4A2 bound transcripts upregulated under hypoxic conditions possess significantly longer and more thermodynamically stable 5'UTRs. Again, this finding supports the final hypothesis presented at the start of this results chapter. These results lead us to the conclusion that eIF4A2 is a master regulator of the molecular adaption to hypoxia, enabling cell proliferation and survival in hypoxia by regulating the translation of proteins in amino

acids synthesis and endocytic pathways. However furthermore investigations remain which will be discussed in the future directions section of this thesis.

6.0 Discussion and Future Directions

The data presented in this thesis for the first time identifies novel eIF4A2 bound transcripts upregulated under hypoxic conditions. Such transcripts were enriched for pathways such as endocytosis, biosynthesis of amino acids, fructose and mannose metabolism and focal adhesion. Data presented in the earlier chapters of this thesis represent the first significant steps in determining the regulation and expression of eIF4A2 under hypoxic conditions. However, this thesis seems to raise more interesting questions and theories the more data is uncovered. There are some key questions that remain following the completion of this thesis which will be discussed in the following section.

6.1 eIF4A2 Hypoxic Regulation and Expression

ChIP of HIF1β would still be valuable in demonstrating that the effect shown in Figure 3.9 through direct transcriptional regulation via the HRE predicted within the 3' exon of the eIFA2 genomic sequence is functional. However there is still a possibility that there are additional transcriptional factors that act to fine tune the regulation of eIF4A2 mRNA expression. It would also be of interest to identify these additional transcription factors and their difference between HCT116 and LS174T cell lines. As shown in Figure, eIF4A2 mRNA expression was significantly upregulated in HCT116 cells under hypoxic conditions, but significantly downregulated following knockout of HIF2α in LS174T cells. Identifying which transcription factors are responsible for eIF4A2 transcription in HCT116 cells would help to explain why it is not under the control of the HIF transcription factors despite containing 2 HREs within its promoter.

An additional crucial experiment would be to investigate if the eIF4A2 protein binds to other sub units of the hypoxic eIF4F complex such as HIF2α, eIF4E2 and eIF4G3 via co-immunoprecipitations performed under normoxic and hypoxic conditions (which has previously never been investigated before in colorectal cancer cells). This would prove that eIF4A2 is directly involved in HIF2α directed hypoxic translation.

An additional question regarding the hypoxic translation of eIF4A2 asks, does eIF4A2 contain an IRES to support its hypoxic translation? IRES translation has been experimentally proven for a number of key proteins required for hypoxic cell survival including EGFR, VEGF, TPI, HMGB1, GLUT1, and many stress regulated transcripts (Webb et al, 2015)(Young et al, 2008). eIF4A2 remains to be one of these identified mRNAs, however if one were to

perform such experiments, a bicistronic reporter assay would be the most appropriate method to use in order to prove the presence of an IRES. A significant upregulation of the eIF4A2 protein was not identified under hypoxic conditions, however eIF4A2 was maintained at the protein level with a slight increasing trend observed, and suggesting it still may play an important role in hypoxic cancer cell survival. An improvement on this methodology would be to investigate the expression of the eIF4A2 protein within the hypoxic polysome of colorectal cancer cells. eIF4A2 may be maintained under hypoxic conditions but also preferentially recruited to the actively translating fraction (the polysome).

An additional remaining question asks, what happens to the helicase activity of eIF4A2 under hypoxic conditions? As previously mentioned, eIF4A2 possess both translational activation and repressive effects and has previously been shown to play a role in stress granule formation (Meijer et al, 2013)(Jongjitwimol et al, 2016). As such, when it is bound to the CCR4-NOT complex, or housed within a stress granule, its helicase activity is not required (as it is not actively unwinding a UTR) and so eIF4A2 would act more like a chaperone molecule in these scenarios, allowing for the recruitment of additional molecules such as mRNA de-capping enzymes or splicing factors. As such, it would be interesting to investigate the helicase activity of eIF4A2 under hypoxic conditions (the effect of hypoxia on the helicase activity of DEAD box proteins is yet to be studied). Helicase assays involve the use of annealed nucleic acid strands, containing a quencher at one end and at the opposite end, a fluorophore, that when separated form a stem loop (Mendoza et al, 2015). As the anneal nucleic acids are unwound by a helicase, the 2 are brought together as the stem loop is formed after strand separation. The fluorescent signal decreases as the helicase further unwinds the substrate (Mendoza et al, 2015). In addition, if eIF4A2 does act as more of a chaperone in these scenarios, what additional proteins is eIF4A2 binding to under hypoxic conditions? eIF4A2 pull down followed by separation of proteins via gel electrophoresis and excision of bands of interested to be analysed by mass spectrometry would be sufficient to identify proteins bound to eIF4A2. As described in the introduction section of this thesis, the helicase activity of eIF4A2 is modulated via its binding to eIF4B and eIF4H; does hypoxia modulate the binding of eIF4A2 to either of these partners is an additional question that remains. Co-immunoprecipitation experiments of colorectal cancer cells exposed to normoxia and hypoxia would be sufficient to answer this.

6.2 Hypoxic eIF4A2 Bound Transcripts

Additional questions remain regarding the 5'UTRs of eIF4A2 bound transcripts, are they enriched for the $(CGG)_4$ motif which is predictive of the presence of an RNA-quadruplex? Motif analysis using the MEME suite software package would allow us to identify if eIF4A2 bound transcripts upregulated under hypoxic conditions contained the $(CGG)_4$ motif or novel enriched motifs within that group of transcripts. Site directed mutagenesis of such identified motifs followed by 5'UTR luciferase reported assays would allow us to determine the specific sequence required for eIF4A2 binding and subsequent translation.

In addition, it would be important to perform additional RIP-SEQ experiments comparing the transcripts bound to eIF4A1 or eIF4A2 and shared across both isoforms. An improvement on the methodology used in this thesis would be to perform RIP/CLIP Seq experiments from the normoxic and hypoxic polysome compared to the monosome. It would then be possible to determine which transcripts eIF4A1 and eIF4A2 are bound to when they are actively or not actively taking part in translation under hypoxic conditions. This could be followed eIF4A1 and eIF4A2 knockdown followed by mass spectrometry from the normoxic and hypoxic polysome and monosome to measure the corresponding protein expression of all transcripts identified from the RIP/CLIP-SEQ experiments. This would allow for the identification of the eIF4A1/eIF4A2 dependent hypoxic translatome. This would then direction future experiments with regards to targeting eIF4A1 and eIF4A2 separately or in combination.

6.3 Targeting Endocytosis in Hypoxia

Drawing conclusions from the data presented in results chapter 3, eIF4A2 inhibition would lead to a reduction in hypoxic autophagy, lysosome transport and other endocytic regulated process leading to a reduction in cancer cell viability (indeed data presented in Figure 5.15 supports the reduction in cell viability following siRNA knockdown of endocytic genes). Current inhibitors of autophagy include chloroquine and hydroxychloroquine. However, previous studies have advised scientists to approach the inhibition of autophagy with caution (Daskalaki et al, 2018). Inhibition of autophagy leads to unpredictable and erratic effects on cell viability within the same cell population at different stages of cancer development and is often referred to as a double edged sword (Yang et al, 2011). Previous studies have demonstrated that knockdown of essential autophagy gene ATG7 actually promoted *in vivo* growth of glioblastoma xenografts (Hu et al, 2012). Inhibition of autophagy in normoxic cells can lead to the promotion of tumorigenesis, whereas inhibition of autophagy under hypoxic conditions leads to a "tumour protective effect";

however when in combination with anti angiogenic therapy, a reduction in xenograft growth rates were observed (Hu et al, 2012). Data presented in Figure 4.3,C suggests that eIF4A2 inhibition (and thus inhibition of endocytic, autophagy and lysosome transcripts) did not lead to any significant reduction in normal colon epithelial cell viability. However, a significant increase in cell viability was observed following eIF4A2 knockdown specifically under hypoxic conditions. Whether this increase in cell viability would eventually give rise to a hyper proliferative state in the normal colon epithelium remains to be uncovered.

6.4 Limitations of Methodology

One limitation of the methodology is the use of oxygen tensions used for the normoxic and hypoxic experimental conditions. As described in the introduction section of the thesis physiological oxygen concentrations (physoxia) vary between organs and is an important factor to consider when studying oxygen concentrations across tumour types. In organs such as the liver and kidneys, oxygen levels range from 5-10% 0_2 (Brooks et al, 2007) (Carreau et al, 2011), the brain 2-6% 0^2, the kidney 7-12% $_{02}$ and the intestine 3.5-6% 0_2. Organs such as the lungs display a gradient distribution in oxygen concentrations (Jagnnathan et al, 2016). Cellular 0_2 concentration is generally defined as normoxia (~20% $0_{2)}$, physoxia (~1-13% 0_2), hypoxia (~0.1-1% 0_2) and anoxia being the lack of oxygen (Soni and Padwad 2017)(McKeown, 2014). Furthermore tumour cells experience dynamic changes in oxygen concentrations with both cycling acute transient bouts of hypoxia and reoxygenation from poorly formed and leaky blood vessels and changes in perfusion and blood flow over time (Vaupel, 2004). So in actual fact we are culturing cells under supra-physiological oxygen conditions under what we call normoxia. In addition, cells are exposed to 48 hours of chronic hypoxia, so perhaps a protocol where cells are exposed to cycling bouts of hypoxia would be more appropriate for future experiments.

6.5 Final Conclusions

In conclusion, the data presented in this thesis identifies eIF4A2 as being required for normoxic and hypoxic colorectal cancer cell survival. In addition, novel eIF4A2 bound transcripts, enriched under hypoxic conditions were identified, such transcripts were enriched for genes involved in the endocytosis, bio synthesis of amino acids and central carbon metabolism pathway, highlighting novel potential mechanisms by which eIF4A2 promotes hypoxic colorectal cancer cell survival. Such eIF4A2 bound transcripts possessed longer and more thermodynamically stable 5'UTRs. These results lead us to the conclusion that eIF4A2 is a master regulator of the molecular adaption at the protein level to hypoxia, enabling cell proliferation and survival in hypoxia by regulating the translation of proteins

in amino acids synthesis and endocytic pathways. This highlights the value of the development of small molecular inhibitors that specifically target eIF4A2 to target the therapy resistance hypoxic tumour microenvironment

7.0 Appendix

qRT-PCR Primers

Target	Primer Sequence (Forward, Reverse)
eIF4A1	TGTCTGCGAGCCAGGATTC CTTCGGGCTCCATCCCA
eIF4A2	TGGTGTCATCGAGAGCAACTG GGCTTCTCAAAACCGTAAGCA
CA9	CTTGGAAGAAATCGCTGAGG TGGAAGTAGCGGCTGAAGTC
HIF1α	GATAGCAAGACTTTCCTCAGTCG TGGCTCATATCCCATCAATTC
HIF2α	CATCATGCGACTGGCAAT GCTTCGGACTCGTTTTCAGA
PDGDH	ATTGCTGTTCAGTTCGTGG AGAGAAGGCACTGGTAAGG
IDH2	CAGCATCTTTGCCTGGACA TCCAGCATCTGGGCAAAC
PGK1	GAGCCAGTTGCTGTAGAACTCA CTTCTGGGCCTACACAGTCC
SHMT2	CGAGTTGCGATGCTGTACTT CTGCGTTGCTGTGCTGAG
PKM1	GCTGTTTGAAGAGCTTGTGC TTATAAGAGGCCTCCACGCT
CTH	CCGTTCTGGAAATCCCACTA TGAAGCAAAGGCCAAACAG
ENO1	TCCCAACATCCTGGAGAATAA ATGCCGATGACCACCTTATC
ENO2	AGGTGGATCTCTATACTGCCAAA AACGCTGTTTGTCTCCATCC
ALDOA	GCCAGAAAAGAGAGGGGCTA AATAGAATCGTTGACGTGTGGA
ALDOC	GGATCAGAACCCGAGCTGT TACGAGTGAGGCATGGTGAC
ENO3	AGCGAAGACATCCCAGGTC CCCTGGAGTCCAAGATTTCC
PLD2	CAA CCG TCT CTT GAC CAT GTC ACT GAC TTC CAG GAA CTC TGT CAT
EDH1	GTTTGGCAACGCTTTCCTC TCGATGATGCTGATGCTGTC
KIF5B	GTGATGATTGCGTCCAAG CTTCTTTGCACAATCGTTG
eIF3a	TACCATGATATTGCCCAGCA ACGGAATTCAGCCTTACGC
FBX02	ATGGACGGAGACGGTGAC GCTCCTCCTCAGCACTCG

Western Blot Primary Antibodies

Target	Host	Predicted Molecular Weight (kDa)	Dilution
eIF4A1	Rabbit	47	1:1000
eIF4A2	Rabbit	47	1:1000
HIF1α	Mouse	93	1:500
HIF2α	Rabbit	118	1:500
CA9	Mouse	55	1:2000
CNOT7	Rabbit	34	1:1000
FOSL2	Rabbit	35-55	1:1000
JUNB	Rabbit	35-39	1:1000
JUND	Rabbit	43	1:1000
LDHA	Rabbit	30	1:1000
NOTCH1	Mouse	114	1:500
SF3B4	Goat	93	1:500
KIF5B	Rabbit	110	1:1000
SHMT2	Rabbit	56	1:1000
EDH1	Rabbit	61	1:1000
PLD2	Rabbit	106	1:500
CTH	Rabbit	45	1:1000
Actin	Goat	37	1:2000

IHC Primary Antibodies

Target	Host	Dilution	Secondary	Dilution
eIF4A2	Rabbit	1:500	Swine anti-rabbit HRP	1:400
CA9	Mouse	1:1000	Goat anti-mouse HRP	1:400
IgG	Mouse	1:500	Goat anti-mouse HRP	1:400

siRNA Sequences

Target	Sequence
eIF4A1	GUAAAGGUGUGGCUUAUUA GAACGAGACGUGAUUAUGA CAACGUGCGUGCUGAGGUG GAAGAUGCAUGCUCGAGAU
eIF4A2	CUACCUACCAAUCGUGAAA CUUGUUGGCUCGCGGGAUU CUUUGUGACUUGUACGAGA CCGCGGAUUAUAACAGAGA
PLD2	GGACAACCAAGAAGAAAUA GGACCGGCCUUUCGAAGAU GACCUGCACUACCGACUGA CAGCAUGGCGGGACUAUAU

EHD1	GGAGAGAUCUACCCAGAAGA CAUCAGCUCCCUCAAGAAAA UGGCAACGUUUCCCUCAAC AUAAAGACUGAGCGGAUGU
KIF5B	GCAGUCAGGUCAAAGAAUA GAACUGGCAUGAUAGAUGA CAACAGACAUGUAGCAGUU GCAGGAACGUCUAAGAGUA
Non Targeting Control	UGGUUUUACAUGUCGACUAA UGGUUUACAUGUUGUGUGA UGGUUUACAUGUUUUCUGA UGGUUUACAUGUUUUCCUA

eIF4A2 shRNA sequences

Clone ID	Sequence
TRCN00000518**69** (sh69)	CCGGCCGGGAGAGTGTTTGATATGTTCTCGAGAACATATCCAAACACTCTCCCGTTTTG
TRCN00003694**84** (sh84)	CCGGAGTCGTGTTCTGATCACTACTCTCTCGAGAGTAGTGATCAGAACACGACTTTTTTG

Urea Lysis Buffer (50ml)

Urea (4M): 12g
Glycerol (5%): 2.5mL
Tris (1.0mM, pH 6.8): 333ul
SDS (0.05%): 0.1g
*Supplemented with fresh 1mM DTT, protease and phosphatase inhibitors

10x TBS (1L)

18.16g Tris Base
81.82 NaCl
pH 7.4

10x TGS (1L)

30g Tris
144g Glycine
10g SDS
pH 8.3

Co-IP Lysis Buffer (1L)

2.4 g Tris-HCl pH 7.4 (20 mM)
8.76 g NaCl (150 mM)
2g MgCl2 (10 mM)
0.15g DTT (1 mM)
0.04g NaF (1 mM)
0.76g β-Glycerophosphate (2.5 mM)
4mL EDTA 0.5M (2 mM)

100mL Glycerol (10%)
10 mL IGEPAL (1% NP-40)

Co-IP Wash Buffer

0.1M sodium phosphate
0.01% Tween20
pH 8.2

cDNA Thermal Cycling Conditions

Settings	Step 1	Step 2	Step 3	Step 4
Temperature	25°C	37°C	85°C	4°C
Time	10 minutes	120 minutes	5 minutes	∞

qPCR Thermal Cycling Conditions

Programme	Cycles	Temperature
Pre Incubation	1	95°C
Amplification	40	60°C
Melting Curve	1	95,65,97°C
Cooling	1	40°C

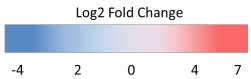
Preliminary Nanopore eIF4A2 RIP-SEQ Screen

AKR1B1	1.00
ALDOA	1.92
ANXA2	1.06
AREG	1.73
ATP5MC1	-1.24
ATP5MC3	-1.35
ATXN3	3.06
BNIP3	2.61
BNIP3L	2.31
BUD23	-1.80
CALB1	4.48
CBX3	-1.50
CD58	2.00
CDA	4.58
CHCHD2	-1.08
CKS2	-0.99
COX5A	0.95
COX5B	-0.61
COX6B1	-0.61
COX7B	-0.73
CSTB	1.69
DANCR	-1.37
DBI	-0.80
ECHS1	-0.74
ESRG	2.54
FABP1	2.28
FXYD3	2.69

G0S2	2.20
GDF15	3.01
GUK1	1.10
H1F0	1.42
H3F3A	-1.00
HIST1H4C	-1.69
HMGN2	-1.34
ID3	-2.41
IFITM3	-1.42
IGFL2	2.09
ISG20	2.34
KCNK1	2.25
KLF6	2.50
KRT19	1.85
LCN2	2.04
LDHA	1.87
LDHB	-1.21
LRRK1	2.35
LSM6	-4.01
MALAT1	3.03
MALL	2.14
MIR210HG	3.57
MRPL13	-2.27
MRPL24	-2.43
MT1E	-0.69
MTRNR2L12	2.03
MTRNR2L8	1.15
MYH9	2.96

NDUFA1	-1.01
NDUFA4	-1.41
NDUFAB1	-1.22
NDUFAF4	-1.70
NDUFB3	-1.27
NDUFB6	-1.59
NOP10	-0.83
NUPR1	1.36
PCBD1	-1.13
PDE4C	1.23
PEBP1	-0.97
PERP	2.02
PGK1	1.02
PHD3	5.44
POLR2L	-1.02
PPIA	-0.79
PRDX3	-1.29
PRR15L	2.27
PRSS23	2.35
PSMA4	-1.96
PSMB2	-1.33
PTPN12	5.29
RAN	-1.26
RBCK1	1.77
REG1A	-2.53
RPL38	-0.81
RPL41	-0.43
RPS12	0.62

RPS2	1.91
S100A10	2.17
S100A11	1.01
S100A16	1.06
S100A6	1.13
S100P	2.00
SERINC2	1.67
SERPINB1	1.45
SF3B5	-2.67
SLC6A8	3.43
SNHG9	-1.10
SNRPD1	-1.27
SNRPD3	-1.35
SNRPF	-1.34
SNRPG	-0.83
SNU13	-1.11
SOD1	-1.09
SRSF3	-1.71
STOML2	-1.39
SUCLG1	-1.49
TFF1	4.88
TFF2	6.10
TFF3	3.70
TMSB4X	1.15
TOMM7	-0.54
TSC22D1	0.84
TUFM	-0.94
TXNIP	2.39
UBE2C	-1.92
UQCRC2	-2.21



eIF4A2 bound enriched transcripts under hypoxic conditions. LS174T cells were exposed to 48 hours 1% 0_2 followed by RNA immunoprecipitation of eIF4A2. Sequencing of transcripts was performed using the Oxford Nanopore MinION. Heat map displays change in transcript abundance in hypoxic RIP fractions compared to normoxic RIP fractions. n=3.

8.0 Bibliography

A Pilot Study of EZN-2968, an Antisense Oligonucleotide Inhibitor of HIF-1alpha, in Adults With Advanced Solid Tumors With Liver Metastases - Full Text View - ClinicalTrials.gov [WWW Document], 2019. . Clinical Trials.gov. URL https://clinicaltrials.gov/ct2/show/NCT01120288 (accessed 12.17.19).

A Study of Hypoxia-inducible Factor 1a (HIF1A) Messenger Ribonucleic Acid (mRNA) Antagonist (RO7070179), to Demonstrate Proof-of-mechanism in Adult Participants With Hepatocellular Carcinoma (HCC) - Full Text View - ClinicalTrials.gov [WWW Document], 2019. . Clinical Trials.gov. URL https://clinicaltrials.gov/ct2/show/NCT02564614 (accessed 12.17.19).

Aguilera, K.Y., Brekken, R.A., 2014. Hypoxia Studies with Pimonidazole in vivo. Bio Protoc 4. Alain, T., Morita, M., Fonseca, B.D., Yanagiya, A., Siddiqui, N., Bhat, M., Zammit, D., Marcus, V., Metrakos, P., Voyer, L.-A., Gandin, V., Liu, Y., Topisirovic, I., Sonenberg, N., 2012. eIF4E/4E-BP ratio predicts the efficacy of mTOR targeted therapies. Cancer Res. 72, 6468–6476.

Andreou, A.Z., Klostermeier, D., 2013. The DEAD-box helicase eIF4A. RNA Biol 10, 19–32.

Aoki, K., Taketo, M.M., 2007. Adenomatous polyposis coli (APC): a multi-functional tumor suppressor gene. Journal of Cell Science 120, 3327–3335.

Armaghany, T., Wilson, J.D., Chu, Q., Mills, G., 2012. Genetic Alterations in Colorectal Cancer. Gastrointest Cancer Res 5, 19–27.

Bailey, S.D., Zhang, X., Desai, K., Aid, M., Corradin, O., Cowper-Sal·lari, R., Akhtar-Zaidi, B., Scacheri, P.C., Haibe-Kains, B., Lupien, M., 2015. ZNF143 provides sequence specificity to secure chromatin interactions at gene promoters. Nature Communications 6, 1–10.

Barbosa, C., Peixeiro, I., Romao, L., 2013. Gene expression regulation by upstream open reading frames and human disease. - PubMed - NCBI. PLoS Genetics 9.

Bárdos, J.I., Ashcroft, M., 2005. Negative and positive regulation of HIF-1: a complex network. Biochim. Biophys. Acta 1755, 107–120.

Barker, N., van de Wetering, M., Clevers, H., 2008. The intestinal stem cell. Genes Dev 22, 1856–1864.

Barrett, L.W., Fletcher, S., Wilton, S.D., 2012. Regulation of eukaryotic gene expression by the untranslated gene regions and other non-coding elements. Cell Mol Life Sci 69, 3613–3634.

Benjamin, D., Colombi, M., Moroni, C., Hall, M.N., 2011. Rapamycin passes the torch: a new generation of mTOR inhibitors. Nat Rev Drug Discov 10, 868–880.

Beppu, K., Nakamura, K., Linehan, W.M., Rapisarda, A., Thiele, C.J., 2005. Topotecan blocks hypoxia-inducible factor-1alpha and vascular endothelial growth factor expression induced by insulin-like growth factor-I in neuroblastoma cells. Cancer Res. 65, 4775–4781.

Bhat, M., Robichaud, N., Hulea, L., Sonenberg, N., Pelletier, J., Topisirovic, I., 2015. Targeting the translation machinery in cancer. Nat Rev Drug Discov 14, 261–278.

Bloomfield, G., Kay, R.R., 2016. Uses and abuses of macropinocytosis. J Cell Sci 129, 2697–2705.

Bohn, J.A., Van Etten, J.L., Schagat, T.L., Bowman, B.M., McEachin, R.C., Freddolino, P.L., Goldstrohm, A.C., 2018. Identification of diverse target RNAs that are functionally regulated by human Pumilio proteins. Nucleic Acids Research 46, 362–386.

Bordeleau, M.-E., Robert, F., Gerard, B., Lindqvist, L., Chen, S.M.H., Wendel, H.-G., Brem, B., Greger, H., Lowe, S.W., Porco, J.A., Pelletier, J., 2008. Therapeutic suppression of translation initiation modulates chemosensitivity in a mouse lymphoma model. J. Clin. Invest. 118, 2651–2660. https://doi.org/10.1172/JCI34753

Botlagunta, M., Krishnamachary, B., Vesuna, F., Winnard, P.T., Bol, G.M., Patel, A.H., Raman, V., 2011. Expression of DDX3 Is Directly Modulated by Hypoxia Inducible Factor-1 Alpha in Breast Epithelial Cells. PLoS One 6.

Bray, F., Ferlay, J., Soerjomataram, I., Siegel, R.L., Torre, L.A., Jemal, A., 2018. Global cancer statistics 2018: GLOBOCAN estimates of incidence and mortality worldwide for 36 cancers in 185 countries. CA: A Cancer Journal for Clinicians 68, 394–424.

Brown, J.M., 2007. Tumor hypoxia in cancer therapy. Meth. Enzymol. 435, 297–321.

Brugarolas, J., Lei, K., Hurley, R.L., Manning, B.D., Reiling, J.H., Hafen, E., Witters, L.A., Ellisen, L.W., Kaelin, W.G., 2004. Regulation of mTOR function in response to hypoxia by REDD1 and the TSC1/TSC2 tumor suppressor complex. Genes Dev. 18, 2893–2904.

Cadigan, K.M., Waterman, M.L., 2012. TCF/LEFs and Wnt Signaling in the Nucleus. Cold Spring Harb Perspect Biol 4.

Carreau, A., Hafny-Rahbi, B., Matejuk, A., Grillon, C., Kieda, C., n.d. Why is the partial oxygen pressure of human tissues a crucial parameter? Small molecules and hypoxia. Journal of Cellular and Molecular Medicine 15, 1239–1253.

Cencic, R., Carrier, M., Galicia-Vázquez, G., Bordeleau, M.-E., Sukarieh, R., Bourdeau, A., Brem, B., Teodoro, J.G., Greger, H., Tremblay, M.L., Porco, J.A., Pelletier, J., 2009. Antitumor activity and mechanism of action of the cyclopenta[b]benzofuran, silvestrol. PLoS ONE 4, e5223.

Cencic, R., Pelletier, J., 2016. Hippuristanol - A potent steroid inhibitor of eukaryotic initiation factor 4A. Translation (Austin) 4, e1137381.

Chee, N.T., Lohse, I., Brothers, S.P., 2019. mRNA-to-protein translation in hypoxia. Molecular Cancer 18, 49.

Chen, J., Ding, Z., Peng, Y., Pan, F., Li, J., Zou, L., Zhang, Y., Liang, H., 2014. HIF-1α Inhibition Reverses Multidrug Resistance in Colon Cancer Cells via Downregulation of MDR1/P-Glycoprotein. PLOS ONE 9, e98882.

Chen, T.-M., Lai, M.-C., Li, Y.-H., Chan, Y.-L., Wu, C.-H., Wang, Y.-M., Chien, C.-W., Huang, S.-Y., Sun, H.S., Tsai, S.-J., 2019. hnRNPM induces translation switch under hypoxia to promote colon cancer development. EBioMedicine 41, 299–309.

Chen, Z.-H., Qi, J.-J., Wu, Q.-N., Lu, J.-H., Liu, Z.-X., Wang, Y., Hu, P.-S., Li, T., Lin, J.-F., Wu, X.-Y., Miao, L., Zeng, Z.-L., Xie, D., Ju, H.-Q., Xu, R.-H., Wang, F., 2019. Eukaryotic initiation factor 4A2 promotes experimental metastasis and oxaliplatin resistance in colorectal cancer. Journal of Experimental & Clinical Cancer Research 38, 196.

Choudhry, H., Harris, A.L., 2018. Advances in Hypoxia-Inducible Factor Biology. Cell Metab. 27, 281–298.

Cintas, C., Guillermet-Guibert, J., 2018. Heterogeneity of Phosphatidylinositol-3-Kinase (PI3K)/AKT/Mammalian Target of Rapamycin Activation in Cancer: Is PI3K Isoform Specificity Important? Front Oncol 7.

Comerford, K.M., Wallace, T.J., Karhausen, J., Louis, N.A., Montalto, M.C., Colgan, S.P., 2002. Hypoxia-inducible factor-1-dependent regulation of the multidrug resistance (MDR1) gene. Cancer Res. 62, 3387–3394.

Copeland, N.G., Jenkins, N.A., 2009. Deciphering the genetic landscape of cancer – from genes to pathways. Trends in Genetics 25, 455–462.

Cummins, E.P., Taylor, C.T., 2005. Hypoxia-responsive transcription factors. Pflugers Arch. 450, 363–371.

Day, D.W., 1984. The adenoma-carcinoma sequence. Scand. J. Gastroenterol. Suppl. 104, 99–107.

de Vries, S., Naarmann-de Vries, I.S., Urlaub, H., Lue, H., Bernhagen, J., Ostareck, D.H., Ostareck-Lederer, A., 2013. Identification of DEAD-box RNA helicase 6 (DDX6) as a cellular modulator of vascular endothelial growth factor expression under hypoxia. J. Biol. Chem. 288, 5815–5827.

Decker, C.J., Parker, R., 2012. P-bodies and stress granules: possible roles in the control of translation and mRNA degradation. Cold Spring Harb Perspect Biol 4, a012286.

Dengler, V.L., Galbraith, M., Espinosa, J.M., 2014. Transcriptional Regulation by Hypoxia Inducible Factors. Crit Rev Biochem Mol Biol 49, 1–15.

Dever, T.E., Green, R., 2012. The Elongation, Termination, and Recycling Phases of Translation in Eukaryotes. Cold Spring Harb Perspect Biol 4.

DeYoung, M.P., Horak, P., Sofer, A., Sgroi, D., Ellisen, L.W., 2008. Hypoxia regulates TSC1/2-mTOR signaling and tumor suppression through REDD1-mediated 14-3-3 shuttling. Genes Dev. 22, 239–251.

Dolfi, S.C., Chan, L.L.-Y., Qiu, J., Tedeschi, P.M., Bertino, J.R., Hirshfield, K.M., Oltvai, Z.N., Vazquez, A., 2013. The metabolic demands of cancer cells are coupled to their size and protein synthesis rates. Cancer Metab 1, 20.

Elvert, G., Kappel, A., Heidenreich, R., Englmeier, U., Lanz, S., Acker, T., Rauter, M., Plate, K., Sieweke, M., Breier, G., Flamme, I., 2003. Cooperative Interaction of Hypoxia-inducible Factor-2α (HIF-2α) and Ets-1 in the Transcriptional Activation of Vascular Endothelial Growth Factor Receptor-2 (Flk-1). J. Biol. Chem. 278, 7520–7530.

Evagelou, S.L., Bebenek, O., Specker, E.J., Uniacke, J., 2019. DEAD-box protein family member DDX28 is a negative regulator of HIF-2α and eIF4E2-directed hypoxic translation. bioRxiv 632331.

Favaro, E., 2013. Cancer Metabolic Pathways Regulated by Hypoxia. (PhD Thesis). Oxford.
Fay, M.M., Lyons, S.M., Ivanov, P., 2017. RNA G-Quadruplexes in Biology: Principles and Molecular Mechanisms. Journal of Molecular Biology 429, 2127–2147.

Fearnhead, N.S., Wilding, J.L., Bodmer, W.F., 2002. Genetics of colorectal cancer: hereditary aspects and overview of colorectal tumorigenesis. Br Med Bull 64, 27–43.

Ferlay, J., Soerjomataram, I., Dikshit, R., Eser, S., Mathers, C., Rebelo, M., Parkin, D.M., Forman, D., Bray, F., 2015. Cancer incidence and mortality worldwide: Sources, methods and major patterns in GLOBOCAN 2012. International Journal of Cancer 136, E359–E386.

Flamant, L., Notte, A., Ninane, N., Raes, M., Michiels, C., 2010. Anti-apoptotic role of HIF-1 and AP-1 in paclitaxel exposed breast cancer cells under hypoxia. Molecular Cancer 9, 191.

Fleming, M., Ravula, S., Tatishchev, S.F., Wang, H.L., 2012. Colorectal carcinoma: Pathologic aspects. J Gastrointest Oncol 3, 153–173.

Fruman, D.A., Rommel, C., 2014. PI3K and cancer: lessons, challenges and opportunities. Nat Rev Drug Discov 13, 140–156.

Fulda, S., Gorman, A.M., Hori, O., Samali, A., 2010. Cellular Stress Responses: Cell Survival and Cell Death. International Journal of Cell Biology 2010.

Galicia-Vázquez, G., Cencic, R., Robert, F., Agenor, A.Q., Pelletier, J., 2012. A cellular response linking eIF4AI activity to eIF4AII transcription. RNA 18, 1373–1384.

Gilks, N., Kedersha, N., Ayodele, M., Shen, L., Stoecklin, G., Dember, L.M., Anderson, P., 2004. Stress granule assembly is mediated by prion-like aggregation of TIA-1. Mol. Biol. Cell 15, 5383–5398.

Gilman, B., Tijerina, P., Russell, R., 2017. Distinct RNA-unwinding mechanisms of DEAD-box and DEAH-box RNA helicase proteins in remodeling structured RNAs and RNPs. Biochem. Soc. Trans. 45, 1313–1321.

Graff, J.R., Konicek, B.W., Vincent, T.M., Lynch, R.L., Monteith, D., Weir, S.N., Schwier, P., Capen, A., Goode, R.L., Dowless, M.S., Chen, Y., Zhang, H., Sissons, S., Cox, K., McNulty, A.M., Parsons, S.H., Wang, T., Sams, L., Geeganage, S., Douglass, L.E., Neubauer, B.L., Dean, N.M., Blanchard, K., Shou, J., Stancato, L.F., Carter, J.H., Marcusson, E.G., 2007. Therapeutic suppression of translation initiation factor eIF4E expression reduces tumor growth without toxicity. J. Clin. Invest. 117, 2638–2648.

Gray, L.H., Conger, A.D., Ebert, M., Hornsey, S., Scott, O.C., 1953. The concentration of oxygen dissolved in tissues at the time of irradiation as a factor in radiotherapy. Br J Radiol 26, 638–648.

Greenberger, L.M., Horak, I.D., Filpula, D., Sapra, P., Westergaard, M., Frydenlund, H.F., Albaek, C., Schrøder, H., Ørum, H., 2008. A RNA antagonist of hypoxia-inducible factor-1alpha, EZN-2968, inhibits tumor cell growth. Mol. Cancer Ther. 7, 3598–3608.

Guertin, D.A., Sabatini, D.M., 2007. Defining the role of mTOR in cancer. Cancer Cell 12, 9–22.

Gupta, S.V., Sass, E.J., Davis, M.E., Edwards, R.B., Lozanski, G., Heerema, N.A., Lehman, A., Zhang, X., Jarjoura, D., Byrd, J.C., Pan, L., Chan, K.K., Kinghorn, A.D., Phelps, M.A., Grever, M.R., Lucas, D.M., 2011. Resistance to the translation initiation inhibitor silvestrol is mediated by ABCB1/P-glycoprotein overexpression in acute lymphoblastic leukemia cells. AAPS J 13, 357–364.

Hallac, R., Zhou, H., Pidikiiti, R., Song, K., Stojadinovic, S., Zhao, D., Solbery, T., Mason, R., n.d. Correlations of noninvasive BOLD and TOLD MRI with pO2 and relevance to tumor radiation response. Magnetic Resonance in Medicine 71, 1863–1873.

Hammond, E.M., Asselin, M.-C., Forster, D., O'Connor, J.P.B., Senra, J.M., Williams, K.J., 2014. The Meaning, Measurement and Modification of Hypoxia in the Laboratory and the Clinic. Clinical Oncology, Advances in Clinical Radiobiology (Part 2) 26, 277–288.

Hanahan, D., Weinberg, R.A., 2011. Hallmarks of Cancer: The Next Generation. Cell 144, 646–674.

Hara, S., Hamada, J., Kobayashi, C., Kondo, Y., Imura, N., 2001. Expression and characterization of hypoxia-inducible factor (HIF)-3alpha in human kidney: suppression of HIF-mediated gene expression by HIF-3alpha. Biochem. Biophys. Res. Commun. 287, 808–813.

Hardt, M., Chantaravisoot, N., Tamanoi, F., 2011. Activating mutations of TOR (target of rapamycin). Genes Cells 16, 141–151.

Harrington, L.S., Findlay, G.M., Lamb, R.F., 2005. Restraining PI3K: mTOR signalling goes back to the membrane. Trends Biochem. Sci. 30, 35–42.

Harris, B.H.L., Barberis, A., West, C.M.L., Buffa, F.M., 2015. Gene Expression Signatures as Biomarkers of Tumour Hypoxia. Clinical Oncology, Biomarkers and Imaging for Precision Radiotherapy 27, 547–560.

Heinimann, K., Müllhaupt, B., Weber, W., Attenhofer, M., Scott, R.J., Fried, M., Martinoli, S., Müller, H., Dobbie, Z., 1998. Phenotypic differences in familial adenomatous polyposis based on APC gene mutation status. Gut 43, 675–679.

Hellen, C.U.T., 2018. Translation Termination and Ribosome Recycling in Eukaryotes. Cold Spring Harb Perspect Biol 10.

Hentze, M.W., Castello, A., Schwarzl, T., Preiss, T., 2018. A brave new world of RNA-binding proteins. Nat. Rev. Mol. Cell Biol. 19, 327–341.

Hershey, J.W.B., Sonenberg, N., Mathews, M.B., 2012. Principles of Translational Control: An Overview. Cold Spring Harb Perspect Biol 4.

Heyer, E.E., Moore, M.J., 2016. Redefining the Translational Status of 80S Monosomes. Cell 164, 757–769.

Hilbert, M., Kebbel, F., Gubaev, A., Klostermeier, D., 2011. eIF4G stimulates the activity of the DEAD box protein eIF4A by a conformational guidance mechanism. Nucleic Acids Res. 39, 2260–2270.

Hinnebusch, A.G., 2011a. Molecular mechanism of scanning and start codon selection in eukaryotes. Microbiol. Mol. Biol. Rev. 75, 434–467, first page of table of contents.

Hinnebusch, A.G., 2011b. Molecular mechanism of scanning and start codon selection in eukaryotes. Microbiol. Mol. Biol. Rev. 75, 434–467, first page of table of contents.

Hinnebusch, A.G., Ivanov, I.P., Sonenberg, N., 2016. Translational control by 5’-untranslated regions of eukaryotic mRNAs. Science 352, 1413–1416.

Hirokawa, G., Kaji, H., Kaji, A., 2007. Inhibition of Antiassociation Activity of Translation Initiation Factor 3 by Paromomycin. Antimicrob Agents Chemother 51, 175–180.

Ho, J.J.D., Wang, M., Audas, T.E., Kwon, D., Carlsson, S.K., Timpano, S., Evagelou, S.L., Brothers, S., Gonzalgo, M.L., Krieger, J.R., Chen, S., Uniacke, J., Lee, S., 2016. Systemic Reprogramming of Translation Efficiencies on Oxygen Stimulus. Cell Reports 14, 1293–1300.

Holcik, M., Sonenberg, N., 2005. Translational control in stress and apoptosis. Nat. Rev. Mol. Cell Biol. 6, 318–327.

Horsman, M.R., Overgaard, J., 2016. The impact of hypoxia and its modification of the outcome of radiotherapy. J Radiat Res 57, i90–i98.

Houlston, R.S., Tomlinson, I.P.M., 2000. Detecting low penetrance genes in cancer: the way ahead. Journal of Medical Genetics 37, 161–167.

Hu, Y.-L., DeLay, M., Jahangiri, A., Molinaro, A.M., Rose, S.D., Carbonell, W.S., Aghi, M.K., 2012. Hypoxia-induced autophagy promotes tumor cell survival and adaptation to anti-angiogenic treatment in glioblastoma. Cancer Res 72, 1773–1783.

Hunter, F.W., Wouters, B.G., Wilson, W.R., 2016. Hypoxia-activated prodrugs: paths forward in the era of personalised medicine. British Journal of Cancer 114, 1071–1077.

Imamura, T., Kikuchi, H., Herraiz, M.-T., Park, D.-Y., Mizukami, Y., Mino-Kenduson, M., Lynch, M.P., Rueda, B.R., Benita, Y., Xavier, R.J., Chung, D.C., 2009. HIF-1alpha and HIF-2alpha have divergent roles in colon cancer. Int. J. Cancer 124, 763–771.
Iommarini, L., Porcelli, A.M., Gasparre, G., Kurelac, I., 2017. Non-Canonical Mechanisms Regulating Hypoxia-Inducible Factor 1 Alpha in Cancer. Front Oncol 7.

Jagannathan, L., Cuddapah, S., Costa, M., 2016. Oxidative stress under ambient and physiological oxygen tension in tissue culture. Curr Pharmacol Rep 2, 64–72.

Jiang, H.-Y., Wek, R.C., 2005. Phosphorylation of the α-Subunit of the Eukaryotic Initiation Factor-2 (eIF2α) Reduces Protein Synthesis and Enhances Apoptosis in Response to Proteasome Inhibition. J. Biol. Chem. 280, 14189–14202.

Jongjitwimol, J., Baldock, R.A., Morley, S.J., Watts, F.Z., 2016. Sumoylation of eIF4A2 affects stress granule formation. J Cell Sci 129, 2407–2415.

Kahvejian, A., Svitkin, Y.V., Sukarieh, R., M'Boutchou, M.-N., Sonenberg, N., 2005. Mammalian poly(A)-binding protein is a eukaryotic translation initiation factor, which acts via multiple mechanisms. Genes Dev 19, 104–113.

Kaluz, S., Kaluzová, M., Liao, S.-Y., Lerman, M., Stanbridge, E.J., 2009. Transcriptional control of the tumor- and hypoxia-marker carbonic anhydrase 9: a one transcription factor (HIF-1) show? Biochim Biophys Acta 1795, 162–172.

Kanehisa, M., Furumichi, M., Tanabe, M., Sato, Y., Morishima, K., 2017. KEGG: new perspectives on genomes, pathways, diseases and drugs. Nucleic Acids Res 45, D353–D361.

Kazazi-Hyseni, F., Beijnen, J.H., Schellens, J.H.M., 2010. Bevacizumab. Oncologist 15, 819–825.

Keith, B., Johnson, R.S., Simon, M.C., 2011. HIF1α and HIF2α: sibling rivalry in hypoxic tumor growth and progression. Nat Rev Cancer 12, 9–22.

Kim, J.-Y., Lee, J.-Y., 2017. Targeting Tumor Adaption to Chronic Hypoxia: Implications for Drug Resistance, and How It Can Be Overcome. Int J Mol Sci 18.

Kobayashi, S., Yamashita, T., Ohneda, K., Nagano, M., Kimura, K., Nakai, H., Poellinger, L., Ohneda, O., 2015. Hypoxia-inducible factor-3α promotes angiogenic activity of pulmonary endothelial cells by repressing the expression of the VE-cadherin gene. Genes to Cells 20, 224–241.

Komar, A.A., Hatzoglou, M., 2011. Cellular IRES-mediated translation. Cell Cycle 10, 229–240.

Koritzinsky, M., Magagnin, M.G., van den Beucken, T., Seigneuric, R., Savelkouls, K., Dostie, J., Pyronnet, S., Kaufman, R.J., Weppler, S.A., Voncken, J.W., Lambin, P., Koumenis, C., Sonenberg, N., Wouters, B.G., 2006. Gene expression during acute and prolonged hypoxia is regulated by distinct mechanisms of translational control. EMBO J. 25, 1114–1125.

Korostelev, A.A., 2011. Structural aspects of translation termination on the ribosome. RNA 17, 1409–1421.

Koumenis, C., Naczki, C., Koritzinsky, M., Rastani, S., Diehl, A., Sonenberg, N., Koromilas, A., Wouters, B.G., 2002. Regulation of protein synthesis by hypoxia via activation of the endoplasmic reticulum kinase PERK and phosphorylation of the translation initiation factor eIF2alpha. Mol. Cell. Biol. 22, 7405–7416.

Kumari, S., Bugaut, A., Huppert, J.L., Balasubramanian, S., 2007. An RNA G-quadruplex in the 5' UTR of the NRAS proto-oncogene modulates translation. Nat. Chem. Biol. 3, 218–221.

Kuznetsov, G., Xu, Q., TenDyke, K., Liu, J., Towle, M., Zhao, N., Marsh, J., Agoulnik, S., Twine, N., Parent, L., Chen, Z., Jiang, Y., Zhang, H., Du, H., Boivin, R., Wang, J. (Yuan), Romo, D., Littlefield, B., 2008. Potent in vitro and in vivo anticancer activities of desmethyl, desamino (DMDA)-pateamine A, an analog of marine natural product pateamine A. Cancer Res 68, 5702–5702.

Kwan, T., Thompson, S.R., 2018. Noncanonical Translation Initiation in Eukaryotes. Cold Spring Harb Perspect Biol a032672.

Lai, M.-C., Chang, C.-M., Sun, H.S., 2016. Hypoxia Induces Autophagy through Translational Up-Regulation of Lysosomal Proteins in Human Colon Cancer Cells. PLoS One 11.

Lang, K.J.D., Kappel, A., Goodall, G.J., 2002. Hypoxia-inducible Factor-1α mRNA Contains an Internal Ribosome Entry Site That Allows Efficient Translation during Normoxia and Hypoxia. Mol Biol Cell 13, 1792–1801.

Laplante, M., Sabatini, D.M., 2009. mTOR signaling at a glance. J. Cell. Sci. 122, 3589–3594.

Lee, A.S., Kranzusch, P.J., Doudna, J.A., Cate, J.H.D., 2016. eIF3d is an mRNA cap-binding protein that is required for specialized translation initiation. Nature 536, 96–99.

Lenz, H.-J., 2007. Cetuximab in the management of colorectal cancer. Biologics 1, 77–91.
Liang, D., Miller, G.H., Tranmer, G.K., 2015. Hypoxia Activated Prodrugs: Factors Influencing Design and Development. Curr. Med. Chem. 22, 4313–4325.

Liang, S., Ju, X., Zhou, Y., Chen, Y., Ke, G., Wen, H., Wu, X., 2017. Downregulation of eukaryotic initiation factor 4A1 improves radiosensitivity by delaying DNA double strand break repair in cervical cancer. Oncology Letters 14, 6976–6982.

Liao, W.-L., Lin, S.-C., Sunny Sun, H., Tsai, S.-J., 2014. Hypoxia-induced tumor malignancy and drug resistance: Role of microRNAs. Biomarkers and Genomic Medicine 6, 1–11.

Lin, C., Miles, W.O., 2019. Beyond CLIP: advances and opportunities to measure RBP–RNA and RNA–RNA interactions. Nucleic Acids Res 47, 5490–5501.

Lin, C.-J., Cencic, R., Mills, J.R., Robert, F., Pelletier, J., 2008. c-Myc and eIF4F are components of a feedforward loop that links transcription and translation. Cancer Res. 68, 5326–5334.

Linder, P., Lasko, P., 2006. Bent out of shape: RNA unwinding by the DEAD-box helicase Vasa. Cell 125, 219–221.

Lindqvist, L., Oberer, M., Reibarkh, M., Cencic, R., Bordeleau, M.-E., Vogt, E., Marintchev, A., Tanaka, J., Fagotto, F., Altmann, M., Wagner, G., Pelletier, J., 2008. Selective Pharmacological Targeting of a DEAD Box RNA Helicase. PLOS ONE 3, e1583.

Livek, K.J., Schmittgen, T.D. 2001. Analysis of relative gene expression data using real time quantitative PCR and the 2-ΔΔ Ct method. Methods. 25,5. 402-408.

Loboda, A., Jozkowicz, A., Dulak, J., 2010. HIF-1 and HIF-2 transcription factors--similar but not identical. Mol. Cells 29, 435–442.

Long, X., Lin, Y., Ortiz-Vega, S., Yonezawa, K., Avruch, J., 2005. Rheb binds and regulates the mTOR kinase. Curr. Biol. 15, 702–713.

Longley, D., Harkin, P., Johnston, P., 2013. 5-Fluorouracil: mechanisms of action and clinical strategies | Nature Reviews Cancer. Nature Reviews Cancer 3, 330–338.

Low, W.-K., Li, J., Zhu, M., Kommaraju, S.S., Shah-Mittal, J., Hull, K., Liu, J.O., Romo, D., 2014. Second-generation derivatives of the eukaryotic translation initiation inhibitor pateamine A targeting eIF4A as potential anticancer agents. Bioorg Med Chem 22, 116–125.

Luoto, K.R., Kumareswaran, R., Bristow, R.G., 2013. Tumor hypoxia as a driving force in genetic instability. Genome Integr 4, 5.

Magnuson, B., Ekim, B., Fingar, D.C., 2012. Regulation and function of ribosomal protein S6 kinase (S6K) within mTOR signalling networks. Biochem. J. 441, 1–21.

Mah, A.T., Yan, K.S., Kuo, C.J., 2016. Wnt pathway regulation of intestinal stem cells. The Journal of Physiology 594, 4837–4847.

Mahboubi, H., Stochaj, U., 2017. Cytoplasmic stress granules: Dynamic modulators of cell signaling and disease. Biochimica et Biophysica Acta (BBA) - Molecular Basis of Disease 1863, 884–895.

Majmundar, A.J., Wong, W.J., Simon, M.C., 2010. Hypoxia-inducible factors and the response to hypoxic stress. Mol. Cell 40, 294–309.

Marchetti, C., Zyner, K.G., Ohnmacht, S.A., Robson, M., Haider, S.M., Morton, J.P., Marsico, G., Vo, T., Laughlin-Toth, S., Ahmed, A.A., Di Vita, G., Pazitna, I., Gunaratnam, M., Besser, R.J., Andrade, A.C.G., Diocou, S., Pike, J.A., Tannahill, D., Pedley, R.B., Evans, T.R.J., Wilson, W.D., Balasubramanian, S., Neidle, S., 2018. Targeting Multiple Effector Pathways in Pancreatic Ductal Adenocarcinoma with a G-Quadruplex-Binding Small Molecule. J. Med. Chem. 61, 2500–2517.

Martineau, Y., Müller, D., Pyronnet, S., 2014. Targeting protein synthesis in cancer cells. Oncoscience 1, 484–485.

Masoud, G.N., Li, W., 2015. HIF-1α pathway: role, regulation and intervention for cancer therapy. Acta Pharm Sin B 5, 378–389.

Mathews, D.H., Turner, D.H., 2006. Prediction of RNA secondary structure by free energy minimization. Current Opinion in Structural Biology, Nucleic acids/Sequences and topology 16, 270–278.

McKenna, D., Errington, R., Pors, K., n.d. Current challenges and opportunities in treating hypoxic prostate tumors. Journal of Cancer Metastasis and Treatment 4.

McKeown, S.R., 2014. Defining normoxia, physoxia and hypoxia in tumours—implications for treatment response. Br J Radiol 87.

Meijer, H.A., Kong, Y.W., Lu, W.T., Wilczynska, A., Spriggs, R.V., Robinson, S.W., Godfrey, J.D., Willis, A.E., Bushell, M., 2013. Translational repression and eIF4A2 activity are critical for microRNA-mediated gene regulation. Science 340, 82–85.

Meijer, H.A., Schmidt, T., Gillen, S.L., Langlais, C., Jukes-Jones, R., de Moor, C.H., Cain, K., Wilczynska, A., Bushell, M., 2019. DEAD-box helicase eIF4A2 inhibits CNOT7 deadenylation activity. Nucleic Acids Res. 47, 8224–8238.

Merrick, W.C., 2004. Cap-dependent and cap-independent translation in eukaryotic systems. Gene 332, 1–11.

Meyuhas, O., Kahan, T., 2015. The race to decipher the top secrets of TOP mRNAs. Biochim. Biophys. Acta 1849, 801–811.

Mistry, I.N., Thomas, M., Calder, E.D.D., Conway, S.J., Hammond, E.M., 2017. Clinical Advances of Hypoxia-Activated Prodrugs in Combination With Radiation Therapy. Int. J. Radiat. Oncol. Biol. Phys. 98, 1183–1196.

Mitchell, S.F., Parker, R., 2014. Principles and Properties of Eukaryotic mRNPs. Molecular Cell 54, 547–558.

Modelska, A., Turro, E., Russell, R., Beaton, J., Sbarrato, T., Spriggs, K., Miller, J., Gräf, S., Provenzano, E., Blows, F., Pharoah, P., Caldas, C., Le Quesne, J., 2015. The malignant phenotype in breast cancer is driven by eIF4A1-mediated changes in the translational landscape. Cell Death Dis 6, e1603.

Mojarad, E.N., Kuppen, P.J., Aghdaei, H.A., Zali, M.R., 2013. The CpG island methylator phenotype (CIMP) in colorectal cancer. Gastroenterol Hepatol Bed Bench 6, 120–128.

Mori, Y., Nagse, H., Ando, H., Horii, A., Ichii, S., Nakatsuru, S., Aoki, T., Miki, Y., Mori, T., Nakamura, Y., 1992. Somatic mutations of the APC gene in colorectal tumors: mutation cluster region in the APC gene. Hum Mol Genet 1, 229–233.

Nguyen, H.T., Duong, H.-Q., 2018. The molecular characteristics of colorectal cancer: Implications for diagnosis and therapy. Oncol Lett 16, 9–18.

NICE, 2019. 1 Recommendations | Colorectal cancer: diagnosis and management | Guidance | NICE [WWW Document]. URL https://www.nice.org.uk/guidance/cg131/chapter/1-Recommendations#management-of-metastatic-disease (accessed 12.17.19).

Nojadeh, J.N., Behrouz Sharif, S., Sakhinia, E., 2018. Microsatellite instability in colorectal cancer. EXCLI J 17, 159–168.

Noll, H., 2008. The discovery of polyribosomes. BioEssays 30, 1220–1234.

Novac, O., 2004. Inhibitors of protein synthesis identified by a high throughput multiplexed translation screen. Nucleic Acids Research 32, 902–915.

Oberer, M., Marintchev, A., Wagner, G., 2005. Structural basis for the enhancement of eIF4A helicase activity by eIF4G. Genes Dev. 19, 2212–2223.

O'Connor, J.P.B., Robinson, S.P., Waterton, J.C., 2019. Imaging tumour hypoxia with oxygen-enhanced MRI and BOLD MRI. Br J Radiol 92, 20180642.

Pakos-Zebrucka, K., Koryga, I., Mnich, K., Ljujic, M., Samali, A., Gorman, A.M., 2016. The integrated stress response. EMBO Rep 17, 1374–1395.

Pal, I., Safari, M., Jovanovic, M., Bates, S.E., Deng, C., 2019. Targeting Translation of mRNA as a Therapeutic Strategy in Cancer. Curr Hematol Malig Rep 14, 219–227.

Pan, L., Woodard, J.L., Lucas, D.M., Fuchs, J.R., Kinghorn, A.D., 2014. Rocaglamide, Silvestrol and Structurally Related Bioactive Compounds from Aglaia Species. Nat Prod Rep 31, 924–939.

Papadopoulos, K., Jonasch, E., Zojwalla, N., Wang, K., Bauer, T., 2018. A first-in-human phase 1 dose-escalation trial of the oral HIF-2a inhibitor PT2977 in patients with advanced solid tumors. | Journal of Clinical Oncology, in: Journal of Clinical Oncology. Presented at the Developmental Theraputics - Clinical Pharmacology and Experimental Theraputics.

Patterson, A.V., Silva, S., Guise, C., Bull, M., Abbattista, M., Hsu, A., Sun, J.D., Hart, C.P., Pearce, T.E., Smaill, J.B., 2015. TH-4000, a hypoxia-activated EGFR/Her2 inhibitor to treat EGFR-TKI resistant T790M-negative NSCLC. JCO 33, e13548–e13548.

Pawlus, M.R., Wang, L., Hu, C.-J., 2014. STAT3 and HIF1α cooperatively activate HIF1 target genes in MDA-MB-231 and RCC4 cells. Oncogene 33, 1670–1679.

Pelletier, J., Graff, J., Ruggero, D., Sonenberg, N., 2015. TARGETING THE eIF4F TRANSLATION INITIATION COMPLEX: A CRITICAL NEXUS FOR CANCER DEVELOPMENT. Cancer Res 75, 250–263.

Pestova, T.V., Kolupaeva, V.G., Lomakin, I.B., Pilipenko, E.V., Shatsky, I.N., Agol, V.I., Hellen, C.U., 2001. Molecular mechanisms of translation initiation in eukaryotes. Proc. Natl. Acad. Sci. U.S.A. 98, 7029–7036.

Peterson, L.W., Artis, D., 2014. Intestinal epithelial cells: regulators of barrier function and immune homeostasis. Nature Reviews Immunology 14, 141–153.

Peterson, T.R., Laplante, M., Thoreen, C.C., Sancak, Y., Kang, S.A., Kuehl, W.M., Gray, N.S., Sabatini, D.M., 2009. DEPTOR is an mTOR inhibitor frequently overexpressed in multiple myeloma cells and required for their survival. Cell 137, 873–886.

Pinkstaff, J.K., Chappell, S.A., Mauro, V.P., Edelman, G.M., Krushel, L.A., 2001. Internal initiation of translation of five dendritically localized neuronal mRNAs. PNAS 98, 2770–2775.

Pooggin, M.M., Ryabova, L.A., 2018. Ribosome Shunting, Polycistronic Translation, and Evasion of Antiviral Defenses in Plant Pararetroviruses and Beyond. Front. Microbiol. 9.
Porru, M., Pompili, L., Caruso, C., Biroccio, A., Leonetti, C., 2018. Targeting KRAS in metastatic colorectal cancer: current strategies and emerging opportunities. J Exp Clin Cancer Res 37.

Powell, S.M., Zilz, N., Beazer-Barclay, Y., Bryan, T.M., Hamilton, S.R., Thibodeau, S.N., Vogelstein, B., Kinzler, K.W., 1992. APC mutations occur early during colorectal tumorigenesis. Nature 359, 235–237.

Price, J.M., Robinson, S.P., Koh, D.M., 2013. Imaging hypoxia in tumours with advanced MRI. Q J Nucl Med Mol Imaging 57, 257–270.

Pringle, E.S., McCormick, C., Cheng, Z., 2019. Polysome Profiling Analysis of mRNA and Associated Proteins Engaged in Translation. Current Protocols in Molecular Biology 125, e79.

Rajesh, K., Krishnamoorthy, J., Kazimierczak, U., Tenkerian, C., Papadakis, A.I., Wang, S., Huang, S., Koromilas, A.E., 2015. Phosphorylation of the translation initiation factor eIF2 α at serine 51 determines the cell fate decisions of Akt in response to oxidative stress. Cell Death & Disease 6, e1591–e1591.

Ramanathan, A., Robb, G.B., Chan, S.-H., 2016. mRNA capping: biological functions and applications. Nucleic Acids Res. 44, 7511–7526.

Ramanathan, M., Porter, D.F., Khavari, P.A., 2019. Methods to study RNA-protein interactions. Nat. Methods 16, 225–234.

Ratcliffe, P.J., 2007. HIF-1 and HIF-2: working alone or together in hypoxia? J. Clin. Invest. 117, 862–865.

Ravenna, L., Salvatori, L., Russo, M.A., 2016. HIF3α: the little we know. The FEBS Journal 283, 993–1003.

Raza, F., Waldron, J.A., Quesne, J.L., 2015. Translational dysregulation in cancer: eIF4A isoforms and sequence determinants of eIF4A dependence. Biochem. Soc. Trans. 43, 1227–1233.

Rogers, D.W., Böttcher, M.A., Traulsen, A., Greig, D., 2017. Ribosome reinitiation can explain length-dependent translation of messenger RNA. PLoS Comput Biol 13.

Rogers, G.W., Richter, N.J., Merrick, W.C., 1999. Biochemical and kinetic characterization of the RNA helicase activity of eukaryotic initiation factor 4A. J. Biol. Chem. 274, 12236–12244.

Rohwer, N., Cramer, T., 2011. Hypoxia-mediated drug resistance: novel insights on the functional interaction of HIFs and cell death pathways. Drug Resist. Updat. 14, 191–201.

Rubio, C.A., Weisburd, B., Holderfield, M., Arias, C., Fang, E., DeRisi, J.L., Fanidi, A., 2014. Transcriptome-wide characterization of the eIF4A signature highlights plasticity in translation regulation. Genome Biol. 15, 476.

Sasikumar, A., Perez, W., Kinzy, T., 2012. The many roles of the eukaryotic elongation factor 1 complex. WIREs RNA 3, 543–555.

Schödel, J., Oikonomopoulos, S., Ragoussis, J., Pugh, C.W., Ratcliffe, P.J., Mole, D.R., 2011. High-resolution genome-wide mapping of HIF-binding sites by ChIP-seq. Blood 117, e207-217.

Schönenberger, M.J., Kovacs, W.J., 2015. Hypoxia signaling pathways: modulators of oxygen-related organelles. Front Cell Dev Biol 3.

Sedlakova, O., Svastova, E., Takacova, M., Kopacek, J., Pastorek, J., Pastorekova, S., 2014. Carbonic anhydrase IX, a hypoxia-induced catalytic component of the pH regulating machinery in tumors. Front Physiol 4.

Semenza, G.L., 2003. Targeting HIF-1 for cancer therapy. Nature Reviews Cancer 3, 721–732.

Sena, J.A., Wang, L., Heasley, L.E., Hu, C.-J., 2014. Hypoxia Regulates Alternative Splicing of HIF and non-HIF Target Genes. Mol Cancer Res 12, 1233–1243.

Shaoyan, X., Juanjuan, Y., Yalan, T., Ping, H., Jianzhong, L., Qinian, W., 2013. Downregulation of EIF4A2 in non-small-cell lung cancer associates with poor prognosis. Clin Lung Cancer 14, 658–665.

Sharma, D.K., Bressler, K., Patel, H., Balasingam, N., Thakor, N., 2016. Role of Eukaryotic Initiation Factors during Cellular Stress and Cancer Progression. Journal of Nucleic Acids. h

Shiokawa, D., Okamoto, K., 2017. Heterogeneity among Lgr5-positive colon stem cells. Mol Cell Oncol 4.

Showkat, M., Beigh, M.A., Andrabi, K.I., 2014. mTOR Signaling in Protein Translation Regulation: Implications in Cancer Genesis and Therapeutic Interventions, Molecular Biology International.

Shveygert, M., Kaiser, C., Bradrick, S.S., Gromeier, M., 2010. Regulation of eukaryotic initiation factor 4E (eIF4E) phosphorylation by mitogen-activated protein kinase occurs through modulation of Mnk1-eIF4G interaction. Mol. Cell. Biol. 30, 5160–5167.

Siddiqui, N., Sonenberg, N., 2015. Signalling to eIF4E in cancer. Biochem. Soc. Trans. 43, 763–772.

Soni, S., Padwad, Y.S., 2017. HIF-1 in cancer therapy: two decade long story of a transcription factor. Acta Oncologica 56, 503–515.

Sørensen, B.S., Busk, M., Overgaard, J., Horsman, M.R., Alsner, J., 2015. Simultaneous Hypoxia and Low Extracellular pH Suppress Overall Metabolic Rate and Protein Synthesis In Vitro. PLoS One 10.

Spiegelberg, L., Houben, R., Niemans, R., de Ruysscher, D., Yaromina, A., Theys, J., Guise, C.P., Smaill, J.B., Patterson, A.V., Lambin, P., Dubois, L.J., 2019. Hypoxia-activated prodrugs

and (lack of) clinical progress: The need for hypoxia-based biomarker patient selection in phase III clinical trials. Clin Transl Radiat Oncol 15, 62–69.

Spriggs, K.A., Stoneley, M., Bushell, M., Willis, A.E., 2008. Re-programming of translation following cell stress allows IRES-mediated translation to predominate. Biol. Cell 100, 27–38.

Stoneley, M., Paulin, F.E., Le Quesne, J.P., Chappell, S.A., Willis, A.E., 1998. C-Myc 5' untranslated region contains an internal ribosome entry segment. Oncogene 16, 423–428.

Sun, Y., Atas, E., Lindqvist, L.M., Sonenberg, N., Pelletier, J., Meller, A., 2014a. Single-molecule kinetics of the eukaryotic initiation factor 4AI upon RNA unwinding. Structure 22, 941–948.

Sun, Y., Atas, E., Lindqvist, L.M., Sonenberg, N., Pelletier, J., Meller, A., 2014b. Single-Molecule Kinetics of the Eukaryotic Initiation Factor 4AI upon RNA Unwinding. Structure 22, 941–948.

Survival | Bowel cancer | Cancer Research UK [WWW Document], 2019. . Cnacer Research UK. URL https://www.cancerresearchuk.org/about-cancer/bowel-cancer/survival (accessed 12.17.19).

Suzuki, C., Garces, R.G., Edmonds, K.A., Hiller, S., Hyberts, S.G., Marintchev, A., Wagner, G., 2008. PDCD4 inhibits translation initiation by binding to eIF4A using both its MA3 domains. Proc. Natl. Acad. Sci. U.S.A. 105, 3274–3279.

Svitkin, Y.V., Pause, A., Haghighat, A., Pyronnet, S., Witherell, G., Belsham, G.J., Sonenberg, N., 2001. The requirement for eukaryotic initiation factor 4A (eIF4A) in translation is in direct proportion to the degree of mRNA 5' secondary structure. RNA 7, 382–394.

Tanabe, A., Tanikawa, K., Tsunetomi, M., Takai, K., Ikeda, H., Konno, J., Torigoe, T., Maeda, H., Kutomi, G., Okita, K., Mori, M., Sahara, H., 2016. RNA helicase YTHDC2 promotes cancer metastasis via the enhancement of the efficiency by which HIF-1α mRNA is translated. Cancer Lett. 376, 34–42.

The colorectal adenoma–carcinoma sequence - Leslie - 2002 - BJS (British Journal of Surgery) - Wiley Online Library [WWW Document], n.d. URL https://bjssjournals.onlinelibrary.wiley.com/doi/abs/10.1046/j.1365-2168.2002.02120.x (accessed 12.17.19).

Thoma, C., Fraterman, S., Gentzel, M., Wilm, M., Hentze, M.W., 2008. Translation initiation by the c-myc mRNA internal ribosome entry sequence and the poly(A) tail. RNA 14, 1579–1589.

Tsumuraya, T., Ishikawa, C., Machijima, Y., Nakachi, S., Senba, M., Tanaka, J., Mori, N., 2011. Effects of hippuristanol, an inhibitor of eIF4A, on adult T-cell leukemia. Biochem. Pharmacol. 81, 713–722.

Tuteja, N., Vashisht, A.A., Tuteja, R., 2008. Translation initiation factor 4A: a prototype member of dead-box protein family. Physiol Mol Biol Plants 14, 101–107.

Umar, S., 2010. Intestinal Stem Cells. Curr Gastroenterol Rep 12, 340–348.

Uniacke, J., Holterman, C.E., Lachance, G., Franovic, A., Jacob, M.D., Fabian, M.R., Payette, J., Holcik, M., Pause, A., Lee, S., 2012. An oxygen-regulated switch in the protein synthesis machinery. Nature 486, 126–129.

Vasen, H.F.A., Blanco, I., Aktan-Collan, K., Gopie, J.P., Alonso, A., Aretz, S., Bernstein, I., Bertario, L., Burn, J., Capella, G., Colas, C., Engel, C., Frayling, I.M., Genuardi, M., Heinimann, K., Hes, F.J., Hodgson, S.V., Karagiannis, J.A., Lalloo, F., Lindblom, A., Mecklin, J.-P., Møller, P., Myrhoj, T., Nagengast, F.M., Parc, Y., Leon, M.P. de, Renkonen-Sinisalo, L., Sampson, J.R., Stormorken, A., Sijmons, R.H., Tejpar, S., Thomas, H.J.W., Rahner, N., Wijnen, J.T., Järvinen, H.J., Möslein, G., 2013. Revised guidelines for the clinical management of Lynch syndrome (HNPCC): recommendations by a group of European experts. Gut 62, 812–823.

Vaupel, P., 2004. The Role of Hypoxia-Induced Factors in Tumor Progression. The Oncologist 9, 10–17.

Vidman, L., Källberg, D., Rydén, P., 2019. Cluster analysis on high dimensional RNA-seq data with applications to cancer research - An evaluation study. bioRxiv 675041.

Vikhreva, P.N., Kalinichenko, S.V., Korobko, I.V., 2017. Programmed cell death 4 mechanism of action: The model to be updated? Cell Cycle 16, 1761–1764.

Villar, D., Ortiz-Barahona, A., Gómez-Maldonado, L., Pescador, N., Sánchez-Cabo, F., Hackl, H., Rodriguez, B.A.T., Trajanoski, Z., Dopazo, A., Huang, T.H.M., Yan, P.S., del Peso, L., 2012. Cooperativity of Stress-Responsive Transcription Factors in Core Hypoxia-Inducible Factor Binding Regions. PLoS One 7.

Wang, G.L., Jiang, B.H., Rue, E.A., Semenza, G.L., 1995. Hypoxia-inducible factor 1 is a basic-helix-loop-helix-PAS heterodimer regulated by cellular O2 tension. Proc Natl Acad Sci U S A 92, 5510–5514.

Wolfe, A.L., Singh, K., Zhong, Y., Drewe, P., Rajasekhar, V.K., Sanghvi, V.R., Mavrakis, K.J., Jiang, M., Roderick, J.E., Van der Meulen, J., Schatz, J.H., Rodrigo, C.M., Zhao, C., Rondou, P., de Stanchina, E., Teruya-Feldstein, J., Kelliher, M.A., Speleman, F., Porco, J.A., Pelletier, J., Rätsch, G., Wendel, H.-G., 2014. RNA G-quadruplexes cause eIF4A-dependent oncogene translation in cancer. Nature 513, 65–70.

Xie, C., Gao, X., Sun, D., Zhang, Y., Krausz, K.W., Qin, X., Gonzalez, F., 2018. Metabolic profiling of the novel HIF2α inhibitor PT2385 in vivo and in vitro. Drug Metab Dispos.

Xu, Z., Li, X.-F., Zou, H., Sun, X., Shen, B., 2017. 18F-Fluoromisonidazole in tumor hypoxia imaging. Oncotarget 8, 94969–94979.

Yamamoto, Y., Singh, C.R., Marintchev, A., Hall, N.S., Hannig, E.M., Wagner, G., Asano, K., 2005. The eukaryotic initiation factor (eIF) 5 HEAT domain mediates multifactor assembly and scanning with distinct interfaces to eIF1, eIF2, eIF3, and eIF4G. PNAS 102, 16164–16169.

Yan, L.X., Wu, Q.N., Zhang, Y., Li, Y.Y., Liao, D.Z., Hou, J.H., Fu, J., Zeng, M.S., Yun, J.P., Wu, Q.L., Zeng, Y.X., Shao, J.Y., 2011. Knockdown of miR-21 in human breast cancer cell lines

inhibits proliferation, in vitro migration and in vivotumor growth. Breast Cancer Research 13, R2.

Yang, Z.J., Chee, C.E., Huang, S., Sinicrope, F.A., 2011. The Role of Autophagy in Cancer: Therapeutic Implications. Mol Cancer Ther 10, 1533–1541.

Young, R.M., Wang, S.-J., Gordan, J.D., Ji, X., Liebhaber, S.A., Simon, M.C., 2008. Hypoxia-mediated selective mRNA translation by an internal ribosome entry site-independent mechanism. J. Biol. Chem. 283, 16309–16319.

Yu, T., Tang, B., Sun, X., 2017. Development of Inhibitors Targeting Hypoxia-Inducible Factor 1 and 2 for Cancer Therapy. Yonsei Med J 58, 489–496.

Zhang, H., Zhang, C., Li, Z., Li, C., Wei, X., Zhang, B., Liu, Y., 2019. A New Method of RNA Secondary Structure Prediction Based on Convolutional Neural Network and Dynamic Programming. Front. Genet. 10.

Zheng, L., Kelly, C., Colgan, S., 2015. Physiologic hypoxia and oxygen homeostasis in the healthy intestine. A Review in the Theme: Cellular Responses to Hypoxia. American Journal of Phsyiology Cell Physiology 309, 350–360.

Ziello, J.E., Jovin, I.S., Huang, Y., 2007. Hypoxia-Inducible Factor (HIF)-1 Regulatory Pathway and its Potential for Therapeutic Intervention in Malignancy and Ischemia. Yale J Biol Med 80, 51–60.

Zuker, M., Stiegler, P., 1981. Optimal computer folding of large RNA sequences using thermodynamics and auxiliary information. Nucleic Acids Res. 9, 133–148.